https://doi.org/10.35662/unine-thesis-2866

Faculty of Science

Laboratory of Technologies for Heritage Materials

Biological strategies for the preservation of waterlogged archaeological wood

A dissertation submitted to the University of Neuchâtel

for the degree of *Docteur ès Sciences*

Presented by

Magdalena Albelda Berenguer

Jury members:

Prof. Edith Joseph, thesis supervisor, University of Neuchâtel, Switzerland

Prof. Pilar Junier, thesis co-supervisor, University of Neuchâtel, Switzerland

Prof. María del Pilar Bosch Roig, Universitat Politècnica de València, Spain

Dr. Jakob Zopfi, Universität Basel, Switzerland

Thesis defended on the 2nd November 2020

UNIVERSITÉ DE NEUCHÂTEL

Faculté des Sciences
Secrétariat-décanat de Faculté
Rue Emile-Argand 11
2000 Neuchâtel – Suisse
Tél : + 41 (0)32 718 21 00
E-mail : secretariat.sciences@unine.ch

IMPRIMATUR POUR THESE DE DOCTORAT

La Faculté des sciences de l'Université de Neuchâtel autorise l'impression de la présente thèse soutenue par

Madame Magdalena ALBELDA BERENGUER

Titre:

"Biological strategies for the preservation of waterlogged archaeological wood"

sur le rapport des membres du jury composé comme suit:

- Prof. ass. Edith Joseph, directrice de thèse, Université de Neuchâtel, Suisse
- Prof. Pilar Junier, co-directrice de thèse, Université de Neuchâtel, Suisse
- Dr. Jakob Zopfi, Université de Bâle, Suisse
- Prof. ass. Maria del Pilar Bosch Roig, Universitàt Politècnica de Valencia, Espagne

Neuchâtel, le 27 novembre 2020

Le Doyen, Prof. A. Bangerter

Abstract

Waterlogged archaeological wood (WAW) is an essential part of our cultural heritage. Wooden objects that have been preserved in waterlogged conditions provide valuable information about past civilizations. However, WAW may encounter serious issues after recovery. When sulfur and iron species have formed and accumulated during burial time, salts precipitation and acidification can appear after exposition to oxygen, leading to severe structural damages. Unfortunately, these alterations are often observed after objects have been consolidated. In response, chemical extraction or neutralization processes are applied. Currently, new trends are opting for less toxic and more environmentally friendly solutions. For example, bio-based treatments are arousing for the preservation of heritage artefacts based on the potential of diverse microbiological metabolisms. The aim of this thesis is to develop a green and sustainable method that would remove sulfur and iron compounds while maintaining the chemical stability and physical structure of WAW heritage. There are only few references of bio-based methods related to the conservation of organic substrates. Therefore, the biotechnological extraction proposed here is an innovative approach for the removal of iron/sulphur species from wood.

This original method adopts two different strategies: 1) the removal of iron using microbial iron chelators (i.e., siderophores) and, 2) the extraction of sulfur species by oxidation with selected bacteria (i.e., *Thiobacillus denitrificans*). Both approaches were studied directly on mineral phases commonly found in WAW, and on model wood samples prepared to simulate WAW. Separately, both biological processes showed positive results extracting iron and sulfur species from model wood samples. Moreover, no further degradation of the wood matrix was detected after application of either extraction method. Further research is still needed to enhance the extraction of iron and sulfur as with more stable mineral phases the dissolution rates were lower. Combined together on model wood samples, the use of siderophores and biological oxidation performed in line to current chemical extraction methods and respected as much as possible the conservation guidelines in terms of appearance, effectiveness and safety. The bio-based treatment results are promising, and future efforts would be made to improve performance and to develop a ready-to use protocol.

Keywords: Waterlogged archaeological wood, heritage conservation, biotechnology, iron sulfides, siderophore, *Thiobacillus denitrificans*

Résumé

Le bois archéologique gorgé d'eau est une partie essentielle de notre patrimoine culturel. Les objets en bois qui ont été préservés dans des sites gorgées d'eau fournissent des informations précieuses sur les civilisations passées. Cependant, le bois gorgé d'eau peut rencontrer de graves problèmes après l'excavation. Lorsque des espèces soufrées et de ferreuses se sont formées et accumulées pendant la période d'enfouissement, la précipitation de sels et l'acidification peuvent apparaître après exposition à l'oxygène, entraînant de graves problèmes structurels. Malheureusement, ces altérations sont souvent observées après que les objets aient été consolidés. Des procédés d'extraction chimique ou de neutralisation sont appliqués en réponse a ces problèmes. Actuellement, les nouvelles tendances optent pour des solutions moins toxiques et plus respectueuses de l'environnement. Par exemple, les traitements biologiques appliqués à la préservation d'artéfacts patrimoniaux basé sur le potentiel de divers métabolismes microbiologiques suscitent l'intérêt. Le but de cette thèse est de développer une méthode verte et durable qui éliminerait les composés soufrés et ferreux tout en maintenant la stabilité chimique et la structure physique du bois gorgé d'eau. Il existe peu de références de méthodes biologiques liées à la conservation des substrats organiques. De ce point de vue, l'extraction biotechnologique proposée ici est une approche innovante pour l'élimination des espèces de fer et soufre du bois.

Cette méthode originale adopte deux stratégies différentes: 1) l'élimination du fer à l'aide de chélateurs microbiens du fer (sidérophores) et, 2) l'extraction d'espèces soufrées par oxydation avec des bactéries sélectionnées (*Thiobacillus denitrificans*). Les deux approches ont été étudiées directement sur les phases minérales couramment trouvées dans le bois gorgé d'eau, et sur des échantillons de bois modèles préparés pour simuler le bois archéologique gorgé d'eau. Les deux processus biologiques ont montré des résultats positifs en extrayant des espèces de fer et de soufre à partir d'échantillons de bois modèles. De plus, aucune dégradation supplémentaire du bois n'a été détectée après l'application des méthodes d'extraction. Néanmoins, des recherches supplémentaires sont nécessaires pour améliorer l'extraction du fer et du soufre car avec des phases minérales plus stables, les taux de dissolution étaient plus faibles. Combinées sur des échantillons de bois modèles, l'utilisation de sidérophores et l'oxydation biologique ont obtenu des résultats dans le cadre des traitements d'extraction chimiques actuels et respectent autant que possible les critères de conservation en termes d'aspect, d'efficacité et de sécurité. Les résultats du traitement biologique sont prometteurs et des efforts futurs seront faits pour améliorer les performances et développer un protocole prêt à l'emploi.

Mots-clés: Bois archéologique gorgé d'eau, conservation du patrimoine, biotechnologie, sulfures de fer, sidérophore, *Thiobacillus denitrificans*

Resumen

La madera arqueológica anegada es una parte esencial de nuestro patrimonio cultural. Los objetos de madera que se han conservado anegados proporcionan información valiosa sobre civilizaciones pasadas. Sin embargo, este tipo de madera puede encontrar problemas graves después de su recuperación. Si compuestos de hierro y azufre se han formado y acumulado durante el periodo de anegamiento, precipitación de sales y formación de ácidos pueden emerger en contacto con oxigeno y humedad. Para la madera esto pueden significar daños estructurales graves. Estas alteraciones a menudo se observan después incluso de que los objetos se hayan consolidado. En respuesta, se aplican procesos de extracción química o neutralización. Actualmente, las nuevas tendencias apuestan por soluciones menos tóxicas y más respetuosas con el medio ambiente. Por ejemplo, los tratamientos biotecnológicos basados en el potencial de diversos metabolismos microbiológicos están en auge en el campo de la preservación del patrimonio. El objetivo de esta tesis es desarrollar un método ecológico y sostenible que elimine los compuestos hierro y azufre, manteniendo la estabilidad química y la estructura física de la madera arqueológica. Hasta la fecha, hay pocas referencias de métodos biológicos para la conservación de sustratos orgánicos. Desde este punto de vista, la extracción biotecnológica propuesta aquí es un enfoque innovador para la eliminación de especies de hierro y azufre de la madera arqueológica anegada.

Este método original adopta dos estrategias diferentes: 1) la eliminación de hierro utilizando quelantes microbianos (sideróforos) y, 2) la extracción de especies de azufre mediante oxidación bacteriana (*Thiobacillus denitrificans*). Ambos enfoques se estudiaron directamente en fases minerales que se encuentran comúnmente en la madera anegada, y en muestras de madera modelo preparadas para simular dicha madera. Ambos procesos biológicos mostraron resultados positivos al extraer hierro y azufre de la madera modelo. Además, no se detectó un incremento en la degradación de la madera después de la aplicación de ningún método de extracción. Aún así, es necesario mejorar el rendimiento de la extracción, ya que, con las fases minerales más estables, las tasas de disolución eran más bajas. El efecto combinado del uso de sideróforos y oxidación biológica obtuvo resultados en línea con los tratamientos de extracción química actuales y, respetó en la medida de lo posible las pautas de conservación en términos de apariencia, efectividad y seguridad. Los resultados del tratamiento biotecnológico son prometedores. Esfuerzos futuros están puestos en mejorar el rendimiento y desarrollar un protocolo listo para usar.

Palabras clave: Madera arqueológica anegada, conservación del patrimonio, biotecnología, sulfuros de hierro, sideróforos, *Thiobacillus denitrificans*

Abbreviations

ASV	Amplicon Sequence Variant
ATR	Attenuated Total Reflectance
CAS	Chrome Azorul S
DFOM	Deferoxamine Mesylate
DTPA	Diethylenetriamine-pentaacetic acid
EB	Erosion Bacteria
EDDHMA	Ethylenediimino-bis(2-hydroxy-4-methylphenyl) acetic acid
EDS	Energy-dispersive X-ray Spectroscopy
EDTA	Ethylenediaminetetraacetic acid
ESEM	Environmental Scanning Electron Microscopy
FTIR	Fourier Transform Infrared Spectroscopy
GYM	Glucose-Yeast-Malt medium
HEPES	N-2-hydroxyethylpiperazine-N'-2-ethane sulphonic acid
IC	Ion Chromatography
ICP-OES	Inductively Coupled Plasma-Optical Emission Spectrometry
ITS	Internal Transcribed Spacer
LMWO	Low Molecular Weight Organic acid
NB	Nutrient Broth
NMR	Nuclear Magnetic Resonance
OD	Optical Density
PCR	Polymerase Chain Reaction
PEG	Polyethylene glycol
pNP	*p*-nitrophenol
pNPG	*p*-nitrophenyl-*β*-D-glucopyranoside
PVD	Pyoverdine
RBBR	Remazol Brilliant Blue R
ROS	Reactive oxygen species
SEM	Scanning Electron Microscopy
SOB	Sulfate-oxidising Bacteria
SRB	Sulfate-reducing Bacteria
Sy-XRF	Synchrotron-X-ray Fluorescence
Tris	Tri(hydroxymethyl)aminomethane
WAW	Waterlogged Archaeological Wood
XRD	X-Ray Diffraction

Table of Contents

Chapter 1

INTRODUCTION

Sites palafittes. © Béat Arnold

Summary

Archaeological discoveries are a way of travelling through time. Archaeological finds bring information about human development and cultural activities of past civilizations. Great discoveries such as Tutankhamun´s tomb will appear in the first page of all-around the world newspapers. As Florian M-L. E. (1990) stated concerning the recovery of the Swedish warship *Vasa*: "[…] hearts must have been bursting and tears flowing. The sight of the ship must have conjured up many different thoughts in the people watching". Archaeological objects awake emotions in people as they feel a connection with past centuries.

In this introductory chapter, the basic concepts about waterlogged archaeological wood (WAW) are explained. The composition of wood and the process of degradation are mentioned to better understand the problematic that wooden objects encounter prior to conservation. WAW suffers serious problems after excavation due to the accumulation of sulfur and iron compounds during burial. Exposure of these compounds to oxygen results in precipitation of salts and acidification, which can lead to serious structural damage, and ultimately the loss of important cultural heritage. Current treatments use strong chemicals with high toxicity, which are not safe for the user or the environment. New trends are looking for more environmentally friendly solutions, such as biological processes. The MICMAC (Microbes for the Archaeological wood Conservation) project proposes a new bio-based treatment for the preservation of WAW.

1.1 Wood: a unique material

Wood is an organic material with a complex chemical composition that functions as structural tissue in the stems of trees and other woody plants. Wood has been defined as the secondary xylem of trees, being the xylem the vascular tissue that conducts water and nutrients from the roots to other parts of the tree [1]. In a living tree, the wood tissue has therefore a support and a transport function, allowing the plant to stand and grow high.

Over time, wood has been widely used by humans as a versatile material. Wood is collected from felled trees and then treated to be used for many different purposes such as construction, energy resource, art, production of paper, etc. Wood has a complex chemical and physical composition that provides unique characteristics and properties to it. The composition of wood is described below from the molecular to the macroscopic level.

Chemical composition

Microscopically, wood is structured in wood fibres composed of elongated cells, which are disposed in longitudinal direction parallel to the main axis. The wood fibres are best defined as a three-dimensional biopolymer consisting of an interconnected network of the three main components of wood: cellulose, hemicelluloses and lignin; with secondary amounts of extractives and inorganics. Sugar based polymers (i.e., carbohydrates: cellulose and hemicelluloses) make up to the 65-75% of the cell wall composition, while lignin only goes up to 18-35%. Overall, the elemental composition of dry wood is 50% carbon, 6% hydrogen, 44% oxygen, and trace amounts of inorganics [1].

Holocellulose

The carbohydrate portion of wood contains the combination of cellulose (40-45%) and hemicelluloses (17-30%) (i.e., holocellulose), and also other sugar polymers such as starch and pectin. The holocellulose fraction is water-insoluble and it can be extracted if lignin and other components are removed from the biomass.

Cellulose

Cellulose is the main component of wood matrix, surrounded by hemicelluloses and lignin. Cellulose is a linear polysaccharide compose of D-glucopyranose units, which are covalent linked together by 1, 4 β-glycosidic bonds. The number of glucose units in a cellulose chain is called degree of polymerization (DP). The cellulose in wood has an average DP of at least 9000-10000 [2] .

Cellulose molecules orientation allows secondary bonding within the chain, and with other adjacent chains. Clusters of cellulose chains form microfibrils. Hydrogen bonds, van der Waals forces and dipole interactions support the cellulose molecules creating a semi-crystalline structure. The distribution of the microfibrils changes the crystallinity of the overall matrix, when the packaging density increases the cellulose structure becomes more crystalline. The strength of the wood fibres depends on the covalent bonds. Cellulose dissolves only in strong acids, but degradation occurs [3].

Hemicelluloses

The hemicellulose fraction is a group of branched polysaccharides polymers with lower crystallinity and DP (around 100-200) than cellulose. They usually contain a backbone structure consisting of one repeating sugar unit bond 1, 4 β with branch points. The amorphous structure of hemicelluloses is more reactive; they are soluble in alkali solutions and are hydrolysed by acids more efficiently than cellulose. The function of hemicelluloses is not yet fully understood but they contribute to the mechanical properties of the cell wall [2].

Lignin

Lignin is a highly complex, amorphous, mostly aromatic polymer of three main monolignols (or phenylpropane derivates). Three different types of ether (C-O-C) bonds and four types of carbon-carbon (C-C) bonds keep the structure together. Moreover, the aromatic rings and hydroxyl groups of lignin allow intermolecular interactions, forming non-covalent and hydrogen bonds with cellulose and hemicelluloses [2].

Lignin plays many roles in the cell wall maintenance. The aromatic structure provides hydrophobicity to the cell wall, as well as inhibits swelling. Moreover, most microorganisms cannot penetrate the cell wall thanks to the lignin barrier. Only some specialized microbes are able to break down the heterogenous lignin structure [4], [5].

Wood extractives

Low molecular mass compounds that can be extracted from wood are known as wood extractives. The total amount of extractives is a small fraction of total composition of the wood; however, wood extractives play different important roles in the tree. Some extractives participate to the metabolism of the living cells, while other protect the tree against fungi and other organisms [1].

The most common wood extractives are resin acids, terpenoids, waxes, fatty acids, and tannins [6]. For instance, tannins are important phenolic extractives in the heartwood of certain species. They are well-known to bind proteins and also inorganics compounds like iron [1], [7].

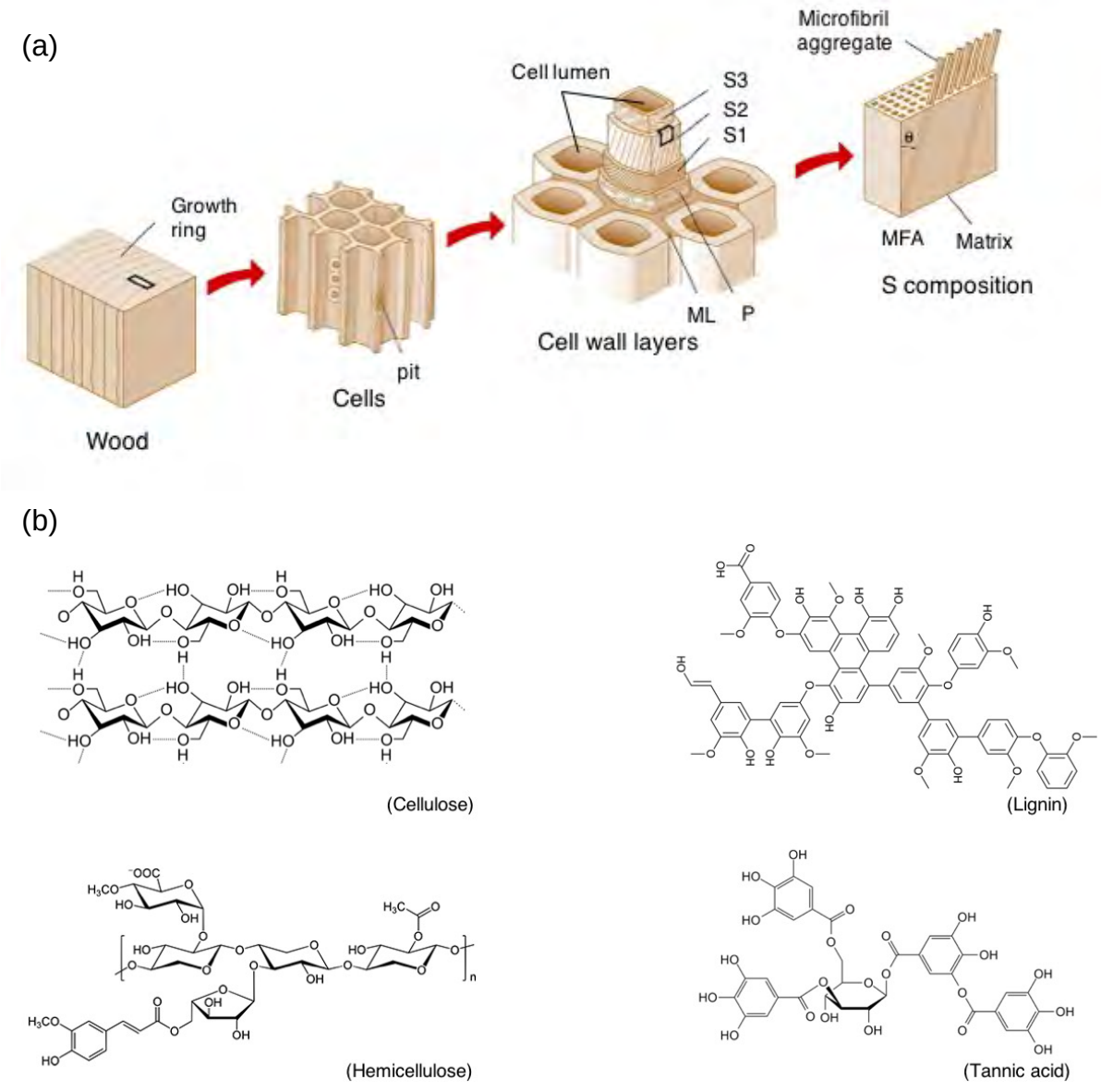

Figure 1.1. *(a) Scheme of the hierarchical structure of wood. At the level of the cell wall, different layers are observed: middle lamella (ML), primary cell wall (P), and secondary cell wall (S1, S2 and S3). The orientation of the cellulose microfibrils in the secondary wall is measured by the microfibril angle (MFA). Adapted from* [8]. *(b) Chemical structure of the main components of the cell wall: cellulose, hemicellulose and lignin, plus some common wood extractives such as tannic acid.*

Cell walls

The cell wall is an important structure in the wood tissue, and therefore is a regular structure within the Plant kingdom. The cell wall consists of three principal regions: the middle lamella, the primary wall, and the secondary wall (Figure 1.1). The chemical composition however differs between the layers, and it can present variations in different parts of the tree, and between different species.

The singular cells of the wood tissue are connected to one another to act as a unified network. Each of the individual cells is linked to the adjacent cells allowing the communication and exchange of biochemicals between them. The middle lamella is the layer between two or more cells that keeps the cells together. This is the first layer in the cell wall. In wood, is mostly composed of lignin. The next cell layer is the primary wall. The composition of this layer is characterised by a high lignin concentration, and a random orientation of cellulose fibrils. In wood, the primary cell wall is so thin that is usually indistinguishable from the middle lamella [3].

Three layers: S1, S2, and S3, constitute the last domain, the secondary cell wall. The first-formed S1 layer is adjacent to the primary wall. This thin layer is characterized by a large microfibril angle. The angle between the orientation of the cellulose fibrils and the long axis of the cell is large (50 to 70 degrees). The next S2 layer presents an opposite distribution of the cellulose fibrils, having a low microfibril angle (5 to 30 degrees). The S2 layer is also characterized by a lower lignin concentration and is the thickest secondary cell wall layer, playing a key role in overall properties of the cell wall. The last S3 layer is again thin and with a high microfibril angle (+70 degrees). The altered orientations of the cellulose fibrils constitute a rigid and advanced construction. The S3 layer has the lowest percentage of lignin due to water transportation through the wood. The S3 layer is in contact with the cell lumen where transportation occurs. Lignin is a hydrophobic macromolecule, and water molecules need enough adhesion to move up in the tree [3], [6].

Wood layers

Macroscopically, wood is also composed by defined layers with different functions (Figure 1.2). The outermost layer, the bark, is a dead layer that provides protection against external damages (physical, mechanical or biological). Underneath the bark is the living phloem (secondary phloem). The main function of this layer is the transport of nutrients. The following layer is the vascular cambium. This very thin layer (about three cell rows) is where the cell

division occurs. The cambium cells originate new phloem to the outside, and xylem to the inside. The xylem layer is divided in sapwood and heartwood. Sapwood is the outer section of the wood and it is the youngest tissue. It performs the fundamental roles of transporting water from the roots to the leaves, storage and distribution of nutrients from the leaves to the rest of the tree. Over the development of the tissue, the xylem cells and vessels lose their cytoplasm, and the cells are then functionally dead. When the cells die, the sapwood becomes heartwood, which functions mainly as support tissue [3]. The chemical transformations that the parenchyma cells experience in the dying process make the heartwood more resistant to decay. In the long-term, the heartwood accumulates a variety of biochemicals, such as resin, phenols and pigments [1].

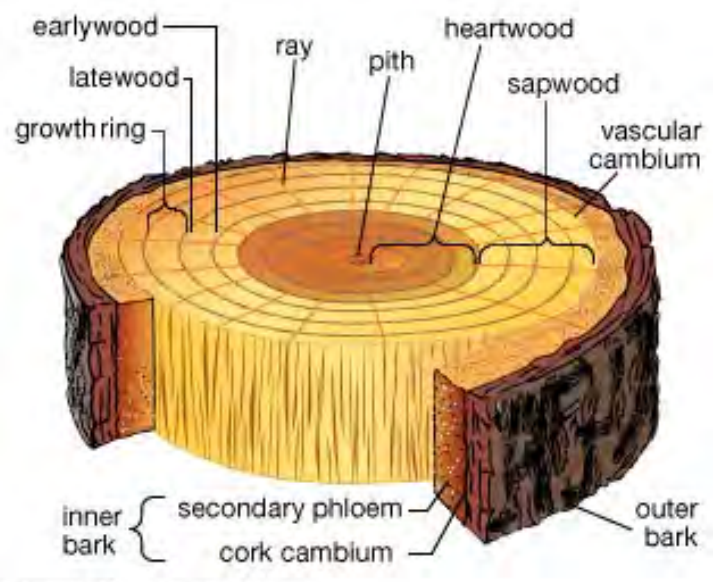

***Figure 1.2**. Schematic representation of the layer structure in wood. © 2006 Merriam-Webster, Inc.*

Annual growth rings are observed in the xylem. Each ring is divided in the earlywood and the latewood. The layers of the wood remain after the tree is chopped down. Measurements of the thickness of the annual rings on a fragment of wood allows the reconstruction of a pattern with wider and narrower tree rings, which corresponds with periods of growth. Afterwards, the patterns are compared with samples of known age from the same area. This methodology, known as dendrochronology, makes possible to follow the history of wooden objects [9]. Moreover, wood separates into two groups: softwoods (e.g., pine) and hardwoods (e.g., oak), based on their composition. Hardwoods have a characteristic type of cell called vessel element (or pore), which is absent in softwoods [3].

Properties of wood

Wood properties may vary according to the tree species or even within the same species due to environmental conditions. Still, wood has some basic properties that are common to all woods.

Anisotropy

Wood is an heterogenous material directionally dependent, which implies different properties in the different planes. For instance, wood is more mechanical resistant in the direction of the axis of the tree. Wood presents three different main planes: cross section or transversal section, radial section, and tangential section (Figure 1.3) [6].

Hygroscopicity

Wood has the capacity to uptake moisture directly from the environment and to hoard it up as liquid water between the spaces of microfibrils. Moreover, wood is able to absorb big quantities of water within the cell lumen [6]. However, increased amounts of water interfere with hydrogen bonding between the organic polymers what decreases the strength of wood [10].

Polarity

Wood is a polar material, which makes it compatible with other polar products such as water, varnishes, etc. [6].

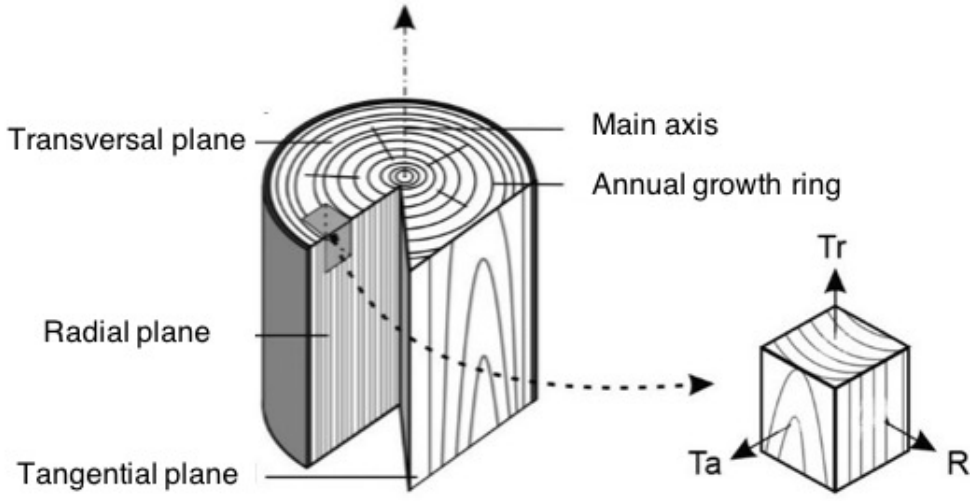

***Figure 1.3**. Graphical representation of the three planes of wood: transversal (Tr), radial (R), and tangential (Ta).*

1.2 Waterlogged archaeological wood (WAW)

Archaeological wood may be defined as wood used by a past human society, preserved in a specific environment and that carries information of human culture [11]. Wood is an exceptionally useful and versatile material that is easy to obtain and easy to find in many diverse environments. Therefore, wood entered in humans life since the beginning of time, and woodworking has played a vital role in the advancement of civilization [12]. In consequence, we may expect many archaeological discoveries to present wood artefacts or traces of them. However, as an organic material, the decay of wooden objects is very likely above ground. At certain oxygen and humidity levels, fungi attack can lead to the total destruction of wooden artefacts [12].

Indeed, specific conditions are required for the long-term survival of wooden objects. Most archaeological finds containing wood are recovered from the seabed, lakes floor or wet soils, where microbial activity is reduced [13]. Under these environments, all the cavities - capillaries and microcapillaries – of the wood are entirely filled with water. However, waterlogged wood may create the wrong illusion; as all the pores spaces are filled with water, the shape remains. But, even underwater, some organisms can still slowly degrade wood. For example, anaerobic microorganisms decay the cellulose and hemicelluloses leaving a mostly a lignin backbone [14]. Waterlogged archaeological wood (WAW) is considered to be in a good state of preservation, because all surface and macroscopic structural details are preserved. However, from a chemical and molecular structural perspective, it can still be highly damaged, presenting a porous and fragile network with a heterogenous chemical composition [15], [16]. Further damage can occur if no conservation methods are put in place.

WAW has allowed historians to better understand the state of development of previous civilizations. Wooden objects that have been preserved in waterlogged conditions give an excellent opportunity to study everyday life activities, like hunting or agriculture, which are invisible if these objects are decomposed. For example, the serial of *Prehistoric Pile Dwellings around the Alps* (UNESCO) is a waterlogged archaeological discovery where the wooden constructions and objects, as well as many other organic materials, have been preserved helping to describe the early life of pre-historical civilizations [17]. Wheels and axles, dugout canoes, handles and shafts are some of the elements found made by wood. Also, the wood species used by these people (oak, fir, ash, willow, lime, and poplar, among others) gives information about their surrounding environment. Moreover, notorious archaeological discoveries are economically significant. For instance, the Vasa Museum in Stockholm, is the most visited

museum in Scandinavia, with 1.5 million visitors per year. Therefore, a lot of efforts are made to better understand the composition and degradation state of WAW for better preservation.

1.3 Degradation processes in waterlogged wood

Biological degradation

Waterlogged wood is usually considered to be well preserved. However, as an organic material, wood is target for degradation by biological processes in nature [12], [13]. Different environmental factors control the rate of biological decay (e.g.: oxygen content, temperature, salinity, etc.). Consequently, the state of preservation of wood varies depending on the local conditions, chemical composition of the wood, and type of wood species [18].

Different types of organisms are involved in the degradation of wood. For instance, in aquatic environments, molluscs such as *Teredo navalis*, and crustaceans like *Limnoria lignorum* and *Sphaeroma terebrans,* can be very aggressive wood-damaging organisms. They produce cavities and holes through the wood structure, but their action is limited to certain environments. Their activity is mostly destructive above the sediments. Moreover, the exposed parts of the *Vasa* were protected from the attack of *T. navalis* due to the low salinity in the Baltic Sea, as the "shipworm" appears to require at least 12‰ salinity [19].

Microorganisms, such as fungi and bacteria, are also involved in wood degradation. Fungi are known to be the most destructive to wood in certain conditions. Indeed, fungi can degrade different wood components, from starch to lignin, leading to a total loss of material. Depending on the decay pattern and components degraded, wood-decaying fungi are divided in three main groups: white-, brown- and soft-rot fungi.

White-rot fungi are characterised for degrading all cell wall components, even lignin, and for producing decolouration of the wood [13]. White-rot are an heterogenous group including many different species of fungi, such as *Ceriporiopsis subvermispora* and *Pleurotus ostreatus* [20]. Some white-rot may decay preferentially lignin over cellulose and hemicellulose, while other white-rot fungi attack all cell wall components simultaneously [20]. In contrast, brow-rot fungi decay almost exclusively polysaccharides. Their degradation of cellulose leads to a considerable loss of wood strength and a brown colouration [13]. Fungi that produce soft-rot usually are classified as Ascomycetes and Fungi Imperfecti [21]. After their attack only the high lignin-content middle lamella remains [21]. They are problematic for wood conservation due to their ubiquitous distribution, attacking wood in terrestrial and aquatic environments [16],

[21]. Waterlogged wood is mainly degraded by soft-rot fungi [22]. In fact, the term "soft-rot" came from describing the degradation of waterlogged wood, as waterlogged wood is soft to the touch. In dry wood, the attack of this group of fungi does not soften the wood [21].

However, like the "shipworm", fungal decay of wood is also restricted to some conditions. In waterlogged locations, evidence of degradation by soft-rot fungi is only observed where oxygen is available [22]. Hence, in aquatic and terrestrial waterlogged places, where oxygen is limited, bacteria are considered to be the main degraders of wood [12]. Bacterial damage causes a loss of strength in wood, but their metabolisms are not as harmful as fungal activity.

Bacterial degradation of wood is complicated due to the defences against it. The high lignin composition in the middle lamella and primary wall makes a barrier that protects against most bacterial enzymatic decomposition. Moreover, some wood extractives may function as toxins [23]. However, some groups of bacteria have acquired the capability to decay the wood components. The primary wood degraders initiate the bacterial colonization of wood increasing the permeability and opening the way to other microbes. The secondary wood degraders, or scavenging bacteria, follow the primary wood degraders attack, and all are part of the total microbial community detected in waterlogged wood [24], [25].

Primary wood degraders

The decay of waterlogged wood has been explained as a progressive process involving several groups of bacteria. Based on microscopically observations, specific morphologies of wood decay were detected, consequently, such bacteria were divided into three groups, i.e. tunnelling, erosion, and cavitation bacteria [25]. These bacteria are typically the first degraders of waterlogged wood. They are the responsible of breaking down the lignocellulose structure of the cell walls in all the wood tissue, even under near anoxic environments.

Erosion bacteria (EB) are the most common group between the primary wood degraders. They are typically rod-shaped and present a firm attachment to cellulosic fibre walls. Most studies have investigated the degradation patterns produced by these microbes, but little is known about the taxonomy of the bacteria involved in biodegradation of WAW. Some studies obtained pure cultures of erosion bacteria, revealing species belonging to the CFB (*Cytophaga–Flavobacterium-Bacteroides*) complex [24], [26]. Bacteria from this group are found in terrestrial and aquatic environments and they have been described by their ability to degrade complex organic materials. Other studies have shown the presence of other bacteria with cellulolytic activity, such as *Pseudomonas* or *Janthinobacterium* [27], [28].

Primary wood degraders are a diverse group. Yet, the entrance of microorganisms to the wood usually follows the same pattern. The bacteria profit different parts of the wood structure, such as pits, vessels, rays and resin canals to access. Then, the degradation process of the cell wall by EB follows the orientation of cellulose microfibrils without damaging the lignified wall. The attack starts in the cell lumen and then moves from the middle lamella to the S3 layer and then into the S2 layer. The erosion caused here is due to enzymatic activity. However, it has not been yet possible to characterize the enzymes produced by these bacteria [29]. The cellulose material for the S2 layer is converted into an amorphous mass of cell wall residues, mainly lignin [25], [30]. Microscopic observations allow to follow the decay caused by EB (Figure 1.4). A distinctive attribute of EB decay is the non-homogenous pattern. Heavily degraded cells can be found between healthy ones (Figure 1.4). At the end of the incursion, bacterial degradation will only leave a fragile skeleton of middle lamella, and the remaining wood structure will collapse irreversibly if the wood is not stored properly (i.e., in wet conditions).

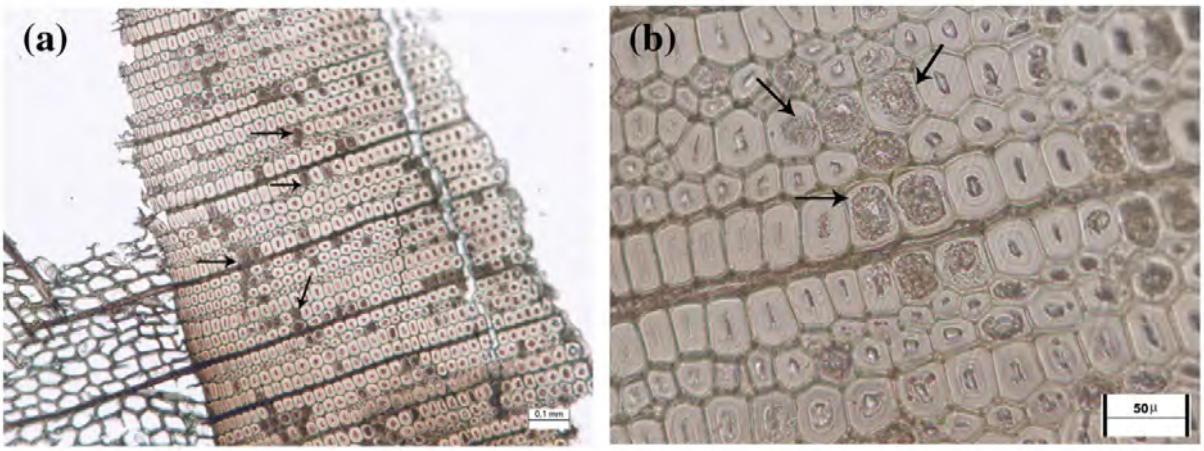

***Figure 1.4**. Light microscope images of a cross section of archaeological wood degraded by erosion bacteria (EB). (a) The typical pattern of decay by EB. Arrows point out single degraded cells surrounded by healthy cells. (b) Higher magnification of the effects of decay by EB (arrows). Adapted from* [30]*. © 2013 Elsevier Ltd.*

Tunnelling bacteria are less described than EB in WAW samples. Tunnelling bacteria activity is condition to an adequate supply of oxygen, while EB can function in near anoxic conditions. However, they are more aggressive as they are able to degrade all cell wall layers regardless the lignin concentration. Moreover, they show tolerance to high concentrations of extractives. These bacteria originate tunnels during the degradation process. The tunnel formation follows every direction, passing through the S1 layer and the middle lamella [29], [30]. Cavitation bacteria are also less recurrent. They begin the penetration at the lumen surface where they

attach themselves via extracellular components. Then, they advance through the S3 layer, to the S2 layer forming small cavities as a result [27].

Secondary wood degraders

Secondary wood degraders or scavenging bacteria are not involved in the initial degradation; they live of using the fermentation and residual products from other wood degraders. They grow using simple sugars from the degraded cell wall materials. They have been described to be partly aerobic, but they can survive in anoxic conditions as well [31].

Sulfate-reducing bacteria (SRB) are anaerobic prokaryotes that can reduce sulfates (SO_4^{2-}) to sulfides when metabolizing simple organic molecules [32]:

$$2(CH_2O) + SO_4^{2-} \rightarrow H_2S_{(aq)} + 2HCO_3 \quad (1)$$

SRB are considered scavenging bacteria in the wood decay. With degradation products from waterlogged wood as carbon source in a sulfate-rich environment, this group of bacteria is considered to be highly active [25]. SRB use a broad variety of compounds as electron donors (e.g. aromatic compounds, sugars, amino acids, inorganic compounds, etc.). However they depend on the degradation products from other organisms, as they are not able to degrade natural biopolymers [32]. The production rates of hydrogen sulfide (H_2S) are elevated in anoxic environments with high concentration of sulfates, such as marine environments or wetlands. Hydrogen sulfide can react with wood components creating organosulfur compounds, and also with iron ions, from co-existing corroding iron parts, forming iron sulfides [33].

The relation between SRB and primary wood degraders is yet not clear. However, it seems that the previous invasion of EB facilitates the entrance of SRB. Suggestions of possible consortia between primary wood degraders and SRB emerge from the isolation of both groups together from degraded waterlogged wood [25]. Also, the apparition of sulfate salts in areas of degraded wood could suggest *in situ* production of hydrogen sulfide in the areas already attacked by EB, but this has not been ruled out. The softened wood could be consequence of the acidity not of previous bacterial erosion. Further studies in the microbial community are needed to reveal the interactions between these communities and how they collaborate in the biodegradation of waterlogged wood.

Chemical degradation. Accumulation of Iron and Sulfur

The well-preserved appearance of WAW is due to favourable burial conditions, i.e., places where the wood decay is limited [34], [35]. However, as stated above, in sulfate-rich

environments, the HS^- ions produced by the SRB go into the wood and react with lignin-rich parts to form organosulfur compounds (thiols and disulfides). Moreover, when iron species are present due to the corrosion of iron items/parts close to the wooden substrate, the sulfide produced by SRB react with the iron ions, forming particles of iron sulfides, that remain in wood cavities [33], [36]. Consequently, the microbial attack to waterlogged wood is often accompanied with the accumulation of sulfur and iron species within the wood structure [36].

Iron sulfides are formed according to the following equations [37]:

$$Fe^{2+} + HS^- \rightarrow FeS_{(s)} + H^+ \quad (2)$$

$$FeS_{(s)} + H_2S \rightarrow FeS_{2(s)} + H_2 \quad (3)$$

Mackinawite (FeS) is the primarily compound formed. Mackinawite will persist inside the wood matrix for long time if conditions remain anoxic and close to neutrality. However, during burial, mackinawite may transform into greigite (Fe_3S_4) if oxygen molecules are present. Partially oxidized mackinawite is an intermediary in this process. Finally, mackinawite may oxidized into pyrite (FeS_2), under anoxic and acidic conditions, if there is an extra supply of sulfur via hydrogen sulfide production [38].

The conservation issue appears because iron sulfides are unstable in oxic environments with high relative humidity level. In such conditions, these compounds start to oxidize producing iron salts and sulfuric acid [39]:

$$FeS_{2(s)} + \frac{7}{2}O_2 + (n+1)H_2O \rightarrow FeSO_4 \cdot nH_2O_{(s)} + H_2SO_{4(aq)} \quad (4)$$

$$FeS_{2(s)} + \frac{15}{4}O_2 + \frac{5}{2}H_2O \rightarrow FeOOH_{(s)} + 2H_2SO_{4(aq)} \quad (5)$$

The high acidity generated causes degradation of the cellulose structure by acid hydrolysis. In consequence, a gradual loss of mechanical strength is observed in the wood. The cellular structure also suffers mechanical damage because of the accumulation of hydrated sulfur salts with a 5-10x volume expansion respect to the previous elemental sulfur molecules [39], [40]. Furthermore, the present iron ions increase the reaction rate for oxidation of sulfur species, catalyse the oxidative degradation of cellulose and, may have a degradation effect on the consolidant agent polyethylene glycol (PEG) [41], [42]. As a transition metal, iron is a highly reactive element and participates in the catalysis of various chemical [43]. In particular, iron is linked with oxidative stress due to Fenton chemistry. Via Fenton reaction, iron catalyses the breakdown of hydrogen peroxide to highly reactive oxygen species (e.g., hydroxyl radicals) that will react with organic molecules:

$$Fe^{2+} + H_2O_2 \rightarrow Fe^{3+} + \bullet OH + -OH \quad (6)$$

$$RH + \bullet OH \rightarrow R\bullet + H_2O \quad (7)$$

Therefore, when iron ions are present in wood, they catalyse the production of free radicals and the oxidative degradation of cellulose is accelerated with a consequent loss of material [44], [45].

Salts precipitation and acidification, therefore, make the long-term preservation of recovered WAW a great challenge. Many products found in waterlogged wood are proof that the oxidation of pyrite occurred over time, and that it is still occurring. Elemental orthorhombic sulfur (α-S_8), which is an intermediate compound in the pyrite oxidation process, is repeatedly detected in archaeological waterlogged wood [46]. Natrajarosite ($NaFe_3(SO_4)_2(OH)_6$) and goethite (α-FeOOH) are also some of the end products of pyrite oxidation that are also commonly found in such wood artefacts. Acidic precipitates of iron(II) and iron(III) sulfates (e.g. rozenite, $FeSO_4 \cdot 4H_2O$) are also often found on surfaces of archaeological wood excavated from marine locations (Figure 1.5).

Over the past years, different studies have focused on recovering information about the different iron and sulfur species inside waterlogged archaeological wooden objects [19], [38], [47], [48]. For example, important wooden artefacts such as the warship *Vasa* in Sweden, or the *Mary Rose* in United Kingdom (Figure 1.5), have been analysed using different high-resolution techniques to establish the total sulfur and iron distribution. The distribution an amount of sulfur depend on the state of wood degradation, the hydrogen sulfides concentration, and the presence of iron(II) ions from corroding iron artefacts. For the *Vasa* the total amount sulfur and iron was mostly detected in the first few centimetres from the surface, while for the Mary Rose the detection was more uniform along the analysed cores of 20 cm [49]. Moreover, the total amount of sulfur content has been estimated to be around 2-3 tons for both shipwrecks, the *Vasa* and the *Mary Rose* [25], [49]. The total amount of iron in the outer 0-2 cm of the *Vasa* hull can be estimated at 5 tons [50]. Freshwater artefacts can also present the accumulation of iron sulfides, as the *Arles Rhône 3* and the *Lyon Saint-Georges 4* shipwreck in France [51], [52]. These results highlight the need for preventive extraction methods of the sulfur and iron species before the wood is exposed to an oxic environment.

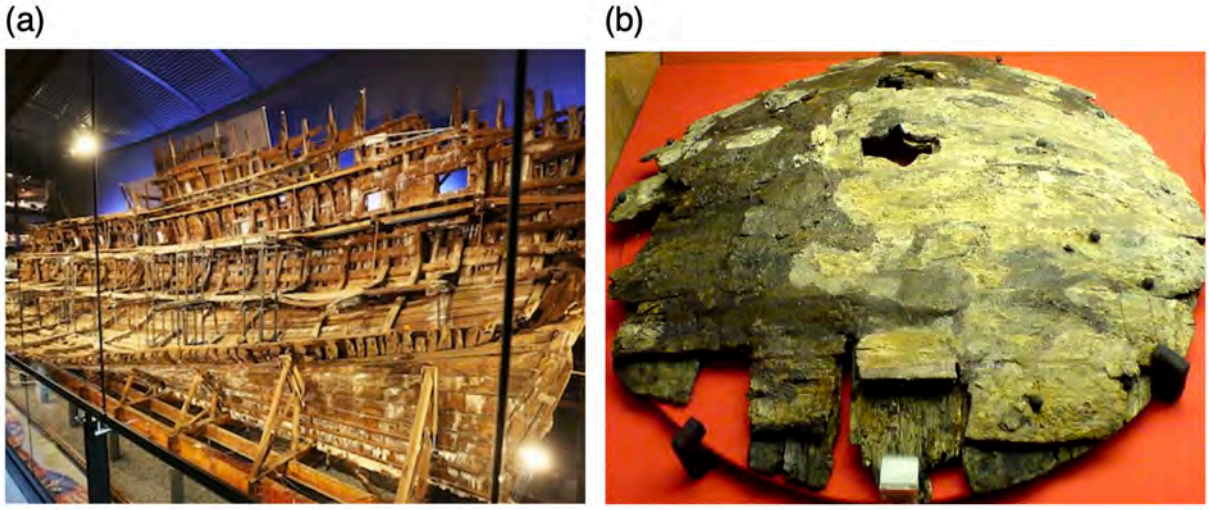

Figure 1.5. *(a) Image of the British warship Mary Rose in exposition in its museum. Salts efflorescence can be appreciated. © Joe Pepler/rex/shutterstock. (b) Detail of a gun shield, belonging to the Mary Rose wreck, presenting precipitation of sulfur salts. Adapted from* [39]. *© Mary Rose Museum.*

1.4 Current Conservation Procedures

Preservation of WAW is needed for future exhibitions and study, as WAW carries priceless information (see section 1.2). Conservation must follow some basic principles: the use of stable and safe materials, the durability and, if possible, the reversibility or at least the retreatability of the treatment [53]. Conservation procedures should respect decayed parts of the artefact trying to consolidate them and not to replace them. Moreover, any treatment should assure minimum intervention. The consequences of natural ageing of the original materials should be respected and not removed [54]. This latest statement enters in ethical conflict when we consider extraction of chemical contaminants. For example, marine archaeological wood is often dark due to iron(III)-tannin complexes or iron oxides particles [48], [49]. The extraction of iron and sulfur from wood is essential for the future preservation of the wooden objects. Even though the wood may appear hard and resistant, the consequences of not removing iron and sulfur species can lead to total loss of the object (see section 1.3). In this case, an ideal treatment should remove the dangerous species keeping as far as possible the aesthetical appearance of the wood. Compromise between safety for the object and appearance has to be made.

After excavation, waterlogged wood should be stored wet to maintain the original dimensions until conservation. Current conservation methods focus on the stabilization of the structure, i.e., consolidation, to avoid collapse upon drying. Over time, consolidation and drying was the main preservation protocol applied to waterlogged wood. However, the apparition of salts and acids in the consolidated archaeological wood aroused interest in investigating possible remediation treatments. Mostly palliative treatments have developed so far, but recently some preventive treatments have started to be also investigated.

Consolidation

Consolidation of the wood matrix has been the key point when treating WAW. This approach has been adopted to harder the wooden structure replacing the water in the wood vessels by a consolidant agent.

Polyethylene glycol (PEG) has been widely used to treat archaeological wood. Commonly, it has become the first step in conservation of waterlogged wood, followed by slow air or freeze drying [55]. PEG is a synthetic, hydrophilic polymer with oxygen (ether) bridges between CH_2CH_2 entities in a chain with terminal hydroxyl groups; $H\text{-}(O\text{-}CH_2CH_2)_n\text{-}OH$. It is used a replacement for water in the wood structure. It provides mechanical support to the softened wood. In the process of PEG preservation different polymers are used. PEG polymers with a

molecular mass around 600 (PEG 600) are used at the beginning of the consolidation process. The water-soluble PEG 600 penetrates the cells walls easily and can bind to the fibrils. Solutions of higher molecular PEG are applied consequently filling out the lumen and bulking the structure [56]. The high molecular PEG enters slower, but it is less hygroscopic giving a less sticky character to the surface. The permeability of wooden objects can vary because of differences in degradation, salts deposits or others. Guidelines are available for the application of PEG based on the maximum water content [54].

During the past years, despite its many advantages, PEG has shown some drawbacks to take into account. When temperature and humidity changed, PEG leaching was observed. Its high hygroscopicity at low-molecular PEG has been problematic, as well as the intense water absorption above 80% relative humidity. Also, as mentioned above, it is susceptible to oxidation reactions catalysed by iron ions (if still present in the wood matrix) leading to its depolymerization and formation of acids that can cause further chemical damage to the wood [57].

Recently, studies have shown the promising results in regards to stability of organosilicon compounds, in particular alkoxysilanes and methyltrimethoxysilane [58]. Alternative consolidants moving towards more renewable and eco-friendly materials like oligoamides and natural polymers such as chitosan, guar, and 2-hydroxyethyl cellulose, have also arisen. These represent promising alternative to PEG. They are more compatible with the wood matrix, cost-effective, and do not produce acids. [57]. Moreover, new trends are trying to focus in tackling various issues at once. Some of the new consolidants present also the capability to chelate iron, preventing further reactions [59]. These materials represent a new line of research where the consolidant is more adapted to the chemical environment of the wood.

Current extraction methods

The appearance of salts efflorescence and associated acidity in wooden artefacts after consolidation and drying has been mostly tackled with curative methods [60]. These methods are mostly designed for local and post-consolidation treatment, and therefore present disadvantages such as the interaction with the consolidant agent (i.e., PEG) previously applied. However, they are necessary to stop the current acidic degradation of the wood. For example, previous experiments used alkaline baths or ammonia (NH_3) gas [49], [61]. Although these treatments are effective at a short-term perspective, the same is not true in the long-term, and in some cases degradation of cellulose and hemicellulose has been reported [61]. Other

alternatives for the de-acidification of wood include the use of alkaline nanoparticles [62], [63]. This treatment showed capability for the long-term neutralization, however, still presents some disadvantages, i.e. toxicity, difficulties in the mechanical removal of sub-products, etc. [64], [65]. Other treatments opt for using passivation agents that stop further oxidation of iron sulfides inside the wood. Several different chemicals have been tested (disodium carbonate, disodium sebacate, and $Mg(OH)_2$ nanoparticles) to prevent acidity and the further oxidation of pyrite [66]. Recently, magnetic nanoparticles have also been proposed as solution to extract iron ions and control acidity. The magnetic function allows the treatment to be target orientated, being able to conduct the nanoparticles in and out of the wood. Initial tests on *Mary Rose* samples showed promising results [67].

The characterization of WAW previous to the consolidation treatment allows to detect possible contamination of the wood with iron sulfides. Preventive extraction methods are then applied to prevent the uncontrolled oxidation of iron sulfides. For instance, Tran et al. (2004), described the use of several oxidants (hydrogen peroxide, sodium hypochlorite, bromate and permanganate) to transform pyrite into soluble compounds. However, the chemical extraction of pyrite was enhanced in acidic conditions. Applying such conditions to dissolve iron sulfides can lead to side damage on the artefacts treated. Thus, gentler methods have been investigated. Tran et al. (2004), suggested in the same study the use of bacteria to oxidise pyrite. Sandström et al. (2005) proposed to test a mild oxidation with singlet oxygen ($^1O_2$) generated by UV radiation. However, UV irradiation could further damage the wood [68]. Chaumat et al. (2019) suggested the use of sodium citrate and active filtration as a greener alternative.

Parallelly, methods focused mostly on active extraction of iron have been also tested. First, electrochemical methods were used. Despite the interesting removal rate, these techniques presented harmful effects on the mechanical resistance of the organic material [35]. In addition, strong iron chelating substances such as derivatives of ethylenediaminetetraacetic acid (EDTA): ethylenediimino-bis (2-hydroxy-4-methylphenyl) acetic acid (EDDHMA), and diethylenetriamine-pentaacetic acid (DTPA), have been used for their the potential to remove iron(III) from the wood [50], [69]. However, the extraction rates were promising only at the surface of the object, making this procedure costly and time-consuming. Moreover, EDDHMA is not available any more for purchase underlying the need for other chelating agents.

1.5 Biotechnology and Conservation

From the fermentation of sugars to create drinks such as beer and cider [70], to the use of bacteria to recover heavy metals in contaminated areas [71], many are the examples of how humans have used microbial metabolisms to their favour during history. In recent years, the interest towards more sustainable and eco-friendly solutions has made researchers in conservation focus on biological metabolisms that can be used to substitute current treatments.

Successful examples of application of bioconservation methods are found in numerous materials (Table 1.1) [72], [73]. Biocleaning approaches are some of the more outstanding biotreatments applied into conservation. Several examples include the removal of organic substances, black crusts, and mineral salts from different materials such as stone, wall paintings, etc. Moreover, different metabolisms have been exploited to different treatments all-leading to the recovery of the surface original appearance [74]. For example, *Pseudomonas stutzeri* has been used for the removal of salts efflorescence by nitrate-reduction and the removal of glue as consequence of chemoorganotrophic respiration [75], [76].

For many years now, biomineralization, i.e., the formation of biogenic minerals, has also been studied for the benefits in preservation of heritage materials. Stone monuments, mainly those compose of carbonate minerals such as limestone and marble, have profited of a process where calcium carbonate precipitates due to bacterial metabolism. The damaged stone is consolidated as result of the formation of calcium carbonate by filling the cracks due to weathering. Practically, this is achieved by the application of exogenous or stone-isolated bacteria along a nutritive solution [77]–[80], or by applying only a nutritive solution to activate the possible carbonatogenic bacteria already existing in the stone microbial community [80]–[82].

Metal substrates have also profited of biomineralization treatments. The minerals formed integrate into the natural corrosion patina creating a compatible passivation layer that is more effective than current coatings [73]. Biopassivation has been studied over more than ten years at the University of Neuchâtel, Switzerland. Specifically, copper-based artefacts have been treated with fungal strains reported to form biogenic oxalates, an ability that allows the transformation of metal compounds into metal oxalates. Metal oxalates, and in particular copper oxalates, create attractive compact patinas that are not associated with cyclical corrosion, providing a good protection of the surface [83], [84].

***Table 1.1**. Some examples of microbial metabolisms applied to conservation of cultural heritage.*

Microbial metabolism	Application	Visual effect*
Chemoorganotrophic respiration	Removal of organic matter from frescoes [75]	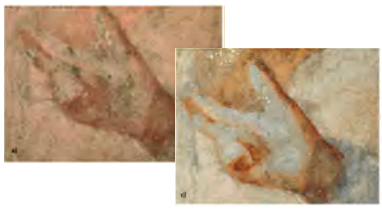
Iron reduction	Biostabilization by biogenic precipitation of minerals [85]	
Nitrate reduction	Biocleaning of salt efflorescence [76]	
Oxalogenesis	Biopassivation of metal surfaces [86]	
Sulfate reduction	Removal of black crust on stone artworks [87]	

*Images adapted from cited references. Images (from top to bottom): © [75]. © 2017 American Society for Microbiology. © 2017 Elsevier Ldt. © Emmanuelle Domon Beuret. Laténium. © Eleonora Gioventù & Paola Lorenzi,

In iron objects, biomineralization enhances the chances of survival of the object if chlorine-containing compounds contaminate the corrosion crust around the object [88]. Iron-reducing bacteria were used under anoxic conditions obtaining as a result the precipitation of stable biogenic iron minerals, such as vivianite [85], [89]. This precipitate increases the stability of the iron artefacts (biostabilization). A different approach focused on the removal of the reactive chlorides-containing corrosion products was also applied. This extraction process used alkaliphile fungal strains that accumulate chlorinated species as detoxification strategy for survival in extreme environments. Promising results showed the removal of the harmful corrosion layer without altering the metal substrate underneath [88].

However, stopping microbial deterioration has been for many years the goal of conservation. Microorganisms drive the elemental cycling in this planet and therefore are involved in opposite pathways. Even though some microorganisms can be beneficial for conservation process, it is usually the case that other microorganisms have been the cause of the problem [73]. Mechanical, physical (e.g. UV radiation) and chemical (e.g. biocides) methods have been used traditionally to eradicate problematic organisms. But even in this field, new trends move towards the use of green biocides and biocontrol [72]. Still, reluctances that may arise when applying microbes to heritage artefacts. Exchange and open discussion are essential in the interdisciplinary research that involves biologists, conservation scientists, and conservators.

The MICMAC project: Microbes for the archaeological wood conservation

The MICMAC (Microbes for the archaeological wood conservation) project deals with the problematic of iron sulfides accumulation in WAW. The aim of the project is to develop and evaluate a preventive bio-based method for the extraction and stabilization of sulfur and iron compounds when the wood is still wet, before the consolidation step.

Biological treatments for the preservation of WAW have not been deeply studied. However, some recent research has described the possibility to use bacteria for the direct consolidation of wood due to the production of bacterial cellulose [90]. Promising results showed that the WAW treated with the bacteria was reinforced, at least in surface, thanks to the accumulation of bacterial cellulose [90]. Still, not many studies have focused on the capabilities of microorganisms to preserve WAW. Indeed, the removal of iron and sulfur species using a biological approach has only been mentioned in few studies [60], [91]. The different metabolisms of some microorganisms could be further exploited for the conservation of WAW.

The specificity of these metabolisms makes them good candidates for treating some of the issues of WAW conservation.

One approach is the solubilisation of problematic iron compounds using microbial iron chelators, i.e., siderophores. Siderophores are iron-binding compounds with high solubility and low molecular weight, produced by many bacteria and fungi under iron starvation. They present high affinity for Fe^{3+} and they have been used in other fields such as in agriculture and medicine [92]. Moreover, their effect in solubilising several iron minerals has been widely studied [93]–[98]. Siderophores will form water-soluble complexes with Fe^{3+} that could be then extracted from the wood.

Furthermore, oxidation of iron sulfides could also enhance extraction of these phases from the wood. Oxidation of iron sulfides by sulfur oxidizing bacteria is a selective process already stablished in "biomining". Bacterial assisted leaching is an efficient and eco-friendly alternative to traditional mining methods [99]. However, even though this microbial process is very successful oxidizing iron sulfides, the high acidic conditions are not ideal in the wood matrix. Candidates for this project should grow at neutral pH. Some different types of chemolithotrophic bacteria, like *Thiobacillus denitrificans*, are able to grow using sulfur and iron compounds as energy source at neutral pH [100], [101]. Moreover, *T. denitrificans*, in an autotrophic bacterium [100]. Carbon dioxide (CO_2) would be an essential nutrient, but it is not expected for this bacterium to attack the wood. *T. denitrificans* is a facultative anaerobe able to oxidise pyrite and other iron sulfides using nitrates (NO_3^-) and producing sulfates (SO_4^{2-}), as the final product of the oxidation [102]:

$$5FeS_{2(s)} + 14NO_3^- + 4H^+ \rightarrow 7N_2 + 5Fe^{2+} + 10SO_4^{2-} + 2H_2O \quad (8)$$

$$5FeS + 8NO_3^- + 8H^+ \rightarrow 4N_2 + 5Fe^{2+} + 5SO_4^{2-} + 4H_2O \quad (9)$$

Therefore, in this approach, extraction of iron sulfides could be done by immersing wood in bacterial cultures and using a trap for sulfates produced. *T. denitrificans* has already been proposed for the removal of iron sulfides from archaeological wood due to its specific metabolism [60]. However, the iron part of the mineral needs to be considered, as well as the sulfur moiety in the siderophore approach.

The combination of siderophores and sulfur-oxidising bacteria, we expect, will enhance the total extraction of iron and sulfur from WAW.

Research outline

The Swiss National Science Foundation granted the MICMAC project (Professorship Grant PP00P2_163653/1, 2016–2020) in 2016. The project continues with the preliminary results obtained during the BActerial Treatment of wood HEritage (BATHE) project, and a following master thesis ("*Applications biotechnologiques à la préservation des biens culturels en bois*", 2015-2016). The MICMAC project is an interdisciplinary research that involves scientists from different backgrounds. This PhD thesis deals with the study of the biological process under revision.

The project is divided in three main working packages (Figure 1.6):

- WP1- Study of the relevant chemical processes in microorganisms.
    - Under WP1, the key goal is to deeply understand the chemical processes involved and to select bacterial strains and extracted siderophores with the best performance.
- WP2- Definition of an application protocol on model samples.
    - Model samples will here be properly altered with sulfur and iron species, fully characterized and an application protocol carefully defined.
- WP3- Evaluation of the treatment's performance: efficiency, durability and impact.
    - In order to have a comprehensive assessment of the treatment's advantages and limits, the following activities are planned: In-depth characterization of the treatment under study and monitoring of the treatment's long-term behaviour.

This PhD is mostly involved with tasks in the first and second work-packages. The objective is to identify and characterize microorganisms or bioproducts that can carry out the desired metabolisms (i.e., sulfur and iron oxidation, and iron complexation) in the wood matrix. Research was conducted in parallel for the different metabolisms under study. A similar experimental plan was followed: first the selection of candidates, and second the optimization of the conditions. The interaction with minerals phases was the first step into the optimization prior to work in the wood matrix. The specific interactions of microbes, or its metabolic products, with iron sulfides and other related minerals are key for the development of a biotreatment that extracts these compounds from WAW. Finally, studying the effects of the treatment on the matrix is essential to evaluate the process.

The first chapters are focused on the metabolic processes. Chapter 2 focuses on iron complexation, and Chapter 3 is directed to the study of sulfur-oxidizing bacteria. Chapter 4 is

about the definition of an application protocol. The combination of the microbial processes under study were investigated together in the wood matrix. Furthermore, investigation was carried out to figure out possible interactions with the autochthonous microbial community of the wood. Finally, Chapter 5 is about the perspectives of the research. The MICMAC project paves the way to promising green alternatives in WAW conservation and this chapter has special weight in discussing the fundamental points to take into account for the further in situ praxis.

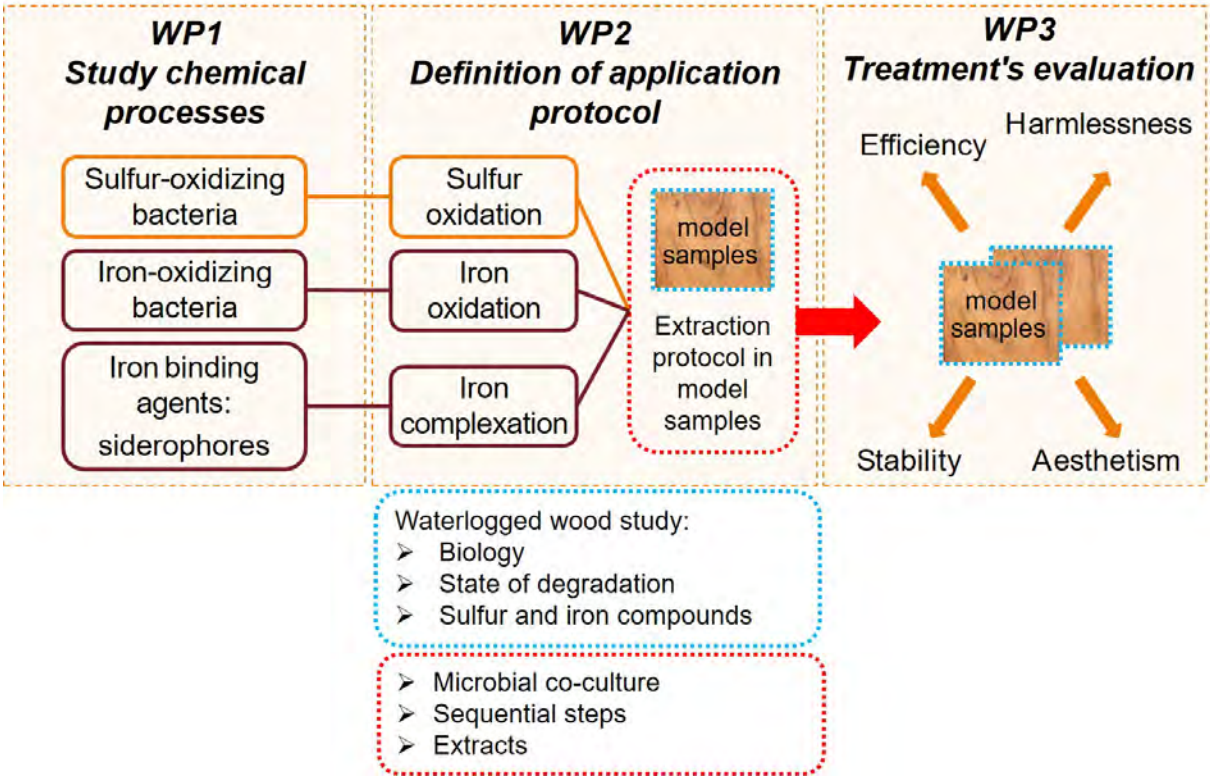

***Figure 1.6**. Schematic representation of the working packages under the MICMAC project.*

References

[1] M. Ek, G. Gellerstedt, and G. Henriksson, Eds., *Wood Chemistry and Biotechnology*. De Gruyter, 2009.

[2] R. M. Rowell, R. Pettersen, J. S. Han, J. S. Rowell, and M. A. Tshabalala, "Cell Wall Chemistry," in *Handbook of Wood Chemistry and Wood Composites*, R. M. Rowell, Ed. CRC Press, 2005, pp. 35–74.

[3] A. C. Wiedenhoeft and R. B. Miller, "Structure and function of wood," in *Handbook of Wood Chemistry and Wood Composites*, R. M. Rowell, Ed. CRC Press LLC, 2012, pp. 9–32.

[4] Á. T. Martínez *et al.*, "Biodegradation of lignocellulosics: Microbial, chemical, and enzymatic aspects of the fungal attack of lignin," *Int. Microbiol.*, vol. 8, no. 3, pp. 195–204, 2005.

[5] I. D. Reid, "Biodegradation of lignin," *Can. J. Bot.*, vol. 73, no. S1, pp. 1011–1018, 1995, doi: 10.1139/b95-351.

[6] S. Vignote Peña and I. Martínez Rojas, *Tecnología de la madera*, 3.ª ed. Madrid: Ediciones Mundi-Prensa, 2006.

[7] N. M. Delimont, M. D. Haub, and B. L. Lindshield, "The Impact of Tannin Consumption on Iron Bioavailability and Status: A Narrative Review.," *Curr. Dev. Nutr.*, vol. 1, no. 2, pp. 1–12, Feb. 2017, doi: 10.3945/cdn.116.000042.

[8] A. Rafsanjani, D. Derome, F. K. Wittel, and J. Carmeliet, "Computational up-scaling of anisotropic swelling and mechanical behavior of hierarchical cellular materials," *Compos. Sci. Technol.*, vol. 72, no. 6, pp. 744–751, 2012, doi: 10.1016/j.compscitech.2012.02.001.

[9] A. Billamboz, "Regional patterns of settlement and woodland developments: Dendroarchaeology in the Neolithic pile-dwellings on Lake Constance (Germany)," *The Holocene*, vol. 24, no. 10, pp. 1278–1287, Oct. 2014, doi: 10.1177/0959683614540956.

[10] J. E. Winandy and R. M. Rowell, "The Chemistry of Wood Strength," in *Handbook of Wood Chemistry and Wood Composites*, R. M. Rowell, Ed. 2005, pp. 303–347.

[11] M.-L. E. Florian, "Scope and History of Archaeological Wood," pp. 3–32, 1989, doi: 10.1021/ba-1990-0225.ch001.

[12] C. G. Björdal, T. Nilsson, and G. Daniel, "Microbial decay of waterlogged archaeological wood found in Sweden. Applicable to archaeology and conservation," *Int. Biodeterior. Biodegrad.*, vol. 43, no. 1–2, pp. 63–73, 1999, doi: 10.1016/S0964-8305(98)00070-5.

[13] R. A. Blanchette, "A review of microbial deterioration found in archaeological wood from different environments," *Int. Biodeterior. Biodegrad.*, vol. 46, no. 3, pp. 189–204, 2000, doi: 10.1016/S0964-8305(00)00077-9.

[14] N. Macchioni, B. Pizzo, and C. Capretti, "An investigation into preservation of wood from Venice foundations," *Constr. Build. Mater.*, vol. 111, no. March, pp. 652–661, 2016, doi: 10.1016/j.conbuildmat.2016.02.144.

[15] J. J. Lucejko, F. Modugno, E. Ribechini, D. Tamburini, and M. P. Colombini, "Analytical instrumental

techniques to study archaeologicalwood degradation," *Appl. Spectrosc. Rev.*, vol. 50, no. 7, pp. 584–625, 2015, doi: 10.1080/05704928.2015.1046181.

[16] C. G. Björdal and Y. Fors, "Correlation between sulfur accumulation and microbial wood degradation on shipwreck timbers," *Int. Biodeterior. Biodegradation*, vol. 140, no. January, pp. 37–42, May 2019, doi: 10.1016/j.ibiod.2019.03.010.

[17] A. Hafner, "UNESCO World Heritage 'Prehistoric pile-dwellings around the Alps': Chances and Challenges for Management and Research of Cultural Heritage Under Water," in *The 5th Baltic Sea Region Cultural Heritage Forum*, 2014, pp. 36–40, [Online]. Available: https://boris.unibe.ch/58972/1/Hafner_2013_UNESCO_Palafittes_Tallinn.pdf.

[18] C. G. Björdal and T. Nilsson, "Reburial of shipwrecks in marine sediments: a long-term study on wood degradation," *J. Archaeol. Sci.*, vol. 35, no. 4, pp. 862–872, 2008, doi: 10.1016/j.jas.2007.06.005.

[19] Y. Fors, A. Rindby, L. Bornmalm, and C. A. Systems, "X-ray fluorescence for cultural heritage : scanning biochemical fingerprints in archaeological shipwrecks," *Spectrosc. Eur.*, vol. 27, no. 1, pp. 11–13, 2015.

[20] A. M. Abdel-Hamid, J. O. Solbiati, and I. K. O. Cann, *Insights into Lignin Degradation and its Potential Industrial Applications*, vol. 82. Elsevier, 2013.

[21] G. Daniel, *Fungal Degradation of Wood Cell Walls*. Elsevier Inc., 2016.

[22] D. J. Huisman, M. R. Manders, E. I. Kretschmar, R. K. W. M. Klaassen, and N. Lamersdorf, "Burial conditions and wood degradation at archaeological sites in the Netherlands," *Int. Biodeterior. Biodegrad.*, vol. 61, no. 1, pp. 33–44, 2008, doi: 10.1016/j.ibiod.2007.06.008.

[23] F. J. Ruiz-Dueñas and Á. T. Martínez, "Microbial degradation of lignin: How a bulky recalcitrant polymer is efficiently recycled in nature and how we can take advantage of this," *Microb. Biotechnol.*, vol. 2, no. 2 SPEC. ISS., pp. 164–177, 2009, doi: 10.1111/j.1751-7915.2008.00078.x.

[24] T. Nilsson, C. Björdal, and E. Fällman, "Culturing erosion bacteria: Procedures for obtaining purer cultures and pure strains," *Int. Biodeterior. Biodegrad.*, vol. 61, no. 1, pp. 17–23, 2008, doi: 10.1016/j.ibiod.2007.06.010.

[25] Y. Fors, T. Nilsson, E. D. Risberg, M. Sandström, and P. Torssander, "Sulfur accumulation in pinewood (Pinus sylvestris) induced by bacteria in a simulated seabed environment: Implications for marine archaeological wood and fossil fuels," *Int. Biodeterior. Biodegrad.*, vol. 62, no. 4, pp. 336–347, 2008, doi: 10.1016/j.ibiod.2007.11.008.

[26] T. Nilsson and C. Björdal, "Culturing wood-degrading erosion bacteria," *Int. Biodeterior. Biodegrad.*, vol. 61, no. 1, pp. 3–10, 2008, doi: 10.1016/j.ibiod.2007.06.006.

[27] E. T. Landy, J. I. Mitchell, S. Hotchkiss, and R. A. Eaton, "Bacterial diversity associated with archaeological waterlogged wood: Ribosomal RNA clone libraries and denaturing gradient gel electrophoresis (DGGE)," *Int. Biodeterior. Biodegrad.*, vol. 61, no. 1, pp. 106–116, 2008, doi: 10.1016/j.ibiod.2007.07.007.

[28] F. Antonelli *et al.*, "Microbiota in waterlogged archaeological wood: Use of next-generation sequencing

to evaluate the risk of biodegradation," *Appl. Sci.*, vol. 10, no. 13, pp. 1–21, 2020, doi: 10.3390/app10134636.

[29] A. P. Singh, Y. S. Kim, and T. Singh, "Bacterial Degradation of Wood," in *Secondary Xylem Biology*, no. July, Elsevier, 2016, pp. 169–190.

[30] N. Macchioni, C. Capretti, L. Sozzi, and B. Pizzo, "Grading the decay of waterlogged archaeological wood according to anatomical characterisation. The case of the Fiavé site (N-E Italy)," *Int. Biodeterior. Biodegradation*, vol. 84, pp. 54–64, Oct. 2013, doi: 10.1016/j.ibiod.2013.05.028.

[31] A. P. Singh and J. A. Butcher, "Bacterial degradation of wood cell walls: a review of degradation patterns," *J. Inst. Wood Sci.*, vol. 12, no. 3, pp. 143–157, 1991.

[32] O. J. Hao, J. M. Chen, L. Huang, and R. L. Buglass, "Sulfate-reducing bacteria," *Crit. Rev. Environ. Sci. Technol.*, vol. 26, no. 2, pp. 155–187, 1996, doi: 10.1080/10643389609388489.

[33] C. Rémazeilles *et al.*, "Microbiologically influenced corrosion of archaeological artefacts:Characterisation of iron(II) sulfides by Raman spectroscopy," *J. Raman Spectrosc.*, vol. 41, no. 11, pp. 1425–1433, 2010, doi: 10.1002/jrs.2717.

[34] C. . G. Björdal, G. Daniel, and T. Nilsson, "Depth of burial, an important factor in controlling bacterial decay of waterlogged archaeological poles," *Int. Biodeterior. Biodegradation*, vol. 45, no. 1–2, pp. 15–26, Jan. 2000, doi: 10.1016/S0964-8305(00)00035-4.

[35] C. Pelé, E. Guilminot, S. Labroche, G. Lemoine, and G. Baron, "Iron removal from waterlogged wood: Extraction by electrophoresis and chemical treatments," *Stud. Conserv.*, vol. 60, no. 3, pp. 155–171, May 2015, doi: 10.1179/2047058413Y.0000000110.

[36] Y. Fors *et al.*, "Sulfur and iron accumulation in three marine-archaeological shipwrecks in the Baltic Sea: The Ghost, the Crown and the Sword," *Sci. Rep.*, vol. 4, no. 1, pp. 1–6, 2014, doi: 10.1038/srep04222.

[37] D. Rickard and G. W. Luther, "Chemistry of iron sulfides," *Chem. Rev.*, vol. 107, no. 2, pp. 514–562, 2007, doi: 10.1021/cr0503658.

[38] C. Rémazeilles, K. Tran, E. Guilminot, E. Conforto, and P. Refait, "Study of Fe(II) sulphides in waterlogged archaeological wood," *Stud. Conserv.*, vol. 58, no. 4, pp. 297–307, 2013, doi: 10.1179/2047058412Y.0000000071.

[39] K. M. Wetherall *et al.*, "Sulfur and iron speciation in recently recovered timbers of the Mary Rose revealed via X-ray absorption spectroscopy," *J. Archaeol. Sci.*, vol. 35, no. 5, pp. 1317–1328, 2008, doi: 10.1016/j.jas.2007.09.007.

[40] J. Preston, A. D. Smith, E. J. Schofield, A. V. Chadwick, M. A. Jones, and J. E. M. Watts, "The effects of Mary Rose conservation treatment on iron oxidation processes and microbial communities contributing to acid production in marine archaeological timbers," *PLoS One*, vol. 9, no. 2, 2014, doi: 10.1371/journal.pone.0084169.

[41] M. Sandström, F. Jalilehvand, I. Persson, U. Gelius, P. Frank, and I. Hall-Roth, "Deterioration of the seventeenth-century warship Vasa by internal formation of sulphuric acid," *Nature*, vol. 415, no. 6874, pp.

893–897, Feb. 2002, doi: 10.1038/415893a.

[42] G. Almkvist and I. Persson, “Degradation of polyethylene glycol and hemicellulose in the Vasa,” *Holzforschung*, vol. 62, no. 1, pp. 64–70, 2008, doi: 10.1515/HF.2008.009.

[43] C. Bolm, J. Legros, J. Le Paih, and L. Zani, “Iron-catalyzed reactions in organic synthesis,” *Chem. Rev.*, vol. 104, no. 12, pp. 6217–6254, 2004, doi: 10.1021/cr040664h.

[44] G. Almkvist and I. Persson, “Fenton-induced degradation of polyethylene glycol and oak holocellulose. A model experiment in comparison to changes observed in conserved waterlogged wood,” *Holzforschung*, vol. 62, no. 6, pp. 704–708, 2008, doi: 10.1515/HF.2008.129.

[45] V. Arantes and A. M. F. Milagres, “Degradation of cellulosic and hemicellulosic substrates using a chelator-mediated Fenton reaction,” *J. Chem. Technol. Biotechnol.*, vol. 81, no. 3, pp. 413–419, Mar. 2006, doi: 10.1002/jctb.1417.

[46] J. A. Bourdoiseau, M. Jeannin, C. Rémazeilles, R. Sabot, and P. Refait, “The transformation of mackinawite into greigite studied by Raman spectroscopy,” *J. Raman Spectrosc.*, vol. 42, no. 3, pp. 496–504, 2011, doi: 10.1002/jrs.2729.

[47] Y. Fors, F. Jalilehvand, E. Damian Risberg, C. Björdal, E. Phillips, and M. Sandström, “Sulfur and iron analyses of marine archaeological wood in shipwrecks from the Baltic Sea and Scandinavian waters,” *J. Archaeol. Sci.*, vol. 39, no. 7, pp. 2521–2532, 2012, doi: 10.1016/j.jas.2012.03.006.

[48] M. Sandström, Y. Fors, F. Jalilehvand, E. Damian, and U. Gelius, “Analyses of sulfur and iron in marine-archaeological wood,” *Proc. 9th ICOM Gr. Wet Org. Archaeol. Mater. Conf. Copenhagen, 2004*, pp. 181–202, 2005.

[49] Y. Fors and M. Sandström, “Sulfur and iron in shipwrecks cause conservation concerns,” *Chem. Soc. Rev.*, vol. 35, no. 5, pp. 399–415, 2006, doi: 10.1039/b507010b.

[50] G. Almkvist and I. Persson, “Extraction of iron compounds from wood from the Vasa,” *Holzforschung*, vol. 60, no. 6, pp. 678–684, 2006, doi: 10.1515/HF.2006.114.

[51] S. Grousset *et al.*, “Study of iron sulphides in long-term iron corrosion processes: Characterisations of archaeological artefacts,” *Corros. Sci.*, vol. 112, pp. 264–275, 2016, doi: 10.1016/j.corsci.2016.07.022.

[52] C. Rémazeilles *et al.*, “Post-treatment Study of Iron/Sulfur-containing Compounds in the Wreck of Lyon Saint-Georges 4 (Second Century ACE),” *Stud. Conserv.*, vol. 65, no. 1, pp. 28–36, Jan. 2020, doi: 10.1080/00393630.2019.1610608.

[53] C. Caple, *Conservation skills: judgement, method and decision making*. Routledge, 2000.

[54] D. W. Grattan and R. W. Clarke, “Conservation of waterlogged wood,” *Conserv. Mar. Archaeol. Objects*, pp. 164–206, Jan. 1987, doi: 10.1016/B978-0-408-10668-9.50015-0.

[55] D. Gregory, P. Jensen, and K. Strætkvern, “Conservation and in situ preservation of wooden shipwrecks from marine environments,” *J. Cult. Herit.*, vol. 13, no. 3 SUPPL., pp. S139–S148, 2012, doi: 10.1016/j.culher.2012.03.005.

[56] M. N. Mortensen, *Stabilization of polyethylene glycol in archaeological wood*. Technical University of Denmark (DTU), 2009.

[57] Z. Walsh *et al.*, "Multifunctional supramolecular polymer networks as next-generation consolidants for archaeological wood conservation.," *Proc. Natl. Acad. Sci. U. S. A.*, vol. 111, no. 50, pp. 17743–8, Dec. 2014, doi: 10.1073/pnas.1406037111.

[58] J. Kowalczuk, A. Rachocki, M. Broda, B. Mazela, G. A. Ormondroyd, and J. Tritt, "Conservation process of archaeological waterlogged wood studied by spectroscopy and gradient NMR methods," *Wood Sci. Technol.*, vol. 53, no. 6, pp. 1207–1222, 2019, doi: 10.1007/s00226-019-01129-5.

[59] Z. Walsh-Korb, E.-R. Janeček, M. Jones, L. Averous, and O. A. Scherman, "New Consolidants for the Conservation of Archeological Wood," in *Heritage Wood*, A. Nevin and M. Sawicki, Eds. Springer, Cham, 2019, pp. 65–77.

[60] K. Tran, N. Bertout, F. Dalard, and J.-P. Magnin, "Trials on chemical and microbiological processes for the oxidation of sulphur compounds in archaeological wood," in *Proceedings of the 9th ICOM Group on Wet Organic Archaeological Materials Conference: Copenhagen, 2004*, 2004, pp. 227–242.

[61] Y. Fors and V. Richards, "The Effects of the Ammonia Neutralizing Treatment on Marine Archaeological Vasa Wood," *Stud. Conserv.*, vol. 55, no. 1, pp. 41–54, Mar. 2010, doi: 10.1179/sic.2010.55.1.41.

[62] R. Giorgi, D. Chelazzi, and P. Baglioni, "Nanoparticles of calcium hydroxide for wood conservation. The deacidification of the Vasa warship," *Langmuir*, vol. 21, no. 23, pp. 10743–10748, 2005, doi: 10.1021/la0506731.

[63] G. Poggi, N. Toccafondi, D. Chelazzi, P. Canton, R. Giorgi, and P. Baglioni, "Calcium hydroxide nanoparticles from solvothermal reaction for the deacidification of degraded waterlogged wood," *J. Colloid Interface Sci.*, vol. 473, pp. 1–8, 2016, doi: 10.1016/j.jcis.2016.03.038.

[64] E. J. Schofield, R. Sarangi, A. Mehta, A. M. Jones, F. J. W. Mosselmans, and A. V. Chadwick, "Nanoparticle de-acidification of the mary rose," *Mater. Today*, vol. 14, no. 7–8, pp. 354–358, 2011, doi: 10.1016/S1369-7021(11)70166-3.

[65] E. J. Schofield, C. Delaveris, and R. Sarangi, "Alkaline earth carbonates for the treatment of problematic sulfur associated with marine archeological wood," *J. Archaeol. Sci. Reports*, vol. 4, pp. 427–433, 2015, doi: 10.1016/j.jasrep.2015.09.021.

[66] G. Chaumat, D. Zahnweh, X. Martinez-Carballal, L. Caillat, T. Guiblain, and M. Dbeaurain, "Development of curative and preventive treatments of waterlogged archaeological wood contaminated by pyrite," 2019.

[67] E. J. Schofield, E. R. Aluri, E. Sanchez Perez, R. O'Reilly, and S. Corr, "The development of localised targeted treatments for the removal of destructive acids from marine archaeological wood," 2019.

[68] A. Cogulet, P. Blanchet, and V. Landry, "Wood degradation under UV irradiation: A lignin characterization," *J. Photochem. Photobiol. B Biol.*, vol. 158, pp. 184–191, 2016, doi: 10.1016/j.jphotobiol.2016.02.030.

[69] A. Berko, A. D. Smith, A. M. Jones, E. J. Schofield, J. F. W. Mosselmans, and A. V. Chadwick, "XAS studies of the effectiveness of iron chelating treatments of Mary Rose timbers," *J. Phys. Conf. Ser.*, vol. 190, p. 012147, Nov. 2009, doi: 10.1088/1742-6596/190/1/012147.

[70] A. Gutiérrez, T. Boekhout, Z. Gojkovic, and M. Katz, "Evaluation of non-Saccharomyces yeasts in the fermentation of wine, beer and cider for the development of new beverages," *J. Inst. Brew.*, vol. 124, no. 4, pp. 389–402, 2018, doi: 10.1002/jib.512.

[71] H. Guo *et al.*, "Bioremediation of heavy metals by growing hyperaccumulaor endophytic bacterium Bacillus sp. L14," *Bioresour. Technol.*, vol. 101, no. 22, pp. 8599–8605, Nov. 2010, doi: 10.1016/J.BIORTECH.2010.06.085.

[72] I. Soffritti *et al.*, "The potential use of microorganisms as restorative agents: An update," *Sustainability (Switzerland)*, vol. 11, no. 14. pp. 1–17, 2019, doi: 10.3390/su11143853.

[73] P. Junier and E. Joseph, "Microbial biotechnology approaches to mitigating the deterioration of construction and heritage materials," *Microb. Biotechnol.*, vol. 10, no. 5, pp. 1145–1148, 2017, doi: 10.1111/1751-7915.12795.

[74] P. Bosch-Roig and G. Ranalli, "The safety of biocleaning technologies for cultural heritage," *Front. Microbiol.*, vol. 5, no. APR, pp. 1–3, 2014, doi: 10.3389/fmicb.2014.00155.

[75] P. Bosch-Roig, J. Regidor-Ros, P. Soriano, and R. Montes-Estelles, "Biocleaning of animal glue on wall paintings by Pseudomonas stutzeri," *Chim. Oggi/Chemistry Today*, vol. 31, pp. 50–53, Jan. 2013.

[76] P. B. Roig, J. L. Regidor Ros, and R. M. Estellés, "Biocleaning of nitrate alterations on wall paintings by Pseudomonas stutzeri," *Int. Biodeterior. Biodegrad.*, vol. 84, pp. 266–274, Oct. 2013, doi: 10.1016/j.ibiod.2012.09.009.

[77] C. Rodriguez-Navarro, M. Rodriguez-Gallego, K. Ben Chekroun, and M. T. Gonzalez-Muñoz, "Conservation of ornamental stone by Myxococcus xanthus-induced carbonate biomineralization," *Appl. Environ. Microbiol.*, vol. 69, no. 4, pp. 2182–2193, Apr. 2003, doi: 10.1128/aem.69.4.2182-2193.2003.

[78] M. I. Daskalakis *et al.*, "Pseudomonas, Pantoea and Cupriavidus isolates induce calcium carbonate precipitation for biorestoration of ornamental stone," *J. Appl. Microbiol.*, vol. 115, no. 2, pp. 409–423, 2013, doi: 10.1111/jam.12234.

[79] J. Ettenauer, G. Piñar, K. Sterflinger, M. T. Gonzalez-Muñoz, and F. Jroundi, "Molecular monitoring of the microbial dynamics occurring on historical limestone buildings during and after the in situ application of different bio-consolidation treatments," *Sci. Total Environ.*, vol. 409, no. 24, pp. 5337–5352, Nov. 2011, doi: 10.1016/j.scitotenv.2011.08.063.

[80] F. Jroundi *et al.*, "Protection and consolidation of stone heritage by self-inoculation with indigenous carbonatogenic bacterial communities," *Nat. Commun.*, vol. 8, no. 1, pp. 1–12, Dec. 2017, doi: 10.1038/s41467-017-00372-3.

[81] C. Jimenez-Lopez, C. Rodriguez-Navarro, G. Piñar, F. J. Carrillo-Rosúa, M. Rodriguez-Gallego, and M. T. Gonzalez-Muñoz, "Consolidation of degraded ornamental porous limestone stone by calcium carbonate

precipitation induced by the microbiota inhabiting the stone," *Chemosphere*, vol. 68, no. 10, pp. 1929–1936, Aug. 2007, doi: 10.1016/j.chemosphere.2007.02.044.

[82] N. Barbabietola *et al.*, "Microbe-Based Technology for a Novel Approach to Conservation and Restoration," *Conserv. Cult. Herit.*, no. February 2015, pp. 69–76, 2012.

[83] E. Joseph *et al.*, "Protection of metal artifacts with the formation of metal-oxalates complexes by Beauveria bassiana," *Front. Microbiol.*, vol. 2, pp. 1–8, 2012, doi: 10.3389/fmicb.2011.00270.

[84] M. Albini *et al.*, "Innovative biological approaches for metal conservation," *Mater. Corros.*, vol. 67, no. 2, pp. 200–206, 2016, doi: 10.1002/maco.201408168.

[85] L. Comensoli, J. Maillard, M. Albini, F. Sandoz, P. Junier, and E. Joseph, "Use of Bacteria To Stabilize Archaeological Iron," *Appl. Environ. Microbiol.*, vol. 83, no. 9, pp. e03478-16, May 2017, doi: 10.1128/AEM.03478-16.

[86] M. Albini, "Fungal biogenic patina: optimization of an innovative conservation treatment for copper-based artefacts," Doctoral Thesis, Université de Neuchâtel, Neuchâtel, 2017.

[87] E. Gioventù and P. Lorenzi, "Bio-Removal of Black Crust from Marble Surface: Comparison with Traditional Methodologies and Application on a Sculpture from the Florence's English Cemetery," *Procedia Chem.*, 2013, doi: 10.1016/j.proche.2013.03.017.

[88] L. Comensoli, S. Bindschedler, P. Junier, and E. Joseph, "Iron and Fungal Physiology: A Review of Biotechnological Opportunities," in *Advances in Applied Microbiology*, vol. 98, Elsevier Ltd, 2017, pp. 31–60.

[89] W. M. Kooli *et al.*, "Bacterial iron reduction and biogenic mineral formation for the stabilisation of corroded iron objects," *Sci. Rep.*, vol. 8, no. 1, p. 764, Dec. 2018, doi: 10.1038/s41598-017-19020-3.

[90] D. Gregory, K. Lyngby, D. Yvonne Shashoua, and N. Braunschweig Hansen, "Anyone for a nice cup of tea? The use of bacterial cellulose for conservation of waterlogged archaeological wood," in *ICOM-CC 18th Triennial Conference Preprints, Copenhagen, 4–8 September 2017*, 2017.

[91] M. Sandström *et al.*, "Sulfur accumulation in the timbers of King Henry VIII's warship Mary Rose: a pathway in the sulfur cycle of conservation concern.," *Proc. Natl. Acad. Sci. U. S. A.*, vol. 102, no. 40, pp. 14165–70, 2005, doi: 10.1073/pnas.0504490102.

[92] L. O. De Serrano, "Biotechnology of siderophores in high-impact scientific fields," *Biomol. Concepts*, vol. 8, no. 3–4, pp. 169–178, 2017, doi: 10.1515/bmc-2017-0016.

[93] T. Yoshida, K. I. Hayashi, and H. Ohmoto, "Dissolution of iron hydroxides by marine bacterial siderophore," *Chem. Geol.*, vol. 184, no. 1–2, pp. 1–9, 2002, doi: 10.1016/S0009-2541(01)00297-2.

[94] X. Liu *et al.*, "Microbial siderophores and root exudates enhanced goethite dissolution and Fe/As uptake by As-hyperaccumulator Pteris vittata," *Environ. Pollut.*, vol. 223, pp. 230–237, 2017, doi: 10.1016/j.envpol.2017.01.016.

[95] P. U. Reichard, R. Kretzschmar, and S. M. Kraemer, "Dissolution mechanisms of goethite in the presence of siderophores and organic acids," *Geochim. Cosmochim. Acta*, vol. 71, no. 23, pp. 5635–5650, Dec.

2007, doi: 10.1016/j.gca.2006.12.022.

[96] S. M. Kraemer, “Iron oxide dissolution and solubility in the presence of siderophores,” *Aquat. Sci.*, vol. 66, no. 1, pp. 3–18, 2004, doi: 10.1007/s00027-003-0690-5.

[97] F. Watteau and J. Berthelin, “Microbial dissolution of iron and aluminium from soil minerals: efficiency and specificity of hydroxamate siderophores compared to aliphatic acids,” *Eur. J. Soil Biol.*, vol. 30, no. 1, pp. 1–9, 1994, Accessed: May 07, 2020. [Online]. Available: http://ci.nii.ac.jp/naid/10015269448/en/.

[98] D. Lukasz, R. Liwia, M. Aleksandra, and S. Aleksandra, “Dissolution of arsenic minerals mediated by dissimilatory arsenate reducing bacteria: Estimation of the physiological potential for arsenic mobilization,” *Biomed Res. Int.*, vol. 2014, 2014, doi: 10.1155/2014/841892.

[99] A. Mahmoud, P. Cézac, A. F. A. Hoadley, F. Contamine, and P. D’Hugues, “A review of sulfide minerals microbially assisted leaching in stirred tank reactors,” *Int. Biodeterior. Biodegrad.*, vol. 119, pp. 118–146, Apr. 2017, doi: 10.1016/j.ibiod.2016.09.015.

[100] H. R. Beller *et al.*, “The genome sequence of the obligately chemolithoautotrophic, facultatively anaerobic bacterium Thiobacillus denitrificans,” *J. Bacteriol.*, vol. 188, no. 4, pp. 1473–1488, 2006, doi: 10.1128/JB.188.4.1473-1488.2006.

[101] S. Hedrich, M. Schlömann, and D. Barrie Johnson, “The iron-oxidizing proteobacteria,” *Microbiology*, vol. 157, no. 6, pp. 1551–1564, 2011, doi: 10.1099/mic.0.045344-0.

[102] S. Vaclavkova *et al.*, “The Importance of Microbial Iron Sulfide Oxidation for Nitrate Depletion in Anoxic Danish Sediments,” *Aquat. Geochemistry*, vol. 20, no. 4, pp. 419–435, Jul. 2014, doi: 10.1007/s10498-014-9227-x.

Chapter 2

IRON COMPLEXATION

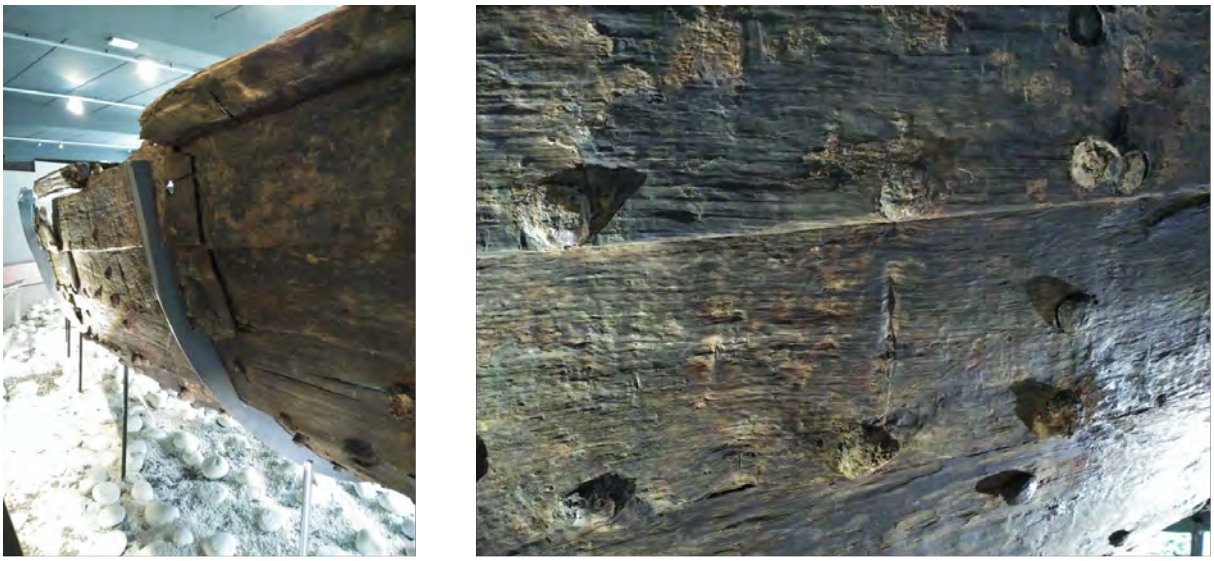

Pecio de Urbieta – Detail of the iron nails. © Magdalena Albelda

The introduction of every section of this chapter is based on the following published review:

- M. Albelda-Berenguer, M. Monachon, and E. Joseph, "Siderophores: From natural roles to potential applications," in *Advances in Applied Microbiology*, vol. 106, G. M. Gadd and S. B. T.-A. in A. M. Sariaslani, Eds. Academic Press, 2019, pp. 193–225.

Results are not published yet.

Summary

Iron is essential for life on Earth. It is involved in many metabolic processes. However, it can be very reactive, and under certain conditions the conversion of iron(II) to iron(III) and vice versa can produce reactive oxygen species (ROS). When wooden objects accumulate iron, ROS can catalyse the degradation of cellulose damaging the wood structure and thereafter the object. In this chapter, we studied different bacteria for their ability to chelate iron from mineral phases that are usually associated to waterlogged archaeological wood (WAW). In the first section we selected four strains that presented the highest production rates of iron chelators (i.e., siderophores). In the following sections, we studied the effect of these bacteria and their siderophores on the dissolution of mineral phases in liquid matrix or in model wood samples. Siderophore-producing bacteria were not as efficient in extracting iron directly from our model wood samples artificially contaminated with iron and sulfur. However, the possibility of using directly siderophores could be ideal for future applications. Promising results were observed with the siderophore deferoxamine, which is commercially available (Desferal®). Similar extraction rates were measured with this siderophore compared to the chemical chelator EDTA. Moreover, the siderophore was able to extract iron from mineral phases directly in solution and in the wood matrix. Especially, its effect in the wood substrate may be less than for the chemical chelator EDTA, as the last enhanced the degradation of cellulosic substrates analogues.

2.1 Selection of siderophore-producing bacteria

Abstract

Siderophore-producing bacteria are widely spread. Seven different bacteria species were selected here to screen their capability to produce siderophores. Chrome Azurol S (CAS) assay was used as general method of detection for iron chelators [1]. *Bacillus* species were not able to produce siderophores in the experimental conditions employed. *Serratia ureilytica*, *Escherichia coli*, *Pseudomonas putida,* and *Streptomyces pilosus*, all presented promising results and were taken to the next step of research.

Introduction

Iron is the fourth most abundant element in the Earth's crust and is essential for almost all forms of life [2]. Indeed, iron is involved in many metabolic processes. For instance, it is an important cofactor of many enzymes and also participates in oxygen transport, respiration, nitrogen fixation, photosynthesis, and synthesis of DNA, fatty acids, and amino acids [3]. However, iron bioavailability is very low. Iron solubility and reactivity strongly depend on pH. At neutral pH, a spontaneous chemical oxidation of iron can be rapid, whereas at low pH this abiotic oxidation occurs very slowly in water. Moreover, at physiological pH, the concentration of free Fe^{3+} ions is limited due to the formation of low-solubility ferric hydroxides [4]. For an optimal bacterial growth, the required concentration of iron(III) varies between 10^{-6} and 10^{-7} M [5]. Therefore, different strategies have been developed to acquire and uptake iron under iron-depleted conditions.

The production of siderophores (from the Greek: "iron carriers") in one of the most common strategies developed by bacteria, fungi, and plants. Siderophores are natural iron chelators, with low molecular weight (400–2000 Da), and high affinity for ferric iron [6], [7]. They are produced under iron starvation with the aim to scavenge iron forming soluble iron(III) complexes. They allow organisms to have access to insoluble iron forms and, in pathogenic microorganisms, they are involved in the stealing of iron from the host proteins [8], [9]. The interest on siderophores has been prolonged since the first studies until today with over 500 different siderophores described [10], and new structures being discovered continuously [11].

In general, siderophores present a higher affinity for iron(III) than iron(II). Fe^{3+} ion acts as a Lewis acid that forms strong complexes with electron-pair donors. Siderophores use negatively charged oxygen groups as donors forming complexes with iron(III) [12]. Most siderophores

have an octahedral geometry, coordinating iron in a thermodynamically favourable hexadentate conformation [13], [14]. This configuration satisfies the coordination sphere of iron, forming a 1:1 complex. Siderophores that form 1:3 or 2:3 complexes, and have a bidentate or tetradentate configuration, respectively, present lower siderophore-iron(III) affinity constants (K_f) than hexadentate chelators [10].

Siderophore production is an efficient and specialized iron-acquisition system that provides a competitive advantage to many bacteria and other organisms in the environment. Organisms produce different types of siderophores and may present more than one iron uptake system with multiple siderophores involved, according to their iron requirements and the environment around. For example, carboxylate siderophores are useful for microbes living in acidic environments. This type of siderophores exhibits carboxyl and hydroxyl donor groups (Figure 2.1). At neutral pH, carboxylates are, in general, less efficient in scavenging iron. However, carboxylate-type siderophores are advantageous at more acidic pH, where they are more effective than catecholates and hydroxamates, which remain protonated [15].

Catecholate siderophores are meanwhile mostly described in bacteria, and includes siderophores such as enterobactin (*Escherichia coli*, *Pseudomonas aeruginosa*) (Figure 2.1), its glycosylated-derivative salmochelin (*Salmonella* spp.), and bacillibactin (*Bacillus* spp.) [16]. Catecholate-type siderophores present the highest ferric iron affinities due to the formation of five-membered chelate rings. In particular, enterobactin has the highest iron affinity constant ($\log K_f = 49.0$) due to its structure with a trilactone backbone with three catechol moieties [10], [17]. Like catecholates, hydroxamates siderophores form five-membered chelate rings but with lower iron affinities. Hydroxamates-type siderophores include types of deferoxamine (i.e., deferoxamine B (DFOB), deferoxamine E (DFOE)) (Figure 2.1), produced by *Streptomyces* species [18].

Mixed type siderophores are characteristic for displaying two or more moieties. These ligands are supported in different chemical structures such as peptides, and di- and tri-aminoalkanes. The peptide chain that carries the ligand sites generally includes cyclic structures at the extremes, which restricts their degradation by proteolytic enzymes. Pyoverdine (PVD), expressed by fluorescent *Pseudomonas* spp., is the main example of a complex peptidic mixed-type siderophore, which contains both hydroxamate and catecholate groups (Figure 2.1) [19]. Other siderophores included in the mixed-type group are aerobactin (produced by *E. coli*) (Figure 2.1), which contains hydroxamate and carboxylate moieties, and petrobactin (produced

by *Marinobacter hydrocarbonoclasticus*) formed by catechol and carboxylate moieties [15], [20].

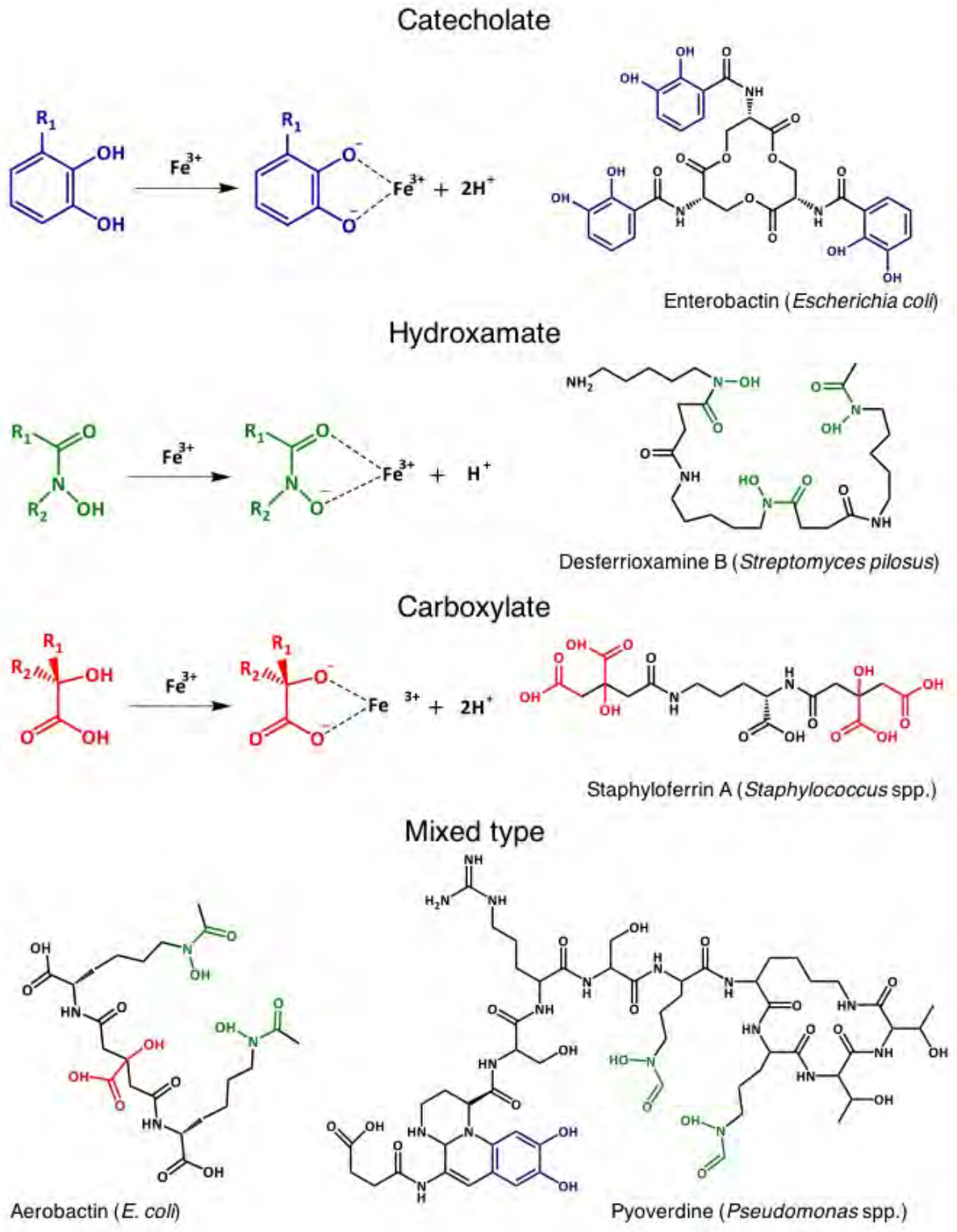

Figure 2.1. *The most common iron-binding moieties (Catecholate, hydroxamate, and carboxylate) found in microbial siderophores and examples. Some siderophores present a combination of the iron-binding moieties and are known as mixed-type siderophores. Adapted from [21]. © 2019 Elsevier Inc.*

In the culture collection at the host institution, we have access to a wide range of different bacteria already isolated and characterized. Bacteria producing different types of siderophores were chosen for the experimental procedure. Thus, the goal of this section is to select bacteria with the best production rates of siderophores that will be further investigated to remove harmful species from waterlogged archaeological wood.

Materials and methods

Bacteria and culture conditions

Bacillus subtilis, *Bacillus thuringiensis* (strain 105NE), *Escherichia coli* (strain K12), *Pseudomonas fluorescens* (strain SN6), *Pseudomonas putida* (strain 90), *Serratia ureilytica* (strain Lr5/4), and *Streptomyces pilosus* (strain ETH 11686) were selected for their ability to produce siderophores. All bacteria, except *S. pilosus*, were cultured in Nutrient Broth (NB) at 28 °C (*Pseudomonas* spp. and *S. ureilytica*) or 37 °C (*Bacillus* spp. and E. coli). *S. pilosus* was kept in Glucose-Yeast-Malt (GYM) medium at 28 ºC. All bacteria, except *S. pilosus*, were obtained from the culture collection of the Laboratory of Microbiology, University of Neuchâtel, Switzerland. *S. pilosus* (DSM 40097) was purchased from the German Collection of Microorganisms and Cell Cultures (DMSZ GmbH, Germany). All media are described in the supplementary material section.

Siderophore production and quantification

Bacterial strains were pre-cultured three times in a modified M9 medium [22] (MM9), prepared in ultrapure Milli-Q® water (Milli-Q® Reference Water Purification System, Merck). All glassware was washed with HCl and Milli-Q® to assure iron-free conditions. Finally, MM9 medium was inoculated from an overnight pre-culture to a final volume of 1% (v/v). Cultures were incubated at 28 °C in high agitation. After the cultures had grown to the stationary phase the capability to produce siderophores was studied using Chrome Azurol S (CAS) assay [1]. We followed the procedure of Alexander and Zuberer (1991). Briefly, the cells were recovered by centrifugation (2500 g for 10 min) and the supernatant was filtered through a 0.22 µm PVDF filters (BGB Analytik, Switzerland). The concentration of siderophores in the filtrate was measured by mixing 100 µL of CAS assay solution, with 100 µL of filtrate in a 96-well plate. After allowing the solutions to equilibrate for 3-4 h, UV-Vis absorbance was measured at 630 nm. Decrease of the absorbance at 630 nm is translated to a higher concentration of iron chelators in the extract. A standard curve with known concentrations of siderophore

(Pyoverdine, Sigma, United States) was achieved following the same procedure as for the samples (Figure S 2.1).

For *Pseudomonas* species, the most common siderophore produced is pyoverdine (PVD), which presents a peak in absorbance around 400 nm ($\varepsilon_{400\,nm}$ $1.85 \cdot 10^4$ $mol \cdot L^{-1} \cdot cm^{-1}$) [23]. Consequently, the production of PVD was registered independently from CAS assay at 400 nm. A standard curve with known concentrations of PVD (Sigma, United States) was prepared (Figure S 2.1).

P. fluorescens was considered as control in this experiment as their capacity to produce siderophores is widely studied. To show the dependency of the production of siderophores to iron levels, *P. fluorescens* was inoculated in MM9 medium amended with 1% of a solution containing: 1 mM $FeCl_3 \cdot 6H_20$ and 1 mM EDTA.

All absorbance values were recorded with an Asys UVM 340 Microplate Reader (Biochrom Ltd, United Kingdom). All media and solutions are described in the supplementary material section.

Results and Discussion

In this preliminary experiment, different bacteria were tested for their capability to produce iron chelators (i.e. siderophores). The study focused on the production of siderophores by microorganisms over other organisms due to the easier handling and faster growth, producing high amounts of siderophores in short-time periods. Moreover, plant siderophores usually present lower stability constants [6]. Furthermore, we selected to work with bacterial siderophores over fungal siderophores for the known capability of some wood-decaying fungi to produce siderophores [6], [24]. In fact, fungal siderophores have been studied as an eco-friendly alternative in bleaching of pulps [6]. Therefore, fungal siderophores could be harmful in our specific application in WAW.

The main criteria to select the bacteria for this experiment were: (1) the capability to produce siderophores, (2) the safety of the object and (3) the potential pathogenicity of the strains. Bacterial siderophores have not been described, in contrast to fungal siderophores, to participate in wood-decay processes. Still, the safety of bacterial siderophores, in regard to wood degradation, is developed later in this chapter.

The other two main criteria were also respected as much as possible. All the bacteria selected in this first experiment, or their genera, have been described before to produce siderophores [3], [25]–[28]. Moreover, all screened bacteria are classified as risk group 1 in Switzerland, and

therefore, are not pathogenic under normal circumstances [29]. However, *Pseudomonas* species carry a special remark: "Pathogenic In Individual Cases, PIIC" [29]. This involves that these bacteria are "shown or suspected to be pathogens in individual cases, predominantly in people with substantial immune deficiency" [29]. Previous studies in bioconservation have used the metabolisms of *Pseudomonas* species under this classification [30]. Therefore, the handling of these specific strains needs to be conducted by trained personal, but their application to preservation of cultural heritage is still possible.

For the screening, CAS assay was selected as method to quantify siderophores production [1]. The addition of any iron chelator in the growth medium will interfere with the final results of the assay. Therefore, the growth media commonly used with CAS assay have reduced level of phosphates, or other interfering components [22]. The growth conditions chosen here were the same for all bacteria, even though this sometimes translated to inefficient growth of some strains. For example, *B. subtilis* and *B. thuringiensis* presented very bad growth in the chosen culture conditions. Both bacteria have been described previously for their production of bacillibactin [15], [28]. However, we could not manage to obtain siderophores production in the experimental conditions. These bacteria were not able to develop correctly in MM9 medium (Table 2.1). In both, solid and liquid cultures, the strains were not able to grow unless casaminoacids or another additional nutritive source were added. However, when casaminoacids were added to the growth medium, no siderophore production was detected. Iron regulates the production of siderophores. Small amounts of iron in solution inhibit the production and secretion of siderophores [31]. Rich media cannot be considered for the production of siderophores, and siderophores studies are usually conducted in minimal media [32]–[34]. *Bacillus* species were not considered further in this project as we could not manage to obtain siderophore production in the experimental conditions chosen.

The next bacterium under study is *S. ureilytica* Lr5/4. This specific strain was isolated from a double layer microbial mat in a source pond at 54 ºC in in the Andean highlands of northern Chile. It presents an optimal growth at 25 ºC and pH 5-6 [35]. The genus *Serratia* has been described previously for the production of siderophores. *S. ureilytica* has been isolated as a plant growth promoting bacteria. This isolated strain was characterized as siderophore-producing [36]. In this study, *S. ureilytica* Lr5/4 was able to grow in the MM9, both liquid and solid, and a high concentration of iron chelators was detected in the bacterial extract up to 20.84 $mg \cdot L^{-1}$ (Table 2.1).

Enterobactin is one of the most studied siderophores. We included *E. coli* in the initial screening due to the high affinity of enterobactin for iron [17]. However, as for the *Bacillus* strains, *E. coli* presented limited growth in MM9 at 28 ºC. Still, we detected a final concentration of iron chelators of 18.17 $mg \cdot L^{-1}$ (Table 2.1).

Pseudomonas strains are well known for their capacity to produce siderophores. Pyoverdine (PVD), the main siderophore produced by *Pseudomonas* spp. has been well characterized in literature [25]. The chromophore group is usually common to all pyoverdines, while the peptide moiety differs among strains and species by the number, length, composition and configuration of amino acids [25]. In this study, two species of fluorescent *Pseudomonas*, *P. fluorescens* and *P. putida*, were selected for their known capacity to produce PVD [37]. The advantage of working with *Pseudomonas* over the previous bacteria is their ability to grow at lower temperature and in poor culture media. In the conditions used here, we obtained concentrations of iron chelators of 26.94 $mg \cdot L^{-1}$, for *P. fluorescens*, and 25.84 $mg \cdot L^{-1}$ for *P. putida*, when measuring with CAS assay (Table 2.1). When using direct detection of PVD, by measuring the absorbance at 400 nm, we detected 12.53 $mg \cdot L^{-1}$ of PVD in the extract of *P. fluorescens*, and 19.33 $mg \cdot L^{-1}$ of PVD in the extract of *P. putida* (Table 2.1). Differences between the two detection methods are expected. CAS assay is not specific of any type of siderophore, while measuring the absorbance at 400 nm give us a reading of only PVD concentration. *Pseudomonas* spp. are known to produce other types of siderophores along with PVD [38], [39]. The higher concentrations detected with CAS assay imply that these bacteria may be producing other iron chelators, apart from PVD, under the experimental conditions.

Finally, an Actionobacteria such as *S. pilosus* was considered in the screening for the recognized capability of this bacterium to produce deferoxamine (DFO). The structure of this hydroxamate siderophore was elucidated by scientists last century [40], and nowadays, DFO is the chemical principle of Desferal®, a commercially available drug used for treating iron or aluminium poisoning [41]. The possibility of having a commercially available siderophore is of great interest for us. An already available “green-chelator” in the market facilitates the application by end-users. We incubated *S. pilosus* in MM9 medium for 20 days to arrive to a final DFO concentration of 27.70 $mg \cdot L^{-1}$. After 7 days, the concentration was about 15.48 $mg \cdot L^{-1}$. Longer times are needed for *S. pilosus* to start producing siderophores in comparison to the other bacteria tested that arrived to peak of production after 1-3 days.

The detection of siderophores when the medium was supplemented with a bioavailable iron source was negligible. Siderophores production was only stimulated under iron-depletion.

***Table 2.1**. Siderophores concentrations calculated in cell-free extracts. CAS assay was used as a general method to quantify siderophores in the bacterial extracts. The production of PVD by Pseudomonas species was followed in parallel at 400 nm.*

	A 630 nm	**Siderophore concentration ($mg \cdot L^{-1}$)**	**A 400 nm**	**PVD concentration ($mg \cdot L^{-1}$)**
Control MM9	0.56 ±0.00	-	0.03	-
Control MM9-Fe (*Pseudomonas fluorescens*)	0.54 ±0.00	-	0.06 ±0.00	-
Bacillus thuringiensis	0.56 ±0.05	-	-	-
Bacillus subtilis	0.57 ±0.01	-	-	-
Escherichia coli	0.22 ±0.01	18.17 ±0.74	-	-
Pseudomonas fluorescens	0.07 ±0.00	26.94 ±0.06	0.15 ±0.02	12.53 ±2.80
Pseudomonas putida	0.09 ±0.01	25.84 ±0.43	0.18 ±0.01	19.33 ±1.02
Streptomyces pilosus	0.06 ±0.00	27.70 ±0.22	-	-
Serratia ureilytica	0.17 ±0.00	20.84 ±0.18	-	-

Values of read absorbance and calculated concentrations ±standard deviation of two or three replicates

Conclusion

The bacteria selected in this study presented different capacities to produce siderophores in the chosen conditions. The *Bacillus* species were not able to grow and therefore no siderophore production was registered in medium MM9. *E. coli* also presented growth issues in the culture conditions, however catecholate siderophores form some of the strongest iron complexes, and we decided to continue with *E. coli* in following experiments. *Pseudomonas* species are well-known siderophore producers. The capacity to produce high amounts of PVD makes them ideal candidates. For next experiments we decided to continue only with *P. putida*.

S. ureilytica turned out to have one of the highest productions of siderophores in MM9 medium. This strain is not as documented as the other selected bacteria. Further analyses are needed to determine the nature of the iron chelators present in the bacterial extract.

Finally, *S. pilosus* presented the highest concentration of siderophores in the cell-free extract. However, to get these amounts we needed to incubate the bacteria for 20 days. Longer times and a fungi-like morphology are not ideal in a possible direct application of *S. pilosus* in the wood matrix. We decided to further study this bacterium as we are interested in the possibility of using the commercial siderophore (i.e., Desferal®) obtained from it.

Supplementary material 2.1

***Table S 2.1**. Composition of Nutrient Broth (NB).*

NB medium	
Peptone	15 g
Yeast extract	3 g
NaCl	6 g
Glucose	1 g
H_2O_d	1000 mL

Final pH 7.5 (±0.2) at 25 °C. Autoclaved

***Table S 2.2**. Composition of Glucose-Yeast-Malt (GYM) medium.*

GYM medium	
Glucose	4 g
Yeast extract	4 g
Malt extract	10 g
H_2O_d	1000 mL

Adjust to pH 7.2. If preparing solid medium add 2 g $CaCO_3$. Autoclaved

***Table S 2.3**. Composition of the modified M9 medium [22]: MM9.*

MM9 medium	
Solution 1	100 mL
Solution 2	10 mL
Milli-Q®	890 mL
Solution 1 (10X)	
PIPES	60,5 g
KH_2PO_4	0,6 g
NaCl	1 g
NH_4Cl	2 g
In 200 mL Milli-Q® water at pH 6.8 (adjusted with NaOH 10M). Autoclaved	
Solution 2 (100X)	
Glucose	20 g
$MgCl_2 \cdot 6H_2O$	4,06 g
$CaCl_2$	0,11 g
$MnCl_2 \cdot 4H_2O$	0,0136 g
H_3BO_3	0,014 g
$CuCl_2 \cdot 2H_2O$	0,27 mg
$ZnCl_2$	5,68 mg
$Na_2MoO4 \cdot 2H_2O$	0,01 g
In 100 mL Milli-Q® water. Filter-sterilized	

***Table S 2.4**. Composition of Chrome Azurol S (CAS) solution [22].*

CAS solution	
HDTMA	21.9 mg
$FeCl_3 \cdot 6H_20$	0.41 mg
CAS	9,1 mg
MES	9.76 g
Milli-Q®	100 mL
pH adjusted to 5.6	

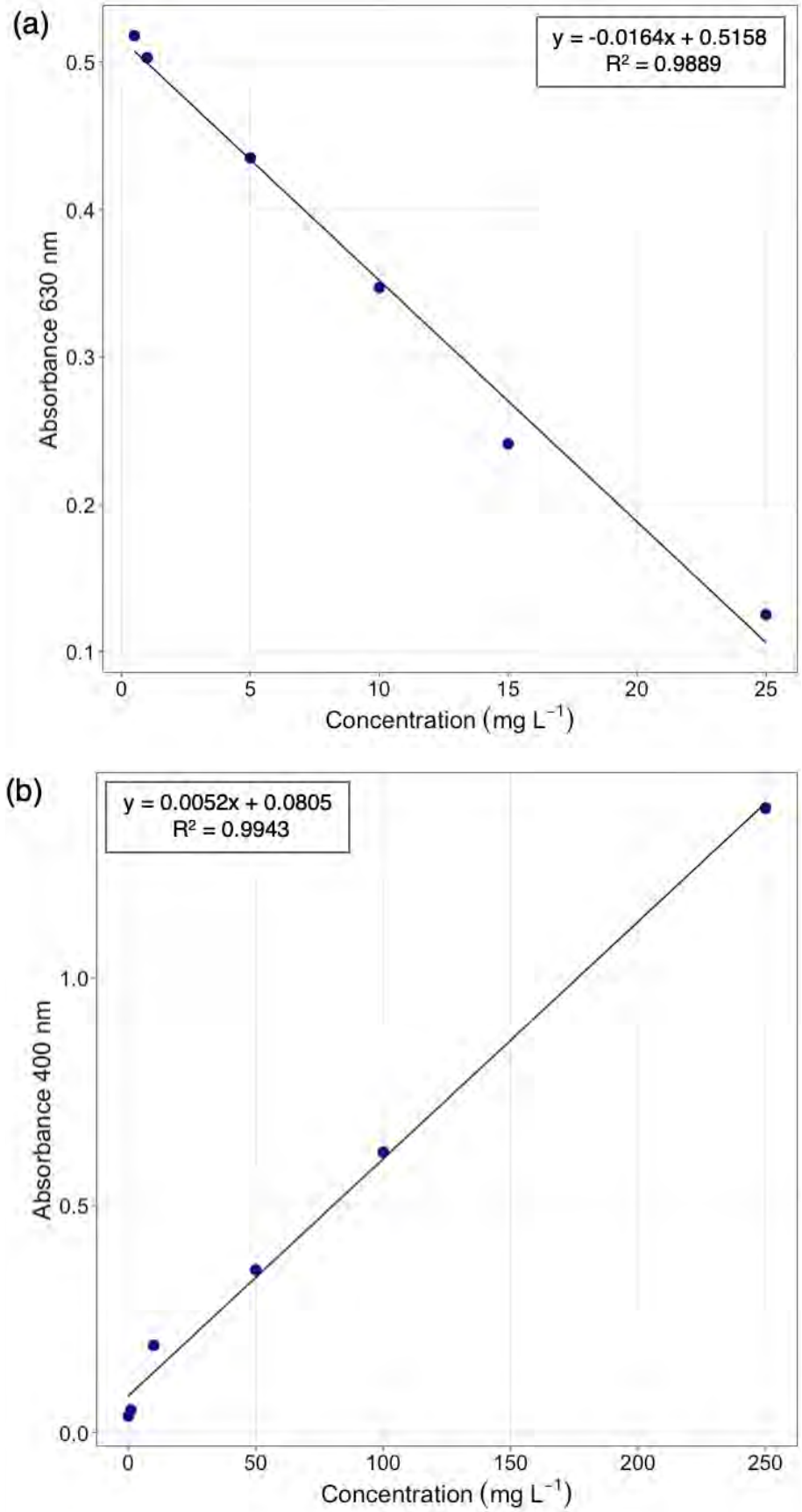

Figure S 2.1. *(a) Standard curve prepared with known amount of commercial PVD for the CAS assay. (b) Standard curve prepared with known concentrations of commercial PVD for the direct measurement of this siderophore's absorbance.*

2.2 Interaction of siderophores with minerals

Abstract

Iron-bearing minerals are a huge reserve of iron in the environment. Microbes have developed tools, such as siderophores to access this low soluble iron. In this section, we studied how the four selected bacteria, *Escherichia coli, Pseudomonas putida, Streptomyces pilosus* and *Serratia ureilytica*, interact with four different iron minerals. Moreover, the purification of pyoverdine from *P. putida* cultures, allowed us to directly study the effect of siderophores in mineral dissolution. The effects of pyoverdine were compared to the commercial siderophore Desferal® and to a chemical chelator. We observed that the bacteria were able to grow with the different mineral phases in a similar way as when bioavailable iron was given. In some of the cases, siderophores were found to be the key for a normal development in presence of iron minerals, while in other cases abiotic oxidation may have released in solution the minimal amounts of iron necessary to growth preventing the production of siderophores. However, the direct interaction of siderophores with the same mineral phases proved that siderophores enhance the dissolution of iron-bearing minerals, being ideal candidates to extract problematic iron from waterlogged wooden artefacts.

Introduction

Waterlogged archaeological wood (WAW) accumulates mostly iron sulfides during burial [42]. However, these species can be quickly oxidized. The formation of iron oxides and oxyhydroxides is commonly detected during the recovery of waterlogged wooden objects [43]. The extraction of iron from wooden artefacts is essential to avoid further degradation via Fenton-like reactions [44]. So far, chemical chelators have been used to extract iron from WAW [45], [46]. However, a biological approach is possible using siderophore-producing bacteria.

The first function of siderophores in nature is to sequester iron from the environment allowing the correct development of organisms. In terrestrial and aquatic environments, iron may be present as part of iron-bearing minerals, forming complexes with ligands, and/or bound to organic materials. In particular, in oxic environments, iron is mostly found as iron(III) oxides and oxyhydroxides [47], whereas in reducing environments, such as waterlogged soils and flooded zones, iron may be found as iron(II) soluble species and oxides. In reducing conditions, ferrous iron sulfides (i.e. pyrite, FeS_2) may ultimately form. Other iron-bearing secondary minerals, such as carbonates (siderites, $FeCO_3$) are also present in soils [48].

The problem for living organisms to access these iron pools is the low solubility and dissolution kinetics of these iron phases. Siderophores have been developed to make the iron present in these minerals available to the organisms. For example, Kraemer (2004) described in detail the process for siderophore-driven solubilization of goethite (α-FeOOH), summarized here in eqs. 1, 2 and 3:

$$\alpha - FeOOH + 3H^+ \rightarrow Fe(III) + 2H_2O \qquad K_S \qquad (1)$$

$$Fe(III) + H_3L \rightarrow FeL + 3H^+ \qquad K_{FeL} \qquad (2)$$

$$\alpha - FeOOH + H_3L \rightarrow FeL + 2H_2O \qquad K_{S,L} \qquad (3)$$

Equation 1 represents the dissolution reaction and the corresponding solubility product K_S. Reaction 2 describes the complexation reaction of iron with a siderophore (L) and the corresponding stability constant K_{FeL}. Equation 3 combines the dissolution reaction in the presence of a siderophore, where $K_{S,L}$ equals K_S x K_{FeL}. Therefore, the concentration of the complex depends on the concentration of the free siderophore, the solubility product of the mineral and the stability constant of the Fe-complex ([FeL] = [H_3L] x $K_{S,L}$ = [H_3L] x K_S x K_{FeL}). Thus, the high affinity constant of siderophores for iron is result of evolution in response to the low solubility of iron oxides at neutral and alkaline pH and to the issue of low concentrations of ligands [47].

The solubility of iron oxides (including iron oxides and iron oxyhydroxides) is also influenced by particle size, pH, and presence of organic ligands [47]. Indeed, low molecular weight organic acids (LMWO) are secreted to promote mineral dissolution [49]. However, siderophores form more stable complexes with iron(III) than organic acids. The affinity constants of ferri-siderophores are in the logarithmical range between 30 to 50 [10], while the log binding affinity for iron(III) of LMWO is lower (e.g. oxalic acid logK_f = 7.5; citric acid logK_f = 17) [50]. Nonetheless, combining LMWO with siderophores has been reported to increase dissolution rates of iron oxyhydroxides due to synergistic effects [49], [51].

In this project, we are interested also in iron sulfides, thus ferrous iron complexation. Not many studies focus on the interaction of siderophores with iron(II). However, some researchers highlight the capacity of siderophores to oxidize iron(II) to iron(III) to establish the stronger bond they form with ferric iron [52], [53]. Moreover, the dissolution of pyrite is enhanced by siderophores [27].

Our goal in this study was to investigate the interaction of the previous selected bacteria and their extracts with different iron oxides and iron sulfides. The aim was to figure out if the

selected bacteria would be able to sequester directly the iron from minerals, in case of a possible direct application of these bacteria to WAW. Furthermore, some experiments focused on the isolation, purification and characterization of the siderophores produced by some of the selected bacteria, and the direct interaction of the extracts with the same mineral phases.

Materials and Methods

Bacteria and culture conditions

Serratia ureilytica (strain Lr5/4), *Escherichia coli* (strain K12), *Pseudomonas putida* (strain 90), and *Streptomyces pilosus* (strain ETH 11686) were selected to analyse the production of siderophores in presence of different iron minerals. All bacteria were cultured in NB (Table S 2.1) at specific temperature, except *S. pilosus* that was kept in GYM (Table S 2.2) medium at 28 ºC.

Iron minerals and chemicals.

Goethite (α-FeOOH) (Alfa Aesar, United States), hematite (Fe_2O_3) (Acros Organics, United States), mackinawite (FeS) (Acros Organics, United States), and pyrite (FeS_2) (Sigma-Aldrich, United States) were selected for this experiment. All minerals were obtained with a purity of 99.8% or higher (trace metal basis). Four minerals can be found in WAW. Minerals were sterilized by autoclaving or washing with ethanol 70% (v/v in deionized water).

Commercial iron chelators were purchased to compare the efficiency with lab extracted siderophores. Deferoxamine mesylate salt (DFOM) was purchased as Desferal® (Novartis AG, Switzerland). Ethylenediaminetetraacetic acid (EDTA) was obtained as salt (Na_2-EDTA) (Apollo Scientific Ldt., United Kingdom). Pyoverdine (PVD) was obtained as a mix of pyoverdines from *P. fluorescens*, with purity higher than 90% (Sigma-Aldrich, United States).

Chemicals to prepare the different buffers used in this experimental section were purchased with a purity over 98%. HEPES, Tris-HCl, citrate and acetate buffers were prepared using: N-2-hydroxyethylpiperazine-N'-2-ethane sulphonic acid (HEPES) (Carl Roth, Germany), tri(hydroxymethyl)aminomethane (Tris) (Acros Organics, United States), citric acid (Carl Roth, Germany), citric acid trisodium salt dihydrate (Acros Organics, Unites States), sodium acetate (Acros Organics, Switzerland), glacial acetic acid (Carl Roth, Germany), respectively.

Ferrozine: (5,6-Diphenyl-3-(2-pyridyl)-1,2,4-triazine-4,4'-disulfonic acid disodium salt hydrate) (Alfa Aesar, United States) and hydroxylammonium chloride (Huber Lab, Switzerland) were obtained also with a purity over 98%.

All solutions were prepared with ultrapure Milli-Q® water (Milli-Q® Reference Water Purification System, Merck, Unites States) with resistivity of 18.2 MΩ.cm (at 25°C) and a Total Organic Carbon (TOC) value below 5 ppb.

Siderophore production and quantification in presence of minerals

Experiments were conducted in 100 mL propylene bottles to avoid iron contamination. Three pre-cultures in MM9 medium (Table S 2.3) were made to assure no iron presence. 50 mL of MM9 were inoculated from an overnight pre-culture to a final volume of 1% (v/v). Minerals were added to a final concentration of 1 $g \cdot L^{-1}$. Cultures where incubated at 26 ºC (±1 ºC) and 120 rpm. Controls without any iron source and with soluble iron (bioavailable iron) were conducted, along with abiotic controls. Iron was supplemented to the medium as 1% (v/v) of a solution containing: 1 mM $FeCl_3 \cdot 6H_20$ and 1 mM EDTA. Samples were withdrawn regularly from the cultures to measure: 1) the growth of the bacteria by increase in the Optical Density (OD) at 600 nm, or in the mass in the case of *S. pilosus*, 2) the siderophore production, and 3) the release of iron from minerals (Ferrozine assay).

Chrome Azurol S (CAS) assay [1], was used for general determination of the concentration of siderophores in the extract of the bacteria. We followed the procedure of Alexander and Zuberer (1991) (see section 2.1). PVD production was registered following the absorbance at 400 nm ($\varepsilon_{400\ nm}$ $1.85 \cdot 10^4$ $mol \cdot L^{-1} \cdot cm^{-1}$[23]). A standard curve with known concentrations of PVD has also been previously prepared (Figure S 2.1).

Purification of siderophores

P. putida was selected for this preliminary test of purification due to the easy detection of PVD. The production of siderophores was conducted in 2 L Erlenmeyer flasks HCl-washed. Three sequent pre-cultures in MM9 medium with succinic acid instead of glucose (MM9-S) were made to assure no iron presence. Glucose was removed from solution 2 (Table S 2.3) and succinic acid was added to a final concentration of 2 $g \cdot L^{-1}$. 1 L of MM9-S per flask was inoculated from the last pre-culture to a final volume of 0.5% (v/v). Cultures where incubated at 26.5 °C and 130 rpm. After reaching the stationary phase, cells were recovered by centrifugation (2500 g for 10 min) and the supernatant was filtered through a 0.22 µm membrane filter (Millipore, United States). Extracts were preserved at 4 °C until final purification.

The solid-phase extract of the cell-free supernatant was prepared using Chromabond C18ec columns containing 500 mg of octadecylsilane (Macherey-Nagel, Germany). The cell-free extract was applied to the C18ec column, which was conditioned with methanol and water. For every 200 – 250 mL of extract one new column was used. The C18ec columns were eluted with 3 mL water (in two times) and with 5 mL of methanol 50% (v/v) (in two times). All eluates were then dried by evaporation (Concentrator plus, Eppendorf, Germany), weighted and kept at -20 °C. UV-Vis spectroscopy and Nuclear Magnetic Resonance (NMR) spectroscopy were applied to determine the nature of the pyoverdines in the different eluates.

Mineral dissolution in presence of siderophores

All dissolution experiments were conducted in 50 mL propylene tubes containing or hematite, goethite, mackinawite, or pyrite with a concentration of 1 $g \cdot L^{-1}$. The tubes were wrapped with aluminium foil to exclude light and shaken continuously on an orbital shaker at 180 rpm at RT. Several experimental conditions were established. The dissolution of the fours minerals was studied under the presence of two siderophores (PVD and DFOM) and one chemical iron chelator (EDTA). The purified PVD, DFOM and EDTA were used in a final concentration of 200 µM. Each mineral was incubated with each iron chelator or alone (control) at different pH. Citrate and acetate buffers were used to maintain pH 5.6. Tris-HCl and HEPES were used to keep pH 7. Dissolution was also studied under no buffered conditions. All solutions were prepared with Milli-Q® water. The total iron concentration was measured in solution after 5 days. Samples were analysed by Inductively Coupled Plasma-Optical Emission Spectrometry (ICP-OES) and Ferrozine assay.

Analytical methods

Ferrozine assay

The Ferrozine® assay [54] measures iron(II) concentrations in solution. Briefly, samples were filtered through a 0.22 µm PVDF filters (BGB Analytik, Switzerland) and then diluted 10:1 in 5 M HCl. 100 µL of the fixed sample was mixed with 900 µL of Ferrozine reagent 0.1% (w/v) prepared in 100 mM HEPES pH 7. To measure total iron, 150 µL of hydroxylamine-HCl were added to the previous mixture. The absorbance was measured at 562 nm after incubation in the darkness at RT. Total iron and iron(II) in solution were calculated using prepared standard curves with known concentrations of iron (Figure S 2.1). Iron(III) concentrations are calculated subtracting iron(II) concentrations to total iron.

Inductively Coupled Plasma-Optical Emission Spectrometry (ICP-OES)

Inductively Coupled Plasma-Optical Emission Spectrometry (ICP-OES) was applied to determine total iron concentrations in the different experimental solutions. Samples were first filtered through a 0.22 µm PVDF membrane (BGB Analytik, Switzerland) and then diluted into the detection range (0-2 ppm). Diluted samples were loaded into the ICP using a peristaltic pump, and a cyclonic spray chamber connected to a nebulizer (Perkin-Elmer, United States) to provide high sample transfer. Total iron concentrations were determined using an Optima 2100 DV (Perkin-Elmer, United States) optical emission spectrometer.

Nuclear magnetic resonance (NMR)

Nuclear magnetic resonance (NMR) spectroscopy was performed on a Bruker Avance II 400 spectrometer equipped with a BBOF+ probe operating at 400 MHz for 1H-NMR. Chemical shifts (δ-values) are reported in parts per million (ppm). Spectra were calibrated according to the deuterated solvents (D_2O) residual proton chemical shifts: 4.79 ppm (1H-NMR). Spectra were analysed using MNova 9.0 (Mestrelab Research) software.

pH measurements

A 691 pH Meter Metrohm (Metrohm AG, Switzerland) was used to control the pH of the solution over time with an ionic electrode (unitrode 6.0259.100) calibrated with buffer solutions (pH 4, 7 and 9).

UV-Visible (UV-Vis) spectroscopy

Absorbance values were registered with a 96-well microplate reader (Asys UVM 340 Microplate Reader, Biochrom Ltd, United Kingdom) when measuring a specific wavelength (i.e., 400, 562, 600, 630 nm for PVD, Ferrozine, OD and CAS, respectively). Whole absorbance spectra (350 to 600 nm) were recorded using a UV-Vis spectrophotometer (Lambda 25 Perkin Elmer, United States).

Statistical analyses

In the mineral dissolution experiment, for each mineral and chelator studied, the statistical significance of the data between the different buffers employed (3 replicates, n = 3) was tested with Welch two sample t-test in RStudio (Version 1.3.1093). The statistical significance threshold was set to 1%.

Results and Discussion

Siderophore production and quantification in presence of minerals

Siderophores drive the dissolution of insoluble iron phases allowing the bacteria to access these iron pools [6]. Iron oxides and oxyhydroxides commonly found in recovered waterlogged wood are solubilized by siderophores in nature [33], [55]. Here, we observed that *Pseudomonas putida* and *Escherichia coli* were able to grow with goethite (α-FeOOH) and hematite (Fe_2O_3), as model for these type of iron minerals, due to the production of siderophores (Figure 2.2 and 2.3).

In particular, the growth of *P. putida* followed a similar trend with bioavailable iron as with goethite and hematite (Figure 2.2). On the contrary, when iron was no present in solution the bacterial growth was much lower (Figure 2.2). The production of pyoverdine (PVD) in presence of goethite and hematite allowed the bacteria to develop in the same conditions as when iron was soluble in the solution. A similar study found that *Pseudomonas mendocina* was able to grow with hematite as with chelated-Fe. Siderophore production was detected in hematite solutions but not in the chelated-Fe extracts [56]. However, the authors also proposed that the reduction of iron plays a role in iron acquisition, as some cell-free extracts showed reduction activity. Still, siderophores were defined as the main mechanism for iron acquisition from hematite [56]. Here, we did not study if the supernatant solution was reductive. But the differences in production of siderophores between the solid-phases solutions and the bioavailable-iron solutions and similar growth in both cases (Figure 2.2), match the hypothesis that siderophores are highly involved in the chelation of iron from goethite and hematite.

The production of siderophores in respect to growth (as measurement of the optical density at 600 nm), reached the maximum levels when no iron source was present (Figure 2.2). However, the absolute amounts of PVD were higher when the minerals were present. The maximum concentration of PVD in solution was 16.50 $mg \cdot L^{-1}$ when hematite was present, 14.52 $mg \cdot L^{-1}$ when goethite was present, and 7.47 $mg \cdot L^{-1}$ when no iron was present.

The dissolution of iron sulfides by siderophores has not been widely studied. Interaction of siderophores with these iron phases are not considered as these minerals will oxidize in oxic environments and, siderophores are mostly related to aerobic bacteria [7], [57]. Indeed, *P. putida* in presence of mackinawite (FeS) and pyrite (FeS_2) produce negligible levels of PVD (Figure 2.2). Moreover, the growth of the bacteria was more important than when iron was bioavailable in solution. Levels of iron between 10 and 40 μM were calculated with the

Ferrozine assay for mackinawite and pyrite solutions (Table S 2.5). These values overpassed the concentration added in the bioavailable iron control. The hypothesis is that mackinawite and pyrite released small amounts of iron under the experimental conditions that was used by the bacterium. Abiotic controls also presented iron in solution confirming abiotic dissolution (Table S 2.5). Regarding goethite and hematite, no iron was detected in solution after the incubation time. The concentrations of siderophores calculated, approximately, using the molecular weight of the most common siderophore for each bacterium (i.e., PVD for *P. putida*), varied from 0 to ~280 μM PVD in hematite solutions, and from 0 to ~245 μM PVD in goethite solutions. These concentrations of siderophores could correlate to extracted amounts of iron in the biological range (10 – 0.1 μM) [58], that couples with the observed growth (Figure 2.2).

The pH of the experimental growth medium (MM9, Table S 2.3) was adjusted to 6.8. Stability of iron minerals is highly related to the pH. Iron oxides present minimum solubility at neutral to alkaline pH [47]. The pH at 6.8 could also explain why no iron was detected in solution when these minerals were present. However, the pH was buffered close to neutrality to favour bacterial growth and siderophore production in this experiment [59].

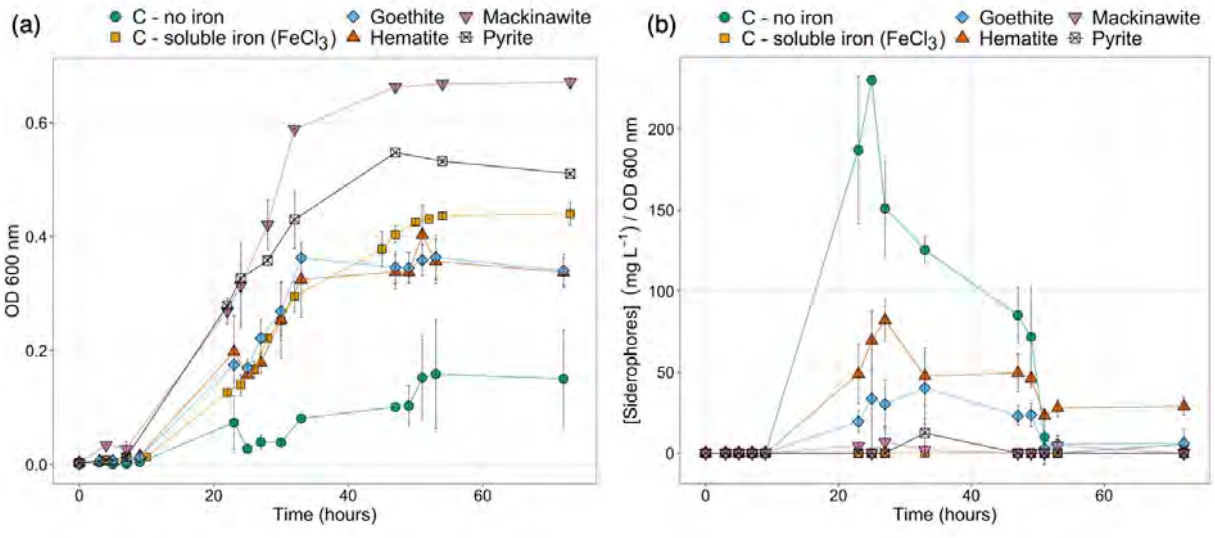

Figure 2.2. *(a) Growth of the bacterium P. putida with the four different iron minerals under study (hematite, goethite, mackinawite and pyrite) in comparison to the controls without iron and with soluble iron, followed by the increase of OD at 600 nm over time. (b) Concentration of PVD (mg·L^{-1}) per relative growth (OD at 600 nm) over time.*

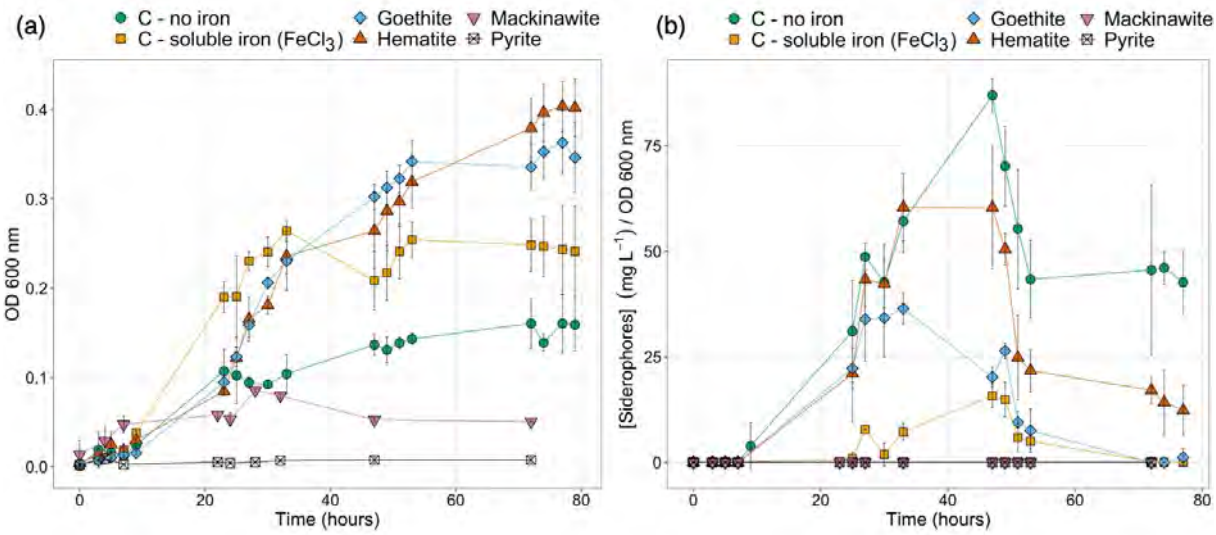

Figure 2.3. *(a) Growth of the bacterium E. coli with the four different iron minerals under study (hematite, goethite, mackinawite and pyrite) in comparison to the controls without iron and with soluble iron, followed by the increase of OD at 600 nm over time. (b) Concentration of siderophores (mg·L^{-1}) per relative growth (OD at 600 nm) over time.*

On the contrary, small growth or no growth was detected when *E. coli* was incubated with mackinawite and pyrite, respectively (Figure 2.3). The temperature was not the optimum for *E. coli*'s growth. However, all experimental set-ups were conducted in the same conditions and growth was observed for the other four conditions. Toxicity has been associated with iron sulfides in nature due to metal contaminants [60]. However, the solid phases used here were pure. Iron was also detected in solution here with these two solid phases (Table S 2.5). Therefore, other associated toxicity or a manipulation mistake may have occurred.

The weathering of iron oxides by *E. coli* siderophores (mostly enterobactin) has not been widely studied. In nature, enterobactin sequesters iron in the gut environment. Therefore, most studies have focused on interaction with human proteins or other iron chelators [61]–[63]. However, presenting the strongest affinities for iron it is likely that enterobactin can favour the dissolution of iron oxides. In this study, *E. coli* was also able to grow in the presence of iron oxides as when iron was soluble in solution (Figure 2.3). In this case, the production of siderophores was also related to the acquisition of iron from iron oxides, and therefore the normal growth of the bacterium (Figure 2.3). The production of siderophores was also higher in respect to growth when no iron source was present (Figure 2.3). The maximum concentration of siderophores was 15.64 mg·L^{-1} when hematite was present, 8.34 mg·L^{-1} when goethite was present, and 10.59

mg·L^{-1} when no iron was present. Small amounts of siderophores (3.30 mg·L^{-1}) were also detected when iron was bioavailable.

The release of iron from goethite and hematite was also here under the detection limit of the Ferrozine assay. Approximate enterobactin calculated levels for *E. coli* solutions ranged from 0 to ~480 μM in hematite solutions, and from 0 to ~250 μM in goethite solutions. This and the solution pH could also translate to iron levels in the range required for bacterial growth (10 – 0.1 μM) [58].

Serratia spp. are known for producing siderophores [28]. Mostly studied as plant-growth promoters, *Serratia* siderophores are part of the soil environment [64], therefore mineral weathering is likely to be influenced by these compounds. Strain Lr5/4 showed promising results in the previous section with high production of siderophores. In this experiment, the levels of iron chelator in solution reached 25.78 mg·L^{-1}, when no iron was present. However, the bacteria failed to grow with hematite (Figure 2.4), and consequently studying the production of siderophores here was not possible. On the contrary, the bacteria were able to use goethite as iron source (Figure 2.4), and siderophore production was registered with a maximum concentration in solution of 12.55 mg·L^{-1}. The production of iron chelator was still higher when no iron was present (Figure 2.4).

In the case of *S. ureilytica*, no iron was either detected in solutions with iron oxides (Table S 2.5). No growth was observed with hematite what could relate with no iron in solution. But iron was not registered either in goethite solutions. *S. ureilytica* Lr5/4 siderophore is not yet identified and an approximative calculation of molar concentration was not possible.

Growth with iron sulfide phases was in the same range as for soluble iron in solution. As in the case of *P. putida*, no siderophore production was registered here (Figure 2.4), but iron was detected in solutions by Ferrozine assay (Table S 2.5). An abiotic oxidation of these minerals could have released iron into solution, allowing the bacteria to profit this iron without the need of metabolically investing in the production of siderophores. However, previous studies have shown the capacity of *Serratia*-siderophores to efficiently dissolve pyrite minerals. Using arsenopyrite, researchers shown that when siderophores were in solution iron concentration increased [27].

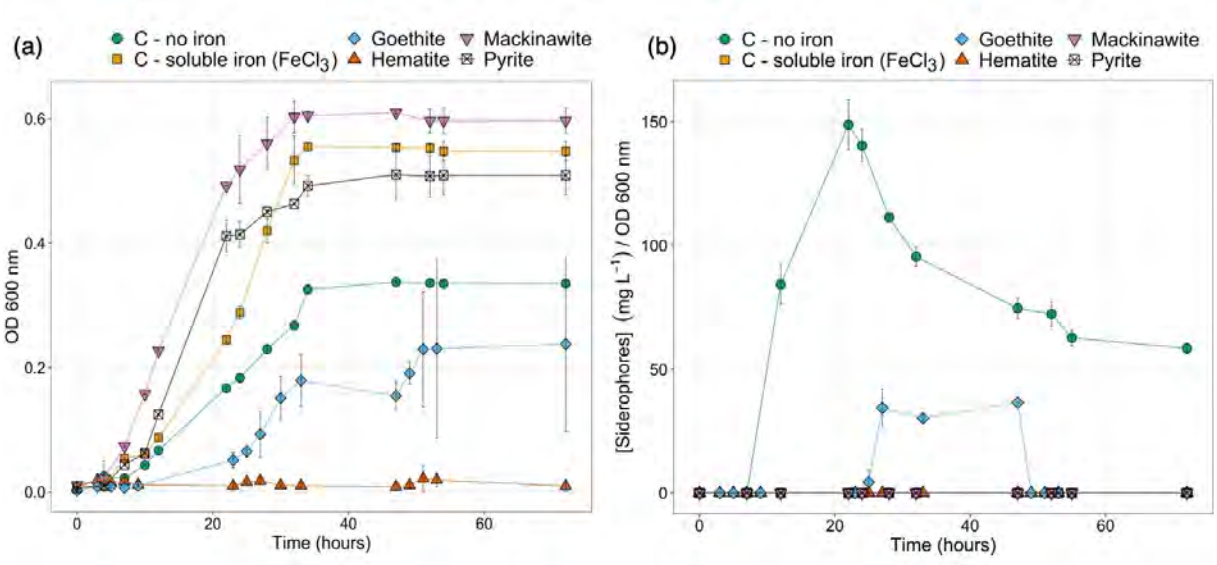

***Figure 2.4**. (a) Growth of the bacterium S. ureilytica with the four different iron minerals under study (hematite, goethite, mackinawite and pyrite) in comparison to the controls without iron and with soluble iron, followed by the increase of OD at 600 nm over time. (b) Concentration of siderophores (mg·L^{-1}) per relative growth (OD at 600 nm) over time.*

The growth of the *Streptomyces pilosus* was followed by the increase in mass over time (Figure 2.5). The correct growth was impossible to follow in presence of the solid phases due to the accumulation of solids inside the mycelia (Figure 2.6). Differences were observed between the independent replicates translating to high standard deviations (Figure 2.5), and consequently, no significative differences were observed in the growth of the bacteria without iron and when iron was bioavailable in solution. Only an initial faster growth was observed in solutions with bioavailable iron (Figure 2.5).

Deferoxamine B (DFOB) has been used as model for many weathering studies [65]–[68]. Direct interaction of *S. pilosus* and minerals also showed that the production of siderophores was one of the factors that enhanced weathering [69]. However, we could not detect the production of siderophores by *S. pilosus* when incubated with the different minerals (Figure 2.5). Moreover, the bacteria were accumulating the minerals inside the mycelia (Figure 2.6). This feature may have aided the bacteria to directly attack the mineral without the need of producing siderophores, or with very low concentrations that are under detection. This characteristic can be interesting in applications for recovery of minerals. For our particular case, it may be difficult to establish a direct application of *S. pilosus* in the wood matrix. The accumulation of iron sulfides in WAW has been described to be mostly on the surface (first few cm) [70]. Still, bacteria need to reach as deep as possible to extract all problematic iron. *S. pilosus* may

encounter problems entering the wood matrix and its effectiveness to extract iron would depend on the adequate diffusion of the siderophores produced.

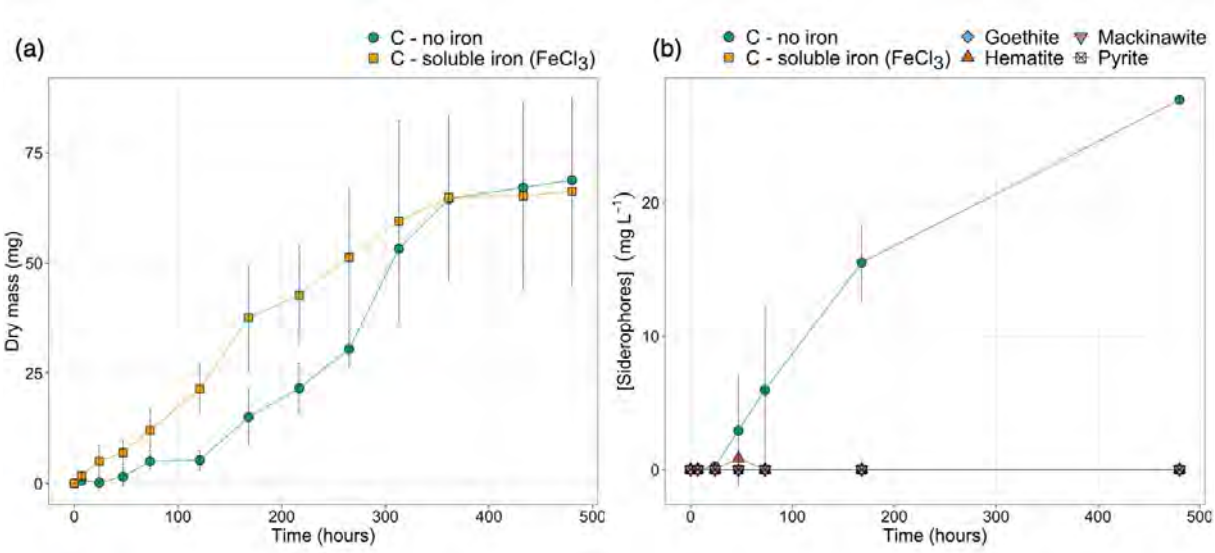

Figure 2.5. *(a) Growth of the bacterium S. pilosus in presence of bioavailable iron or without iron, followed by the increase of dry mass (mg) over time. (b) Increase in the concentration of siderophores (mg·L^{-1}) over time when the bacteria are in presence of five different sources of iron, or without iron (control).*

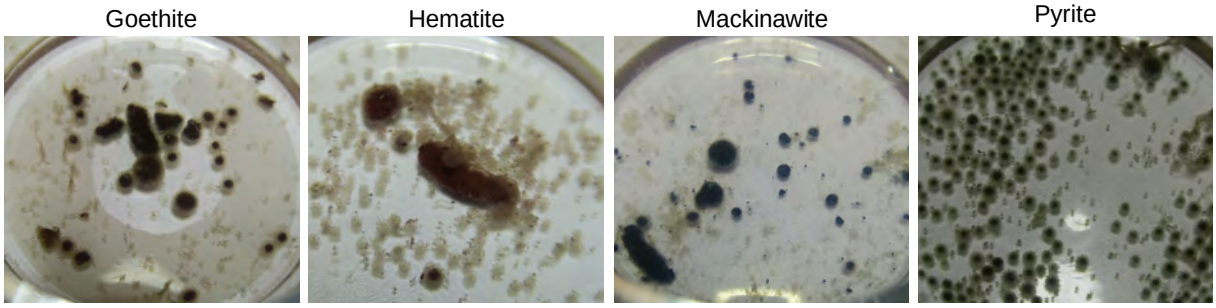

Figure 2.6. *Visual aspect of the cultures of S. pilosus during incubation with different minerals: goethite, hematite, mackinawite, and pyrite. The minerals have been captured within the bacteria mycelia.*

Purification of siderophores

The direct application of microorganisms in the field of bioconservation is a common praxis [71]–[73]. Previous studies have even investigated the advantages of applying directly active cells over the use of enzymatic extracts [74]. For their application, the direct employment of bacteria was favoured as other secondary metabolites, apart from enzymes, helped in the biocleaning process. The use of enzymes alone had a reduced effectiveness as they only worked in their specific substrate [74]. However, for our application, we decided to isolate and study the direct effect of siderophores in iron extraction. In the previous section, we observed that when using active cells, the amount of siderophores released in solution varied over time and was just enough for obtaining iron for bacterial development. Purification of siderophores will allow the use of constant and higher concentrations of the chelators.

The main siderophore produced by *P. putida* (i.e., pyoverdine (PVD)) is a well-known siderophore, extensively characterised and studied. PVD is the main type of siderophore produced by fluorescent *Pseudomonas* under iron-depletion [23]. It was discovered in 1892, and since then, more than 50 different types of pyoverdines have been studied [37]. All pyoverdines have three main structural parts: 1) a dihydroxyquinoline chromophore, 2) a side chain involving a dicarboxylic acid or a dicarboxylic amide, and 3) a variable peptide chain of six to twelve amino acids [37], [75] (Figure 2.1). *P. putida* and PVD were selected for the first attempt of purifying siderophores due to the performance observed in previous experiments.

P. putida was able to produce considerable amounts of siderophores, in comparison to the other microorganisms tested. With *P. putida*, we were able to increase the production arriving to 87.50 ±0.14 $mg \cdot L^{-1}$ of PVD in solution, when using MM9-S. The carbon source influences the production yields of PVD. Succinic acid enhances the synthesis of PVD over other carbon sources such as glucose. The PVD molecule has a succinate moiety and having this compound in the culture medium is beneficial for the cell [76]. However, the presence of succinic acid and other medium components gave problems with using directly the free-cell extracts in downstream applications. The amounts of these compounds interfered with the analytical methods. Therefore, the purification of PVD also helped to remove undesired compounds from the extract.

Another advantage of working with *Pseudomonas* spp. is the easy detection of PVD. After solid-phase purification, we obtained several eluates with absorbance properties. PVD was detected in both water eluates and 50% methanol eluates. For 1 L of culture, the final solid weight was 122.50 ±11.45 mg and 32.25 ±2.89 mg for all water eluates and all methanol eluates,

respectively. The first fraction of the water eluates was discarded because we assumed still contained medium components. The solid weight in the first fraction of water eluates was always higher than in the other fractions of water eluates but the absorbance at 400 nm was in the same range. We assumed some loss of PVD to gain purity. The final solid weight recovered, taking into account all eluates, was 69.75 ±15.77 mg per 1 L of *P. putida* supernatant. The recuperation yield calculated was 79.71%, based on the concentration of PVD in the extract before purification (87.50 ±0.14 $mg \cdot L^{-1}$). Although we lost PVD during the purification, the process allowed to eliminate most of the medium components and to recover considerable amounts of PVD to be used in further experiments.

Moreover, we could characterize our PVD extract as a mix of pyoverdines. The two elution products obtained (water eluates vs methanol eluates) showed different absorbance spectra (Figure 2.7). While the mix of water fractions (elute H_2O) showed a maximum peak at 403 nm, all 50% methanol eluates (elute MeOH) presented a maximum peak at 380 nm with a shoulder at 365 nm (Figure 2.7). Xiao and Kisaalita 1995, showed that absorbance in pyoverdines is dependent of the pH. At lower pH (3 to 5), the spectra had double peaks around 365 and 384 nm. At higher pH (7 to 9), the spectra showed a single peak close to 407 nm. We did not check the pH of our elutes before analysing. However, the spectrum registered before purification, where the pH was 6.7, showed two peaks, one around 405 nm and one around 384 nm (Figure 2.7). This suggested that *P. putida* strain 90 could be producing two different types of pyoverdines [25], [75], that were separated during the solid-phase purification.

Indeed, further NMR characterization of the two eluates showed differences between them in the side chain region of the spectra (Figure S 2.3). Eluate H_2O matched previous references for succinimide dihydro-pyoverdine, while eluate MeOH presented a mix of pyoverdines with succinic and succinimide moieties [77]. Deeper characterization would be needed to confirm the specific phases found in the two eluates. However, when we compared the absorbance spectrum of a commercial mix of pyoverdines (Sigma, United States) with our eluates (Figure 2.7); we found that the spectra of the commercial PVD matched eluate MeOH. The commercial mix of pyoverdines mainly contains the succinic acid and succinimide forms of PVD, the same found in eluate MeOH.

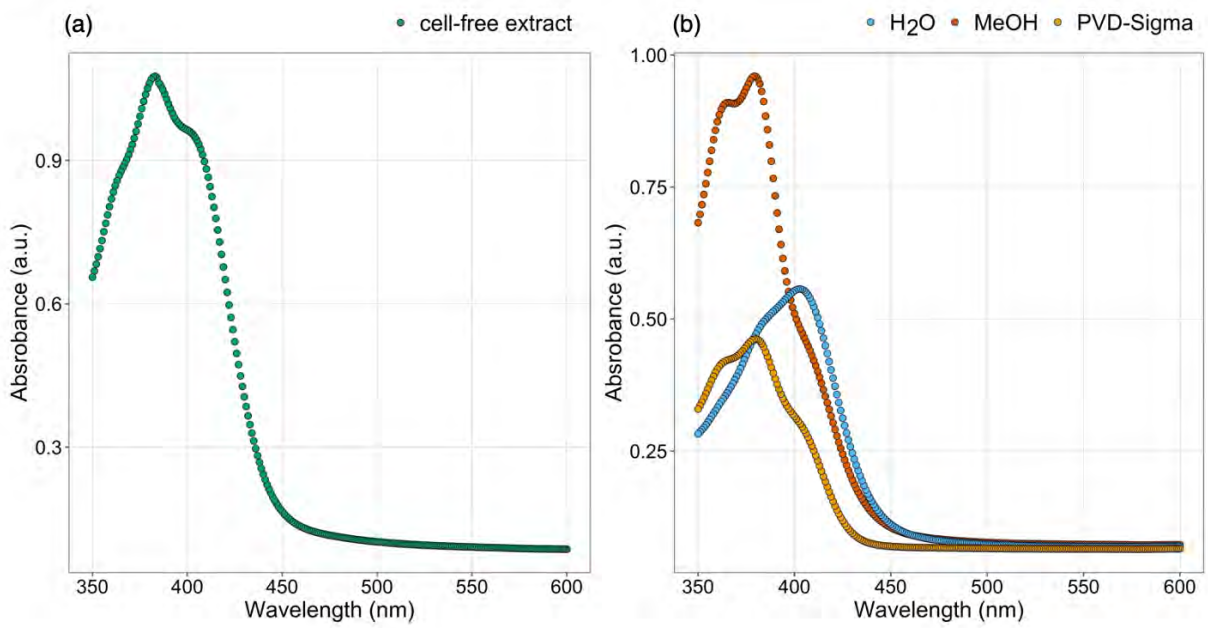

***Figure 2.7**. Spectra UV-Vis of (a) cell-free supernatant obtained from a culture of P. putida after reaching stationary phase; (b) two elutes (H_2O and 50% MeOH fractions) obtained from the cell-free supernatant of P. putida after solid-phase chromatography, compared to a commercial PVD (Sigma-Aldrich, United States).*

Mineral dissolution in presence of siderophores

Iron oxides and oxyhydroxides can be found along with iron sulfides in WAW [43]. Usually, more oxygen sensitive phases such as mackinawite are detected inside the wood, while iron(III) oxidised phases are found at the surface [43]. Regardless, all iron species present a risk for the long-term stability of wooden objects. Thus, the solubilisation of four representative iron species: goethite, hematite, mackinawite and pyrite, was studied in presence of different iron chelators. The purified mix of pyoverdines was compared to a commercial siderophore (deferoxamine mesylate (DFOM), Desferal®), and to the typically used chemical chelator, EDTA [46]. Additionally, four different buffers were tested with the different chelators.

The pH of the solution was maintained with the different buffers. Even if the buffers interacted with iron ions, the pH was stable at the adjusted pH. For HEPES and Tris-HCl buffers the pH was 7 ±0.3, and for citrate and acetate buffers the pH was 5.6 ±0.5. When no buffer was included (using Milli-Q® water only), the pH of the solution varied. In general, DFOM and PVD solutions turned from pH ~5-6 towards neutrality (DFOM: pH 7-7.7; PVD: pH 6.3-7.2). EDTA solutions presented alkaline pH (pH 8.8-9.3) at the end of the experiment time. In all families of siderophores, the formation of the complexes is clearly pH dependent. In nature, iron competes with protons (H^+) for the free siderophores, and the iron-siderophore complex will be more stable at neutral to alkaline pH [78]. On the contrary, the solubility of iron oxides increases

at more acidic pH values [47]. Here, the two selected working pHs, one in the neutrality (pH 7), and one more acidic (pH 5.6) are a compromise between the wood matrix, where very alkaline or very acidic pH can be harmful for wood components [79], and stability of siderophores and iron solid phases.

Moreover, two different buffers were selected for each pH. At pH 7, HEPES buffer was selected for not having any expected interference with iron chelation [80]. On the other hand, Tris-HCl buffer interferes with metals [80], and may have a synergic effect with the chelators under study. However, we did not observe any improvement in the dissolution of the four solid phases when using Tris-HCl buffer (Figure 2.8). In fact, for both siderophores and all solid phases, there were no significant differences between these two buffers (DFOM pH 7 HEPES vs DFOM pH 7 Tris-HCl: with hematite *p*-value = 0.5803, with goethite *p*-value = 0.2601, with pyrite *p*-value = 0.876, with mackinawite *p*-value = 0.2516; PVD pH 7 HEPES vs PVD pH 7 Tris-HCl: with hematite *p*-value = 0.9512, with goethite *p*-value = 0.962, with pyrite *p*-value = 0.01057, with mackinawite *p*-value = 0.3851). Differences were only detected with EDTA as chelator in these buffers. The dissolution of goethite, hematite and pyrite was significantly higher with HEPES buffer, while the dissolution of mackinawite was not significantly different between pH 7 buffers (EDTA pH 7 HEPES vs EDTA pH 7 Tris-HCl: with hematite *p*-value = 0.0002231, with goethite *p*-value = 2.69e-05, with pyrite *p*-value = 0.001228, with mackinawite *p*-value = 0.1275) (Figure 2.8).

At pH 5.6, both buffers selected are expected to interact with iron ions. However, we observed significant differences between citrate and acetate buffers for almost all minerals with all chelators (DFOM pH 5.6 citrate vs DFOM pH 5.6 acetate: with hematite *p*-value = 0.001868, with goethite *p*-value = 0.003242, with pyrite *p*-value = 5.078e-06, with mackinawite *p*-value = 0.0004247; PVD pH 5.6 citrate vs PVD pH 5.6 citrate: with hematite *p*-value = 0.0001484, with goethite *p*-value = 0.0002434, with pyrite *p*-value = 0.6027,withmackinawite *p*-value = 9.035e-05; EDTA pH 5.6 citrate vs EDTA pH 5.6 citrate: with hematite *p*-value = 3.112e-07, with goethite *p*-value = 1.686e-06, with pyrite *p*-value = 0.8582, with mackinawite *p*-value = 0.007234) (Figure 2.8). In general, for all solid phases, the presence of citrate in the solution enhanced the dissolution (Figure 2.8). Indeed, controls without chelator but with citrate buffer, presented amounts of dissolved iron in solution, in some cases, equal or higher than when a chelator was also present (Figure 2.8). On the contrary, the solids amounts were quite stable in the other three buffers tested and without a buffer. Only pyrite and mackinawite seemed more solubilised without a buffer being used (Figure 2.8).

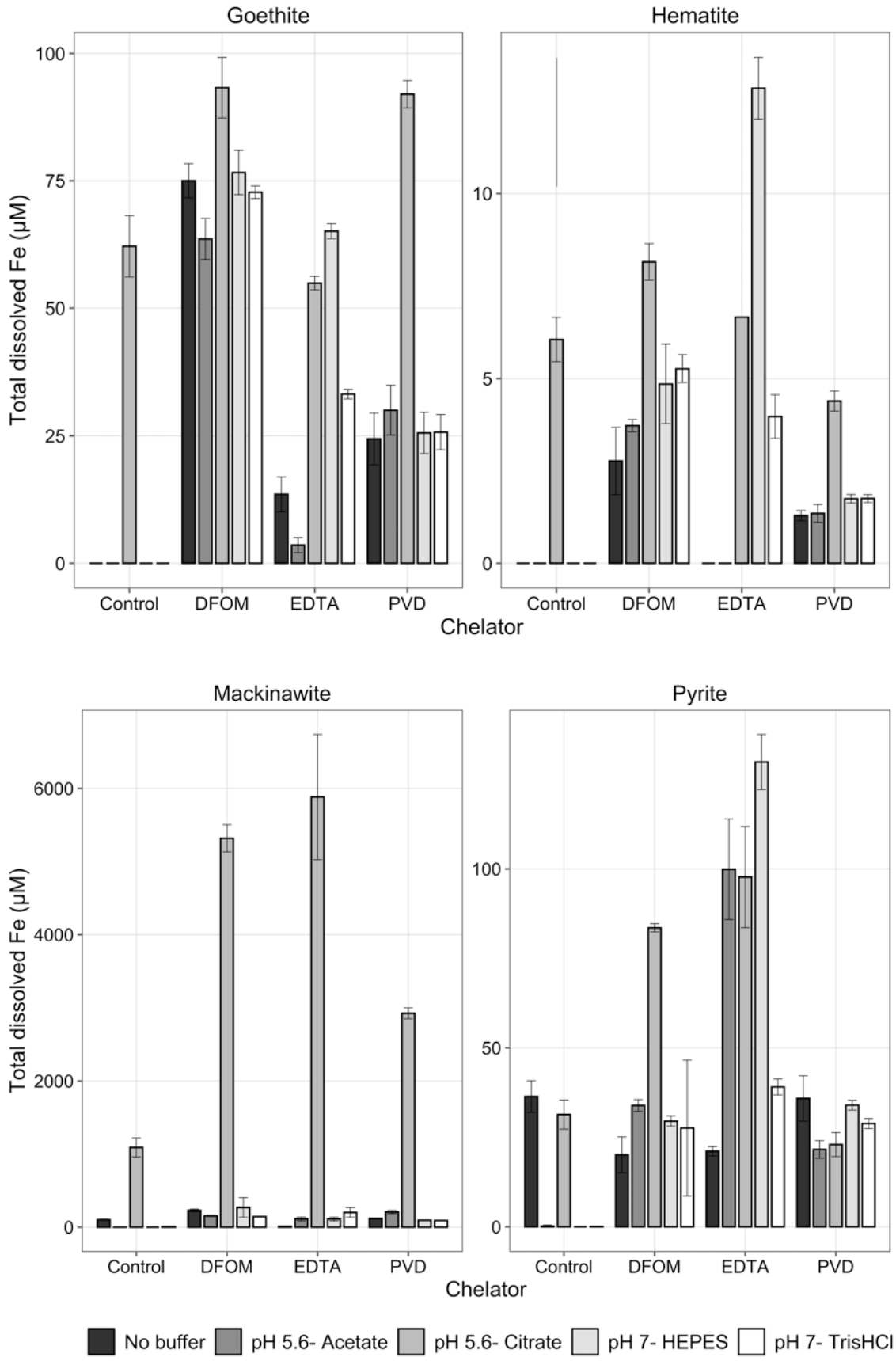

Figure 2.8. *Total dissolved Fe (µM) following addition of (1 g·L^{-1}) goethite, hematite, mackinawite, and pyrite solutions, with bacterial siderophores (purified PVDs and DFOM) and chemical chelators (EDTA), in four different buffer conditions or without a buffer. Three independent replicates were conducted.*

DFOM benefited from the synergic effect of citrate buffer. The amounts of iron detected in solution were higher using citrate buffer than with the other buffers with all minerals (Figure 8). This was also the case for the purified PVD, except with pyrite where all conditions had the same effect in the dissolution (Figure 2.8). Overall, EDTA effect was also improved with citrate buffer in respect to acetate buffer, however, in this case HEPES buffer was still giving better results, with the exception of mackinawite (Figure 2.8).

Actually, mackinawite was the less stable mineral in presence of citrate buffer, detecting iron concentrations up to ~6 mM in the solution (Figure 2.8). The values obtained with citrate buffer were between 10 to 60 times higher than with the other buffer conditions. Mackinawite solubility depends on pH in acidic conditions (pH<6). Mackinawite is highly soluble in acidic conditions, and citric acid has been used to help remove problematic mackinawite from flow lines in the oil and gas industry. Citric acid prevents the formation of insoluble iron salts [81].

Above pH 6, however, mackinawite solubility is not well understood and it is assumed to be independent from pH [82], [83]. This could explain solubility differences between acidic pH buffers and HEPES and Tris-HCl buffers, where iron solubility may be highly related to the presence of iron chelators, but not the pH. However, citrate buffer conditions still have much bigger effect than acetate buffer conditions, even both being in the acidic region. This could be explained due to differences in pK_a between these buffers. Acetate pK_a is 4.76, while citrate has three pK_a values: 3.13, 4.76 and 6.40. Citric acid has been studied for a greater chelating capacity over acetic acid, in stainless steel [84]. Hematite dissolution was also enhanced by citrate buffer in almost all cases (Figure 2.8). However, hematite was a much more stable phase (Figure 2.8). Iron concentrations in solution were not higher than 15 μM. Similar results have been observed previously, where the dissolution of goethite and other minerals was higher than hematite, in presence of *Pseudomonas* extracts [75]. Indeed, the solubility constant of hematite (K_s = –0.53) is lower than the one of goethite (K_s = 0.36) [47]. The higher stability of hematite also explains why more siderophores were produced by the bacteria (*P. putida* and *E. coli*) in presence of this mineral, in the previous section (Figure 2.2 and 2.3). Also, iron released from hematite in presence of PVD correlates with the observed above. 200 μM PVD extracted amounts of iron under the detection limit of the Ferrozine assay, but sufficient for bacterial development [58].

Goethite and pyrite presented similar results in terms of iron concentrations detected in solution. For both minerals maximum concentration value was ~100 μM (Figure 2.8). All chelators used form 1:1 complex with iron. Here, the highest iron detection was around half the value of concentration of the chelator (200 μM). Previous studies have shown similar relation of

dissolved iron/concentration of chelator, when studying the dissolution of goethite in presence of deferoxamine B [49].

Conclusion

Siderophore-producing bacteria are an interesting group of microorganisms with high potential for different applications. They are currently used to extract minerals from different ores thanks to the production of siderophores. Here, we showed how siderophores are involved in the dissolution of different iron-bearing minerals. However, depending on the mineral phase siderophores may not be needed. For instance, when the bacteria were incubated with pyrite and mackinawite, the bacteria were able to grow without the metabolic need of producing siderophores. Moreover, some bacteria, such as *S. pilosus*, may present other mechanisms to trap iron that does not need the production of siderophores. Therefore, it is important to do basic studies to figure out the best candidates for future applications. Depending on the final goal, i.e., recovery of a specific element, dissolutions of the mineral, etc., we should select one or another microorganism.

For instance, if the aim is the dissolution of iron-bearing minerals, the direct use of siderophores could be a good alternative. The siderophores tested here, DFOM and PVD, showed overall similar extraction rates to the reference iron chelator EDTA. The recovery of iron from goethite, hematite, mackinawite, and pyrite was enhanced by the presence of siderophores. Moreover, the addition of other chelating agents such as organic acids presented a synergic effect in most of the cases increasing the dissolution rate. Therefore, it has been proven that siderophores can be applied to the extraction of iron from problematic iron minerals found in WAW.

Supplementary material 2.2

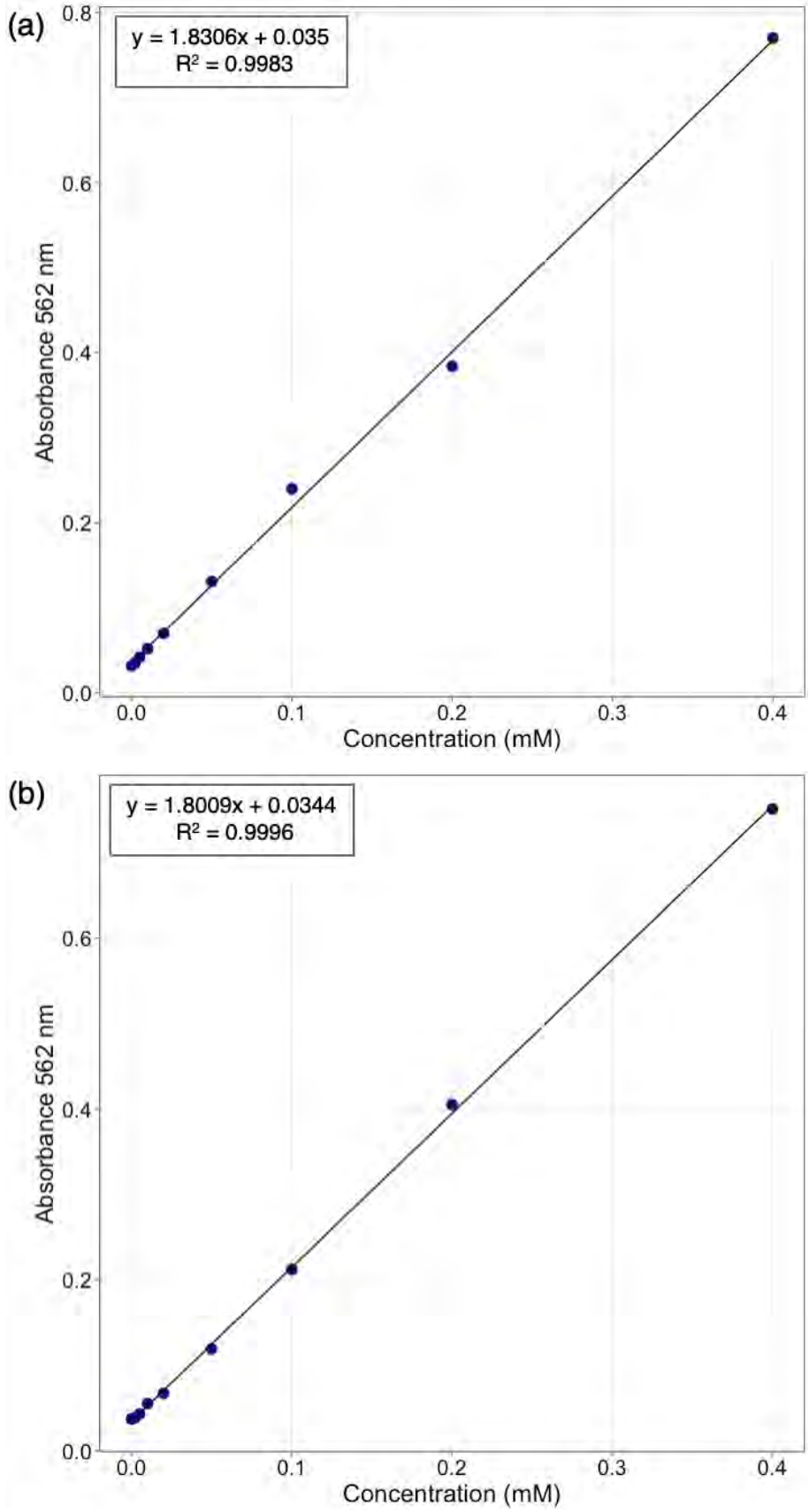

Figure S 2.2. *(a) Standard curve for calculating iron(II) concentrations via Ferrozine assay prepared with known amounts of iron(II). (b) Standard curve for calculating total iron concentrations via Ferrozine assay prepared with known amounts of iron(III) mixed with hydroxylamine-HCl.*

***Table S 2.5**. Total Fe concentrations calculated with Ferrozine assay at the end of the incubation time of the different bacteria with the minerals under study. In the experimental conditions, the levels of iron were under the detection limits in the solutions with goethite and hematite (-).*

	Goethite	**Hematite**	**Mackinawite**	**Pyrite**
	Total Fe (μM)	Total Fe (μM)	Total Fe (μM)	Total Fe (μM)
Control	-	-	35.04 ±6.67	15.88 ±1.58
Escherichia coli	-	-	35.31 ±8.54	19.21 ±5.88
Pseudomonas putida	-	-	40.68 ±5.87	14.58 ±4.65
Streptomyces pilosus	-	-	27.82 ±5.10	7.55 ±5.49
Serratia ureilytica	-	-	31.98 ±9.63	15.51 ±12.23

Values of registered absorbance and calculated concentrations ±standard deviation of three replicates

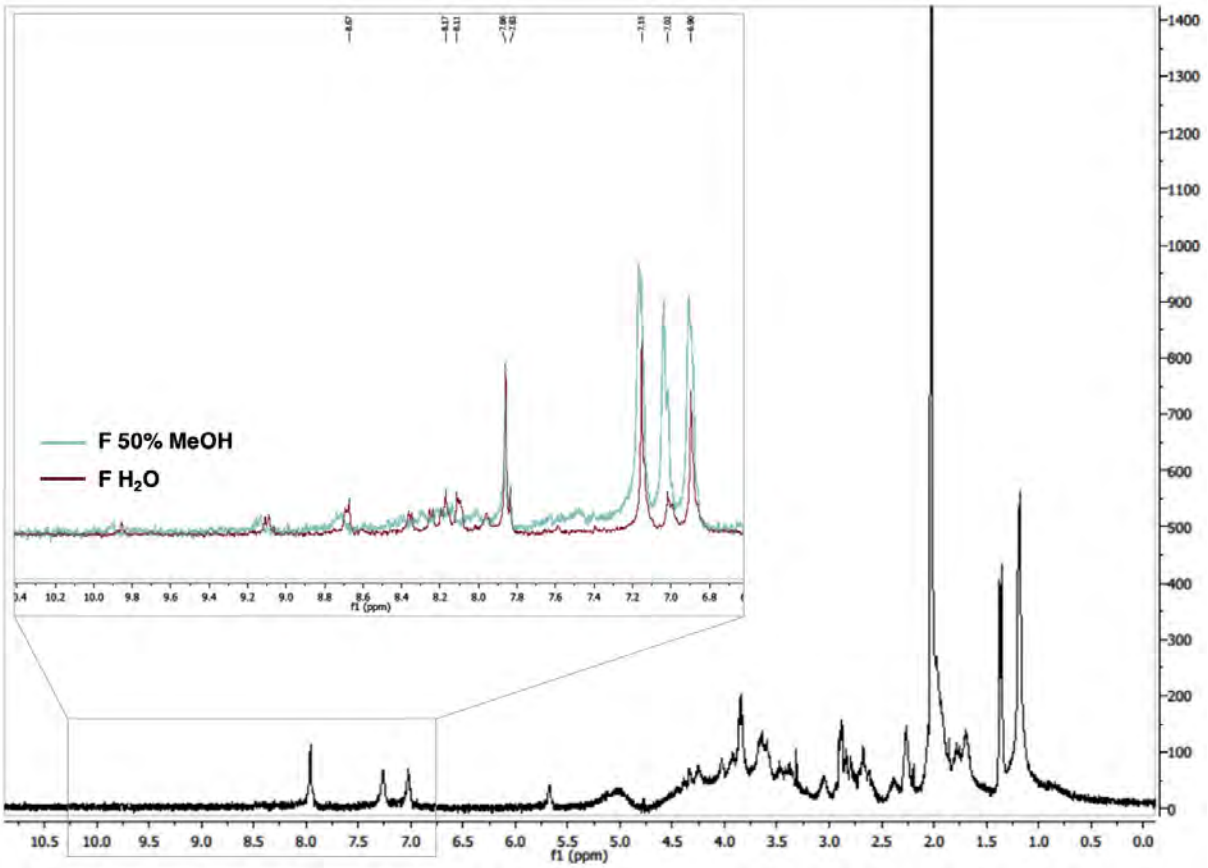

Figure S 2.3. *Comparative analysis of 400 MHz 1H NMR spectra of the two eluates obtained from PVD purification. An amplification of the side chain region is included as differences were not observed in the other regions of the spectra.*

2.3 Extraction of iron from model wood samples

Abstract

Iron species can be an issue in the long-term conservation of waterlogged archaeological wood. Current conservation procedures use strong iron chelators to extract the problematic iron from the wood. Here, we proposed to use siderophore-producing bacteria and their siderophores to solubilise iron-bearing minerals. Model wood samples were prepared by artificial contamination with iron and sulfur species. The direct use of siderophore-producing bacteria registered some effects in the model samples. However, iron extraction was very limited, and we assume that no siderophore production occur. The bacteria probably had enough available iron in solution and did not need the secretion of siderophores. On the other hand, the extraction of iron from the model samples using siderophores had remarkable results. Even though our purified siderophore (PVD) did not give the expected results, we still found promising the use of the commercial siderophore. The use of DFOM was comparable to EDTA in terms of iron extraction, and DFOM was more compatible with the wood substrate.

Introduction

In cultural heritage conservation iron ions are considered highly harmful. Paper artefacts, for example, are in danger due to the presence of iron corrosion products. In paper, iron contaminants are introduced during the manufacture, from airborne dust, due to supporting materials in contact with the paper object, or with the presence of certain inks (i.e., iron gall ink) [85], [86]. The removal of iron corrosion products is considered essential for the preservation of valuable objects. Different strategies have been proposed for the removal of iron from paper. Ferric iron can be complexed with chemical chelating agents such as EDTA, removed by acid solubilization, or reduced to the more soluble Fe^{2+} ions by, for example, sodium dithionite.

Iron-related problems have been widely investigated also in wooden heritage artefacts [87]–[89], as presented in the introduction chapter. Iron-contaminated wood is common since wooden objects are frequently associated with iron parts (e.g., nails, etc.) employed as fixation materials. Iron in waterlogged wood can be present in both oxidation states, Fe^{2+} and Fe^{3+}. The most frequent types of iron compounds in waterlogged wood are various iron(III) hydroxides and oxides (e.g., goethite and lepidocrocite) along with iron(II) salts and iron in reduced sulfur compounds such as pyrite and pyrrhotite. The presence of iron compounds is a problem in preservation of waterlogged archaeological wood and induces three main threats. First, salts

precipitation as consequence of oxidation of iron sulfides can lead to mechanical damage [90]. This oxidation may generate acids, which can lead to hydrolysis of polysaccharides and thus degradation of wood. Finally, the participation of iron in Fenton-type reactions. Therefore, it is essential to extract the problematic iron compounds before any further treatment being applied to the wood.

In the same manner than paper artefacts, wooden objects are an important part of the human historical patrimony. In consequence, extraction treatments have been proposed to remove iron from wood matrix (refer to chapter 1). Mainly, strong iron chelators have been used. New trends are opting for less toxic and greener methods in the field of conservation. Siderophores could be stablished as bio-based solution for the chelation of iron in iron-contaminated organic materials. Already a few studies have mentioned them as possible solution for iron contamination in paper and wooden artefacts [91]–[93]. Rapti et al. (2017) compared the efficacy of DFOM, EDTA, and DTPA, being DFOM the more effective in removing iron corrosion products from wooden cubes artificially stained.

At this stage of the research, the aim was to investigate the possible application of the selected bacteria directly to model wood samples contaminated with iron species, mostly iron sulfides. Furthermore, the efficiency to extract iron from model wood samples contaminated with iron species of our bacterial extract of PVD was compared to the commercial siderophore Desferal® and EDTA. The safety of applying siderophores to wooden objects was evaluated here always in comparison to the chemical chelator EDTA.

Materials and Methods

Model wood samples

Balsa (*Ochroma pyramidale*) wood cubes with the following dimensions: 1×1×1 cm^3, were prepared to reproduce the characteristics of waterlogged wood. The samples were impregnated with iron and sulfur solutions by immersing them in 1 L iron(II) chloride tetrahydrate (0.5 M $FeCl_2 \cdot 4\ H_2O$) solution under vacuum (-600 mbars) for 4 h. The samples were dried overnight at 45 °C. Afterwards, the samples were immersed in a solution of hydrated sodium sulfide (0.5 M $Na_2S \cdot nH_2O$) under vacuum (-600 mbars) for also 4 h. Samples were kept immersed in N_2-flushed water. Before any experimental procedure, cubes samples were washed by ultrasonic bath until no more impregnation solution was released and conductivity values closed to deionized water.

Extraction of iron from wood using siderophore producing bacteria

Serratia ureilytica (strain Lr5/4), *Escherichia coli* (strain K12), *Pseudomonas putida* (strain 90), and *Streptomyces pilosus* (strain ETH 11686) were pre-cultured in MM9 medium three times before inoculation of the experiment to assure no iron presence. After, 60 mL of MM9 were inoculated from the last pre-culture to a final volume of 1% (v/v). One model wood cube was included per bottle. Cultures where incubated at 28 ºC (±2 ºC) and 120 rpm. Controls without any bacteria were conducted. Three independent replicates of controls and samples were carried out. Samples were taken over time from the cultures to measure: 1) the growth of the bacteria by increase in the Optical Density (OD) at 600 nm, or in mass, in the case of *S. pilosus*, 2) the siderophore production, and 3) the levels of iron, sulfates, and other anions in solution.

CAS (Chrome Azurol Sulfonate) assay [1], was used for general determination of the concentration of siderophores in the extract of the bacteria. We followed the procedure of Alexander and Zuberer (1991) (see section 2.1). Pyoverdine (PVD) production was registered following the absorbance at 400 nm ($\varepsilon_{400\ nm}$ $1.85 \cdot 10^4$ $mol \cdot L^{-1} \cdot cm^{-1}$ [23]). Absorbance values were registered with a 96-well microplate reader (Asys UVM 340 Microplate Reader, Biochrom Ltd, United Kingdom).

Extraction of iron from wood using purified siderophores

Wood cubes artificially contaminated were treated with the previously purified PVDs (section 2.2), the commercial siderophore, DFOM (purchased as Desferal®, Novartis, Switzerland), and the chemical chelator, EDTA. The final concentration of the chelating agent was 10 mM. The extraction was conducted in HEPES buffer (pH 7) and citrate buffer (pH 5.6), and in no buffered solution. All solutions were prepared with Milli-Q® water. Wood samples were extracted at room temperature under orbital agitation (100 rpm) for 15 days. Light was avoided using aluminium foil. Samples were taken over time for further analysis.

Analytical methods

Colorimetric measurements

A Minolta CM-508D spectrophotometer was used for the colour measurements, with the following parameters: Specular Component Included (SCI), Illuminant D65 (daylight containing UV component, colour T 6504K), d/8° geometry, 10° observer, measurement area diameter 10 mm, illumination with Xe flashlight source 100% UV containing all UV components or 0% UV containing no UV components, CIELab 1976 colour space. On each

wood sample, a measurement was carried out on the centre of three faces (i.e., three measurements per cube). Measurements were carried out on fresh, artificially contaminated, treated and control wood samples.

Inductively Coupled Plasma-Optical Emission Spectrometry (ICP-OES)

Total iron and sulfur concentrations were determined in the solutions of the different extraction experiments using Inductively Coupled Plasma-Optical Emission Spectrometry (ICP-OES). Samples were filter, diluted and then analysed with an Optima 2100 DV (Perkin-Elmer, United States) optical emission spectrometer. Specific parameters applied are described in the previous section.

Ion chromatography (IC)

Sulfates (SO_4^{2-}), phosphates (PO_4^{3-}) and other anions concentrations were measured by ion chromatography (Dionex ICS-1600). The instrument was equipped with a conductivity detector, a Dionex Ion Pac™ AS14A (4 x 250 mm) anion exchange column, and a Dionex Ion PacTM RFIC™ (4 x 50 mm) guard column. A solution of 8 mM Na_2CO_3 and 1 mM $NaHCO_3$ was used at a flow rate of 1.3 $mL \cdot min^{-1}$ as mobile phase. The detection limit was 0.05 $mg \cdot L^{-1}$. Before analysis samples were filtered with 0.22 µm PVDF filters (BGB Analytik, Switzerland) and then correctly diluted. Data was analysed with the Chromeleon™ software (Thermo Fisher Scientific, United States).

pH measurements

A 691 pH Meter Metrohm (Metrohm AG, Switzerland) was used to control the pH of the solution over time with an ionic electrode (unitrode 6.0259.100) calibrated between pH 4 and pH 7 or pH 7 and pH 9 buffer solutions. The pH of the cubes was measured with a surface electrode (flat membrane electrode 6.0256.100), also correctly calibrated, at the beginning and end of the experiment.

Raman spectroscopy

A Jobin Yvon Horiba™ spectrophotometer coupled with Olympus BX41 microscope (Horiba Ltd., Japan) was used for measurements. Spectra were recorded at a wavelength of 632 nm, hole of 800 µm, slit of 200 µm, 100-1200 cm^{-1} range, filter 25%, 50xLWD objective and 5 sec of acquisition with 10 accumulations. The spectra were processed with LabSpec® 5 software (automatic baseline correction). Reference spectra from spectra libraries and literature were used to identify the compounds formed. Measurements were carried out on the surface of impregnated, treated and control wood samples.

Scanning Electron Microscopy coupled with Energy Dispersive X-Ray Spectroscopy (SEM-EDS) analyses

Wood samples treated with siderophore producing bacteria were rinsed after the incubation time, and small slices were obtained using a razor blade. Wood segments were fixed at RT with 3% (v/v) glutaraldehyde solution in 0.1 M sodium cacodylate (pH 7.2) for 3h, washed twice and then dehydration steps were performed using different concentrations of ethanol (25%, 50%, 75%, 90%, 100% (v/v)) and then pure acetone. Finally, samples were dried in a CO_2 atmosphere.

Samples were mounted on stubs using carbon conductive tape. Samples were examined under low vacuum without coating using a Thermo Scientific™ Scios™ 2 DualBeam™ (Thermo Fisher Scientific, United States) equipped with an energy-dispersive X-ray analyser (EDAX, United States). Afterwards, the same samples were coated with a layer of gold using a Leica EM SCD050 (60 mA current, 5 cm, 5 s duration, argon gas), and examined again at high vacuum using the same instrument. The samples were observed using an EDT detector (secondary electron acquisition), an acceleration potential of 10 kV and 7 mm working distance.

Interaction of siderophores with analogues of wood

Degradation of p-nitrophenyl-β-D-glucopyranoside

The degradation of *p*-nitrophenyl-*β*-D-glucopyranoside (pNPG) was determined by monitoring the release of *p*-nitrophenol (pNP). pNPG has been widely used to study *β*-glucosidases and degradation of cellulose [94]. If pNPG breaks down, pNP is released and this molecule can be easily monitored in the supernatant with an absorbance occurring at 410 nm.

Following a previously described method [24], the reaction mixture consisted of 1.6 mL of pNPG 0,1% (w/v) (Sigma-Aldrich, Switzerland) in sodium acetate buffer 50 mM pH 5, 200 µL of 2 mM iron chelator, 100 µL of 40 mM H_2O_2 and 100 µL of 4 mM $FeCl_3 \cdot 6H_2O$ (freshly prepared). The mixtures were incubated in a water bath (50 °C) for 56 h, samples were taken at 0, 1, 3, 5, 7, 24, 30, 48, and 56 h. Samples were immediately mixed with 10% sodium bicarbonate in a 2:3 ratio and absorbance measured. Basic pH slows the enzymatic reaction and enhances the colour of the pNP released during the reaction. Samples included Fe^{3+}/H_2O_2 to evaluate if the iron chelators participate in the production of reactive oxygen species (ROS) by Fenton reaction, and if these species are the responsible for the breakdown of pNPG.

Several controls were set up: 1) containing no iron chelators but only H_2O_2 and Fe^{3+}, 2) containing siderophores but not H_2O_2 and Fe^{3+} and 3) only the substrate, pNPG, in sodium

acetate buffer. All samples were run in triplicates. Absorbance was measured with a UV-Vis spectrophotometer (Lambda 25 Perkin Elmer, United States).

Degradation of Remazol Brilliant Blue R (RBBR)

RBBR is a dye used as an indicator of ligninolytic activity. The degradation of RBBR was studied following the ratio between the maximum absorbance of the dye at 590, with a reference absorbance value at 500 nm (Abs 590/Abs 500). The reaction mixture consisted of 1.6 mL of RBBR 0,01% (w/v) (Sigma-Aldrich, Switzerland) in sodium acetate buffer 50 mM pH 5, 200 µL of 2 mM iron chelators, 100 µL of 40 mM H_2O_2 and 100 µL of 4 mM $FeCl_3 \cdot 6H_2O$ (freshly prepared). The mixtures were incubated in a water bath (50 °C) for 48 h, samples were taken at 1, 3, 5, 7, 24 and 48 h and measured. As above, Fe^{3+}/H_2O_2 were included to evaluate the production of ROS. Same controls as before were carried out. All samples were run in triplicates. Absorbance was measured with a UV-Vis spectrophotometer (Lambda 25 Perkin Elmer, United States).

Statistical analyses

One-way ANOVA was used to calculate the significance of the data in the extraction of iron from artificially contaminated wood for each chelator employed (2 replicates, n = 2). Student's t-test was used to calculate significant differences in the RBBR degradation analysis. Both analytical tests were conducted in Microsoft® Excel (Version 16.43). The statistical significance threshold was set to 1%.

Results and Discussion

Extraction of iron using siderophore-producing bacteria

Many examples show the feasibility of using living microbes for the conservation of cultural heritage (see Chapter 1.5). Here, the first approach to extract iron from contaminated waterlogged wood was the direct use of four selected bacterial strains (*E. coli*, *P. putida, S. pilosus* and *S. ureilytica*). As seen previously, these bacteria showed the capacity to produce siderophores that helped the dissolution of iron mineral phases and, therefore, were further tested in model samples of waterlogged archaeological wood (WAW).

Figure 2.9. *Visual appearance of the wood cubes after incubation with siderophore-producing bacteria. Balsa wood was artificially impregnated with iron sulfides, and then treated with E. coli, P. putida, S. pilosus and, S. ureilytica. Control M refers to the cube incubated in MM9 medium without bacteria.*

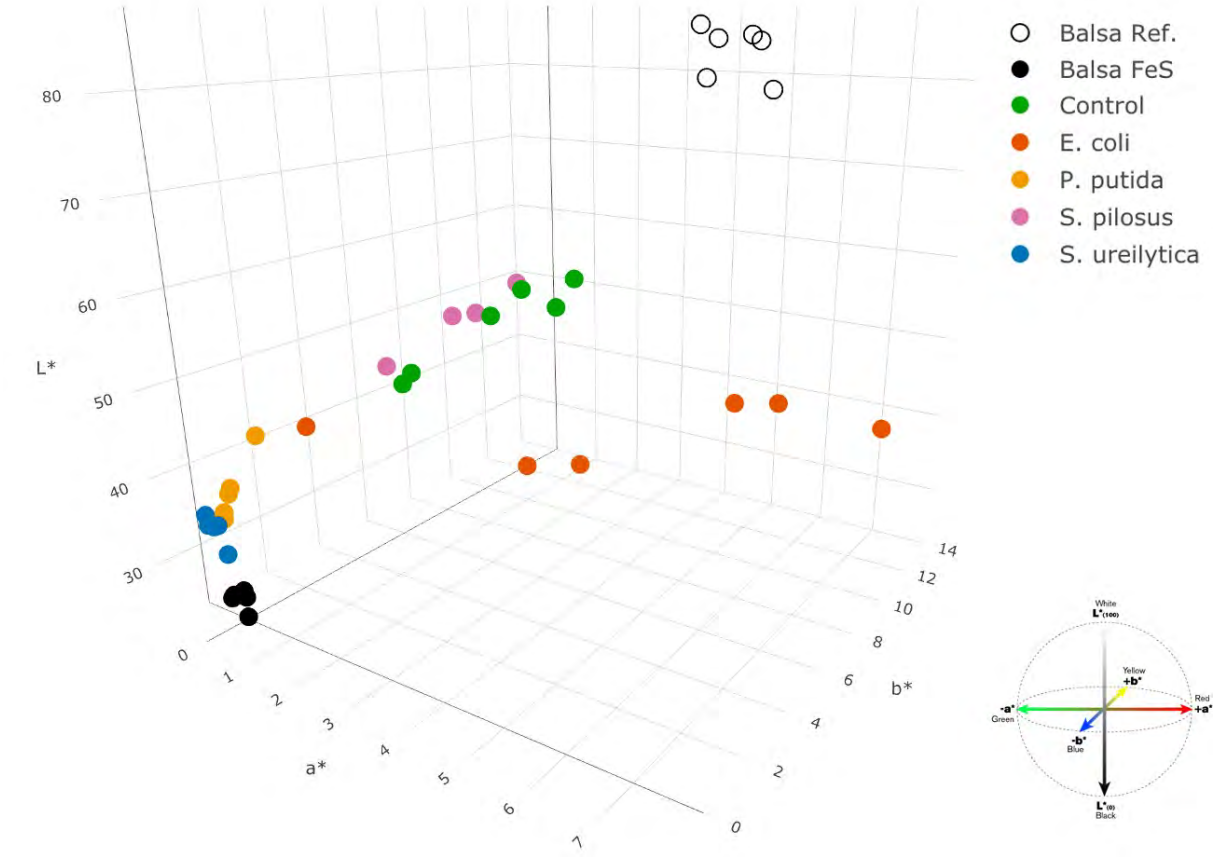

Figure 2.10. *Colorimetry plot representing colour coordinates: L* (lightness/bright-dark), a* (red/green opponent colours) and b* (yellow/blue opponent colours). Colour measurements were taken on the wood surface of all samples after the incubation time. Wood cubes were treated with E. coli, P. putida, S. pilosus and, S. ureilytica. Control M refers to the cube incubated in MM9 medium without bacteria. Fresh balsa (Balsa Ref.) and balsa impregnated with iron sulfides (Balsa FeS) are included as reference.*

Balsa wood was selected to prepare artificially contaminated waterlogged wood as it presents a similar porosity to WAW. Moreover, its light colour facilitates monitoring the colour variation of the samples during the contamination protocol [95]. The goal of the artificial contamination is to obtain iron sulfides (i.e., greigite, mackinawite and pyrite) within the wood, and also decrease the holocellulose content to achieve similar characteristics to WAW. The preparation of similar model samples has been reported in previous studies for the assessment of extraction methods [46], [88].

The four bacterial strains were able to grow in presence of the model wood (Figure S 2.4), in growth medium MM9 (Table S 2.3). However, the exact growth of *S. pilosus* was impossible to follow. This bacterium grew attached to the surface of the wood, and sampling to measure the increase of mass over time was not feasible.

E. coli and *S. ureilytica* presented a fast growth arriving to stationary phase after 13-17 h. *P. putida* took over 30 h to arrive to stationary phase (Figure S 2.4). Growth was faster than observed previously with minerals, but differences could be due to a more active inoculum. Like in the previous experiment with pure mineral phases, the pH of the solution was adjusted at 6.8 to favour bacterial development and siderophore production. However, in presence of the artificially contaminated wood, no siderophores production was registered for any of the bacteria using CAS assay. The absorbance at 630 nm did not decrease over time. The presence of iron in solution could explain the lack of siderophores production. Iron in solution can be present as residual from the artificial contamination solution, or as partial dissolution of the minerals formed. Indeed, total iron levels measured with ICP-OES at the end of the experiment revealed some iron in solution (see below).

However, even though there was no detectable production of siderophores, the bacteria had a clear visual impact on the wood cubes (Figure 2.9). After the impregnation protocol, model wood samples presented a dark hue (Figure 2.9). Colorimetric analyses plotted the model wood samples near the 0.0.0 (L* a* b*) coordinates (Figure 2.10). Iron and sulfur species are responsible for the dark colour of WAW [70]. The extraction or transformation of these species may translate into a change in colour. For instance, after rinsing and removing the biomass, cubes extracted with *S. pilosus* presented a grey-yellowish hue (Figure 2.9). The appearance of *S. pilosus*-treated cubes to the wood in the control without bacteria (control M), as confirmed on the colorimetric plot (Figure 2.10). Therefore, we assume that the colour changes in these cases were most likely due to abiotic reactions, not to the effect of microorganisms (*S. pilosus*). On the contrary, *E. coli* treatment made the cubes turn towards a reddish tonality (Figures 2.9

and 2.10). An oxidation of iron sulfides forming iron oxides could have been the cause for this colour change [46]. Finally, treatment with *P. putida* or *S. ureilytica* kept unchanged the black colour of the artificially impregnated wood samples (Figure 2.9 and 2.10). Only, *P. putida* presented some greyish areas, especially at the edges of the cubes (Figure 2.9).

Colour changes may be a result of the transformations of the mineral phases occurring in the model wood. Raman spectroscopy allowed us to determine some of the phases formed. Mackinawite (FeS) and greigite (Fe_3S_4) were identified in artificially contaminated samples after the impregnation protocol (Figure S 2.5). The Raman shifts at 255 and 290 cm^{-1} are attributed to partially-oxidized mackinawite [96]. Furthermore, the presence of greigite, with corresponding vibrational bands at 354 and 363 cm^{-1}, can be a confirmation of the partial oxidation of mackinawite, as it is a product of this reaction [97]. In addition to iron sulfides, elemental sulfur (α-S_8) was also identified with vibrational bands at 150, 219 and 473 cm^{-1} [43] (Figure S 2.5).

Mostly elemental sulfur was detected by Raman spectroscopy in all wood samples after incubation with the different bacteria (Figures 2.11, 2.12, 2.13, 2.14 and 2.15 and Table S 2.6). However, the relative intense Raman shifts observed for elemental sulfur made difficult the correct identification of other phases. For instance, hematite (Fe_2O_3) and lepidocrocite characteristic bands appear at 225 and 250 cm^{-1} [98], respectively, that could be covered by those of elemental sulfur in the same region (220 and 248 cm^{-1}) [43].Other phases occurrence could also be underestimated due to the strong intensity of elemental sulfur.

In fact, complementary SEM-EDS analyses revealed that not only sulfur was present on the wood surface after incubation with the different bacteria. On the *S. pilosus*-treated samples, for example, analyses of surface areas showed precipitates that were mainly composed by iron and phosphorous (Figure 2.12). Iron phosphates are yellowish precipitates, what could explain the colour change these cubes (Figure 2.9). Some studies have shown that in presence of phosphates, iron and sulfur species are highly reactive [82]. Iron(III) phosphates are able to react with sulfides (S^{2-}) leading to elemental sulfur and iron(II) phosphates [99]. These transformations would explain the co-detection of elemental sulfur (by Raman spectroscopy), iron and phosphorous (by EDS).

Similar results were observed with the control samples (control M). The cubes had an identical appearance to *S. pilosus* cubes (Figure 2.9). SEM-EDS revealed phosphorous and iron on cross-sections (Figure 2.11 and S 2.5), along with elemental sulfur detected by Raman analysis.

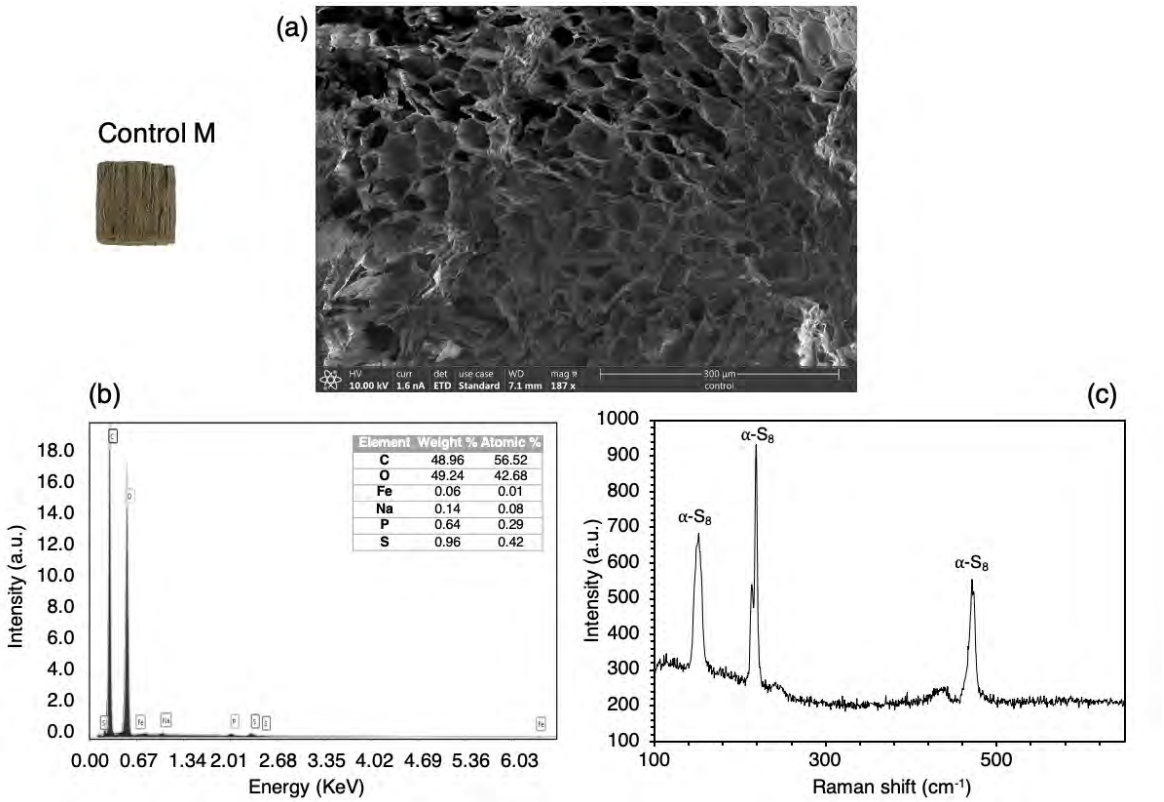

Figure 2.11. *(a) Secondary electron micrograph of a cross-section of the control wood sample. (b) EDS spectrum of a whole cross-section area. (c) Raman spectrum obtained from the surface of the control wood sample. Characteristic Raman shifts of elemental sulfur (α-S_8) are tagged.*

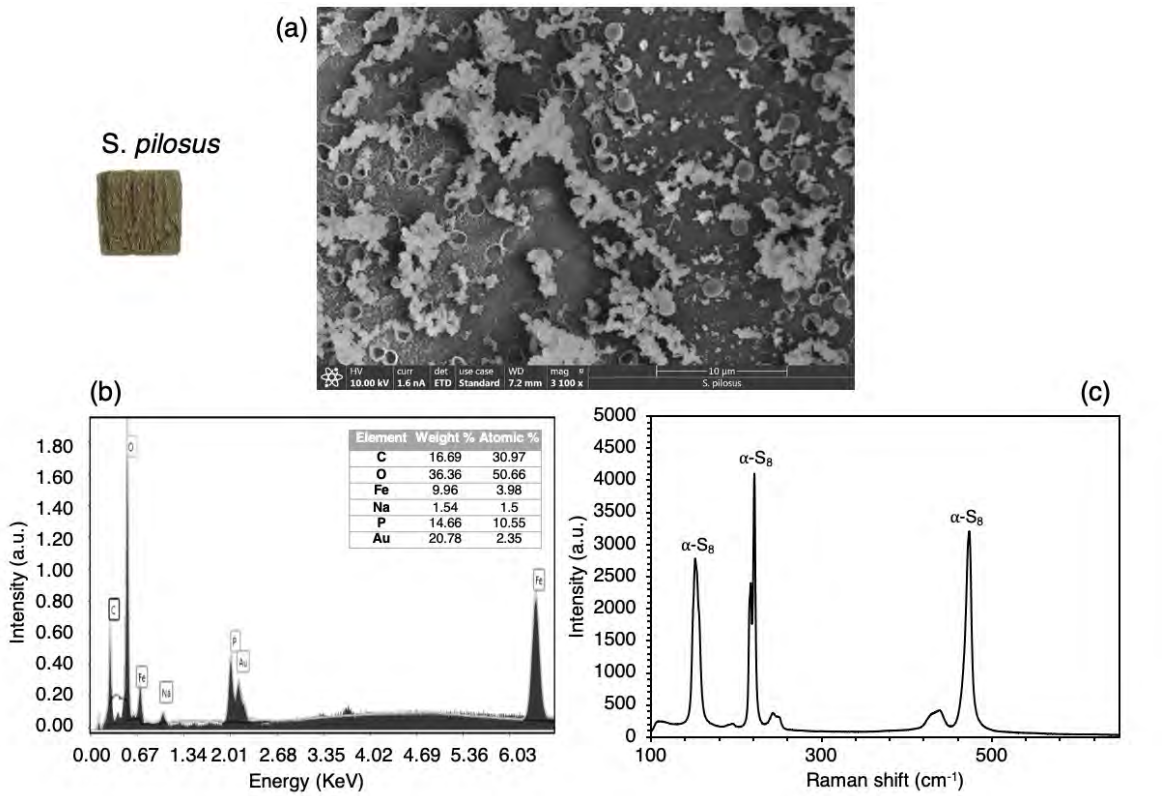

Figure 2 12. *(a) Secondary electron micrograph of precipitates found on the surface of wood samples treated with S. pilosus. (b) EDS spectrum of the solid phase. (c) Raman spectrum obtained from the surface of the wood sample. Characteristic peaks of elemental sulfur (α-S_8) are tagged.*

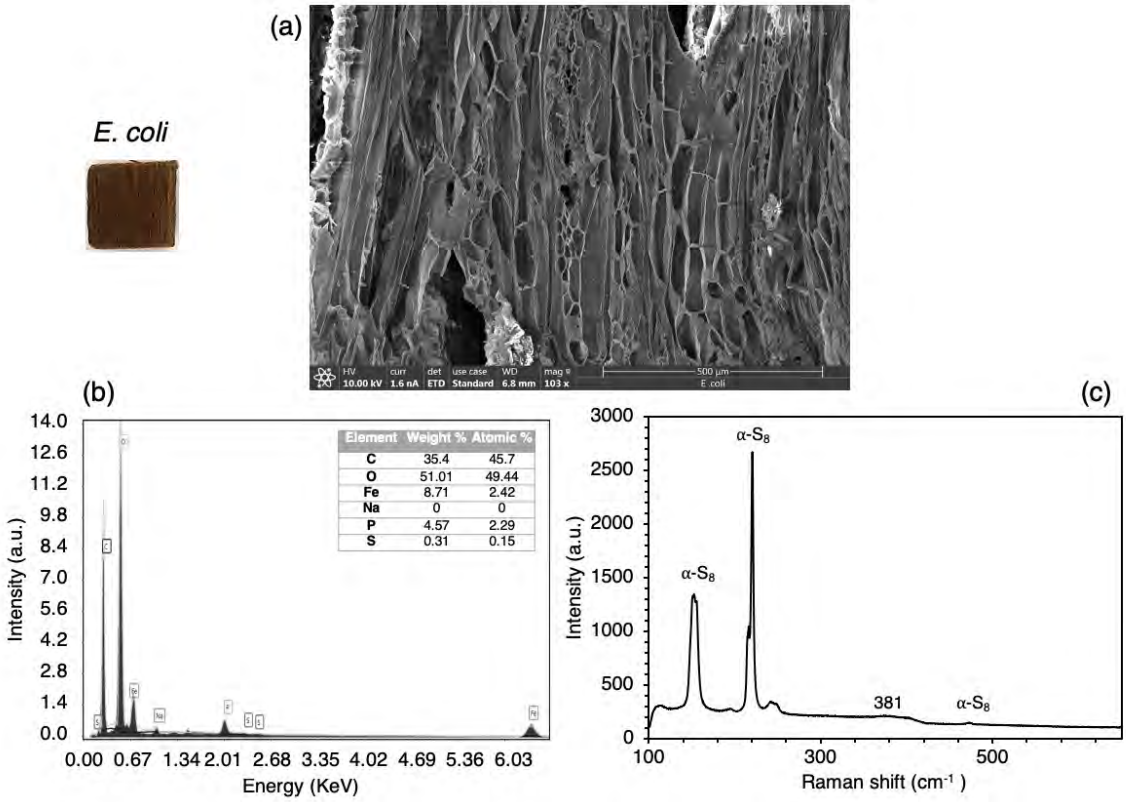

Figure 2.13. *(a) Secondary electron micrograph obtained from a tangential section of E. coli wood samples. (b) EDS spectrum of a superficial tangential cut. (c) Raman spectrum obtained from the surface of the wood sample. Characteristic peaks of elemental sulfur (α-S8) are tagged.*

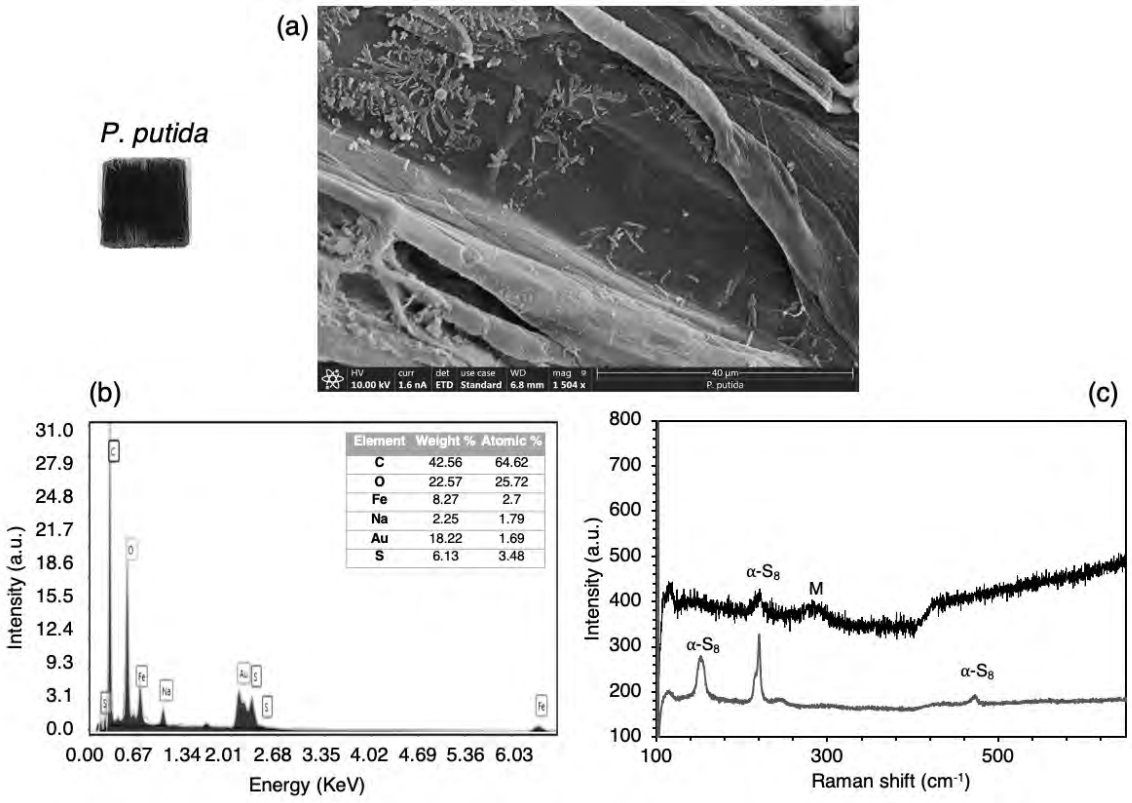

Figure 2.14. *(a) Secondary electron micrograph of precipitates found on the wood samples treated with P. putida. (b) EDS spectrum of the precipitates. (c) Raman spectra obtained from the surface of the wood sample. Characteristic peaks of elemental sulfur (α-S8) and mackinawite (M) are tagged.*

Other less registered bands also occur in Raman analyses. On the samples treated with *E. coli*, a small peak at ~381 cm^{-1} was registered (Figure 2.13). This band could be attributed to goethite (α-FeOOH) [98], or pyrite [43], or to cellulose [100]. In fact, this peak has been currently detected in our Raman analyses, therefore we assumed that must correspond to wood components as it was detected in all types of samples. Still, the strongest goethite band occurs at 385 cm^{-1} [101]. Other shifts could be covered by sulfur bands or, the relative intensity could be underestimated due to the strong intensity of elemental sulfur. In this case, considering the red coloration that *E. coli*-treated cubes acquired (Figure 2.9), the peak could be assigned to goethite. Indeed, complementary SEM-EDS analyses on *E. coli* wood cubes showed that on surface, where the colour of the cube had a red tonality, iron was the most abundant element after oxygen and carbon (Figure 2.13). Moreover, Raman spectroscopy did not detect the presence of iron sulfides on the surface of the cubes after incubation with this bacterium. An oxidation of iron sulfides on surface is likely to have occurred here (Figure 2.13). On the contrary, inner cuts of the *E. coli*-treated wood exposed a black interior. ESD analysis of this area showed mostly sulfur (Figure S 2.6).

After incubation, just some bands at 284 and 308 cm^{-1}, related to iron sulfides (mackinawite) [96], were detected in *P. putida* and *S. ureilytica* wood samples, respectively (Figure 2.14 and 2.15). The persistence of these species on the wood surface of these cubes could explain why these woods kept the dark hue (Figure 2.9). Moreover, elemental sulfur intensities registered with Raman in *P. putida*- and S. *ureilytica*-treated wood were much lower than in the other woods. The elemental sulfur here must remain from the artificial contamination protocol, while in the other cubes, new precipitation of elemental sulfur could have happened, as discussed above.

Indeed, SEM-EDS analyses on the surface of the wood cubes extracted with *P. putida* showed some mineral formation mainly composed of iron and sulfur, that correlates with the mackinawite detected by Raman spectroscopy (Figure 2.14). Sodium also detected can come from the artificial impregnation solution. In the same SEM micrograph, we can observe some bacteria cells, proving the capability of the bacteria to grow within the wood (Figure 2.14). Wood cubes extracted with *P. putida* only presented slight changes with respect to before treatment at some edges. Analyses in that region also showed some phosphorous amounts (Figure S 2.7).

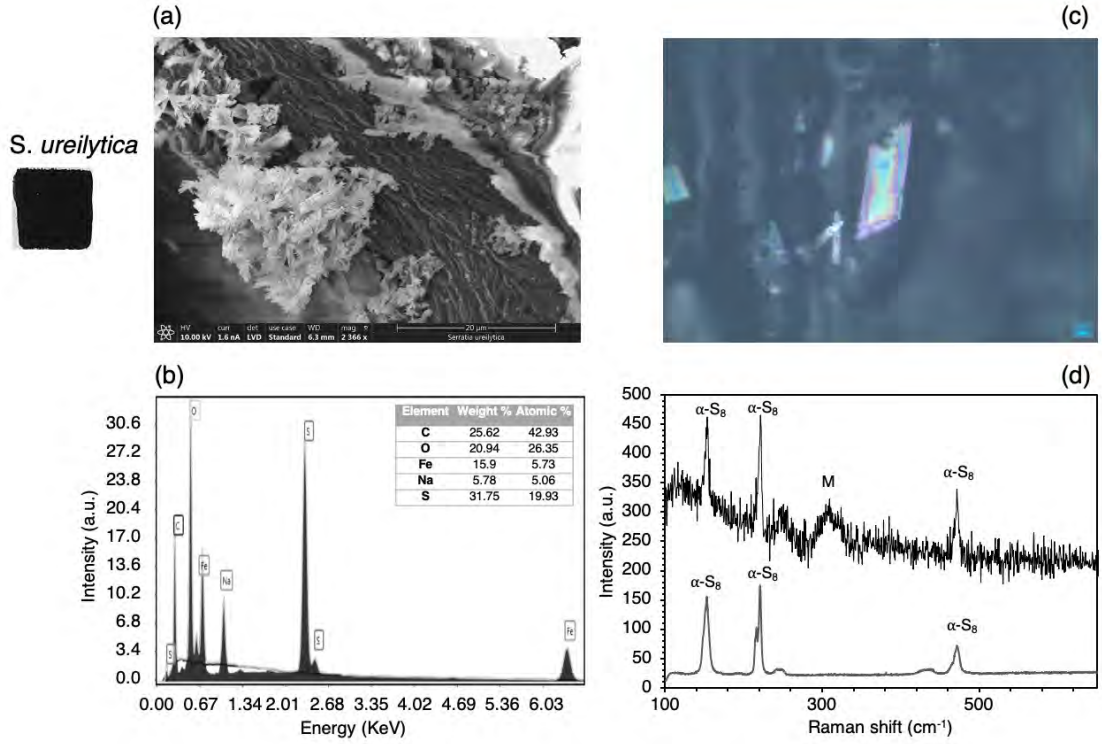

***Figure 2.15**. (a) Secondary electron micrograph of precipitates found on the wood samples treated with S. ureilytica. (b) EDS spectrum of the solid phase. (c) Raman microscopy image of a crystal-like found on the surface of the wood cubes treated with S. ureilytica. (d) Raman spectra obtained from the surface of the wood sample. Characteristic peaks of elemental sulfur (α-S8) and mackinawite (M) are tagged.*

Wood samples treated with *S. ureilytica* remained exactly as before treatment. The only difference was the emergence of small crystal-like aggregates over the surface (Figure 2.15). SEM-EDS analyses also detected the formation of aggregates, with chemical composition of sulfur, iron and sodium (Figure 2.15). However, Raman characterisation of these compounds was difficult as, even using a filter to decrease the laser energy impulse, these aggregates were decomposing during analysis. Iron sulfides, such as mackinawite, pyrite, or greigite have been detected previously with Raman spectroscopy [42], [43]. Here, we still detected mackinawite (Figure 2.15). Then, it is possible that these compounds are other sulfur and iron phases that cannot be detected under the experimental conditions applied. For example, $NaFeS_2$ could have been formed [102], as the artificial contamination of the samples is done using a solution of $Na_2S{\cdot}nH_2O$ and sodium was detected by EDS. Further characterization with X-ray diffraction (XRD) is needed for identification [103].

Previous studies have suggested the dual role of microorganisms in corrosion [104]. As commented in the introduction chapter, microbes drive the elemental cycles on Earth, and are involved in many different pathways. In fact, *Pseudomonas* and *Serratia* species have previously shown prevention of microbiologically influenced corrosion (MIC). Their

metabolisms prevented other microorganisms from corroding steel [105]. In a similar way, these bacteria could have prevented here the oxidation of iron sulfides, keeping the original appearance of the artificial contaminated wood, especially *S. ureilytica*-treated cubes (Figure 2.9).

The different bacteria had clear diverse effects on the treated wood. Analyses of the solutions helped to better understand what occurred. For example, phosphates are present in MM9 medium with an initial concentration of 210 $mg \cdot L^{-1}$. IC analyses revealed that at the end of the incubation time, no phosphates remained in the solutions of the control M and *S. pilosus* (Table 2.2). This could corroborate the hypothesis that the changes in these cubes are due to the formation of iron phosphates. Phosphates also decreased from the original concentration in the other bacterial solutions (Table 2.2). Indeed, some phosphorous was still detected in *E. coli* and *P. putida* samples (Figures 2.13 and S 2.7). Moreover, these bacteria are known to accumulate polyphosphates, also explaining the drop in phosphates in the solutions [106], [107]. *S. ureilytica* solutions also registered a decrease in phosphates over time. At the end of the experimental time, half the amount of phosphates was measured in the solutions in respect to the original concentration of 200 $mg \cdot L^{-1}$. As no phosphates were detected within the wood by EDS, this bacterium must have also used phosphates for growth and/or reserve.

Sulfates were detected by IC at the end of the incubation time. This could mean oxidation of sulfur species present in the wood by the bacteria. However, the amounts of sulfates were similar between all bacteria solutions and the control M (Table 2.2), indicating abiotic oxidation. Finally, total iron levels were also measured in solution using ICP-OES. No iron was detected in the solutions of the control M, while iron was measured in the solutions with the bacteria (Table 2.2). Siderophore production was not detected with CAS assay for any bacteria. In these conditions, other iron acquisition systems may have participated. There are systems that operate under iron sufficiency (>10 μM) [31]. Moreover, oxidation of iron sulfides to iron oxides in *E. coli*-treated cubes could explain why *E. coli* solutions presented the highest amounts of iron in solutions [108] (Table 2.2). Still, iron levels registered here were much lower than the extracted levels by isolated iron chelators in the next section.

The use of some of the bacteria, like *P. putida* or *S. ureilytica*, or phosphates in the medium composition, as seen in the control M and *S. pilosus*, could be beneficial as we have seen that the phases formed were less subjected to abiotic oxidation. *S. ureilytica*-treated wood samples kept the original dark appearance for over months, while untreated samples oxidise quickly in water. Therefore, some of the bacterial treatments may allow a stabilisation of the compounds

present. Current WAW treatments already target stabilisation of iron sulfides and wood parts, preventing the formation of harmful acids with extraction methods and/or neutralisation processes [109]. In the long-term perspective it would be better to extract the harmful iron and sulfur species as much as possible [70]. However, when extraction is difficult and time-consuming, parallel stabilization can have interesting outcomes.

***Table 2.2**. Total iron, sulfates and phosphates detected in solution at the end of the extraction time. Total iron was measured using ICP-OES, while anions were measured with IC.*

Bacteria	**Total iron (mg·L^{-1})**	**Sulfates (mg·L^{-1})**	**Phosphates (mg·L^{-1})**
Control M	0.00 ±0.00	2979.17 ±31.11	0.00 ±0.00
Escherichia coli	23.47 ±2.26	2989.03 ±15.98	70.18 ±14.99
Pseudomonas putida	2.63 ±0.85	2998.26 ±21.25	34.71 ±7.88
Streptomyces pilosus	1.28 ±0.36	3021.59 ±40.55	0.00 ±0.00
Serratia ureilytica	1.51 ±0.67	2993.59 ±12.43	101.07 ±13.71

Extraction of iron from wood using purified siderophores

The direct use of siderophore-producing bacteria to extract iron from model wood samples did not succeed in removing the iron species formed during artificial impregnation. Although, some protective effects were observed, iron extraction rates were very low. In this section, we applied directly some bacterial siderophores to extract higher quantities of iron from the model balsa wood.

Following the results from section 2.2, we decided to work with three different buffer conditions. The model wood samples were extracted with DFOM, PVD and EDTA as chelating agents, in HEPES and citrate buffers, independently, as well as without any buffer. HEPES buffer is not expected to interfere with iron chelation [110], while citric acid has proven before to increase the dissolution effect of different siderophores [6], [111]. Citric acid is indeed used by some microorganisms as chelating agent [112].

In general, any treatment should intend minimum intervention. The original appearance should be respected as much as possible [113]. Two criteria have been previously followed: colour and

wood shrinkage [46]. Shrinkage evaluates the physical impact of the treatment on the wood. However, samples were not dried after treatment to properly follow shrinkage variations [46]. Visual observations were made at this point. Considering colour, the artificial contamination resulted in an homogenous black coloration (Figure 2.16), that resembled WAW dark hue [70], [89]. Iron extraction, however, would tend to recover the clear colour of the reference wood [46]. As far as possible, the extraction of iron should be high and respect the dark hue of WAW.

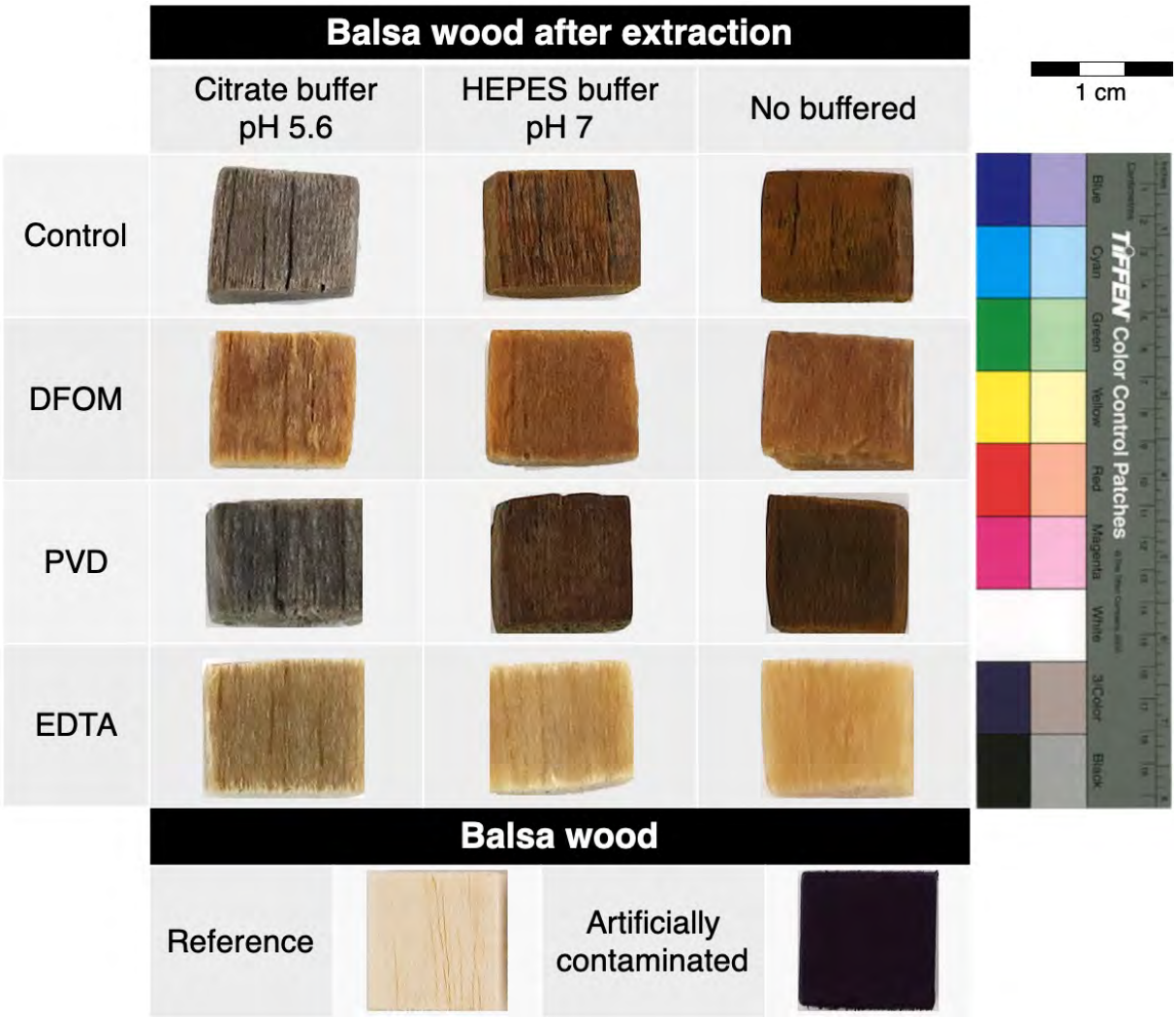

***Figure 2.16**. Visual appearance of the wood cubes after 15 days extraction with 10 mM of different iron chelators. Balsa wood was artificially impregnated with iron sulfides, and then treated with DFOM, PVD, and EDTA, in three different conditions: pH 7, pH 5.6 or not buffered solution. Control refers to the cubes incubated without any iron chelator.*

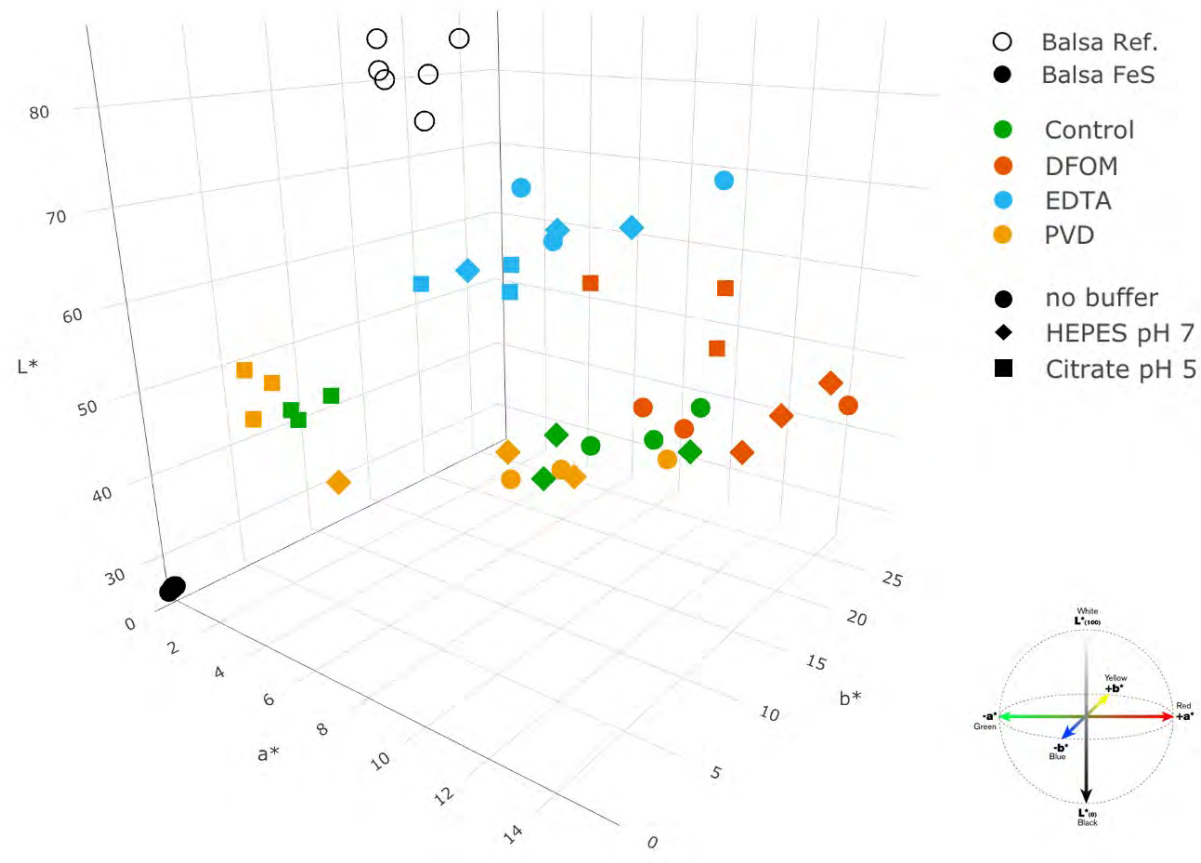

Figure 2.17*. Colorimetry plots representing colour coordinates: L* (lightness/bright-dark), a* (red/green opponent colours) and b* (yellow/blue opponent colours). Colour measurements were taken on the wood surface of all samples after extraction. Artificially contaminated balsa was extracted with DFOM, EDTA or PVD in three different conditions: pH 7, pH 5.6 or not buffered solution. Controls for the buffer solution without any iron chelator were included. Fresh balsa (Balsa Ref.) and balsa impregnated with iron sulfides (Balsa FeS) are included as references.*

PVD-extracted samples in citrate buffer presented a clearer and greyish hue than samples extracted in the other two buffer conditions (Figure 2.16). Colorimetric measurements confirmed that these cubes had a clearer tone (higher L*) and were close to 0 in a*b* coordinates (Figure 2.17). PVD samples in HEPES buffer or without a buffer kept a darker hue with a red tonality (Figures 2.16 and 2.17). Control samples, without any chelating agent, also presented different appearance when treated with citrate buffer than in the other conditions (Figure 2.16). Iron species seemed to oxidize in HEPES and no-buffer cubes, turning cubes appearance from a black hue to a red coloration (Figures 2.16 and 2.17). Citrate-buffered samples became greyish and stayed in a*b* coordinates closer to 0 (Figure 2.17). PVD and control wood samples plotted together in the colour scale (Figure 2.17).

DFOM samples also presented differences between the different buffer conditions. When extracted in citrate buffer, samples presented a lighter hue and L* values were higher (Figure

2.17). However, all DFOM extracted cubes gained a red tonality, and therefore a shift towards higher a* values was observed (Figure 2.17). Iron-DFOM complex results in an orange-red solution [114], what could have stained the wood. Finally, EDTA-treated samples presented a clearer appearance than the wood cubes treated with the other chelating agents (Figure 2.16). The L* values observed were higher (Figure 2.17). EDTA seems successful in recovering the original colour of balsa wood. However, in the next section, we further analysed if this discolouration was only due to iron extraction, or the chelator interfered with wood components.

Raman analyses helped to better understand the colour changes observed. In these cubes, Raman spectroscopy measures were conducted on the surface as well as in the core, after cutting the wood cubes in half. As in the previous section, mostly elemental sulfur was detected in all samples (Figures 2.18, 2.19, S 2.8 and S 2.9 and Table S 2.7). However, here we were able to clearly spot some iron oxides and oxyhydroxides, such as hematite and lepidocrocite, in some of the control and PVD cubes (Figure S 2.7). Therefore, the change of colour observed in control and PVD samples was confirmed to be because of the formation of iron oxide species. In control samples, we observed that even in citrate buffer, where the surface of the cubes did not have a red colouration, right under the surface there was oxidation occurring (Figure S 2.8). WAW samples usually show iron oxides and oxyhydroxides on the surface and oxygen-sensitive iron sulfides in the inside [43]. The observed oxidation and remaining the black core, indicate incomplete extraction.

Just by appearance, PVD treatment seemed to have had a lower effect than the other two iron chelators tested. Wood cubes resembled and clustered together with control samples (Figures 2.16 and 2.17). Raman analyses also pointed towards that assumption as lepidocrocite was also detected on the surface of samples treated with PVD (Figure 2.18), but not in any other samples. Here, we also observed that the cores of the wood cubes remained black. Therefore, PVD was not able to reach and extract iron from the inside of the wood cubes.

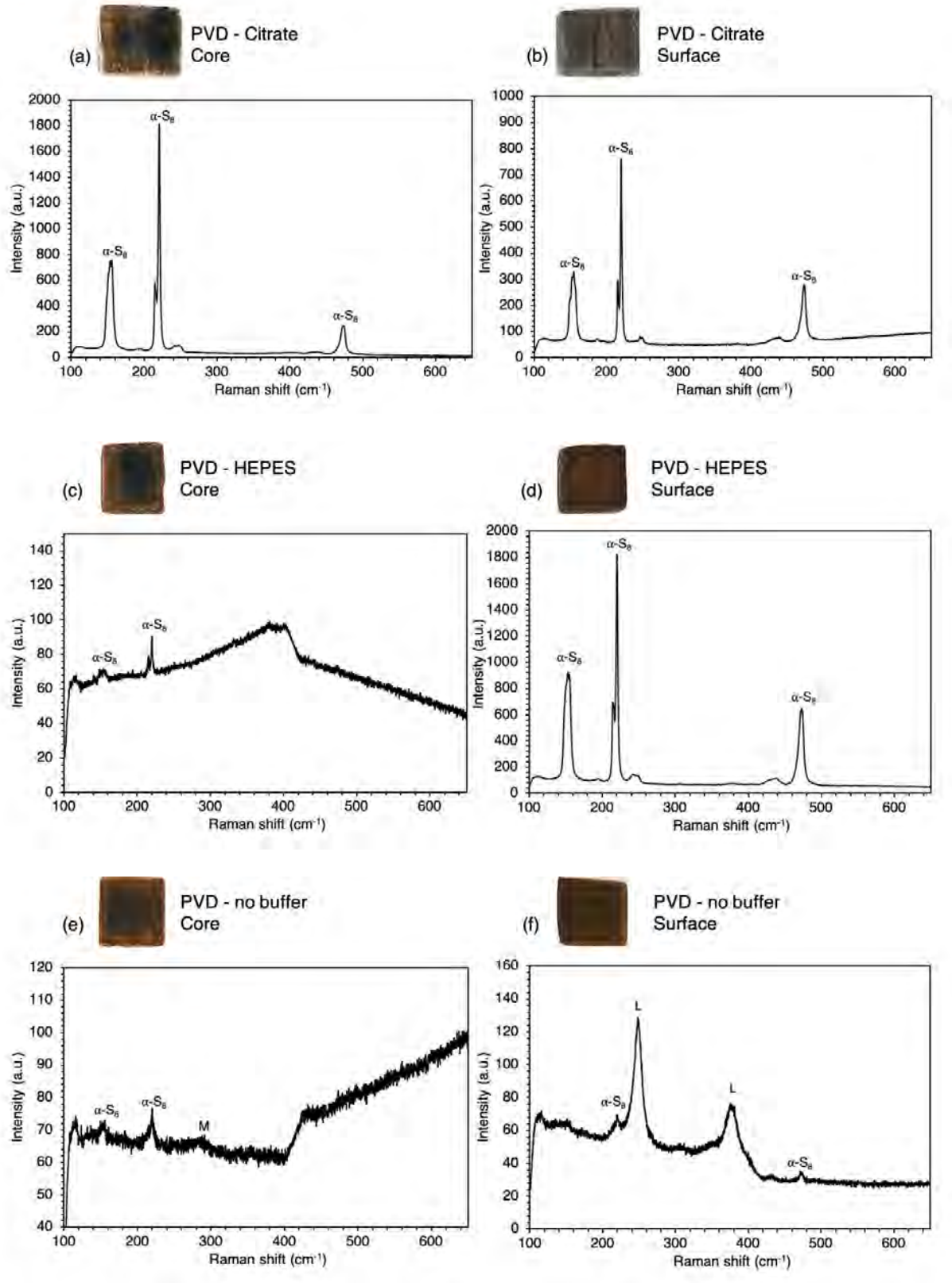

Figure 2.18. *Raman spectra obtained from the PVD-extracted wood cubes in citrate buffer: (a) core and (b) surface; HEPES buffer: (c) core and (d) surface; and without any buffer: (e) core and (f) surface. Characteristic peaks of elemental sulfur (α-S_8), lepidocrocite (L), and mackinawite (M) are tagged.*

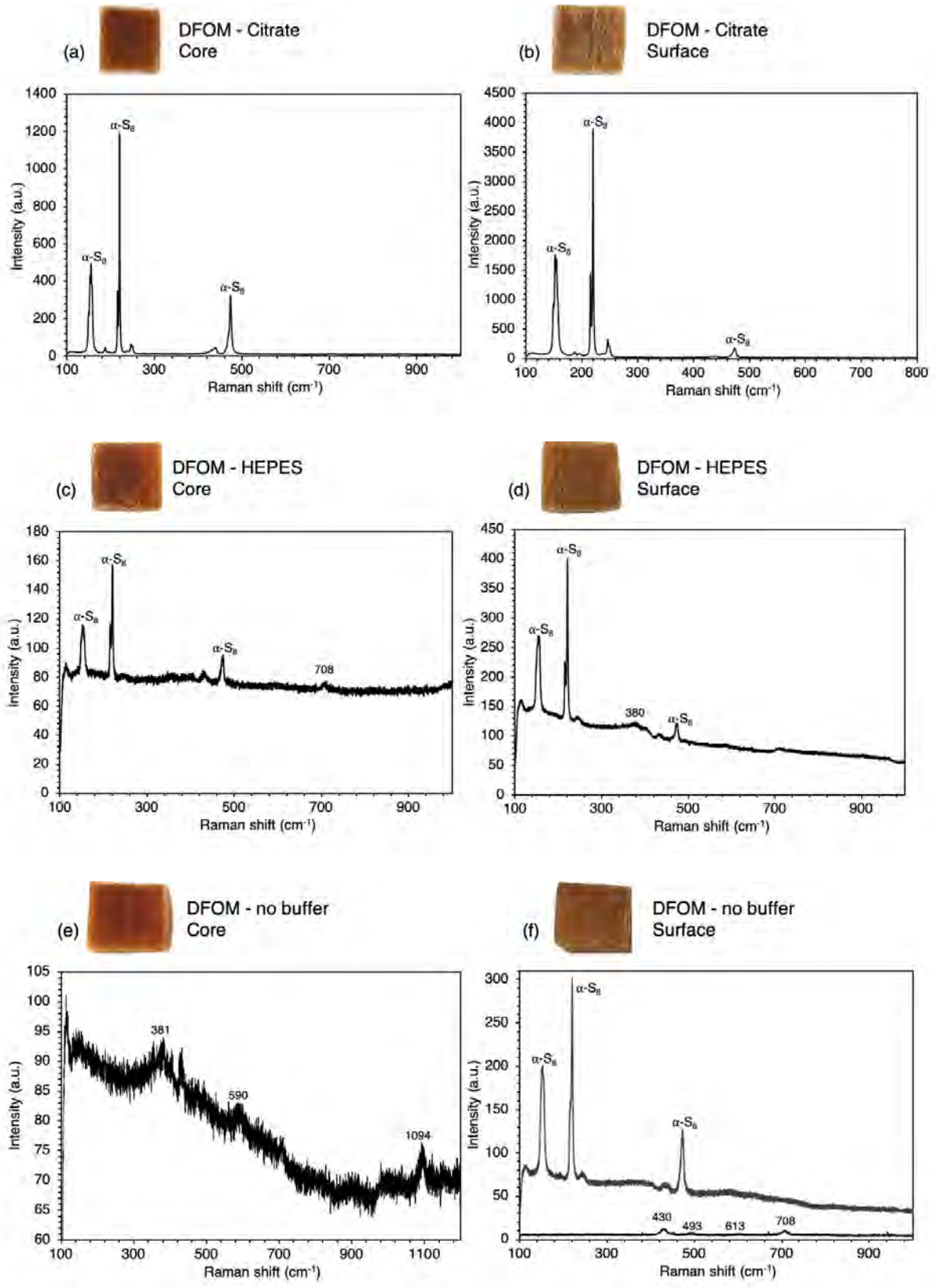

Figure 2.19. *Raman spectra obtained from the DFOM extracted wood cubes in citrate buffer: (a) core and (b) surface; HEPES buffer: (c) core and (d) surface; and without any buffer: (e) core and (f) surface. Characteristic peaks of elemental sulfur (α-S_8), along with some unidentified peaks.*

DFOM treatment showed that the inside of the cubes presented a similar appearance to the surface (Figure 2.19). We can assume that in this case, the siderophore was able to reach the core of the wood cubes. Moreover, Raman analyses showed mostly elemental sulfur (Figure 2.19). However, the band ~381 cm^{-1} was also registered here in some of the spectra (Figure 2.19). As discussed in the previous section, this band could be associated to goethite [98], pyrite [43], or cellulose [100]. Above, this Raman shift was argued to be goethite thanks to the parallel detection of iron by EDS analysis and the lack of other associated Raman bands. In this case, however, the band appeared in some cases associated with shifts corresponding for wood components also (~590 and ~1094 cm^{-1} [100], [115]) (Figure 2.19). Moreover, on the surface of DFOM treated wood cubes in no buffered solution, we registered a spectrum with major peaks at ~430 and ~708 cm^{-1}, and minor peaks at ~493 and ~613 cm^{-1}, and in some other spectra (Figure 2.19), the band at ~708 cm^{-1} also appeared. These shifts could be attributed to wood components, such as cellulose and lignin [100]. Overall, it seemed that DFOM treatment had a better performance than PVD treatment, as the core of the cubes was efficiently extracted, and the detection of iron oxides was not as clear as in PVD samples.

Raman analyses of EDTA samples mostly detected elemental sulfur (Figure S 2.9), in both surface and core spectra. Still, in some of the cubes extracted with EDTA, we also registered the bands at ~430 and ~708 cm^{-1}, as well as the band at ~380 cm^{-1} (Figure S 2.9). EDTA samples did not have a black core. The treatment with chemical chelator of reference seemed to efficiently extract iron from both surface and inner areas.

Indeed, ICP-OES analyses of total iron extracted showed that the extraction of iron was much higher for both DFOM and EDTA, where the cores were not black, than for PVD and control samples (Figure 2.20). Actually, PVD extraction was the same as in the control in HEPES buffer and without any buffer. Only with citrate buffer the extraction increased with respect to the control, but only in one of the replicates as represented by the big standard deviations.

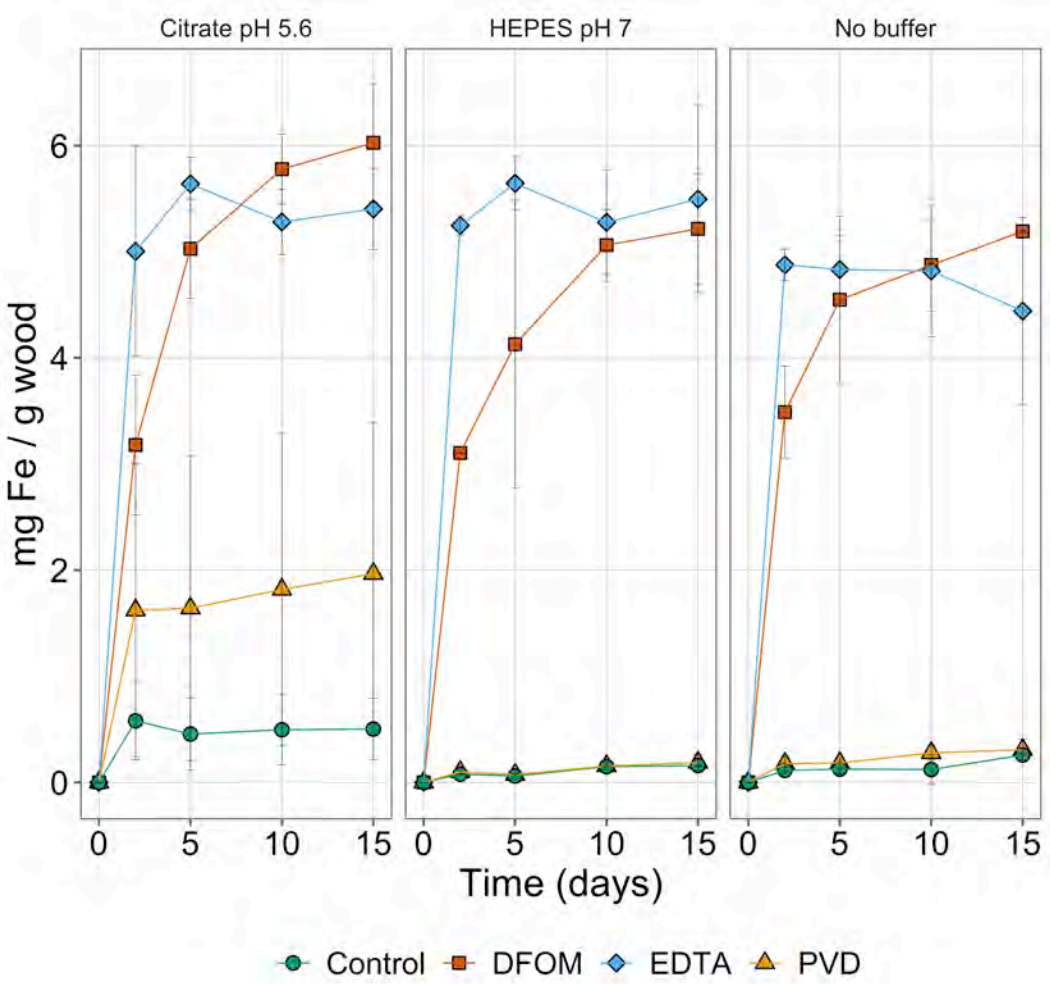

Figure 2.20. *Total iron extracted from the model wood samples (mg Fe/g wood) using DFOM, PVD, EDTA, or no chelator (control), over time. The extraction was conducted in three different conditions: citrate buffer (pH 5.6), HEPES buffer (pH 7), or without any buffer.*

The lower extraction observed using our purified PVD could be due to a lower concentration of this siderophore compared to the other two chelating agents. The concentration of our PVD extract was calculated experimentally. Also, PVD was kept regularly at -20 °C to prevent degradation. However, some deterioration could have occurred during storage time. Stabilization of the purified extract should be considered in the future. Formation of a PVD salt, as in the case of DFOM (deferoxamine mesylate salt), could increase stability.

DFOM presented very similar results to the reference chemical chelator. Both chelating agents arrived at similar extraction values after 15 days extraction (Figure 2.20). The main difference was that EDTA reached saturation in only 2 days, while DFOM started to reach saturation after 15 days (Figure 2.20). Diffusion into the wood seems to have been different for both chelators. Even though DFOM has a higher affinity for iron ($\log K_f = 30.5$) than EDTA ($\log K_f = 25.1$) [10], the faster diffusion of EDTA may have compensated this fact in the experimental time. EDTA

has a lower molecular weight than DFOM. Longer extraction times may have translated to bigger extraction rates of DFOM, as in some of the conditions the extraction curve was still not flat (Figure 2.20). However, diffusion rate is a key point in the extraction of iron from wood [116]. Lower diffusion rates would increase treatments duration, making the overall process time-consuming. Still, the benefits of using a greener chelator may overcome this drawback.

Overall, the use of citrate buffer improved extraction rates for the siderophores (Figure 2.20). Still, previous studies have shown that in some cases citric acid does not have a synergic effect in the dissolution of iron minerals due to adsorption competition in the minerals surface [49]. Moreover, the concentration of the chelating agent here was higher (10 mM) than in the study of dissolution of mineral phases (200 μM). In particular for DFOM, this fact could explain why in this experience the differences observed between citrate buffer and the other buffer conditions were not as notable as in the dissolution of minerals, especially for mackinawite. In this case the extraction of iron was mostly influenced by DFOM, while in the previous section citric acid may have been the key player. Extraction with EDTA was not significatively different between buffers (*p*-value = 0.413) (Figure 2.20).

Solutions with citrate buffer increased the pH from ~5.6 ±0.1 to 7.3 ±1.0, 7.6 ±0.2, 8.0 ±1.0, and 8.4 ±0.1, for DFOM, PVD, EDTA, and control, respectively. The pH values showed that citrate buffer interacted with iron as the buffer effect was lost for all cases. HEPES buffer kept a stable pH ~7, while the solutions without a buffer went from pH ~5.9 ±1.0 to 8.0 ±0.3, 7.8 ±0.7, 8.2 ±2.2, and 7.8 ±0.2, for DFOM, PVD, EDTA, and control, respectively. All pH increased when no buffered was added as with citrate buffer. The impregnation solution has a highly basic pH, even if the cubes were rinsed, this could explain the increase in pH in the solutions.

Complementary IC analyses were carried out to detect any oxidation of sulfur species. However, the high amounts of dissolved sulfide (hydrogen sulfide H_2S, hydrosulfide ions HS^- or sulfides S^{2-}) contaminated the chromatography column not allowing to read other anions. Nonetheless, ICP-OES measured gave us values of total sulfur in solution. Extraction of iron is usually accompanied with the extraction of other compounds [45]. The chelation of iron from iron sulfides should also release sulfur species into solution. After 2 days extraction we measured high quantities of sulfur in solution (Figure S 2.10). However, over the extraction time, sulfur in solution decreased (Figure S 2.10). This fact explains the high quantities of elemental sulfur detected on the cubes with Raman analyses. To avoid the precipitation of

elemental sulfur and other sulfur species an oxidant could be included. The oxidation of the sulfur species co-extracted with iron is a theme of discussion in the next chapters of this thesis.

Interaction of siderophores with analogues of wood

Green chelators, such as siderophores, are quite recent in the field of conservation. Therefore, is essential to assess any secondary reaction with wood components. As we have seen, DFOM had a different effect in the model wood samples to EDTA. Both chelating agents extracted the same amount of iron (figure 2.20). Still, the final appearance of the wood cubes was significatively different (Figure 2.16).

Siderophores play an important role in the metabolism of different microorganisms. Therefore, even though their use in conservation is new, their interaction with wood has been previously study. For example, some studies have been interested in the role that fungal siderophores play in the degradation of cellulosic substrates [24]. Following a similar experimental plan to the cited reference, we tested the effect of our purified PVD, DFOM and EDTA in some wood analogues. For instance, Remazol brilliant blue R (RBBR) have been tested before to study ligninolytic activities [117]. We incubated the RBBR in presence of the three chelating agents with or without Fe^{3+}/H_2O_2, to exclude that the degradation is due to the production of reactive oxygen species (ROS) by Fenton reaction. After 3 days of incubation, no significant decrease in absorbance was observed for any chelator in any condition (Table S 2.8). Therefore, no degradation of RBBR was observed in the experimental conditions.

Parallelly, we also studied the degradation of p-nitrophenyl-β-D-glucopyranoside (pNPG). We studied if siderophores are involved in depolymerization of cellulose by Fenton rection, using the pNPG analogue. After 56 h, both siderophores had released pNP to values close to the control without any chelator. DFOM even presented lower pNP values than the control (Figure 2.21). On the contrary, EDTA in presence of Fe^{3+}/H_2O_2 released high levels of pNP, therefore, EDTA interfered in the breakage of pNPG. Needs to be noted that controls without Fe^{3+}/H_2O_2, and only the chelating agent did not release any pNP (Figure S 2.11). Consequently, this reassures that the breaking of pNPG observed in presence of EDTA, Fe^{3+} and H_2O_2 is due to Fenton reaction and the production of ROS.

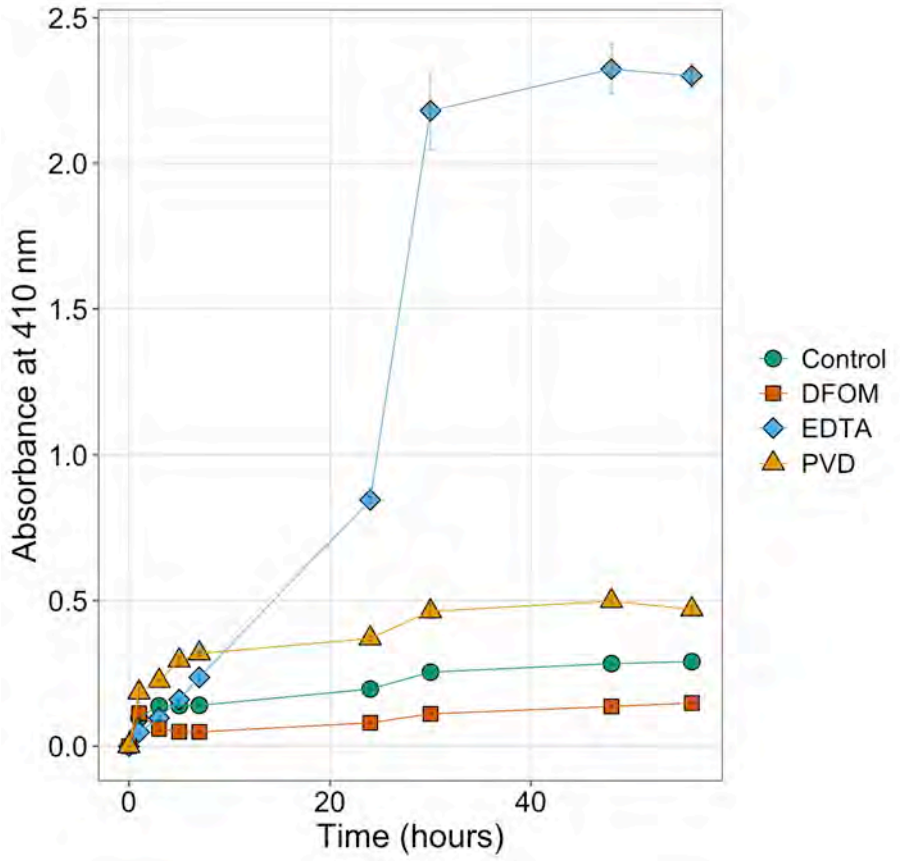

***Figure 2.21**. p-nitrophenol (pNP) released from pNPG by DFOM-Fe^{3+}/H_2O_2, PVD-Fe^{3+}/H_2O_2, EDTA-Fe^{3+}/H_2O_2, and the control with only Fe^{3+}/H_2O_2.*

The redox potential is an important parameter for the stability of iron-siderophore complexes. The standard redox potential (E°) of the iron(III)/iron(II) couple in water at pH 2 is +770 mV, however this value can vary due to iron chelation and pH. Indeed, when stable iron-siderophore complexes are formed, the redox potentials observed shift to negative. For most iron-siderophores complexes, the redox potentials are in the range from -350 to -750 mV, meaning that the chelated iron(III) will not react with most of the biological reducing agents [15].

This low redox potential also prevents participation of iron as a catalyst in redox processes such as the Haber-Weiss cycle, which produces ROS. A positive redox potential in an aerobic environment will lead to the production of highly harmful hydroxyl radicals [12]. For example, EDTA is well-known to promote the formation of hydroxyl radicals [93]. Iron(III)-EDTA/iron(II)-EDTA redox potential is +96 mV [118], more positive than in the case of iron-siderophore complexes. Consequently, siderophores are a safer option to use in organic materials as the production of ROS is likely in the presence of EDTA and iron ions in an oxidative environment.

Moreover, the use of EDTA as chelator is under risk assessment [119], [120]. The high emissions of EDTA into the natural environment and its low biodegradability justifies the reduction in the use of this chemical [120]. Furthermore, although EDTA has been evaluated as low risk for human health, this implies that protective measures are taken to minimise users exposure [121].

Conclusion

Siderophore-producing bacteria were not able to efficiently extract iron from artificially contaminated model wood samples. However, each bacterium showed very different effect in the wood. Some, like *S. ureilytica* and *P. putida*, prevented the oxidation of iron sulfides. This could be interesting as new trends in conservation of WAW are looking at prevention instead of intervention. However, further analyses are needed to deeply understand the chemical changes that prevent the oxidation.

On the other hand, the use of siderophores reported very good results. DFOM presented comparable results to the chemical chelator, EDTA. Even though the extraction times were longer with DFOM than EDTA, EDTA promoted the degradation of wood analogues and the final appearance of the cubes was further away from the typical WAW dark hue. Therefore, DFOM is safer alternative for the wooden objects. Moreover, current trends in green chelators are looking to reduce the usage of EDTA in favour of more biodegradable compounds that do not accumulate in the environment [119], [120].

DFOM presented better results than purified siderophore, PVD. The instability of this siderophore may have accounted for the differences observed. The use of commercial, stable siderophores can be, however, attractive for end users.

Supplementary material 2.3

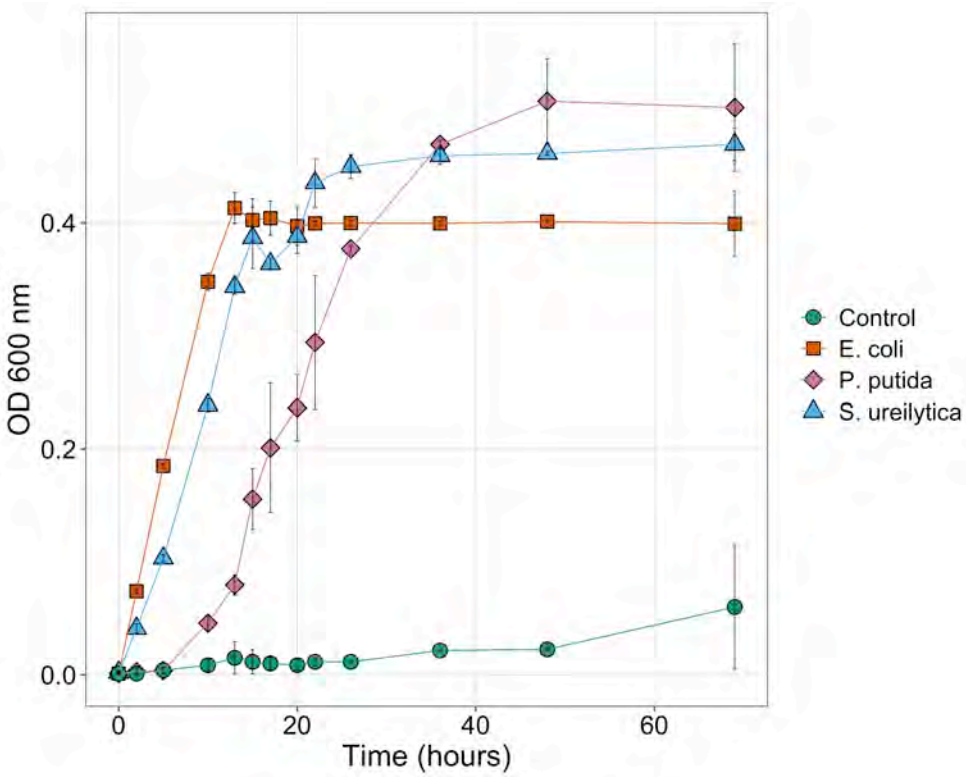

Figure S 2.4. *Growth of the different siderophore-producing bacteria: E. coli, P. putida, and S. ureilytica, in MM9 medium with model wood samples; compared to the abiotic control.*

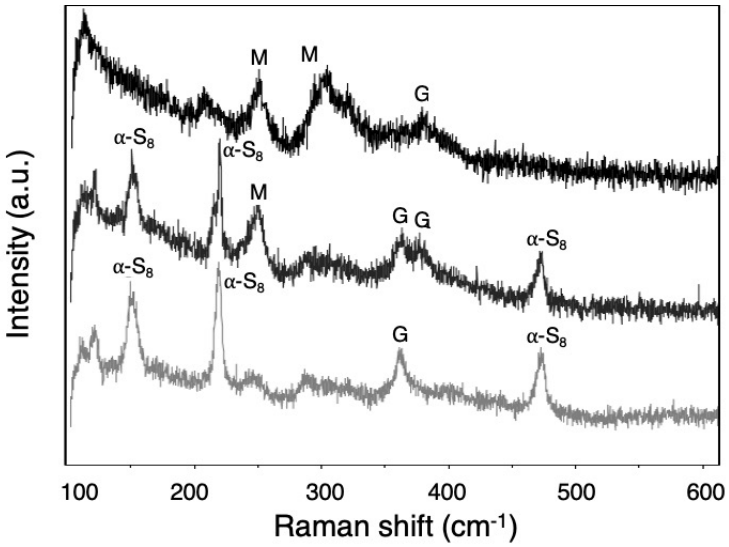

***Figure S 2.5**. Raman spectra obtained from the artificially contaminated wood sample before any extraction treatment. Characteristic peaks of elemental sulfur (α-S8), mackinawite (M), and greigite (G) are tagged.*

***Table S 2.6**.Compounds identified by Raman spectroscopy after 3 days of extraction with different siderophore-producing bacteria, or without bacteria (control M), compared to the compounds identified in the reference wood before any treatment (Figure S 2.5).*

	Compounds identified	**Bands observed (cm^{-1})**
Artificially contaminated balsa	Mackinawite	255, 290
	Greigite	354, 363
	Elemental sulfur	150, 219, 473
Control M	Elemental sulfur	150, 218, 242, 437, 470
Escherichia coli	Elemental sulfur	153, 220, 242, 472
	Goethite*/cellulose*	381
Pseudomonas putida	Elemental sulfur	150, 220, 472 / 220
	Mackinawite	284
Streptomyces pilosus	Elemental sulfur	151, 216, 221, 245, 432, 474
Serratia ureilytica	Elemental sulfur	153, 220, 245, 435, 471
	Mackinawite	308

References: [43], [96], [98].
Compounds marked (*) are not confirmed.

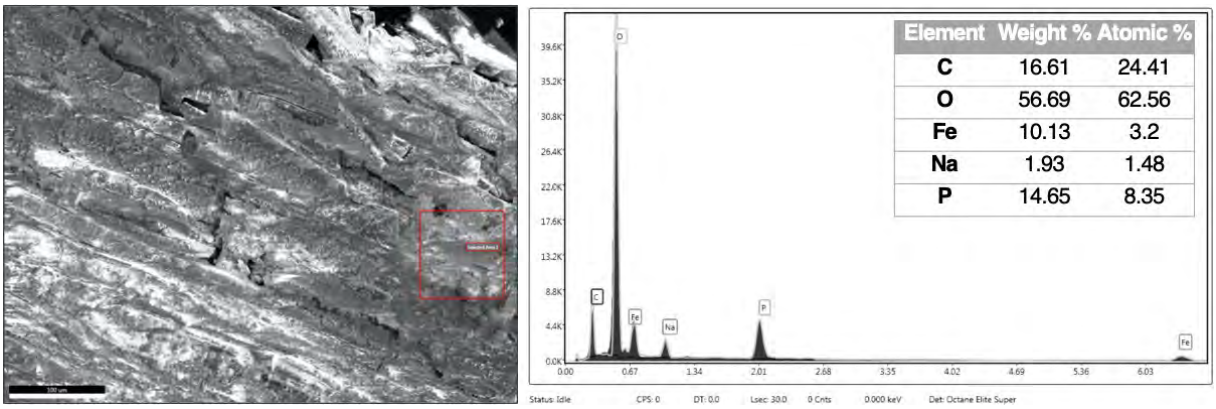

***Figure S 2.6**. Secondary electron micrograph of a tangential cut of a control M wood sample, with the complementary EDS spectrum. The EDS analysis is corresponding to the red area indicated on the SEM image.*

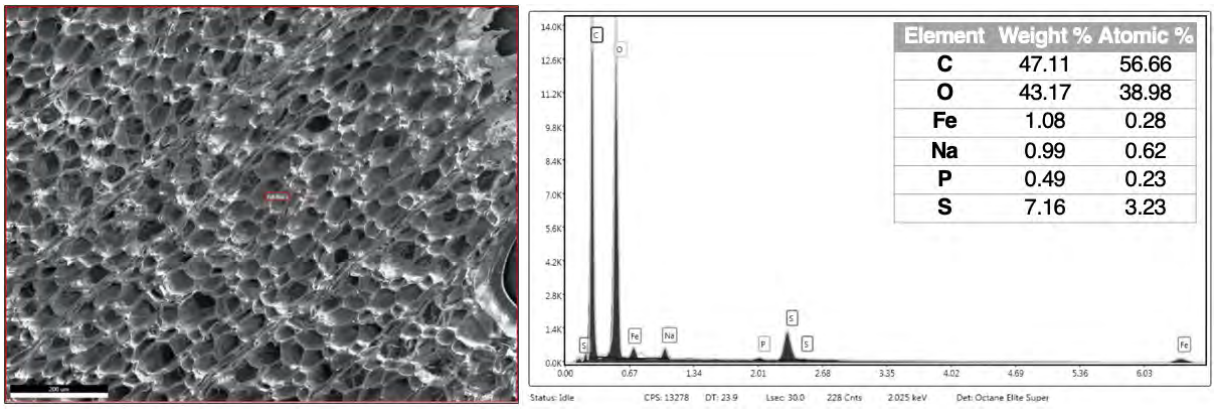

***Figure S 2.7**. Secondary electron micrograph of a cross section cut of one E. coli wood sample, with the complementary EDS spectrum. The EDS analysis correspond to the whole area visible on the SEM image.*

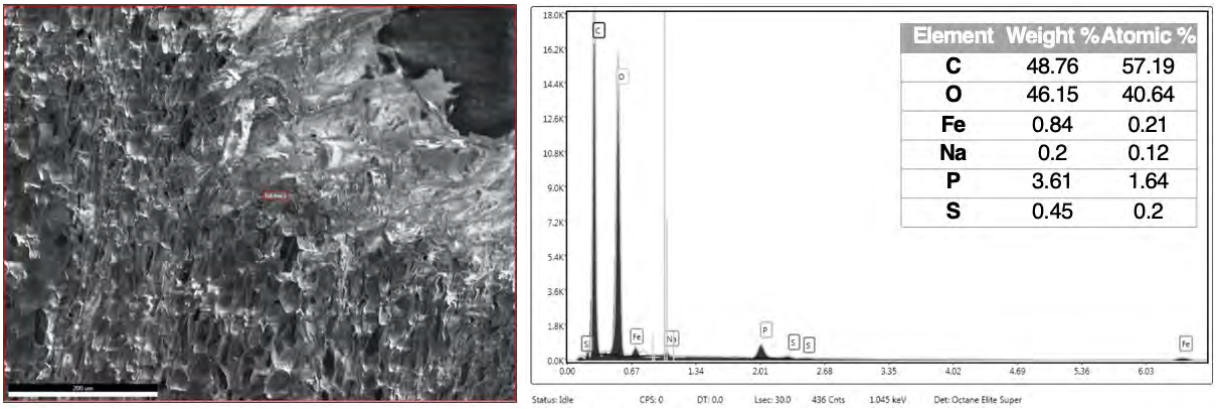

***Figure S 2.8**. Secondary electron micrograph of a cross section cut of one P. putida wood sample, with the complementary EDS spectrum. The EDS analysis correspond to the whole area visible on the SEM image.*

Table S 2.7*. Compounds identified by Raman spectroscopy after 3 days of extraction with different siderophore-producing bacteria, or without bacteria (control M), compared to the reference before any treatment.*

	Buffer	Compounds identified	Main bands observed (cm^{-1})
Artificially contaminated balsa		Mackinawite	255, 290
		Greigite	354, 363
		Elemental sulfur	150, 219, 473
Control	Citrate pH 5.6	Elemental sulfur	154, 220, 473
		Hematite	227, 245, 293, 412
	HEPES pH 7	Elemental sulfur	154, 220, 473
		Goethite* or cellulose*	382
		Elemental sulfur	221, 429, 474
		Goethite* or cellulose*	380
	No buffered	Elemental sulfur	154, 220, 248, 473
		Goethite* or cellulose*	380
		Elemental sulfur	152, 221, 244, 474
		Elemental sulfur	155, 220
		Lepidocrocite + Goethite	252, 379, 480
DFOM	Citrate pH 5.6	Elemental sulfur	155, 220, 474
		Elemental sulfur	152, 220, 474
	HEPES pH 7	Elemental sulfur	153, 220, 473
		Wood substrate*	708
		Elemental sulfur	155, 220, 474
		Goethite* or cellulose*	380
	No buffered	Goethite* or cellulose*	381
		Wood substrates*	589, 1094
		Elemental sulfur	152, 220, 471
		Wood substrates*	430, 493, 630, 708
PVD	Citrate pH 5.6	Elemental sulfur	154, 220, 474
		Elemental sulfur	154, 220, 477
	HEPES pH 7	Elemental sulfur	155, 220
		Elemental sulfur	154, 220 473
	No buffered	Elemental sulfur	152, 220
		Mackinawite	305
		Elemental sulfur	220, 472
		Lepidocrocite	248, 375
EDTA	Citrate pH 5.6	Elemental sulfur	155, 220, 474
		Elemental sulfur	154, 221, 474
	HEPES pH 7	Elemental sulfur	153, 220
		Wood substrates*	432, 709
		Elemental sulfur	153, 220, 474
	No buffered	Elemental sulfur	155, 220
		Elemental sulfur	152, 220, 472
		Goethite* or cellulose*	380
		Elemental sulfur	155, 221, 474

References: [43], [96], [98].
Compounds marked (*) are not confirmed.

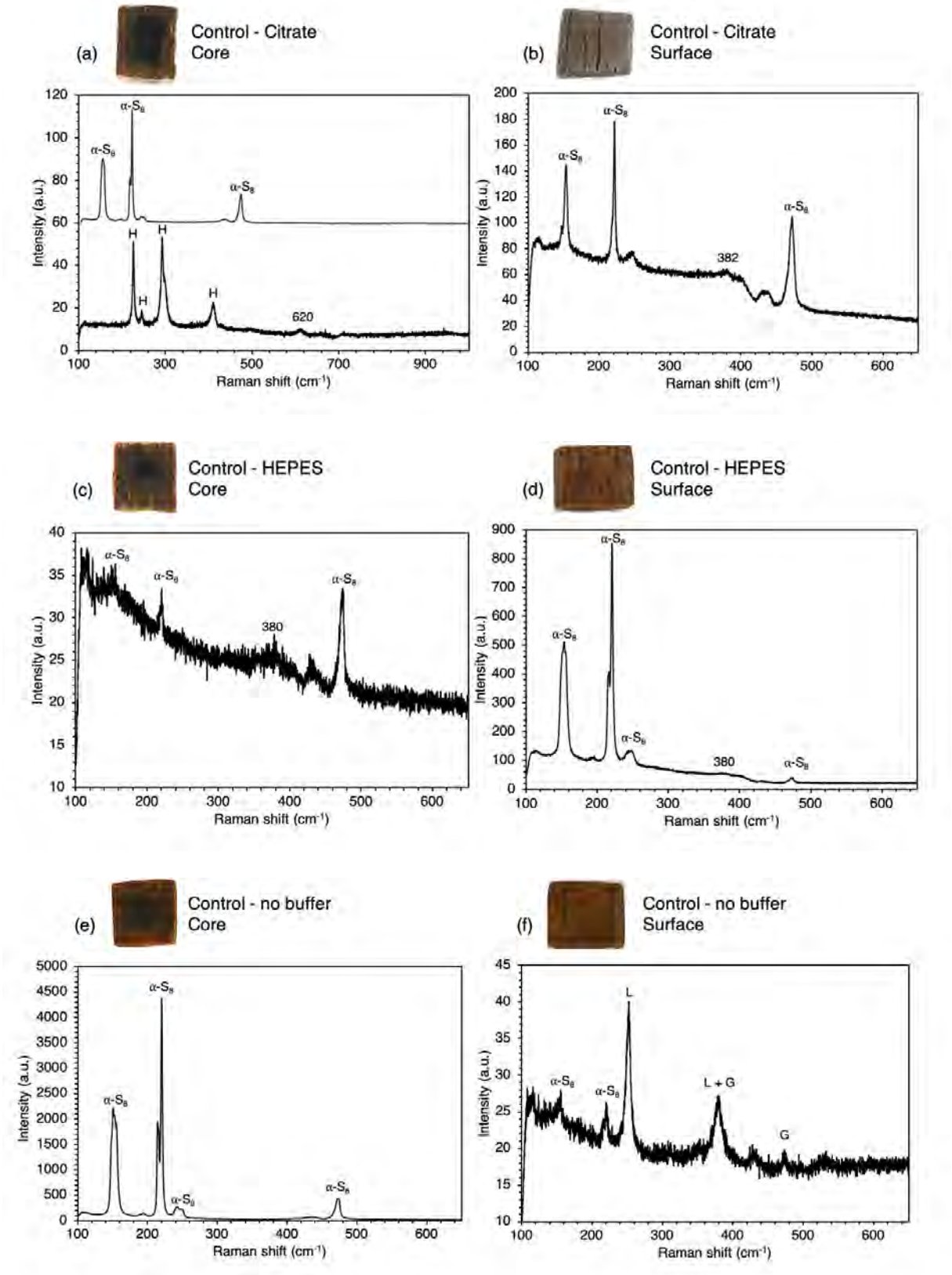

Figure S 2.9. *Raman spectra obtained from the control wood cubes in citrate buffer: (a) core and (b) surface; HEPES buffer: (c) core and (d) surface; and without any buffer: (e) core and (f) surface. Characteristic peaks of elemental sulfur (α-S_8), hematite (H), and lepidocrocite (L) are tagged, along with some unidentified peaks.*

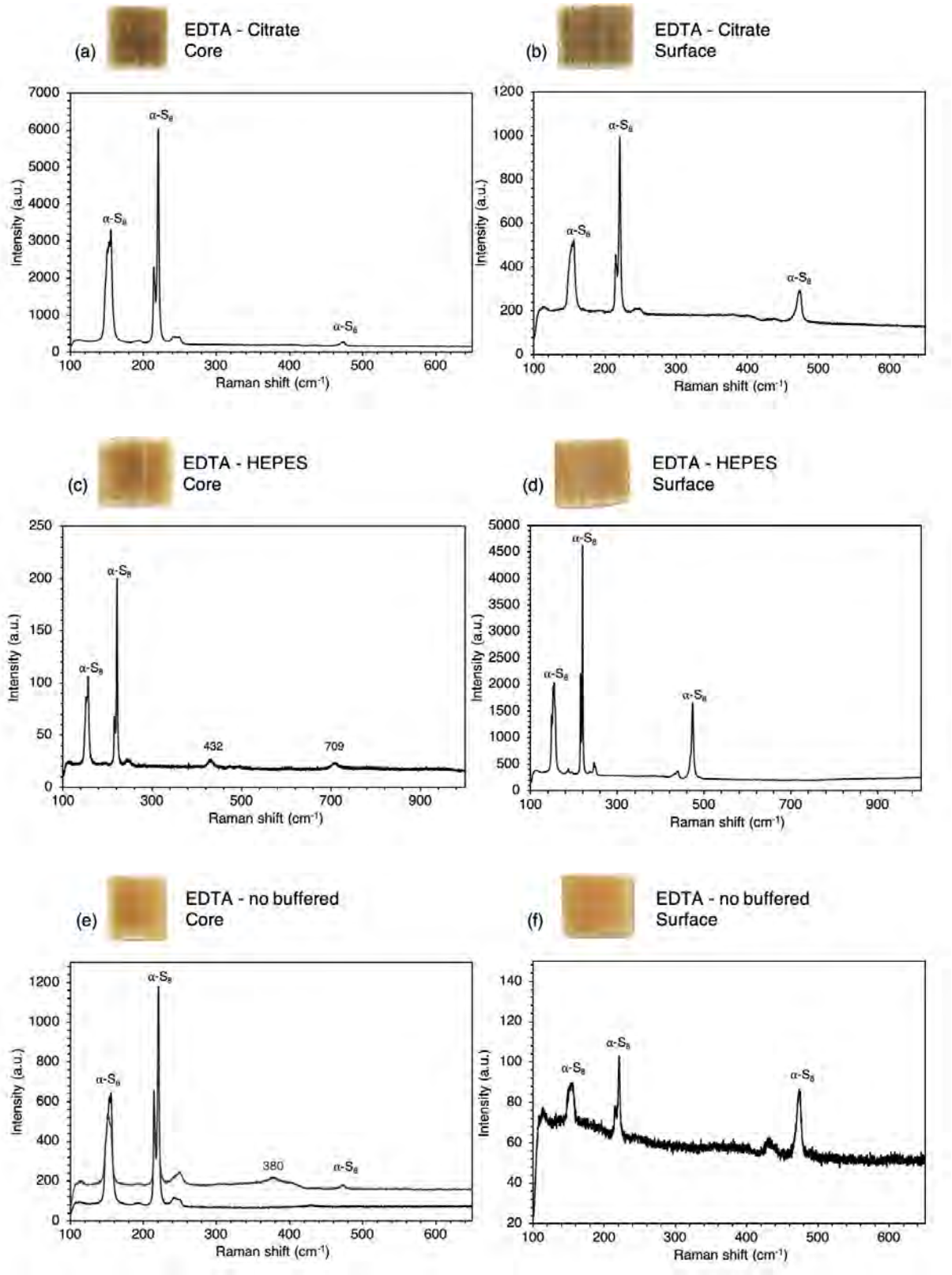

Figure S 2.10. *Raman spectra obtained from the EDTA extracted wood cubes in citrate buffer: (a) core and (b) surface; HEPES buffer: (c) core and (d) surface; and without any buffer: (e) core and (f) surface. Characteristic peaks of elemental sulfur (α-S_8) are tagged, along with some unidentified peaks.*

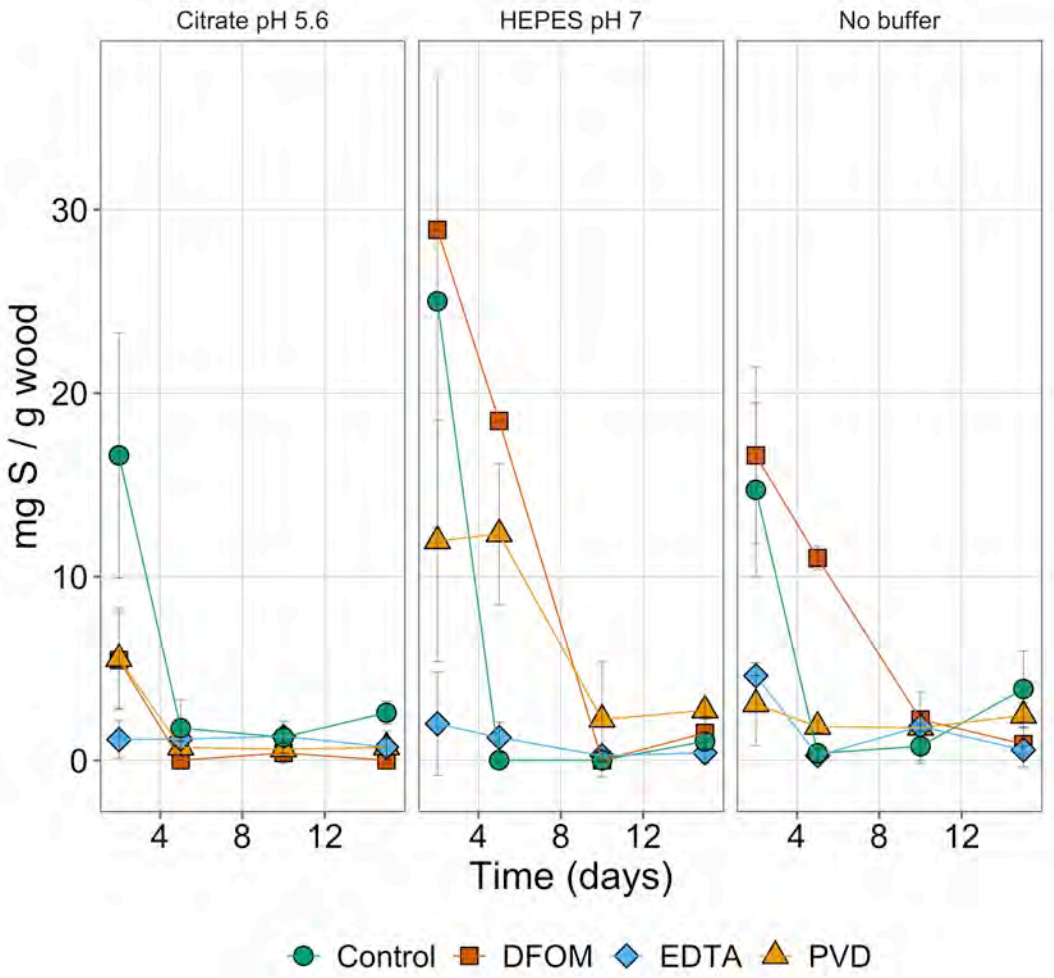

Figure S 2.11. *Total sulfur extracted from the model wood samples (mg S/g wood) using EDTA (♦), DFOM (■), PVD (▲), or no chelator (control (●)), over time. The extraction was conducted in three different conditions: citrate buffer (pH 5.6), HEPES buffer (pH 7), or without any buffer.*

Table S 2.8. *Ratios of absorbance between the maximum absorbance of RBBR (590 nm), and a reference absorbance (500 nm), for the different chelating agents and RBBR, at T0 and TF (3 days).*

	Abs 595/Abs 500 at T0	**Abs 595/Abs 500 at TF**	***p*-value (t-test)**
RBBR-Fe^{3+}/H_2O_2	1.45 ±0.10	1.46 ±0.10	0.85
DFOM-Fe^{3+}/H_2O_2	1.27 ±0.03	1.27 ±0.03	0.78
EDTA-Fe^{3+}/H_2O_2	1.69 ±0.10	1.67 ±0.10	0.59
PVD-Fe^{3+}/H_2O_2	1.19 ±0.03	1.12 ±0.06	0.10

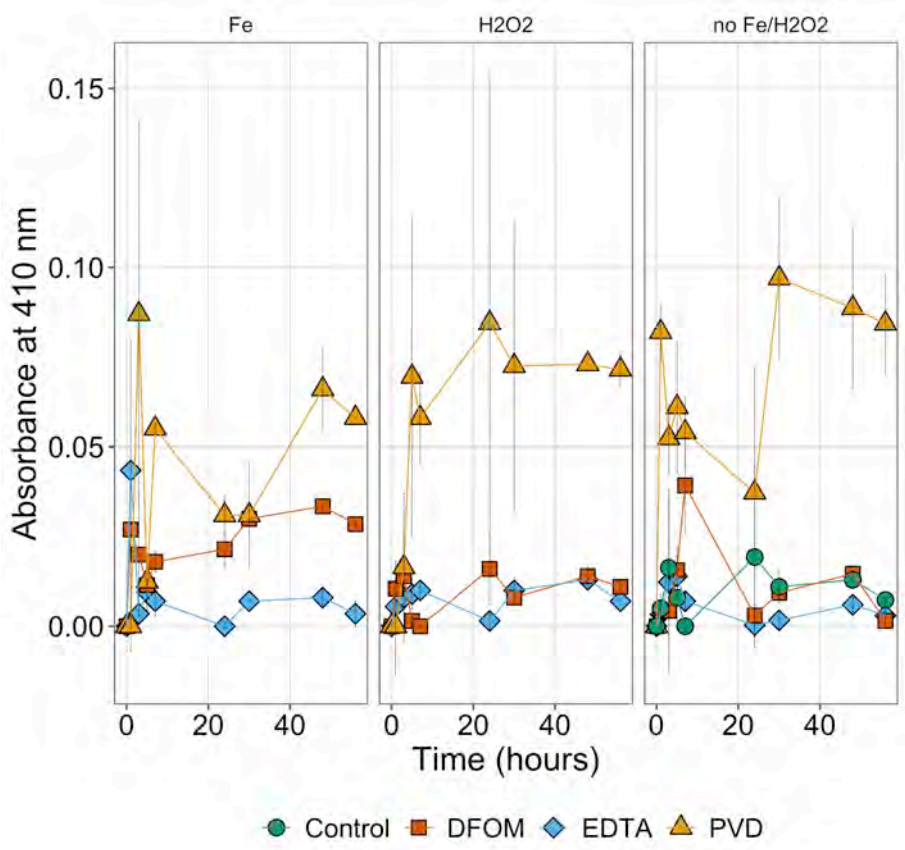

Figure S 2.12. *p-nitrophenol (pNP) released from pNPG by DFOM, PVD, EDTA in presence of with only Fe^{3+}, only H_2O_2, or without any additive. A control with only pNPG and without Fe^{3+}nor H_2O_2 is also included.*

Author contribution

MA-B designed and performed all experiments, analysed the data and wrote the published review and this chapter. MM assisted with Raman and SEM-EDS analyses. EJ supervised the experimental design, analysed the data, wrote and corrected the published review and this chapter.

References

[1] B. Schwyn and J. B. Neilands, "Universal chemical assay for the detection and determination of siderophores," *Anal. Biochem.*, vol. 160, no. 1, pp. 47–56, 1987, doi: 10.1016/0003-2697(87)90612-9.

[2] K. A. Weber, L. A. Achenbach, and J. D. Coates, "Microorganisms pumping iron: anaerobic microbial iron oxidation and reduction," *Nat. Rev. Microbiol.*, vol. 4, no. 10, pp. 752–764, 2006, doi: 10.1038/nrmicro1490.

[3] L. O. De Serrano, A. K. Camper, and A. M. Richards, "An overview of siderophores for iron acquisition in microorganisms living in the extreme," *BioMetals*, vol. 29, no. 4, pp. 551–571, Aug. 2016, doi: 10.1007/s10534-016-9949-x.

[4] T. C. Johnstone and E. M. Nolan, "Beyond iron: non-classical biological functions of bacterial siderophores," *Dalt. Trans.*, vol. 44, no. 14, pp. 6320–6339, 2015, doi: 10.1039/C4DT03559C.

[5] J. Brandel, N. Humbert, M. Elhabiri, I. J. Schalk, G. L. A. Mislin, and A. M. Albrecht-Gary, "Pyochelin, a siderophore of Pseudomonas aeruginosa: Physicochemical characterization of the iron(iii), copper(ii) and zinc(ii) complexes," *Dalt. Trans.*, vol. 41, no. 9, pp. 2820–2834, 2012, doi: 10.1039/c1dt11804h.

[6] E. Ahmed and S. J. M. Holmström, "Siderophores in environmental research: Roles and applications," *Microb. Biotechnol.*, vol. 7, no. 3, pp. 196–208, 2014, doi: 10.1111/1751-7915.12117.

[7] J. B. Neilands, "Siderophores : Structure and Function of Microbial Iron Transport Compounds Siderophores : Structure and Function of Microbial Iron Transport Compounds *," *J. Biol. Chem.*, vol. 270, no. 45, pp. 26723–26726, 1995, doi: 10.1074/jbc.270.45.26723.

[8] R. J. Abergel *et al.*, "Anthrax pathogen evades the mammalian immune system through stealth siderophore production," *Proc. Natl. Acad. Sci.*, vol. 103, no. 49, pp. 18499–18503, Dec. 2006, doi: 10.1073/pnas.0607055103.

[9] K. D. Krewulak and H. J. Vogel, "Structural biology of bacterial iron uptake," *Biochim. Biophys. Acta - Biomembr.*, vol. 1778, no. 9, pp. 1781–1804, 2008, doi: 10.1016/j.bbamem.2007.07.026.

[10] R. C. Hider and X. Kong, "Chemistry and biology of siderophores," *Nat. Prod. Rep.*, vol. 27, no. 5, pp. 2129–2138, 2010, doi: 10.1039/b906679a.

[11] R. Hermenau *et al.*, "Gramibactin is a bacterial siderophore with a diazeniumdiolate ligand system," *Nat. Chem. Biol.*, pp. 1–3, 2018, doi: 10.1038/s41589-018-0101-9.

[12] S. Dhungana and A. L. Crumbliss, “Coordination chemistry and redox processes in siderophore-mediated iron transport,” *Geomicrobiol. J.*, vol. 22, no. 3–4, pp. 87–98, 2005, doi: 10.1080/01490450590945870.

[13] H. Boukhalfa and A. L. Crumbliss, “Chemical aspects of siderophore mediated iron transport,” *BioMetals*, vol. 15, no. 4, pp. 325–339, 2002, doi: 10.1023/A:1020218608266.

[14] C. S. Carroll and M. M. Moore, “Ironing out siderophore biosynthesis: a review of non-ribosomal peptide synthetase (NRPS)-independent siderophore synthetases,” *Crit. Rev. Biochem. Mol. Biol.*, vol. 53, no. 4, pp. 356–381, 2018, doi: 10.1080/10409238.2018.1476449.

[15] M. Miethke and M. A. Marahiel, “Siderophore-Based Iron Acquisition and Pathogen Control,” *Microbiol. Mol. Biol. Rev.*, vol. 71, no. 3, pp. 413–451, 2007, doi: 10.1128/MMBR.00012-07.

[16] A. Butler and R. M. Theisen, “Iron(III)-siderophore coordination chemistry: Reactivity of marine siderophores,” *Coord. Chem. Rev.*, vol. 254, no. 3–4, pp. 288–296, 2010, doi: 10.1016/j.ccr.2009.09.010.

[17] K. N. Raymond, E. A. Dertz, and S. S. Kim, “Enterobactin: An archetype for microbial iron transport,” *Proc. Natl. Acad. Sci.*, vol. 100, no. 7, pp. 3584–3588, 2003, doi: 10.1073/pnas.0630018100.

[18] R. Saha, N. Saha, R. S. Donofrio, and L. L. Bestervelt, “Microbial siderophores: A mini review,” *J. Basic Microbiol.*, vol. 53, no. 4, pp. 303–317, 2013, doi: 10.1002/jobm.201100552.

[19] I. J. Schalk, M. Hannauer, and A. Braud, “New roles for bacterial siderophores in metal transport and tolerance,” *Environ. Microbiol.*, vol. 13, no. 11, pp. 2844–2854, 2011, doi: 10.1111/j.1462-2920.2011.02556.x.

[20] V. I. Holden and M. A. Bachman, “Diverging roles of bacterial siderophores during infection,” *Metallomics*, vol. 7, no. 6, pp. 986–995, 2015, doi: 10.1039/C4MT00333K.

[21] M. Albelda-Berenguer, M. Monachon, and E. Joseph, “Siderophores: From natural roles to potential applications,” in *Advances in Applied Microbiology*, vol. 106, G. M. Gadd and S. B. T.-A. in A. M. Sariaslani, Eds. Academic Press, 2019, pp. 193–225.

[22] D. B. Alexander and D. A. Zuberer, “Use of chrome azurol S reagents to evaluate siderophore production by rhizosphere bacteria,” *Biol. Fertil. Soils*, vol. 12, no. 1, pp. 39–45, 1991, doi: 10.1007/BF00369386.

[23] P. Jacques, M. Ongena, F. Bernard, R. Fuchs, H. Budzikiewicz, and P. Thonart, “Fluorescent Pseudomonas mainly produce the dihydro form of pyoverdine at low specific growth rate.,” *Lett. Appl. Microbiol.*, vol. 36, no. 5, pp. 259–62, 2003, [Online]. Available: http://www.ncbi.nlm.nih.gov/pubmed/12680934.

[24] V. Arantes and A. M. F. Milagres, “Degradation of cellulosic and hemicellulosic substrates using a chelator-mediated Fenton reaction,” *J. Chem. Technol. Biotechnol.*, vol. 81, no. 3, pp. 413–419, Mar. 2006, doi: 10.1002/jctb.1417.

[25] C. Cezard, N. Farvacques, and P. Sonnet, “Chemistry and Biology of Pyoverdines, Pseudomonas Primary Siderophores,” *Curr. Med. Chem.*, vol. 22, no. 2, pp. 165–186, 2014, doi: 10.2174/09298673216661410111946 24.

[26] S. Sajeed Ali and N. N. Vidhale, “Bacterial Siderophore and their Application : A review,” *Int . J . Curr . Microbiol . App . Sci*, vol. 2, no. 12, pp. 303–312, 2013, [Online]. Available:

https://www.researchgate.net/profile/Syed_Sajeed_Ali/publication/303913491_Bacterial_Siderohore_and_their_Application_A_review/links/575d34ab08aec91374ae795c.pdf.

[27] D. Lukasz, R. Liwia, M. Aleksandra, and S. Aleksandra, "Dissolution of arsenic minerals mediated by dissimilatory arsenate reducing bacteria: Estimation of the physiological potential for arsenic mobilization," *Biomed Res. Int.*, vol. 2014, 2014, doi: 10.1155/2014/841892.

[28] L. O. De Serrano, "Biotechnology of siderophores in high-impact scientific fields," *Biomol. Concepts*, vol. 8, no. 3–4, pp. 169–178, 2017, doi: 10.1515/bmc-2017-0016.

[29] J. Frey, "Classification of Organisms Part 1: Bacteria," no. January. Federal Office for the Environment FOEN, Federal Office of Public Health FOPH, pp. 1–203, 2013.

[30] P. Bosch-Roig, J. Regidor-Ros, P. Soriano, and R. Montes-Estelles, "Biocleaning of animal glue on wall paintings by Pseudomonas stutzeri," *Chim. Oggi/Chemistry Today*, vol. 31, pp. 50–53, Jan. 2013.

[31] S. C. Andrews, A. K. Robinson, and F. Rodríguez-Quiñones, "Bacterial iron homeostasis," *FEMS Microbiol. Rev.*, vol. 27, no. 2–3, pp. 215–237, 2003, doi: 10.1016/S0168-6445(03)00055-X.

[32] C. M. H. Ferreira, Â. Vilas-Boas, C. A. Sousa, H. M. V. M. Soares, and E. V. Soares, "Comparison of five bacterial strains producing siderophores with ability to chelate iron under alkaline conditions," *AMB Express*, vol. 9, no. 1, 2019, doi: 10.1186/s13568-019-0796-3.

[33] D. A. Ams, P. A. Maurice, L. E. Hersman, and J. H. Forsythe, "Siderophore production by an aerobic Pseudomonas mendocina bacterium in the presence of kaolinite," *Chem. Geol.*, vol. 188, no. 3–4, pp. 161–170, 2002, doi: 10.1016/S0009-2541(02)00077-3.

[34] M. S. Sonawane, R. D. Chaudhary, Y. S. Shouche, and R. Z. Sayyed, "Insect Gut Bacteria: A Novel Source for Siderophore Production," *Proc. Natl. Acad. Sci. India Sect. B - Biol. Sci.*, vol. 88, no. 2, pp. 567–572, 2018, doi: 10.1007/s40011-016-0785-0.

[35] S. Filippidou *et al.*, "Adaptive strategies in a poly-extreme environment: Differentiation of Vegetative Cells in Serratia ureilytica and Resistance to Extreme Conditions," *Front. Microbiol.*, vol. 10, no. FEB, pp. 1–13, Feb. 2019, doi: 10.3389/fmicb.2019.00102.

[36] D. Barnawal, N. Bharti, D. Maji, C. S. Chanotiya, and A. Kalra, "1-Aminocyclopropane-1-carboxylic acid (ACC) deaminase-containing rhizobacteria protect Ocimum sanctum plants during waterlogging stress via reduced ethylene generation," *Plant Physiol. Biochem.*, vol. 58, pp. 227–235, Sep. 2012, doi: 10.1016/j.plaphy.2012.07.008.

[37] P. Visca, F. Imperi, and I. L. Lamont, "Pyoverdine siderophores: from biogenesis to biosignificance," *Trends Microbiol.*, vol. 15, no. 1, pp. 22–30, Jan. 2007, doi: 10.1016/j.tim.2006.11.004.

[38] C. Ferret, T. Sterckeman, J. Y. Cornu, S. Gangloff, I. J. Schalk, and V. A. Geoffroy, "Siderophore-promoted dissolution of smectite by fluorescent Pseudomonas," *Environ. Microbiol. Rep.*, vol. 6, no. 5, pp. 459–467, 2014, doi: 10.1111/1758-2229.12146.

[39] T. A. Ronnebaum and A. L. Lamb, "Nonribosomal peptides for iron acquisition: pyochelin biosynthesis as a case study," *Curr. Opin. Struct. Biol.*, vol. 53, pp. 1–11, 2018, doi: 10.1016/j.sbi.2018.01.015.

[40] H. Bickel, G. E. Hall, W. Keller-Schierlein, V. Prelog, E. Vischer, and A. Wettstein, "Stoffwechselprodukte von Actinomyceten. 27. Mitteilung. Über die Konstitution von Ferrioxamin B," *Helv. Chim. Acta*, vol. 43, no. 7, pp. 2129–2138, 1960, doi: 10.1002/hlca.19600430732.

[41] D. Kalinowski and D. Richardson, "The evolution of iron chelators for the treatment of iron overload disease and cancer," *Pharmacol. Rev.*, vol. 57, no. 4, pp. 547–583, 2005, doi: 10.1124/pr.57.4.2.547.

[42] C. Rémazeilles *et al.*, "Microbiologically influenced corrosion of archaeological artefacts:Characterisation of iron(II) sulfides by Raman spectroscopy," *J. Raman Spectrosc.*, vol. 41, no. 11, pp. 1425–1433, 2010, doi: 10.1002/jrs.2717.

[43] C. Rémazeilles, K. Tran, E. Guilminot, E. Conforto, and P. Refait, "Study of Fe(II) sulphides in waterlogged archaeological wood," *Stud. Conserv.*, vol. 58, no. 4, pp. 297–307, 2013, doi: 10.1179/2047058412Y.0000000071.

[44] S. Norbakhsh, I. Bjurhager, and G. Almkvist, "Impact of iron(II) and oxygen on degradation of oak – modeling of the Vasa wood," *Holzforschung*, vol. 68, no. 6, pp. 649–655, 2014, doi: https://doi.org/10.1515/hf-2013-0197.

[45] G. Almkvist and I. Persson, "Extraction of iron compounds from wood from the Vasa," *Holzforschung*, vol. 60, no. 6, pp. 678–684, 2006, doi: 10.1515/HF.2006.114.

[46] C. Pelé, E. Guilminot, S. Labroche, G. Lemoine, and G. Baron, "Iron removal from waterlogged wood: Extraction by electrophoresis and chemical treatments," *Stud. Conserv.*, vol. 60, no. 3, pp. 155–171, May 2015, doi: 10.1179/2047058413Y.0000000110.

[47] S. M. Kraemer, "Iron oxide dissolution and solubility in the presence of siderophores," *Aquat. Sci.*, vol. 66, no. 1, pp. 3–18, 2004, doi: 10.1007/s00027-003-0690-5.

[48] A. Robin, G. Vansuyt, P. Hinsinger, J. M. Meyer, J. F. Briat, and P. Lemanceau, "Chapter 4 Iron Dynamics in the Rhizosphere," in *Advances in Agronomy*, vol. 99, no. 08, 2008, pp. 183–225.

[49] P. U. Reichard, R. Kretzschmar, and S. M. Kraemer, "Dissolution mechanisms of goethite in the presence of siderophores and organic acids," *Geochim. Cosmochim. Acta*, vol. 71, no. 23, pp. 5635–5650, Dec. 2007, doi: 10.1016/j.gca.2006.12.022.

[50] J. L. Pierre and I. Gautier-Luneau, "Iron and citric acid: A fuzzy chemistry of ubiquitous biological relevance," *BioMetals*, vol. 13, no. 1, pp. 91–96, 2000, doi: 10.1023/A:1009225701332.

[51] Z. Wang, W. D. C. Schenkeveld, S. M. Kraemer, and D. E. Giammar, "Synergistic Effect of Reductive and Ligand-Promoted Dissolution of Goethite," *Environ. Sci. Technol.*, vol. 49, no. 12, pp. 7236–7244, Jun. 2015, doi: 10.1021/acs.est.5b01191.

[52] E. Farkas, É. A. Enyedy, L. Zékány, and G. Deák, "Interaction between iron(II) and hydroxamic acids: Oxidation of iron(II) to iron(III) by desferrioxamine B under anaerobic conditions," *J. Inorg. Biochem.*, vol. 83, no. 2–3, pp. 107–114, 2001, doi: 10.1016/S0162-0134(00)00197-5.

[53] R. Xiao and W. S. Kisaalita, "Fluorescent pseudomonad pyoverdines bind and oxidize ferrous ion," *Appl. Environ. Microbiol.*, vol. 64, no. 4, pp. 1472–1476, 1998.

[54] L. L. Stookey, “Ferrozine-A New Spectrophotometric Reagent for Iron,” vol. 42, no. 7, pp. 779–781, 1970, doi: 10.1021/ac60289a016.

[55] T. Yoshida, K. I. Hayashi, and H. Ohmoto, “Dissolution of iron hydroxides by marine bacterial siderophore,” *Chem. Geol.*, vol. 184, no. 1–2, pp. 1–9, 2002, doi: 10.1016/S0009-2541(01)00297-2.

[56] P. Larry E. Hersman, Allison Huang, “Siderophore Production and Iron Reduction by Pseudomonas mendocina in Response to Iron Deprivation,” *Geomicrobiol. J.*, vol. 17, no. 4, pp. 261–273, Oct. 2000, doi: 10.1080/01490450050192965.

[57] C. M. Fennessey, M. E. Jones, M. Taillefert, and T. J. Dichristina, “Siderophores are not involved in Fe(III) solubilization during anaerobic Fe(III) respiration by shewanella oneidensis MR-1,” *Appl. Environ. Microbiol.*, vol. 76, no. 8, pp. 2425–2432, 2010, doi: 10.1128/AEM.03066-09.

[58] A. Robin, G. Vansuyt, P. Hinsinger, J. M. Meyer, J. F. Briat, and P. Lemanceau, “Iron Dynamics in the Rhizosphere. Consequences for Plant Health and Nutrition,” *Adv. Agron.*, vol. 99, no. 08, pp. 183–225, 2008, doi: 10.1016/S0065-2113(08)00404-5.

[59] V. K. S., S. Menon, H. Agarwal, and D. Gopalakrishnan, “Characterization and optimization of bacterium isolated from soil samples for the production of siderophores,” *Resour. Technol.*, vol. 3, no. 4, pp. 434–439, 2017, doi: 10.1016/j.reffit.2017.04.004.

[60] S. C. M. Haaijer, L. P. M. Lamers, A. J. P. Smolders, M. S. M. Jetten, and H. J. M. Op de Camp, “Iron sulfide and pyrite as potential electron donors for microbial nitrate reduction in freshwater wetlands,” *Geomicrobiol. J.*, vol. 24, no. 5, pp. 391–401, 2007, doi: 10.1080/01490450701436489.

[61] R. J. Abergel *et al.*, “The Siderocalin/Enterobactin Interaction: A Link between Mammalian Immunity and Bacterial Iron Transport 1,” *J. Am. Chem. Soc.*, vol. 130, no. 34, pp. 11524–11534, Aug. 2008, doi: 10.1021/ja803524w.

[62] B. Qi and M. Han, “Microbial Siderophore Enterobactin Promotes Mitochondrial Iron Uptake and Development of the Host via Interaction with ATP Synthase,” *Cell*, vol. 175, no. 2, pp. 571-582.e11, 2018, doi: 10.1016/j.cell.2018.07.032.

[63] V. Gasser *et al.*, “Catechol siderophores repress the pyochelin pathway and activate the enterobactin pathway in Pseudomonas aeruginosa: An opportunity for siderophore-antibiotic conjugates development,” *Environ. Microbiol.*, vol. 18, no. 3, pp. 819–832, 2016, doi: 10.1111/1462-2920.13199.

[64] G. Berg, “Plant–microbe interactions promoting plant growth and health: perspectives for controlled use of microorganisms in agriculture,” *Appl. Microbiol. Biotechnol.*, vol. 84, no. 1, pp. 11–18, Aug. 2009, doi: 10.1007/s00253-009-2092-7.

[65] B. E. Kalinowski, L. J. Liermann, S. Givens, and S. L. Brantley, “Rates of bacteria-promoted solubilization of Fe from minerals: A review of problems and approaches,” *Chem. Geol.*, vol. 169, no. 3–4, pp. 357–370, 2000, doi: 10.1016/S0009-2541(00)00214-X.

[66] C. Poggenburg, R. Mikutta, P. Liebmann, M. Koch, and G. Guggenberger, “Siderophore-promoted dissolution of ferrihydrite associated with adsorbed and coprecipitated natural organic matter,” *Org.*

Geochem., 2018, doi: 10.1016/J.ORGGEOCHEM.2018.09.004.

[67] X. Liu *et al.*, "Microbial siderophores and root exudates enhanced goethite dissolution and Fe/As uptake by As-hyperaccumulator Pteris vittata," *Environ. Pollut.*, vol. 223, pp. 230–237, 2017, doi: 10.1016/j.envpol.2017.01.016.

[68] S. F. Cheah, S. M. Kraemer, J. Cervini-Silva, and G. Sposito, "Steady-state dissolution kinetics of goethite in the presence of desferrioxamine B and oxalate ligands: Implications for the microbial acquisition of iron," *Chem. Geol.*, vol. 198, no. 1–2, pp. 63–75, 2003, doi: 10.1016/S0009-2541(02)00421-7.

[69] L. J. Liermann, B. E. Kalinowski, S. L. Brantley, and J. G. Ferry, "Role of bacterial siderophores in dissolution of hornblende," *Geochim. Cosmochim. Acta*, vol. 64, no. 4, pp. 587–602, Feb. 2000, doi: 10.1016/S0016-7037(99)00288-4.

[70] Y. Fors and M. Sandström, "Sulfur and iron in shipwrecks cause conservation concerns," *Chem. Soc. Rev.*, vol. 35, no. 5, pp. 399–415, 2006, doi: 10.1039/b507010b.

[71] L. Comensoli, J. Maillard, M. Albini, F. Sandoz, P. Junier, and E. Joseph, "Use of Bacteria To Stabilize Archaeological Iron," *Appl. Environ. Microbiol.*, vol. 83, no. 9, pp. e03478-16, May 2017, doi: 10.1128/AEM.03478-16.

[72] E. Joseph *et al.*, "Protection of metal artifacts with the formation of metal-oxalates complexes by Beauveria bassiana," *Front. Microbiol.*, vol. 2, pp. 1–8, 2012, doi: 10.3389/fmicb.2011.00270.

[73] P. B. Roig, J. L. Regidor Ros, and R. M. Estellés, "Biocleaning of nitrate alterations on wall paintings by Pseudomonas stutzeri," *Int. Biodeterior. Biodegrad.*, vol. 84, pp. 266–274, Oct. 2013, doi: 10.1016/j.ibiod.2012.09.009.

[74] G. Ranalli *et al.*, "Biotechnology applied to cultural heritage: Biorestoration of frescoes using viable bacterial cells and enzymes," *J. Appl. Microbiol.*, vol. 98, no. 1, pp. 73–83, 2005, doi: 10.1111/j.1365-2672.2004.02429.x.

[75] H. Wei and L. Aristilde, "Structural characterization of multiple pyoverdines secreted by two Pseudomonas strains using liquid chromatography-high resolution tandem mass spectrometry with varying dissociation energies," *Anal. Bioanal. Chem.*, vol. 407, no. 16, pp. 4629–4638, 2015, doi: 10.1007/s00216-015-8659-5.

[76] A. Chiadò, L. Varani, F. Bosco, and L. Marmo, "Opening study on the development of a new biosensor for metal toxicity based on pseudomonas fluorescens pyoverdine," *Biosensors*, vol. 3, no. 4, pp. 385–399, 2013, doi: 10.3390/bios3040385.

[77] I. Gwose and K. Taraz, "Pyoverdine aus Pseudomonas putida (Pyoverdins from Pseudomonas putida)," *Naturforsch*, vol. 47c, pp. 487–502, Feb. 1992.

[78] H. Boukhalfa, S. D. Reilly, R. Michalczyk, S. Iyer, and M. P. Neu, "Iron(III) coordination properties of a pyoverdin siderophore produced by Pseudomonas putida ATCC 33015," *Inorg. Chem.*, vol. 45, no. 14, pp. 5607–5616, 2006, doi: 10.1021/ic060196p.

[79] Y. Fors and V. Richards, "The Effects of the Ammonia Neutralizing Treatment on Marine Archaeological

Vasa Wood," *Stud. Conserv.*, vol. 55, no. 1, pp. 41–54, Mar. 2010, doi: 10.1179/sic.2010.55.1.41.

[80] C. M. H. Ferreira, I. S. S. Pinto, E. V. Soares, and H. M. V. M. Soares, "(Un)suitability of the use of pH buffers in biological, biochemical and environmental studies and their interaction with metal ions-a review," *RSC Adv.*, vol. 5, no. 39, pp. 30989–31003, 2015, doi: 10.1039/c4ra15453c.

[81] H. Gamal, K. Abdelgawad, and S. Elkatatny, "New environmentally friendly acid system for iron sulfide scale removal," *Sustain.*, vol. 11, no. 23, 2019, doi: 10.3390/su11236727.

[82] D. Rickard and G. W. Luther, "Chemistry of iron sulfides," *Chem. Rev.*, vol. 107, no. 2, pp. 514–562, 2007, doi: 10.1021/cr0503658.

[83] D. Rickard, "The solubility of FeS," *Geochim. Cosmochim. Acta*, vol. 70, no. 23 SPEC. ISS., pp. 5779–5789, 2006, doi: 10.1016/j.gca.2006.02.029.

[84] N. Mazinanian, I. Odnevall Wallinder, and Y. Hedberg, "Comparison of the influence of citric acid and acetic acid as simulant for acidic food on the release of alloy constituents from stainless steel AISI 201," *J. Food Eng.*, vol. 145, no. March 1973, pp. 51–63, 2015, doi: 10.1016/j.jfoodeng.2014.08.006.

[85] S. Choi, "Foxing on paper: a literature review," *Jaic*, vol. 46, no. 2, pp. 137–152, 2007, doi: 10.1179/019713607806112378.

[86] H. Xing, O. Ma, Q. Yong, C. Yang, X. Chao, and Y. Li, "Study on Removal of Iron Rust from Paper Objects with Thiourea Dioxide," *IOP Conf. Ser. Mater. Sci. Eng.*, vol. 364, p. 012081, 2018, doi: 10.1088/1757-899X/364/1/012081.

[87] G. Almkvist and I. Persson, "Distribution of iron and sulfur and their speciation in relation to degradation processes in wood from the Swedish warship Vasa," *New J. Chem.*, vol. 35, no. 7, p. 1491, 2011, doi: 10.1039/c1nj20056a.

[88] J. Preston, A. D. Smith, E. J. Schofield, A. V. Chadwick, M. A. Jones, and J. E. M. Watts, "The effects of Mary Rose conservation treatment on iron oxidation processes and microbial communities contributing to acid production in marine archaeological timbers," *PLoS One*, vol. 9, no. 2, 2014, doi: 10.1371/journal.pone.0084169.

[89] M. Sandström, Y. Fors, F. Jalilehvand, E. Damian, and U. Gelius, "Analyses of sulfur and iron in marine-archaeological wood," *Proc. 9th ICOM Gr. Wet Org. Archaeol. Mater. Conf. Copenhagen, 2004*, pp. 181–202, 2005.

[90] K. M. Wetherall *et al.*, "Sulfur and iron speciation in recently recovered timbers of the Mary Rose revealed via X-ray absorption spectroscopy," *J. Archaeol. Sci.*, vol. 35, no. 5, pp. 1317–1328, 2008, doi: 10.1016/j.jas.2007.09.007.

[91] S. Rapti, S. Rivers, and A. Pournou, "Removing iron corrosion products from museum artefacts : Investigating the effectiveness of innovative green chelators," no. November 2015, 2016.

[92] S. Rapti, S. Boyatzis, S. Rivers, A. Velios, and A. Pournou, "Removing iron stains from wood and textile objects: assessing gelled siderophores as novel green chelators," Aug. 2017.

[93] M. Strlič, J. Kolar, and B. Pihlar, "Some preventive cellulose antioxidants studied by an aromatic

hydroxylation assay," *Polym. Degrad. Stab.*, vol. 73, no. 3, pp. 535–539, Jan. 2001, doi: 10.1016/S0141-3910(01)00120-3.

[94] J. A. Méndez-Líter, J. Gil-Muñoz, M. Nieto-Domínguez, J. Barriuso, L. I. De Eugenio, and M. J. Martínez, "A novel, highly efficient β-glucosidase with a cellulose-binding domain: Characterization and properties of native and recombinant proteins," *Biotechnol. Biofuels*, vol. 10, no. 1, pp. 1–15, 2017, doi: 10.1186/s13068-017-0946-2.

[95] M. Monachon *et al.*, "Characterization of model samples simulating degradation processes induced by iron and sulfur species on waterlogged wood," *Microchem. J.*, vol. 155, p. 104756, 2020.

[96] J. A. Bourdoiseau, M. Jeannin, R. Sabot, C. Rémazeilles, and P. Refait, "Characterisation of mackinawite by Raman spectroscopy: Effects of crystallisation, drying and oxidation," *Corros. Sci.*, vol. 50, no. 11, pp. 3247–3255, 2008, doi: 10.1016/j.corsci.2008.08.041.

[97] J. A. Bourdoiseau, M. Jeannin, C. Rémazeilles, R. Sabot, and P. Refait, "The transformation of mackinawite into greigite studied by Raman spectroscopy," *J. Raman Spectrosc.*, vol. 42, no. 3, pp. 496–504, 2011, doi: 10.1002/jrs.2729.

[98] M. Hanesch, "Raman spectroscopy of iron oxides and (oxy)hydroxides at low laser power and possible applications in environmental magnetic studies," *Geophys. J. Int.*, vol. 177, no. 3, pp. 941–948, 2009, doi: 10.1111/j.1365-246X.2009.04122.x.

[99] P. Wilfert *et al.*, "Sulfide induced phosphate release from iron phosphates and its potential for phosphate recovery," *Water Res.*, vol. 171, p. 115389, 2020, doi: 10.1016/j.watres.2019.115389.

[100] U. P. Agarwal and S. A. Ralph, "FT-Raman Spectroscopy of Wood: Identifying Contributions of Lignin and Carbohydrate Polymers in the Spectrum of Black Spruce (Picea Mariana)," *Appl. Spectrosc.*, vol. 51, no. 11, pp. 1648–1655, Nov. 1997, doi: 10.1366/0003702971939316.

[101] D. L. A. De Faria, S. Venâncio Silva, and M. T. De Oliveira, "Raman microspectroscopy of some iron oxides and oxyhydroxides," *J. Raman Spectrosc.*, vol. 28, no. 11, pp. 873–878, 1997, doi: 10.1002/(sici)1097-4555(199711)28:11<873::aid-jrs177>3.0.co;2-b.

[102] P. Taylor and D. W. Shoesmith, " The nature of green alkaline iron sulfide solutions and the preparation of sodium iron(III) sulfide, NaFeS 2 ," *Can. J. Chem.*, vol. 56, no. 22, pp. 2797–2802, 1978, doi: 10.1139/v78-462.

[103] A. Lassin, P. Piantone, C. Crouzet, F. Bodénan, and P. Blanc, "Estimated thermodynamic properties of NaFeS2 and erdite (NaFeS2:2H2O)," *Appl. Geochemistry*, vol. 45, pp. 14–24, 2014, doi: 10.1016/j.apgeochem.2014.02.015.

[104] N. Kip and J. A. Van Veen, "The dual role of microbes in corrosion," *ISME J.*, vol. 9, no. 3, pp. 542–551, 2015, doi: 10.1038/ismej.2014.169.

[105] A. Pedersen and M. Hermansson, "Inhibition of metal corrosion by bacteria," *Biofouling*, vol. 3, no. 1, pp. 1–11, 1991, doi: 10.1080/08927019109378157.

[106] N. N. Rao, S. Liu, and A. Kornberg, "Inorganic polyphosphate in Escherichia coli: The phosphate regulon

and the stringent response," *J. Bacteriol.*, vol. 180, no. 8, pp. 2186–2193, 1998, doi: 10.1128/jb.180.8.2186-2193.1998.

[107] K. M. Tobin, J. W. McGrath, A. Mullan, J. P. Quinn, and K. E. O'Connor, "Polyphosphate accumulation by Pseudomonas putida CA-3 and other medium-chain-length polyhydroxyalkanoate-accumulating bacteria under aerobic growth conditions," *Appl. Environ. Microbiol.*, vol. 73, no. 4, pp. 1383–1387, 2007, doi: 10.1128/AEM.02007-06.

[108] P. J. Sullivan, J. L. Yelton, and K. J. Reddy, "Iron sulfide oxidation and the chemistry of acid generation.," *Environ. Geol. Water Sci.*, vol. 11, no. 2, pp. 289–295, 1988.

[109] G. Chaumat, D. Zahnweh, X. Martinez-Carballal, L. Caillat, T. Guiblain, and M. Dbeaurain, "Development of curative and preventive treatments of waterlogged archaeological wood contaminated by pyrite," 2019.

[110] Y. Yoshimura, Y. Matsuzaki, T. Watanabe, K. Uchiyama, K. Ohsawa, and K. Imaeda, "Effects of Buffer Solutions and Chelators on the Generation of Hydroxyl Radical and the Lipid Peroxidation in the Fenton Reaction System.," *J. Clin. Biochem. Nutr.*, vol. 13, no. 3, pp. 147–154, 1992, doi: 10.3164/jcbn.13.147.

[111] O. Wiche, D. Tischler, C. Fauser, J. Lodemann, and H. Heilmeier, "Effects of citric acid and the siderophore desferrioxamine B (DFO-B) on the mobility of germanium and rare earth elements in soil and uptake in Phalaris arundinacea," *Int. J. Phytoremediation*, vol. 19, no. 8, pp. 746–754, 2017, doi: 10.1080/15226514.2017.1284752.

[112] M. L. Guerinot, E. J. Meidl, and O. Plessner, "Citrate as a siderophore in Bradyrhizobium japonicum," *J. Bacteriol.*, vol. 172, no. 6, pp. 3298–3303, 1990, doi: 10.1128/jb.172.6.3298-3303.1990.

[113] D. W. Grattan and R. W. Clarke, "Conservation of waterlogged wood," *Conserv. Mar. Archaeol. Objects*, pp. 164–206, Jan. 1987, doi: 10.1016/B978-0-408-10668-9.50015-0.

[114] J. M. Domínguez-Vera, "Iron(III) complexation of Desferrioxamine B encapsulated in apoferritin," *J. Inorg. Biochem.*, vol. 98, no. 3, pp. 469–472, 2004, doi: 10.1016/j.jinorgbio.2003.12.015.

[115] V. A. Gerasimov *et al.*, "Raman spectroscopy for identification of wood species," *J. Phys. Conf. Ser.*, vol. 741, no. 1, 2016, doi: 10.1088/1742-6596/741/1/012131.

[116] G. Almkvist, "The chemistry of the Vasa," Doctoral Thesis, Uppsala, 2008.

[117] N. N. Sing, A. Husaini, A. Zulkharnain, and H. A. Roslan, "Decolourisation Capabilities of Ligninolytic Enzymes Produced by Marasmius cladophyllus UMAS MS8 on Remazol Brilliant Blue R and Other Azo Dyes," *Biomed Res. Int.*, vol. 2017, 2017, doi: 10.1155/2017/1325754.

[118] K. L. Straub, M. Benz, and B. Schink, "Iron metabolism in anoxic environments at near neutral pH," *FEMS Microbiol. Ecol.*, vol. 34, no. 3, pp. 181–186, 2000, doi: 10.1016/S0168-6496(00)00088-X.

[119] N. J. Dixon, "Greener Chelating Agents," in *Handbook of Green Chemistry Volume 9: Designing Safer Chemicals*, First Edit., R. Boethling and A. Voutchkova, Eds. Wiley-VCH Verlag GmbH & Co. KGaA, 2012, pp. 281–307.

[120] K. Asemave, "Greener Chelators for Recovery of Metals and Other Applications," *Org. Med. Chem. Int.*

J., vol. 6, no. 4, May 2018, doi: 10.19080/OMCIJ.2018.06.555694.

[121] F. I. for O. S. and H.-N. Unit, "EDETIC ACID (EDTA) Summary Risk Assessment Report," Dortmund, Germany, 2004. [Online]. Available: https://echa.europa.eu/documents/10162/5ed7db13-e932-4999-8514-378ce88ca51f.

Chapter 3

BIOLOGICAL OXIDATION OF SULFUR SPECIES

Pyrite. © Barta IV

Section 3.2.1 of this chapter is based on the following published article:

- M. Albelda Berenguer., M. Monachon, C. Jacquet, P. Junier, C. Rémazeilles, E. J. Schofield and E. Joseph, "Biological oxidation of sulfur compounds in artificially degraded wood," *Int. Biodeterior. Biodegradation*, vol. 141, pp. 62–70, Jul. 2019, doi: 10.1016/j.ibiod.2018.06.009.

Results from sections 3.1 and 3.2.2 are not published.

Summary

Sulfur oxidation is an early metabolic pathway. Several bacteria are able to oxidise sulfur compounds to obtain energy. In this chapter, we worked with the chemolithotroph bacterium *Thiobacillus denitrificans* as model for the oxidation of sulfur species under neutral pH in denitrifying conditions, or oxic environment. First, the solubilisation of three common sulfur compounds found in waterlogged wood was studied. *T. denitrificans* was able to oxidise elemental sulfur using nitrates and oxygen. However, the oxidation of mackinawite and pyrite was more challenging, and biological oxidation was not clearly observed in the experimental conditions, especially for pyrite. On the other hand, *T. denitrificans* was able to metabolise synthetic sulfur compounds present in model wood samples (oak and balsa wood). In particular, the bacteria were able to solubilise partially oxidised mackinawite. Although, secondary abiotic reactions were detected. The formation of phosphate precipitates was observed in both samples and abiotic controls. When other buffer agent was included in the medium solution, it seemed that iron oxides precipitation occurred. In both cases, iron was not co-extracted with sulfur species highlighting the need for an extraction treatment that includes sulfur and iron mobilisation.

3.1 Oxidation of mineral sulfur phases

Abstract

Iron sulfides are common compounds in the Earth crust, being pyrite the most abundant. The oxidation of these phases in anoxic conditions is not well-understood. In particular, discussion still exists about the possibility of microbial oxidation of pyrite in these conditions. The solubilisation of these species is of interest in many fields, here we are interested in the removal of iron sulfides and other sulfur species from waterlogged archaeological wood (WAW). The bacterium *Thiobacillus denitrificans* was selected as model to carry out the oxidation of elemental sulfur, mackinawite and pyrite under several experimental conditions. The oxidation of elemental sulfur to sulfates was possible under all conditions. Mackinawite was also oxidised but with very low conversion rates and not in all set-ups. Finally, pyrite is still under discussion. As other researchers found before, the oxidation of pyrite was not clearly driven by solely biological processes and further investigations are needed.

Introduction

Iron sulfides establish a diverse group of solids and dissolved complexes that are an essential component in the biogeochemical cycles of iron and sulfur [1]. The connection between the iron and sulfur cycles is strongly influenced by microbial activity. For instance, sulfate anions (SO_4^{2-}), which are reduced to sulfides by bacteria, react with ferrous iron (Fe^{2+}) to form iron sulfides [2]. The further oxidation of the iron sulfides minerals and other sulfur species is closing the cycle. The involvement of microorganisms in the last step has been studied in natural environments [3], [4]. For example, pyrite (FeS_2) oxidation under oxic and low pH conditions has been extensively studied. Acidophilic microbes, represented by *Acidothiobacillus ferrooxidans*, enhance pyrite dissolution through aerobic ferrous iron oxidation, which produces soluble Fe^{3+} ions that chemically attack the pyrite [5], [6]. Even though this microbial process is very successful oxidizing iron sulfides, these conditions are not ideal in a wood matrix. Acidic conditions promote acid hydrolysis of cellulose [7]. However, the oxidation of iron sulfides has also been observed in in sediments, shallow aquifers, and soils that present an anoxic and circumneutral environment [25]. Oxidation in these conditions is more suitable for the further application in a wood matrix.

Nitrates consumption related to sulfates production has been detected at several pyrite-bearing aquifers over the past few years [3], [8], [25]. Field studies suggested that the nitrates reduction and sulfates production observed was caused by the mediated microbial nitrate-dependent

oxidation of pyrite [4], [9]. However, laboratory experiments are contradictory. Using the bacterium *Thiobacillus denitrificans* as model for such oxidation, some studies showed the capability of the bacteria to couple the reduction of nitrates with the production of sulfates [10]. On the contrary, other studies failed to correlate the oxidation of pyrite to the reduction of nitrates. In the latest, the oxidation of co-existent elemental sulfur on the pyrite surface is proposed as the source for sulfates production [11]. Pyrite is an acid-non-soluble metal; thus, all valence bands are derived from metal orbitals. In this metal sulfide, the covalent bonds between sulfur and metal element are kept until six successive one-electron oxidation steps occur and thiosulfates are produced. The oxidation of pyrite is so far known exclusively as the transfer of valence band electrons to Fe^{3+} ions [12]. The bacteria here acquire energy through iron-assisted electron shuttling.

However, two pathways have been proposed for the anaerobic pyrite oxidation at neutral pH [13]. The indirect mechanism is the already described oxidation of pyrite by Fe^{3+} ions. As for aerobic acidophiles, microbial oxidation of ferrous iron would occur, but in this case coupled to nitrate reduction. However, this would require an acidic micro niche or chelated iron species, as in neutral pH free aqueous iron(III) tends to precipitate. In these conditions, a second mechanism postulates a direct attack of the pyrite surface by cell attachment and destabilization of pyrite surface [13]. More experimental evidence however is required to validate both pathways, and the microbial pyrite oxidation remains unclear. On the contrary, iron monosulfides, such as mackinawite (FeS), are acid-soluble minerals and the proton-promoted dissolution pathway is clearly defined. Sulfur-oxidizing bacteria (SOB) oxidise free hydrogen sulfide (H_2S), which is formed during proton attack of the iron sulfide, to sulfuric acid. Thus, the protons previously consumed by the metal sulfide dissolution are regenerated [12].

The oxidation of iron sulfides and elemental sulfur has been investigated for different applications. In particular, the denitrification of wastewater by SOB is possible with the addition of iron sulfides or elemental sulfur [14], [15]. Recently, *T. denitrificans* has been proposed for the dissolution of pyrite inside waterlogged wood [16]. The capability of conducting nitrate-dependent oxidation of pyrite at neutral pH will open many lines of application.

T. denitrificans was the first non-filamentous chemolithoautotrophic bacteria discovered to be able to use inorganic sulfur as energy source [17], [18]. The goal of this study is to evaluate the capacity of *T. denitrificans* to oxidise mineral sulfur phases commonly found in waterlogged archaeological wood. Elemental sulfur (α-S_8), mackinawite (FeS) and pyrite (FeS_2) were used

as main mineral phases. The oxidation was conducted under different conditions to evaluate diverse possible application protocols.

Materials and Methods

Bacteria and culture conditions

Thiobacillus denitrificans (DSM 12475) was obtained from the German Collection of Microorganisms and Cell Cultures (DMSZ GmbH, Germany). The strain was cultivated using standard anaerobic techniques at 30 °C in the dark using 113 medium (2017 DMSZ).

Sulfur mineral phases

Elemental sulfur (α-S_8) was purchased with a purity of 99.998% based on trace metals analysis (Sigma-Aldrich, Unites States). Mackinawite (FeS) was obtained with a purity of 99.9%, (trace metal basis) and -100 mesh (Acros Organics, Unites States). Minerals were sterilized washing with ethanol 70% (v/v).

Natural pyrite (FeS_2) crystals (1-2 cm in diameter) acquired from *Pierre qui Roule* (http://www.pierrequiroule.ch), Nods, Switzerland, were pre-ground under ambient atmosphere in an agate mortar to a particle size of 1-5 mm. The final grinding was done also under ambient atmosphere in an automatic mortar grinder RM 200 (Retsch, Germany). After the grinding, the pyrite powder was sieved for a more uniform final product. The sieve used had a pore size of 45 µm (Sigma-Aldrich, Unites States). The resulting powder was resuspended in 200 mL N_2-flushed Milli-Q® water and sonicated for 45 min. After removing the water, the pyrite powder was washed twice in 200 mL of 1 M HCl shaking for 1 h at 180 rpm. Afterwards, the pyrite powder was washed three time in 200 mL of pure acetone shaking for 20 min at 220 rpm. Finally, the powder was rinsed twice in N_2-flushed Milli-Q® water. After removing the maximum water possible the pyrite powder was frozen at -20 ºC and lyophilized. Some samples of pyrite were only washed with HCl. The resulting dried powders was analysed by SEM-EDS, and XRD.

Oxidation experiments

Oxidation of mineral sulfur phases

The oxidation of the three mineral sulfur phases was conducted under several conditions (Table 3.1). *T. denitrificans* was grown at 30 °C in 113 medium (2017 DSMZ) for 5 days. Then, the cells were recovered by centrifugation and washed three time in medium 113 without nitrates,

or any sulfur or iron source. *T. denitrificans* was inoculated to every experiment to the final cell concentration mentioned in Table 3.1.

***Table 3.1**. Overview of the different experimental conditions for the study of biological oxidation of elemental sulfur, mackinawite or pyrite.*

	Experiment I	**Experiment II**	**Experiment II**	**Experiment IV**	**Experiment V**
Cell concentration (cells·mL^{-1})	~1x10^6	~1x10^6	~1x10^6	~1x10^6	~1x10^8
Initial nitrate concentration (mM)	20	20	20	20	20
Oxygen	-	-	yes	yes	-
Initial concentration of mineral (mM)	30	30	30	30	30
Additional sulfur source	-	2 or 8 mM thiosulfates	-	8 mM thiosulfates	-

[a]Exp. V was only conducted with pyrite powder.

In experiments without oxygen, the solution was degassed under vacuum (-960 mbar) and then N_2-flushed. Experiments were conducted in glass serum bottles sealed with butyl rubber stoppers and flushed with CO_2/N_2 (20/80%) at 30 °C in the darkness. Experiments where oxygen was not removed from the solution were carried out in no sealed bottles at 30 ªC in the dark. The oxidation medium consisted of a modified 113 medium where all the sulfur and iron compounds were removed. The final composition of the modified medium was: 15 mM KH_2PO_4, 20 mM KNO_3, 19 mM NH_4Cl, 3.2 mM $MgCl_2·6H_2O$, 30 mM $NaHCO_3$, and 2 mL of modified SL-4 oligo-elements solution (Table S 3.2). The bottles were filled with 100 mL of extraction medium and 30 mM of mineral. In experiment II, $Na_2S_2O_3·5H_2O$ was added anoxically to a final concentration of 2 or 8 mM (Exp. II.1 and II.2, respectively). In experiment IV, $Na_2S_2O_3·5H_2O$ was added to a final concentration of 8 mM Samples of the solutions and mineral powder were taken over time for further analyses.

Several controls were carried out to evaluate secondary reactions. Some bottles contained the mineral and nitrates but no *T. denitrificans* (abiotic oxidation control), others contained only the mineral and *T. denitrificans* but no nitrates (oxygen controls in experiments I, II and V). Controls for the additional sulfur source included $Na_2S_2O_3·6H_2O$ at the correct concentration, nitrates and *T. denitrificans*. Finally, controls for internal accumulation of sulfur contained only

nitrates and *T. denitrificans,* but no sulfur source. Experiments were performed in three independent replicates, whereas the controls were run in duplicate. One sample and one control bottle were not sampled over time to dismiss differences due to sampling.

Oxidation of iron sulfides in presence of iron chelators

The oxidation of pyrite is promoted by the presence of iron(III). To evaluate if the presence of chelated iron enhances the dissolution of pyrite, *T. denitrificans* was incubated with pyrite and three different iron chelators independently.

T. denitrificans was prepared as described above. Then, inoculated to the modified 113 medium where all the sulfur and iron compounds were removed. The solution was degassed under vacuum (-960 mbar) and then N_2-flushed. Experiments were conducted in glass serum bottles sealed with butyl rubber stoppers and flushed with CO_2/N_2 (20/80%) at 30 °C in the darkness. The final concentration of pyrite was 30 mM. Bottles containing 30 mM mackinawite were also inoculated and studied in the same way for comparison. The three iron chelators used were EDTA, and two siderophores, deferoxamine mesylate (DFOM, purchased as Desferal®, Novartis AG, Switzerland) and our purified pyoverdine (PVD). The final concentration of chelator in the solution was 0.8 mM. Samples of the solutions and mineral powder were taken over time for further analyses.

Several controls setup out to evaluate secondary reactions. Some bottles contained the mineral and the iron chelator but no *T. denitrificans* (abiotic oxidation control with chelator), others contained only the mineral (abiotic oxidation). Controls with the mineral, the iron chelator and *T. denitrificans* but no nitrates (oxygen controls). Controls with only the iron chelator and *T. denitrificans* (oxidation of chelator). Finally, controls for internal accumulation of sulfur containing only nitrates and *T. denitrificans* were also included. Experiments were performed in three independent replicates, whereas the controls were run in duplicate. One sample and one control bottle were not sampled over time to dismiss differences due to sampling.

Analytical methods

Ferrozine assay

In the experiments containing iron sulfides, iron oxidation was evaluated by the quantification of iron(II) with the Ferrozine assay [19]. Iron concentrations were measured over time in samples taken from the supernatant and from the solid fraction. Samples from the solution were filtered through a 0.22 µm PVDF membrane (BGB Analytik, Switzerland) to remove solid particles. Both samples were fixed mixing 800 µL of sample with 200 µL of 2 M sulfamic acid

(H_3NSO_3). In solid samples, iron will get solubilized from the solid phase. To calculate iron(II), 100 µL of the fixed solution were mixed with 900 µL of 0.1% (w/v) Ferrozine reagent (Sigma-Aldrich, United States) prepared in 100 mM HEPES (Sigma-Aldrich, United States) solution adjusted to pH 7. For the measurement of total iron, 150 µL of 1.5 M hydroxylamine-HCl were added to the previous mix. The absorbance was measured after 2 h at 562 nm with an Asys UVM 340 Microplate Reader (Biochrom, United Kingdom). Total iron and iron(II) in solution were calculated using the prepared standard curves with known concentrations of iron (supplementary material 2.2). Iron(III) concentrations are calculated subtracting iron(II) concentrations to total iron.

Ion chromatography (IC)

For the determination of the concentration of sulfates (SO_4^{2-}), nitrates (NO_3^-), nitrites (NO_2^-), and phosphates (PO_4^{3-}), samples were filtered at 0.22 µm (BGB Analytik, Switzerland) to remove residual particulate matter. Filtered samples were correctly diluted and analysed by ion chromatography (Dionex ICS-1600). The instrument was equipped with a conductivity detector, a Dionex Ion Pac™ AS14A (4 x 250 mm) anion exchange column, and a Dionex Ion PacTM RFIC™ (4 x 50 mm) guard column. A solution of 8 mM Na_2CO_3 and 1 mM $NaHCO_3$ was used at a flow rate of 1.3 $mL \cdot min^{-1}$ as mobile phase. The detection limit was 0.05 $mg \cdot L^{-1}$. Data was analysed with the Chromeleon™ software (Thermo Fisher Scientific, United States).

pH measurements

A 691pH Meter Metrohm (Metrohm AG, Switzerland) standard pHmeter was used to control the pH of the solution over time with an ionic electrode (unitrode 6.0259.100) calibrated with buffer solutions (pH 4, 7 and 9).

Scanning Electron Microscopy coupled with Energy Dispersive X-Ray Spectroscopy (SEM-EDS) analyses

Samples after incubation with the bacteria were prepared before observation as follows. Cultures were centrifuged and fixed for 1 h with 2.5% glutaraldehyde solution in 0.1 M sodium cacodylate, washed twice by centrifugation with the same solution and fixed again for 2 h with 1% osmium tetraoxide in 0.1 M sodium cacodylate. After the secondary fixation, the samples were washed twice with distilled water. Then dehydration steps were performed using different concentrations of ethanol (25%, 50%, 75%, 90%, 100% (v/v)) and then pure acetone. Finally, samples were mounted on stubs using carbon conductive tape. Elemental sulfur samples were coated with a layer of carbon using a Leica EM SCD050 (60 mA current, 5 cm, 5 s duration, argon gas). Samples were examined using a Thermo Scientific™ Scios™ 2 DualBeam™

(Thermo Fisher Scientific, Unites States) equipped with an energy-dispersive X-ray analyser (EDAX, Unites States). The samples were observed using an EDT detector (secondary electron acquisition), an acceleration potential of between 20-10 kV and a 7 mm working distance.

X-Ray Diffraction (XRD)

X-Ray diffraction (XRD) analyses were performed on pyrite powder at the end of the preparation protocol. The diffraction patterns were collected for $20 < 2\theta < 99$ using PANalyticalX'PertProMPD diffractometer equipped with a fast-linear detector and sample spinner. The measurement time was 60 h to acquire high statistics for better signal-to-noise ratio. The sensitivity of the XRD phase analyses was about 1 % weight.

Results and Discussion

Pyrite characterisation

X-ray diffractogram (XRD) patterns of the analysed powders corresponded to pyrite phase (Figure 3.1). However, an extra low intensity peak at 2theta of 26.6 ° was observed when the pyrite powder was washed with acetone. This peak was absent for samples only washed in HCl (Figure 3.1). No phase could be attributed to the extra peak. Moreover, EDS analyses revealed a Fe:S ratio of approximately 1:2 suggesting that the powder consisted of pyrite (Figure 3.2). Some minor contaminations were detected (Figure 3.2). Overall, pure pyrite crystals were assumed.

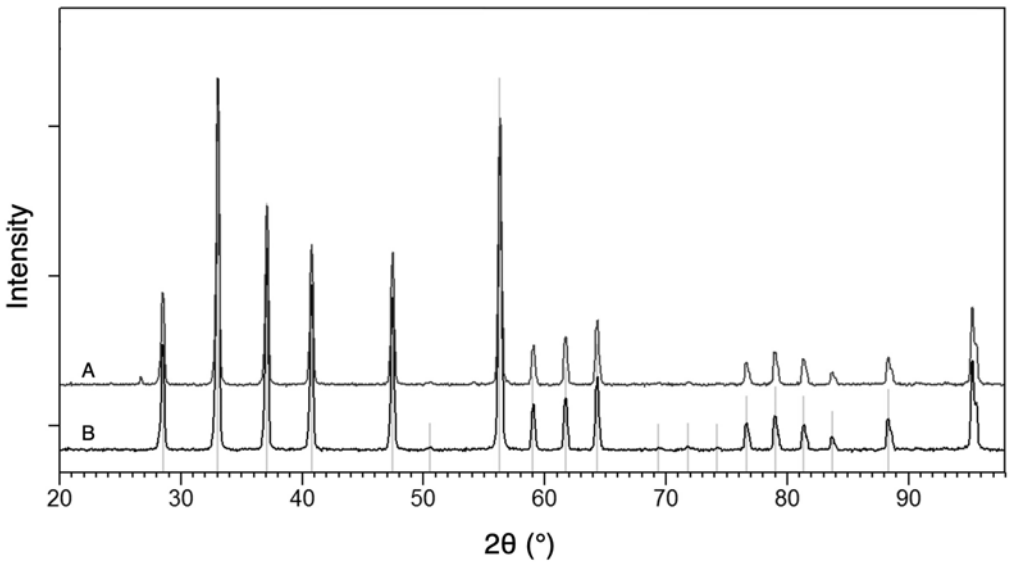

Figure 3.1. *X-ray diffractogram of pyrite HCl-acetone washed (A), and pyrite HCl washed (B). Vertical grey lines indicate the reference pyrite (FeS_2) pattern.*

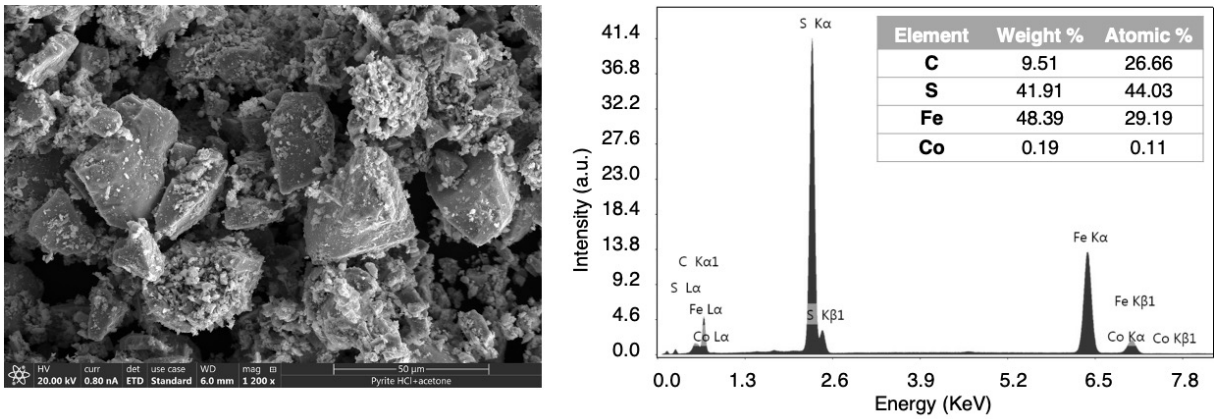

***Figure 3.2**. SEM image and corresponding EDS spectrum of the ground pyrite after HCl and acetone wash.*

The ground pyrite had a crystalline cubic structure, and due to the sieving, particles were of 50 µm or smaller (Figure 3.2). A wide range of sizes up to 50 µm were observed. The pyrite particles within the wood varies from nm to 20-50 µm [20], [21]. The HCl washing helped to remove the nanosized structures. However, some nanoparticles were still detected on the surface of bigger pyrite crystals (Figure 3.2). Previous studies have shown the capacity of *T. denitrificans* of oxidise the nanoparticulate fraction of pyrite [10]. The range of sizes in the experiment helped to figure out if the oxidation of pyrite by the bacteria is limited to the nanosized structures.

Oxidation of mineral sulfur phases

Elemental sulfur (α-S_8), mackinawite (FeS) and pyrite (FeS_2) are recurrent sulfur species detected in waterlogged wooden objects [20]. The extraction of these phases is important for the stability of the artefacts. Here, we studied the oxidation of the three compounds in different conditions.

First, we considered the oxidation of the three phases under anoxic environment. After 72 days of incubation, *T. denitrificans* was able to oxidise elemental sulfur, but the biological oxidation of mackinawite and pyrite was not as clear (Figure 3.3). The bacteria were able to develop with elemental sulfur more successfully than the other two sulfur species (Figure 3.3). *T. denitrificans* consumed 9.75 ±1.24 mM nitrates and generated 7.62 ±1.18 sulfates and 4.08 ±0.57 mM nitrites, respectively, in presence of elemental sulfur (Table 3.2). On the contrary, the bacteria only consumed 0.57 ±0.26 mM nitrates and produced 0.68 ±0.14 mM sulfates and 0.23 ±0.20 mM nitrites, respectively, in presence of mackinawite (Table 3.2). In the pyrite experiment, no significant consumption of nitrates (ΔNO_3^- = 0.19 ±0.06 mM), no production of nitrites and no significant release of sulfates (ΔSO_4^{2-} = 0.26 ±0.27 mM) was found (Table 3.2).

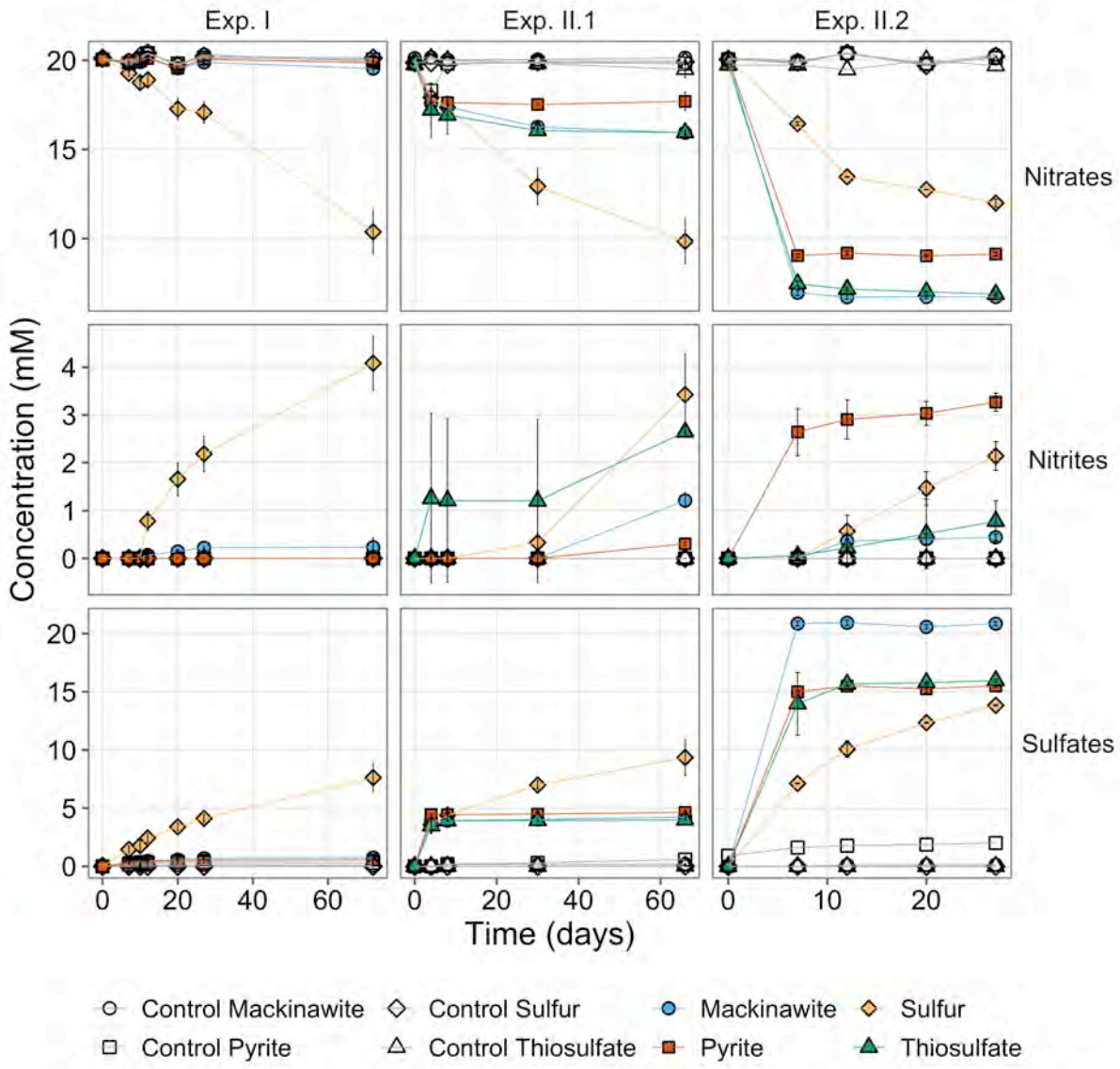

***Figure 3.3**. Concentration over time of nitrates, nitrites, and sulfates in presence of T. denitrificans (closed symbols) or abiotic controls without bacteria (open symbols), in the anoxic experimental set-ups (Exp. I, II.1 and II.2) for the different mineral sources under study: elemental sulfur, mackinawite, and pyrite. In experiments with thiosulfates addition (Exp. II.1 and II.2), sodium thiosulfate control is included. Error bars show standard deviation of two or three replicates.*

Similar studies have found that *T. denitrificans* is indeed able to use elemental sulfur as energy source, but not crystalline pyrite [11]. The changes observed with pyrite, are likely due to abiotic oxidation by residual oxygen in the solution. Similar amounts of sulfates were detected in the controls, and the standard deviations for consumption of nitrates suggest that the depletion observed is just due to measurement variations (Table 3.2). On the other hand, the results obtained with mackinawite point towards a biological oxidation. Even though the quantities detected were smaller than for elemental sulfur, sulfates detected in the samples were significantly higher than in the control. Moreover, nitrites were not detected in the controls

(Figure 3.3). Previous studies have also recorded a slight production of nitrites in *T. denitrificans* cultures amended with nitrates and FeS [10].

Calculated stoichiometry ratios (depleted nitrates/produced sulfates ($\Delta NO_3^-/\Delta SO_4^{2-}$) and depleted nitrates/produced nitrites ($\Delta NO_3^-/\Delta NO_2^-$)) for the elemental sulfur samples approached the following standard oxidation reaction [11]:

$$17S_{(0)} + 24NO_3^- + 8H_2O \rightarrow 6NO_2^- + 9N_2 + 17SO_4^{2-} + 16H^+ \quad (1)$$

The theoretical ratios for this reaction are 1.4 and 4 for $\Delta NO_3^-/\Delta SO_4^{2-}$ and $\Delta NO_3^-/\Delta NO_2^-$, respectively. Calculated ratios were 1.28 ±0.04 and 2.39 ±0.03 for the same ratios, respectively (Table 3.2). More sulfates and nitrites were produced experimentally than expected for equation 1. However, a reaction without production of nitrogen would translate to more nitrites and less sulfates:

$$S_{(0)} + 3NO_3^- + H_2O \rightarrow 3NO_2^- + SO_4^{2-} + 2H^+ \quad (2)$$

The bacteria were metabolising elemental sulfur mostly through reaction 1, but complementary pathways, as equation 2, could also be happening. With mackinawite we also expect that the bacteria went through a partial denitrification:

$$1.5FeS + 3NO_3^- + 2H^+ \rightarrow N_2 + NO_2^- + 1.5Fe^{2+} + 1.5SO_4^{2-} + H_2O \quad (3)$$

The theoretical ratios for this reaction are 2 and 3 for $\Delta NO_3^-/\Delta SO_4^{2-}$ and $\Delta NO_3^-/\Delta NO_2^-$, respectively. While calculated ratios were 0.72 ±0.26 and 2.65 ±0.94, respectively. We observed a smaller ratio for $\Delta NO_3^-/\Delta SO_4^{2-}$, implying that there may have been also total denitrification [3]:

$$5FeS + 8NO_3^- + 8H^+ \rightarrow 4N_2 + 5Fe^{2+} + 5SO_4^{2-} + 4H_2O \quad (4)$$

This latest reaction involves more production of sulfates for less consumption of nitrates.

In the next experiments, an additional sulfur source (i.e., thiosulfates) was included to help initial growth of the bacteria to have a higher cell concentration in the solutions. Prior work has related the cell concentration with higher oxidation rates [11]. Elemental sulfur samples and mackinawite samples followed a similar path where the $\Delta NO_3^-/\Delta SO_4^{2-}$ ratio would decrease, while the $\Delta NO_3^-/\Delta NO_2^-$ ratio would increase (with an exception for mackinawite in exp. II.1) (Table 3.2). The decrease in the $\Delta NO_3^-/\Delta SO_4^{2-}$ ratio can be related to a higher production of sulfates via thiosulfates oxidation, that involve less consumption of nitrates [22], [23]:

$$5S_2O_3^{2-} + 8NO_3^- + H_2O \rightarrow 10SO_4^{2-} + 4N_2 + 4H^+ \quad (5)$$

***Table 3.2**. Mass balance of educts and products for the different experimental set-ups after the incubation time[a].*

		NO_3^- depleted (mM)	SO_4^{2-} produced (mM)[b]	NO_2^- produced (mM)	$\Delta NO_3^-/\Delta SO_4^{2-}$ ratio	$\Delta NO_3^-/\Delta NO_2^-$ ratio
Mineral sulfur (α-S_8)	Exp. I	9.75 ±1.24	7.62 ±1.18	4.08 ±0.57	1.28 ±0.04	2.39 ±0.03
	Exp. II.1	10.02 ±1.26	9.32 ±1.52	3.43 ±0.0.86	1.08 ±0.05	3.11 ±1.15
	Exp. II.2	8.07 ±0.23	13.83 ±0.06	2.14 ±0.30	0.58 ±0.01	3.82 ±0.65
	Exp. III	0.00	5.22 ±1.27	0.10 ±0.17	-	-
	Exp. IV	5.20 ±0.02	15.06 ±0.22	0.70 ±0.21	0.35 ±0.00	7.75 ±2.29
Macki-nawite (FeS)	Exp. I	0.57 ±0.26	0.68 ±0.14	0.23 ±0.20	0.72 ±0.26	2.65 ±0.94
	Exp. II.1	4.19 ±0.15	4.04±0.22	1.22 ±0.15	1.04 ±0.08	3.47 ±0.34
	Exp. II.2	13.39 ±0.13	20.70 ±0.17	0.44 ±0.07	0.65 ±0.01	30.47 ±4.92
	Exp. III	0.00	0.11 ±0.11	0.00	-	-
	Exp. IV	11.05 ±0.10	19.17 ±0.05	0.00	0.58 ±0.01	-
Pyrite (FeS_2)	Exp. I	0.19 ±0.06	0.26 ±0.27	0.00	-	-
	Exp. II.1	2.12 ±0.51	4.07 ±0.18	0.31 ±0.03	0.52 ±0.15	7.00 ±1.91
	Exp. II.2	10.92 ±0.11	13.49 ±0.07	3.27 ±0.19	0.81 ±0.00	3.35 ±0.23
	Exp. III	0.00	0.18 ±0.29	0.00	-	-
	Exp. IV	13.33 ±0.10	14.63 ±0.16	9.30 ±0.01	0.91 ±0.00	1.45 ±0.01
	Exp. V	0.00	0.04 ±0.05	0.00	-	-
Thio-sulfates ($S_2O_3^-$)	Exp. II.1	3.83 ±0.10	3.96 ±0.03	2.64 ±0.01	0.97 ±0.03	1.45 ±0.04
	Exp. II.2	12.86 ±0.12	15.96 ±0.14	0.78 ±0.43	0.81 ±0.01	19.39 ±10.50
	Exp. IV	11.38 ±0.02	15.45 ±0.05	2.10 ±0.05	0.74 ±0.00	5.43 ±0.13

[a]Values are after 72 days of incubation for exp. I and 66 days for exp. II.1, while values for exp. II.2, III, IV, and V are after 27 days of incubation.

[b]Sulfates concentrations, and therefore the calculated ratios, have been adjusted by removing the amounts of sulfates detected in the abiotic controls.

Moreover, the previous reaction also explains the increase in $\Delta NO_3^-/\Delta NO_2^-$ ratio. Thiosulfates should be an easier source for complete denitrification, reducing of nitrates directly to nitrogen gas. However, the detection of nitrites in the controls with bacteria and only thiosulfates (Table 3.2 and Figure 3.3) could mean that *T. denitrificans* not always metabolizes thiosulfates to nitrogen gas. Still, we observed differences between exp. II.1 and II.2. The detection of nitrites was especially high in exp. II.1, where the $\Delta NO_3^-/\Delta SO_4^{2-}$ ratio (0.97 ±0.03) was also higher than the theoretical ratio of equation 5. While, in exp. II.2, the production of nitrites was negligible and the $\Delta NO_3^-/\Delta SO_4^{2-}$ ratio (0.81 ±0.01) matched the theoretical ratio. Therefore, a transformation of nitrates to nitrites could have occurred independently of the oxidation of thiosulfate in exp. II.1 [14], or the bacteria could have used an alternative route [23]:

$$2S_2O_3^{2-} + 8NO_3^- + 2H_2O \rightarrow 4SO_4^{2-} + 8NO_2^- + 4H^+ \quad (6)$$

Moreover, in the case of mackinawite, the reduction of nitrates and production of sulfates followed a very similar tendency to the controls with only bacteria and thiosulfates (Figure 3.3). Especially in exp II.1, the curves were identical. Therefore, we cannot assure here that the sulfates detected belong to the oxidation of mackinawite or thiosulfates.

Similar results were obtained with pyrite. The addition of thiosulfates made the bacteria grow initially. Yet, we could not point out if they switched and grow also using pyrite. In exp II.2, identical $\Delta NO_3^-/\Delta SO_4^{2-}$ ratios of ~0.8 were observed for the pyrite samples and the thiosulfates controls (Table 3.2). The only difference between the controls and the samples was the amounts of nitrites detected. When growing with pyrite and thiosulfates the production of nitrites was much higher (Figure 3.3 and Table 3.2). This could indicate oxidation of pyrite in these conditions [10]. However, as we have discussed before, the production of nitrites was variable when using only thiosulfates. This could not assure that the nitrites observed are due to thiosulfates or pyrite metabolism. Indeed, in exp II.1, the production of nitrites was much lower for the pyrite samples than for the controls with thiosulfates (Figure 3.3). Moreover, exp II.1 was the only one where the $\Delta NO_3^-/\Delta SO_4^{2-}$ ratio was not identical to the thiosulfates control ratio. Here, the $\Delta NO_3^-/\Delta SO_4^{2-}$ ratio was 0.52 ±0.15, due to a lower consumption of nitrates or a higher production of sulfates (Figure 3.3). However, the oxidation of pyrite usually involves higher consumptions of nitrates having $\Delta NO_3^-/\Delta SO_4^{2-}$ ratios above 1 [10], [14], [24]:

$$5FeS_2 + 14NO_3^- + 4H^+ \rightarrow 5Fe^{2+} + 10SO_4^{2-} + 7N_2 + 2H_2O \quad (7)$$

$$5FeS_2 + 15NO_3^- + 10H_2O \rightarrow 5Fe(OH)_3 + 10SO_4^{2-} + 7.5N_2 + 5H^+ \quad (8)$$

$$FeS_2 + 7.5NO_3^- + 3.5H_2O \rightarrow Fe(OH)_3 + 2SO_4^{2-} + 7.5NO_2^- + 4H^+ \quad (9)$$

Also, the last of the three equations presented above suggest a total oxidation of pyrite. Iron determination brought some insight to the total oxidation of pyrite.

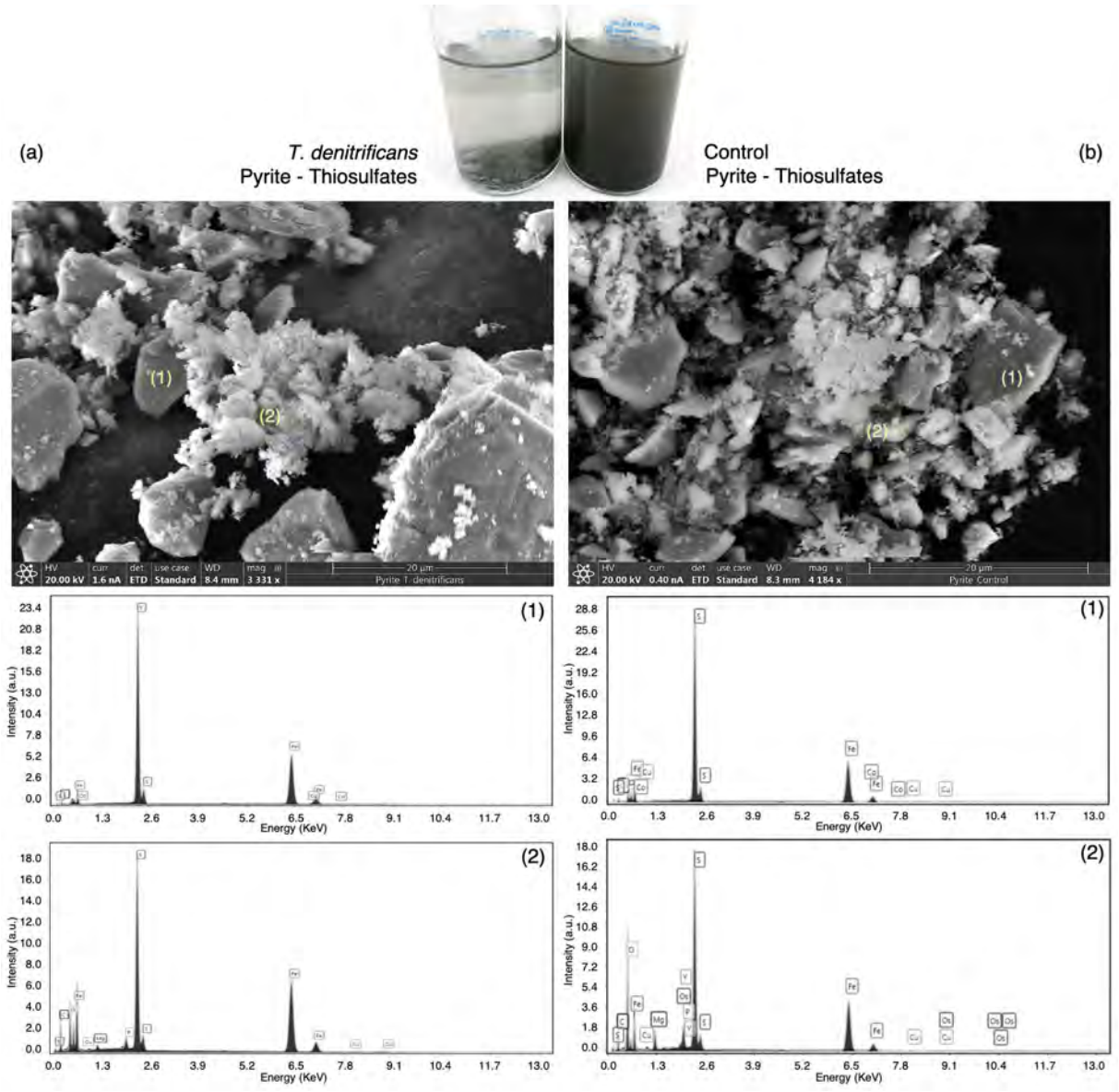

***Figure 3.4**. Visual appearance and complementary secondary electron micrograph of the cultures with pyrite and thiosulfates (Exp II.1) and abiotic controls with pyrite and thiosulfates. Images of the cultures were taken right after manual agitation. SEM images are accompanied by EDS spectra of the areas indicated with numbers.*

Although, the previous evidence pointed towards only an abiotic oxidation of pyrite, an increase in the turnover iron(III)/iron(II) was observed in the samples with thiosulfates and pyrite (Figure S 3.1). In the controls, we mostly measured Fe^{2+} on pyrite particles during the whole experiment, while in samples we detected increase in Fe^{3+}. Moreover, the measurement of iron from pyrite in thiosulfate amended experiments was difficult. Over the incubation time, the

pyrite clustered together and, even with manual agitation of the bottles no particles went into solution (Figure 3.4). This could suggest that the biomass produced thanks to the oxidation of thiosulfates created a "biofilm" around pyrite facilitating the oxidation [25].

Complementary, SEM analyses, however, did not identified bacteria growing on the surface of the pyrite (Figure 3.4). Some aggregates with different composition to pyrite were observed, but they were also detected in the controls (Figure 3.4). Some of the elements detected: copper, magnesium, phosphorous, are part of the 113-medium composition. Precipitates from the medium compounds is possible. Other elements like osmium, are residual from the sample fixation protocol. Therefore, these aggregates are not consequence of bacterial activity. Maybe the biomass produced during growth was enough to aggregate the pyrite particles in solution but did not resist the fixation protocol. Moreover, prior work has shown that although *T. denitrificans* can colonize pyrite surface, most of the cells remained free-living in solution, but that both may interfere in the process of pyrite oxidation [26].

On the contrary, the biofilms originated around elemental sulfur particles were clearly identified by naked eyes in all sulfur samples, and they survived the fixation protocol (Figure 3.5).

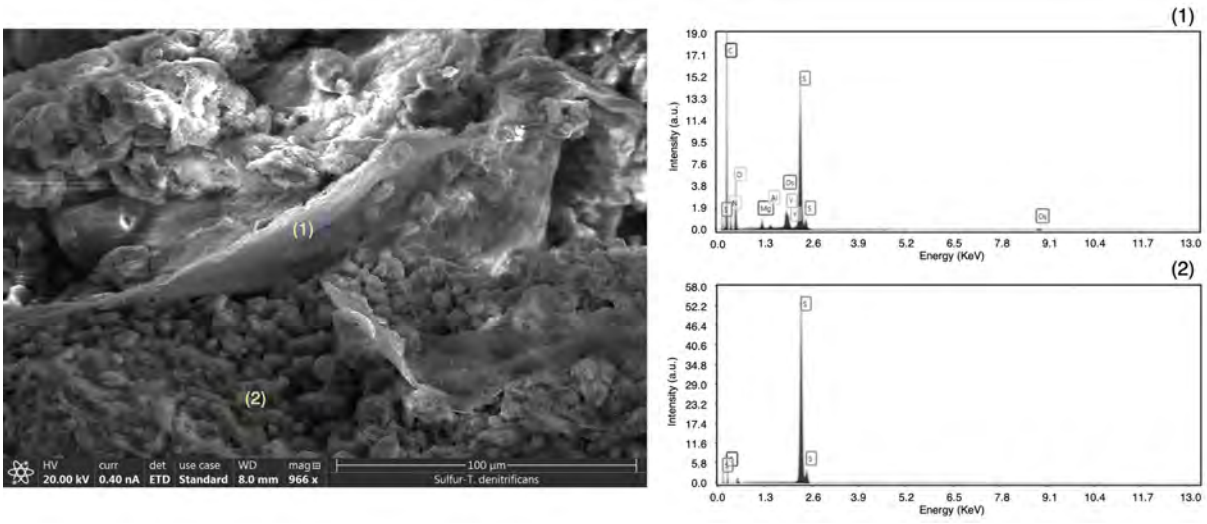

***Figure 3.5**. Secondary electron micrograph of the fixated sulfur sample (Exp. I) with corresponding EDS spectra. The areas where the EDS analyses were performed are indicated with numbers.*

We conducted a following experiment (Exp. V), where we increased the initial concentration of bacteria cells, but we did not add an extra sulfur source. An initial higher biomass could have a similar effect than the supplementary sulfur source in the oxidation rates of pyrite. However, in these conditions we did not observe production of sulfates different to that recorded for

abiotic controls (Figure S 3.2). The biomass here may not have been as active as in the previous experiment, or the incubation time was too short (30 days compared to 66 days).

Anoxic conditions are ideal to prevent abiotic oxidation of sulfur species but, maintaining an oxygen-free solution may be challenging in the conservation field. Therefore, we also tried to carry out the oxidation of these compounds in presence of oxygen. Similar conditions as discussed above were conducted.

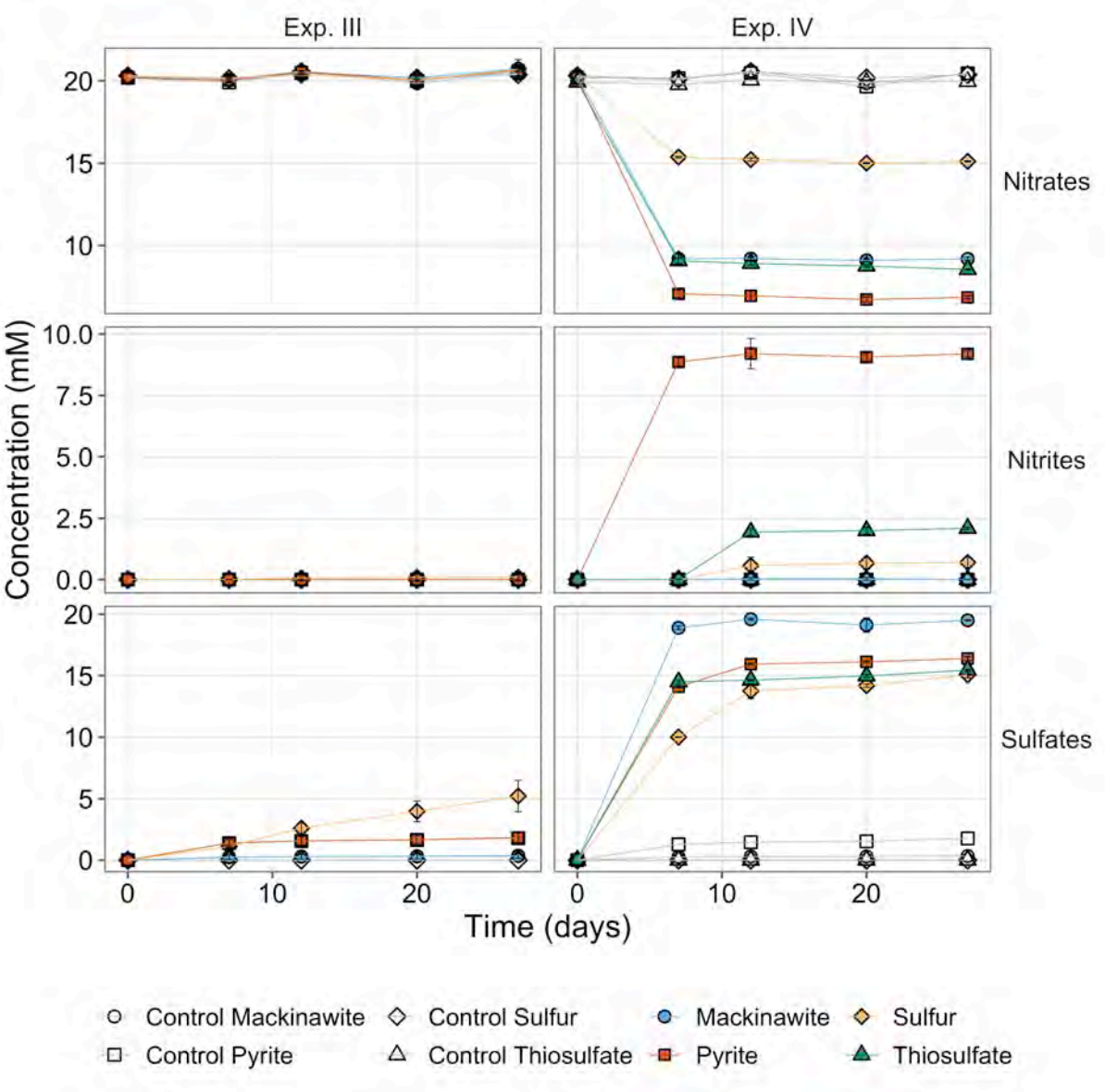

***Figure 3.6**. Concentration over time of nitrates, nitrites, and sulfates in presence of T. denitrificans (closed symbols) or abiotic controls without bacteria (open symbols), in oxic experimental set-ups (Exp. III and IV) for the different mineral sources under study: elemental sulfur, mackinawite, and pyrite. In experiments with thiosulfates, sodium thiosulfate control is included. Error bars show standard deviation of two or three replicates.*

Without an additional sulfur source, in presence of oxygen only elemental sulfur was oxidised by the bacteria (Figure 3.6). Moreover, the oxidation was using the dissolved oxygen present in solution not the added nitrates (Table 3.2) [2]:

$$S_{(0)} + 1.5O_2 + H_2O \rightarrow + SO_4^{2-} + 2H^+ \quad (10)$$

The previous reaction is more favourable than oxidation coupled to denitrification. Equation 10 has a ΔG° of -587.1 kJ/reaction, while oxidation with nitrates has a ΔG° of -547.6 kJ/reaction [2]. Moreover, no sulfates were detected in the abiotic controls. Therefore, all sulfates detected were produced due to the bacteria metabolism, and elemental sulfur was stable in the experimental conditions without bacteria. This is interesting towards a future application, as no nitrates would be needed and no secondary compounds, such as nitrites produced. Nitrates are a concern in wastewater treatment, where the use of reduced sulfur has already been suggested a possible remediation [27], [28]. Moreover, nitrites are regulated due to health risk potential [29]

The addition of thiosulfates in oxic conditions showed that the oxidation of thiosulfates was mostly via denitrification even in presence of oxygen (Figure 3.6). Only a slight reduction in the consumption of nitrates was registered (Figure 3.6 and Table 3.2). Overall, very similar results were obtained with regard to exp. II.2. Again, mackinawite samples and thiosulfate controls presented a consumption of nitrates almost identical, while the production of sulfates was higher for mackinawite samples suggesting possible oxidation of the mineral (Figure 3.6). For pyrite samples in this case, the consumption of nitrates was higher than in the thiosulfates controls, but we observed a very high production of nitrites (Figure 3.6). The high nitrates/nitrites conversion could explain this increased consumption of nitrates, especially since the production of sulfates was the same (Table 3.2).

In general, elemental sulfur was clearly metabolized by the bacteria in all conditions. Mackinawite, on the contrary, was only clearly oxidized by *T. denitrificans* in exp. I (anoxic conditions without any extra sulfur source). In oxic conditions, the oxidation was in the same range as in the controls. With an extra sulfur source, the oxidation of mackinawite seemed to have occurred as well, but it was difficult to assure that the extra sulfur source increased the oxidation rates of the mineral. The oxidation of pyrite to sulfates by *T. denitrificans* was not clear in any condition. Without an extra sulfur source, the sulfates produced were due to abiotic oxidation. In thiosulfate-amended cultures, production of sulfates matched the expected production for oxidation of thiosulfates (Table 3.2). Only in Exp. II.1, we observed higher

production of sulfates than expected. But the reduction of nitrates was not increased. Still, in these conditions we observed iron oxidation (Figure S 3.1). This observation is line with previous suggestions that *T. denitrificans* could oxidase the ferrous iron moiety preferentially over the sulfide one [30]. The extra sulfates observed here could have been produced by more accessible oxidation of the sulfide moiety once the bacteria oxidized the ferrous iron. Therefore, of all conditions, only here we could argue nitrate-dependent oxidation of pyrite driven by *T. denitrificans*.

Oxidation of iron sulfides in presence of iron chelators

The addition of chelating agents increased the concentration of iron in solution (Figure 3.7), which was under the detection limit in all experiments above.

Iron levels in DFOM solutions with mackinawite were the same between abiotic controls and samples with the bacteria. In both cases we measured concentrations of total iron of ~160-180 µM, after the incubation time. On the other hand, with pyrite, in presence of DFOM, and *T. denitrificans* the concentrations of iron in solution reached higher values than in abiotic controls. Maximum concentration detected was of ~135 µM in controls, and ~220 µM in bacterial cultures. These differences pointed towards a synergic effect between DFOM and *T. denitrificans*.

EDTA abiotic controls presented higher concentration of iron than the samples with bacteria, in the case of mackinawite. With pyrite, iron concentration in solution was similar between samples and controls (Figure 3.7). EDTA had a different effect on mackinawite than on pyrite dissolution. The concentrations of iron detected in solution were between 190 to 270 µM in mackinawite samples and controls, respectively, while concentrations of only ~45 µM were detected with pyrite samples and controls. DFOM was more efficient in solubilising pyrite than EDTA in the experimental conditions, while closer results between the two chelators were obtained for mackinawite (Figure 3.7).

In the case of PVD, iron levels detected in solution with pyrite and mackinawite were lower than for the other chelators used (Figure 3.7). We observed that experimental results with PVD varied more than with the other two chelators under study. As already mentioned in the previous chapter, the concentrations of this chelator were calculated experimentally. Also, the stability of PVD over time could be reduced.

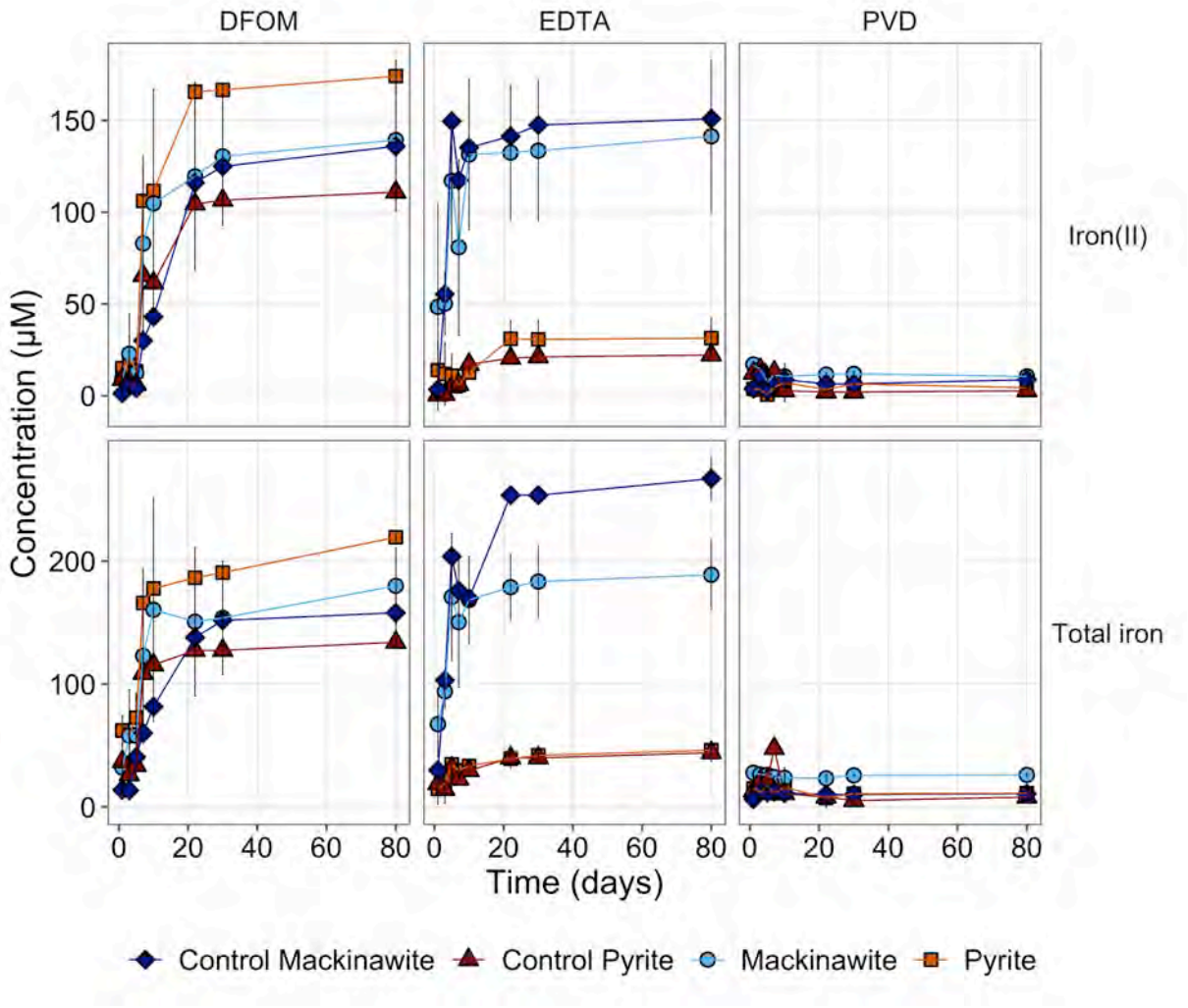

Figure 3.7*. Total iron and iron(II) concentrations measured in solution over time for samples with T. denitrificans and pyrite or mackinawite plus one of the chelating agents under study (DFOM, EDTA or PVD), compared to abiotic controls without the bacteria. Error bars show standard deviation of two or three replicates.*

The destabilization of the iron sulfide minerals via iron chelation could enhance the oxidation of the sulfur moiety by the bacteria. A slight oxidation of mackinawite was registered. Sulfates in abiotic controls with chelators were not detected while sulfates were present in the solutions with bacteria for all chelators (Figure 3.8). However, the oxidation was not enhanced compared to the previous experience without chelators. Amounts of ~0.10 to 0.25 mM of sulfates were detected at the end of the incubation time here, while in the previous section, exp. I, we detected ~0.68 mM (Table 3.2). Moreover, sulfates production were the lowest in EDTA samples, while they registered the highest concentrations of iron release from mackinawite.

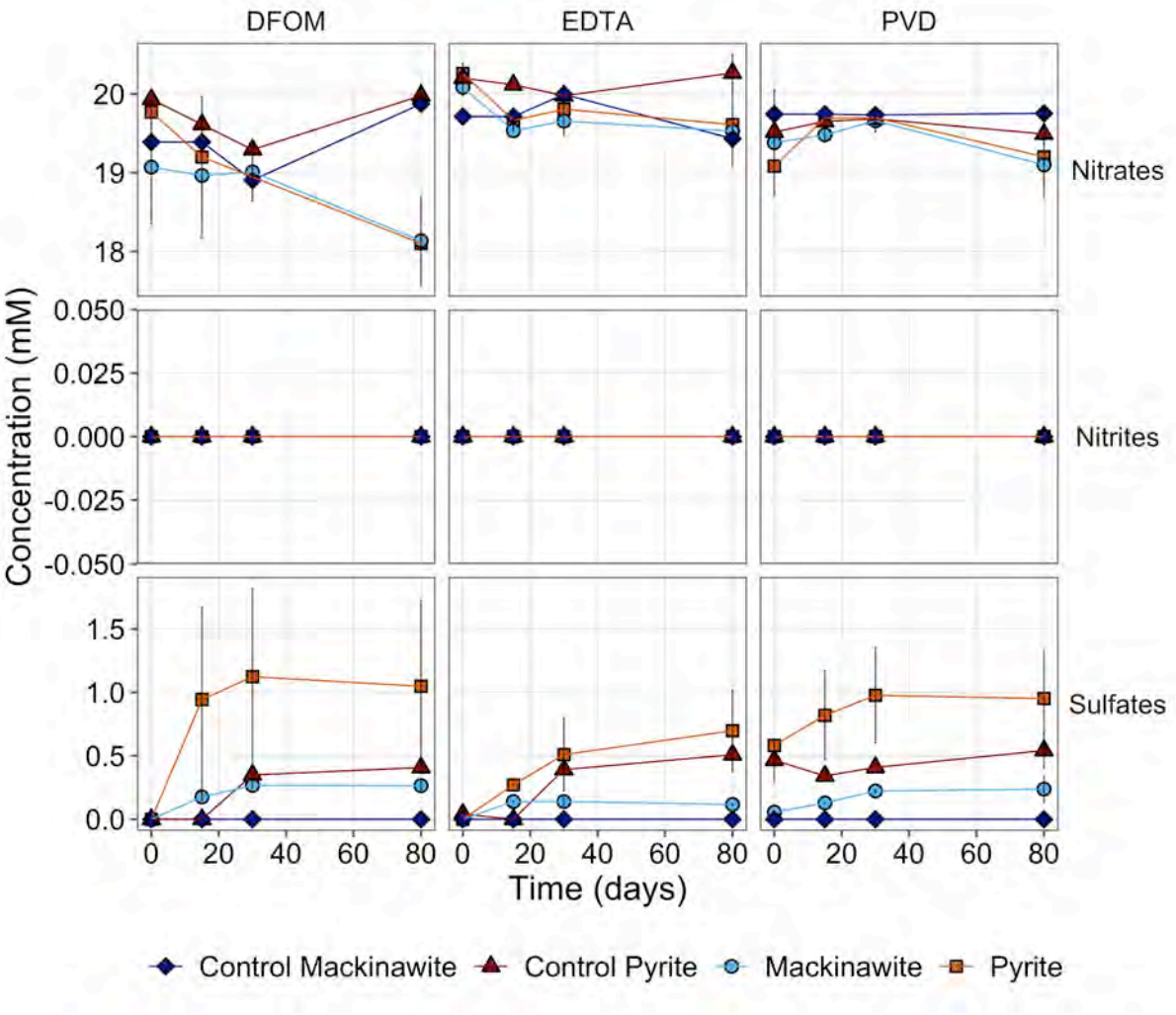

Figure 3.8. *Concentration over time of nitrates, nitrites, and sulfates in presence of T. denitrificans and pyrite or mackinawite plus one of the chelating agents under study (DFOM, EDTA or PVD). Controls refer to abiotic controls with chelators. Error bars show standard deviation of two or three replicates.*

Sulfates production in pyrite samples was not significantly higher than in abiotic controls for any condition (Figure 3.8). The solubilization of pyrite by the chelators did not seem to enhance the oxidation of pyrite by the bacteria. Only one DFOM-sample pointed towards biotic oxidation. This sample presented high production of sulfates arriving to ~1.5 mM after the incubation time. Moreover, $\Delta NO_3^-/\Delta SO_4^{2-}$ ratio for this sample was 1.36, close to the theoretical ratios of reactions 7 and 8. Moreover, although SEM-EDS analyses showed no colonies on the surface of pyrite crystals (Figure 3.9), we could detect some possible oxidation on the pyrite surface. The sulfur component was reduced, and iron and oxygen elements were increased in some crystals, maybe due to iron oxides formation (Figure 3.9). The calculation of oxidized iron on pyrite particles was difficult due to interferences with the total iron in solution. However, this could point towards biological oxidation of pyrite in this sample. The other

DFOM-pyrite samples had around the same sulfates levels as the controls, giving the high standard deviations observed (Figure 3.8). Concentration of sulfates registered in EDTA samples were the same as in controls proving abiotic oxidation. PVD samples did not show either decrease in nitrates, and sulfates production were not significantly different to the controls (Figure 3.8).

Overall, the addition of a chelator agent promoted the dissolution of both pyrite and mackinawite. The dissolution, however, did not enhance the oxidation of the sulfur moiety. With mackinawite similar sulfates values as the experience above, without chelating agents, were detected. In mackinawite samples, the addition of ferric iron should not increase oxidation as it is an acid-soluble iron sulfide [1], [12]. In pyrite samples (except one), sulfate concentrations were the same in samples with the bacteria and chelators, abiotic controls with chelators and abiotic controls without chelators. Therefore, the presence of chelated iron did not promote either oxidation of pyrite. Pyrite oxidation is catalysed by Fe^{3+} ions in certain conditions [12]. Iron needs to be soluble for the oxidation to occur. That is why the hypothesis suggests the existence of acidic micro niches or chelating agents [13]. Recent work suggests that in anoxic and neutral pH, the oxidation of pyrite is possible with a redox potential higher than +200 mV, as for some cellular components [25]. But, redox potential of the iron-complexes formed here are lower than +200 mV [31], [32], as discussed in chapter 2. The formed iron-complexes may actually prevent the iron ions to participate in redox reactions [31].

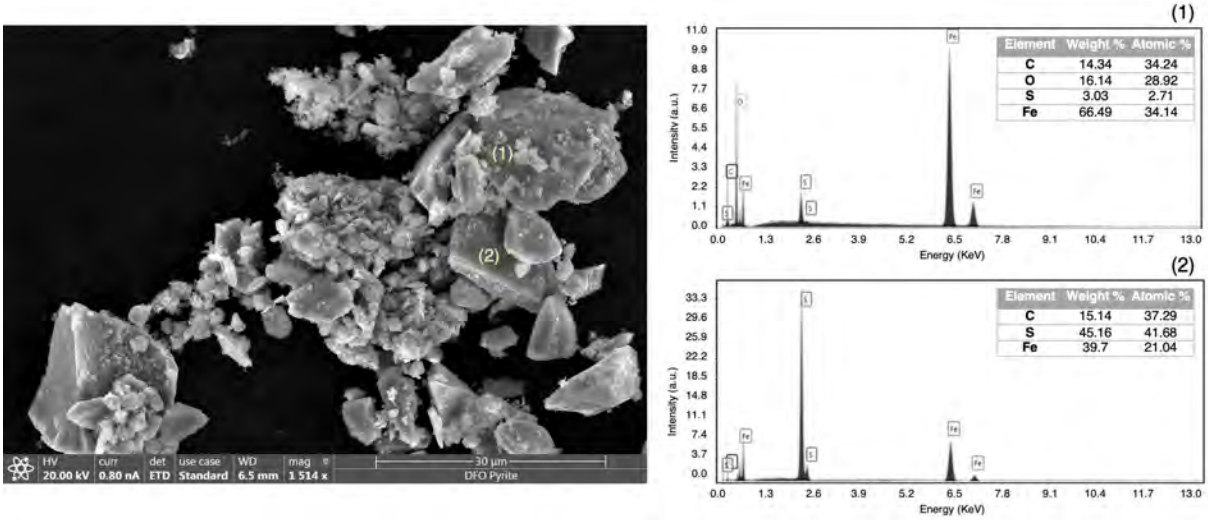

***Figure 3 9**. Secondary electron micrograph of the fixated DFOM-pyrite sample with correspondent EDS spectra. The areas where the EDS analyses were performed are indicated with numbers.*

Conclusion

T. denitrificans is a well-known sulfur-oxidising bacterium. In this study, it was able to oxidise elemental sulfur under all the experimental conditions. The capability of *T. denitrificans* of solubilising elemental sulfur to sulfates is promising for its removal in waterlogged wood artefacts. Moreover, the possibility of using oxygen as electron acceptor reduces the use of nitrates and the accumulation of nitrites. However, the oxidation of mackinawite and pyrite was not as efficient. Mackinawite was oxidised under anoxic conditions, but the oxidation rate was very slow. The addition of an extra sulfur source or a chelating agent did not improve the oxidation rates for mackinawite or pyrite. In fact, pyrite oxidation was not clearly detected in the experimental conditions. Only, under some conditions some oxidation of the iron phase was observed, but the production of sulfates was always similar to the abiotic controls. In general, the biological oxidation of pyrite is challenging in circumneutral pH and deeper studies are needed. The use of an iron- and sulfur-oxidising consortium could enhance the oxidation of pyrite allowing to develop practical applications.

Supplementary material 3.1

***Table S 3.1**. Composition of 113. Thiobacillus denitrificans medium (© 2017 DSMZ GmbH).*

113 medium	
Solution A	
KH_2PO_4	2 g
KNO_3	2 g
NH_4Cl	1 g
$MgSO_4 \cdot 7H_2O$ or $MgCl_2 \cdot 6H_2O$	0.8 g / 0.66 g
Trace element solution SL-4	2 mL
H_2O_d	960 mL
Adjust pH to 7.0 with NaOH 100% N_2 gas atmosphere. Autoclave	
Solution B	
$Na_2S_2O_3 \cdot 5H_2O$	5 g
H_2O_d	20 mL
100% N_2 gas atmosphere. Autoclave	
Solution C	
$NaHCO_3$	1 g
H_2O_d	20 mL
80% N_2 and 20% CO_2 gas atmosphere. Filter-sterile	
Solution D	
$FeSO_4 \cdot 7H_2O$	2 mg
H_2O_d	1 mL
100% N_2 gas atmosphere. Autoclave	

Appropriate amounts of solutions B, C and D are added to the sterile solution A.
Note: A small amount of white precipitate forms after autoclaving, but this has no negative effect on growth.

***Table S 3.2**. Composition of trace element solution SL-4 (14. Clostridium formicoaceticum medium (© 2015 DSMZ GmbH)) and modified version.*

Trace element solution SL-4	
Na_2-EDTA	0.5 g
$FeSO_4 \cdot 7H_2O$	0.2 g
$ZnSO_4 \cdot 7H_2O$	0.1 g
$MnCl_2 \cdot 4H_2O$	0.03 g
H_3CO_3	0.3 g
$CoCl_2 \cdot 6H_2O$	0.2 g
$CuCl_2 \cdot 2H_2O$	0.01 g
$NiCl_2 \cdot 6H_2O$	0.02 g
$Na_2MoO_4 \cdot 2H_2O$	0.03 g
H_2O_d	1000 mL
Adjust pH to 7	
Modified trace element solution SL-4	
$ZnCl_2$	0.05 g
$MnCl_2 \cdot 4H_2O$	0.03 g
H_3CO_3	0.3 g
$CoCl_2 \cdot 6H_2O$	0.2 g
$CuCl_2 \cdot 2H_2O$	0.01 g
$NiCl_2 \cdot 6H_2O$	0.02 g
$Na_2MoO_4 \cdot 2H_2O$	0.03 g
H_2O_d	1000 mL
Adjust pH to 7	

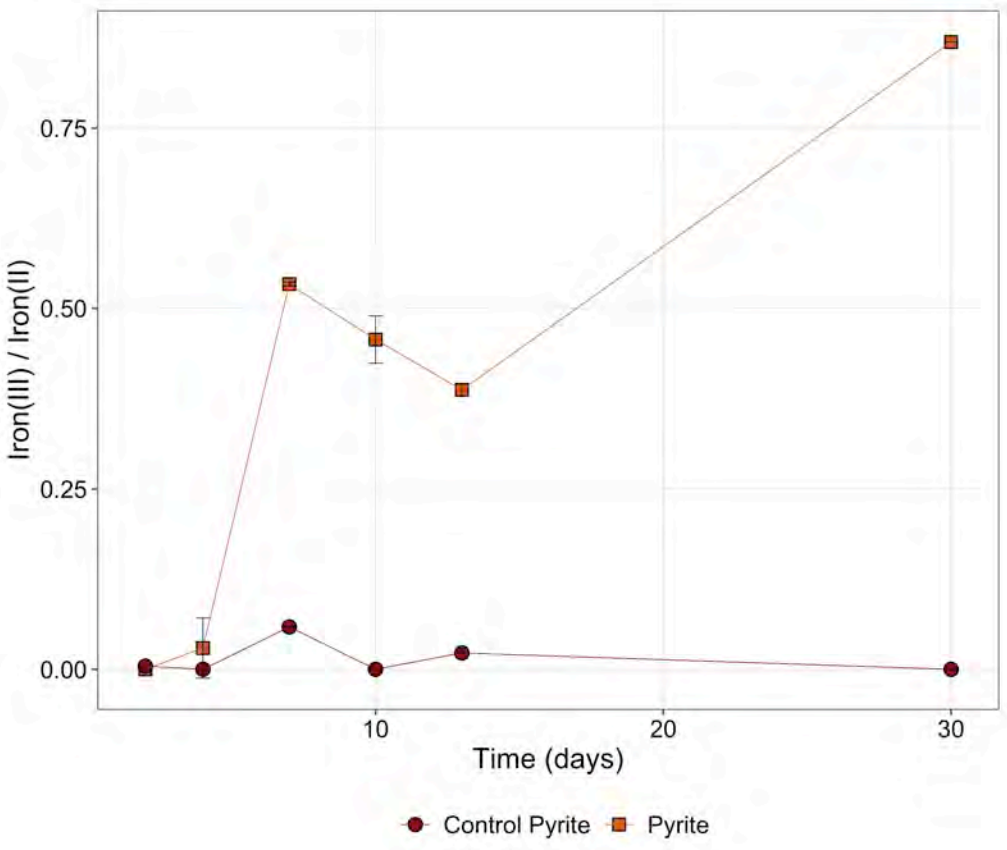

Figure S 3.1. *Iron(III)/iron(II) concentration ratio over time measured in pyrite particles incubated with T. denitrificans or without bacteria (abiotic control) in experimental set-up II.1. Error bars show standard deviation of two or three replicates.*

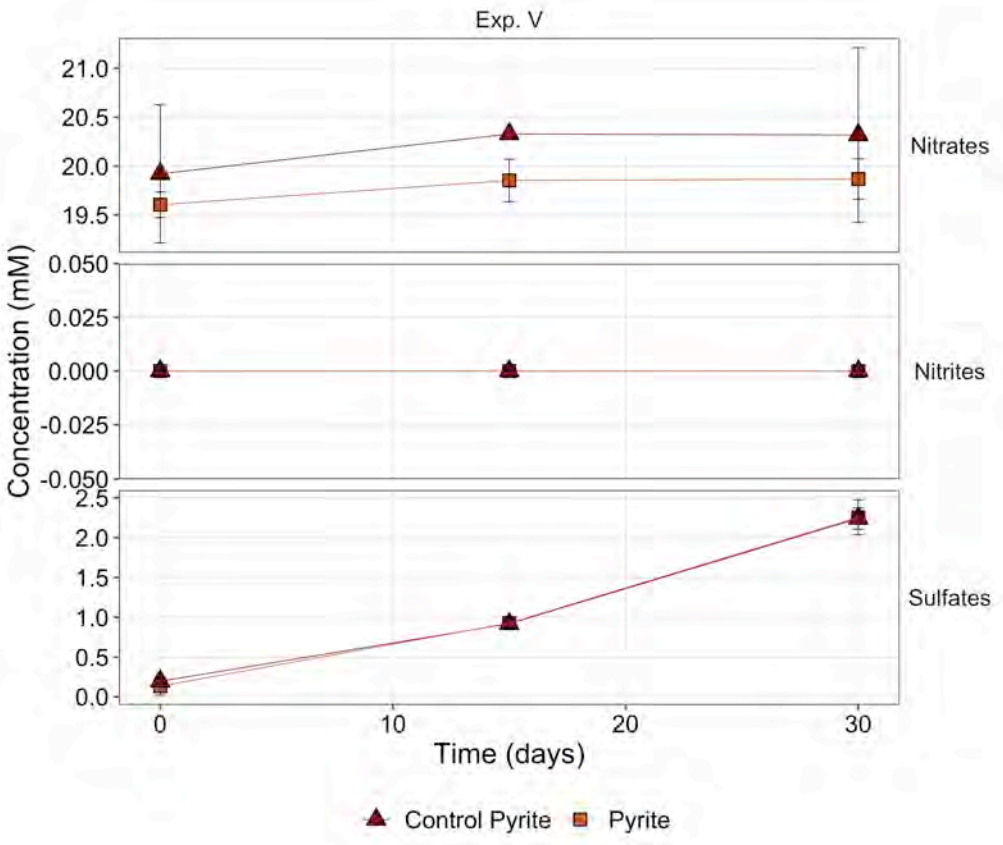

***Figure S 3.2**. Concentration over time of nitrates, nitrites, and sulfates in presence of pyrite and ~1x10^{8} cells·mL^{-1} of T. denitrificans or abiotic control, in anoxic experimental set-up (Exp. V). Error bars show standard deviation of two or three replicates.*

3.2 Biological oxidation of sulfur compounds in wood

Abstract

In this study, we evaluated the capacity of the bacterium *Thiobacillus denitrificans* to transform synthesised sulfur compounds commonly in waterlogged wood mock-ups, to more readily extractable compounds thereby eliminating the threat of degradation. First, oak samples, impregnated with a solution containing iron(II) and sulfides, were used to assess the efficiency of the bacterial treatment. Before treatment, mackinawite (FeS) and mineral sulfur (α-S_8) were detected in the impregnated wood. After treatment with *T. denitrificans*, even though some elemental sulfur remained in the sample, the predominant phase corresponded to oxidized sulfur compounds. This demonstrates that *T. denitrificans* was able to use the reduced sulfur compounds present in the wood samples as an energy source, producing more soluble oxidized sulfur compounds. In addition, non-invasive techniques such as FTIR spectroscopy, showed no negative effect on the wood after the treatment in comparison with the reference-impregnated wood. This first trial demonstrated the feasibility of a biotechnological procedure for the preventive extraction of sulfur species from WAW. In a second step, we tried to improve the application protocol varying the cell concentration, the electron acceptor and the buffer agent. In this case, impregnated balsa wood model samples showed similar results to oak samples, indicating compatibility with different types of wood. However, the change in experimental conditions did not improve the extraction efficiency.

Introduction

Waterlogged environments can promote the preservation of archaeological wooden artefacts, as the burial conditions are advantageous, i.e. places where the wood decay is limited [33]. However, sulfur species are formed in the wood as a consequence of the metabolic activity of sulfate-reducing bacteria (SRB). In anoxic sulfate-rich environments (i.e., seabed), with wood as carbon and energy source, SRB produce hydrogen sulfide. Inside the wood, the concomitant presence of contemporary iron pieces, that corrode and generate iron ions, leads to the formation of iron sulfides that accumulate in the wood [34], [35]. Upon exposure to oxygen, damaging compounds can be formed. On one hand, the oxidation of iron sulfides under high levels of relative humidity leads to the formation of sulfuric acid, responsible for the degradation of the wood cellulosic compounds by acid hydrolysis. Moreover, mechanical damage of the wood structure is also observed due to a physical swelling during the transformation of elemental sulfur or sulfides to hydrated sulfate salts [36], [37]. On the other hand, iron itself is responsible

for the catalysis of different reactions such as oxidative degradation of cellulose and oxidation of sulfur compounds, accelerating the production of acids [38]. In consequence, sulfur and iron accumulation within WAW is a matter of concern for long-term preservation of this valuable cultural heritage [7].

Mild biological oxidation processes could be explored for the extraction of insoluble sulfur phases from WAW. The use of bacteria is extended to mobilise metals [39], [40]. Moreover, some specific bacteria, like the above studied chemolithotroph *Thiobacillus denitrificans*, are able to grow using sulfur compounds as energy source at neutral pH [17], [41], allowing their application in the wood matrix. *T. denitrificans* has been previously studied for the use of this metabolism in different applications, such as the treatment of wastewater [14], [42]. Also, it was proposed for the preservation of waterlogged wood [16]. However, the aim was to determine if *T. denitrificans* was able to grow with mineral phases containing up to 10% pyrite and no further experiments with wood samples were reported.

Our goal is to develop a green and sustainable extraction method that would specifically remove sulfur compounds while maintaining the physical structure, chemical stability, and aesthetic appearance of waterlogged wood heritage. In this study, we used different analytical techniques to assess the feasibility of a preventive biotechnological treatment for the extraction of sulfur compounds from archaeological wood.

3.2.1 Proof of concept

Materials and methods

Model samples

Oak (*Quercus* sp.) was employed to reproduce the characteristics of waterlogged wood. Oak is widely found in archaeological discoveries. Different oak samples were prepared with the following dimensions: 1×1×1 cm^3as cube and 4×1×0.1 cm^3as transversal and longitudinal slices. Each sample was first autoclaved at 121 °C for 15 min. After, the samples were impregnated with iron sulfides by immersing them in 1 L iron(II) chloride tetrahydrate (0.5 M $FeCl_2 \cdot 4H_2O$) solution under vacuum (-600 mbars) for 4 h. The samples were dried overnight at 45 °C. Afterwards, the samples were immersed in a solution of hydrated sodium sulfide (0.5 M $Na_2S \cdot nH_2O$) under vacuum (-600 mbars) for another 4 h. The impregnated samples were kept inside Anaerocult® A mini (Merck, Germany) bags to prevent oxidation.

Bacteria and culture conditions

Thiobacillus denitrificans (NEU 1109) was obtained from the culture collection of the University of Neuchâtel, Switzerland. The strain was cultivated using standard anaerobic techniques at 30 °C using medium 113 (2010 DMSZ).

Oxidation experiments

Experiments were conducted in glass serum bottles sealed with butyl rubber stoppers and flushed with CO_2/N_2 (20/80%) at 30 °C in agitation (150 rpm) for 7, 14 and 28 days. Each bottle was previously autoclaved at 121 °C for 15 min. The extraction medium consisted of a modified 113 medium (DSMZ, 2010). In the modified medium all the sulfur and iron compounds were removed. The final composition of the modified medium was: 15 mM KH_2PO_4, 20 mM KNO_3, 19 mM NH_4Cl, 3.2 mM $MgCl_2 \cdot 6H_2O$, 30 mM $NaHCO_3$, and 2 mL of SL4 oligo-elements solution. The pH was adjusted to 7 (with the addition of 1 M NaOH). $NaHCO_3 \cdot 5H_2O$ was sterilized by filtration under a gas mixture atmosphere, CO_2/N_2 (20/80%), and then added to the autoclaved medium under 100% N_2 gas atmosphere. The bottles were filled with 50 mL of extraction medium and four impregnated wood samples (2 cubes and 2 slices). *T. denitrificans* was then inoculated from an overnight pre-culture to a final volume of 1% (v/v). Negative controls without bacteria were carried out to evaluate the possible interaction of the medium with the wood substrate. Wood impregnated with iron sulfides but not incubated with bacteria was considered as reference. Experiments and controls were performed in three independent replicates.

Analytical methods

Environmental scanning electron microscopy (ESEM) - Energy-dispersive X-ray spectroscopy (EDS)

A Philips ESEM XL30 FEG environmental scanning electron microscope equipped with an energy-dispersive X-ray analyser was used to obtain high-resolution images and to determine the elemental composition of the samples. Observations were performed on thin cross-sections obtained with a scalpel from the surface and inner part of wood cubes. The observations were performed at 65-70% RH, low pressure (4 Torr) and a voltage of 20 kV. Samples were placed on a Peltier plate cooled to 4 °C.

Fourier transform infrared spectroscopy (FTIR)

Fourier transform infrared spectroscopy (FTIR) analysis was conducted to assess the risk of the microbiological treatment for the wood substrate. FTIR spectra were obtained with a Nicolet

iS5 Thermo Fisher™ spectrophotometer (Thermo Fisher Scientific, United States) equipped with a diamond Attenuated Total Reflectance (ATR) crystal plate (iD5™ ATR accessory) at ambient temperature. Measurements were performed directly on the surface of fresh, reference (impregnated), treated and control wood samples. Average spectra from 32 scans were collected in the range of 400 to 4000 cm^{-1} with a 4 cm^{-1} spectral resolution. Spectra were analysed using OMNIC™ software (Thermo Fisher Scientific, United States). In order to evaluate the eventual wood degradation, the intensity ratios between lignin absorbance band (1505 cm^{-1}) against carbohydrates absorbance bands (either 1368, 1157 or 897 cm^{-1}) were calculated. These bands are assigned respectively to aromatic skeletal vibration in lignin, C–H deformation in cellulose and hemicellulose, C–O–C vibration in cellulose and hemicellulose and C–H deformation in cellulose [43]. ANOVA tests were then performed to evaluate significant differences between the calculated ratios.

Ion chromatography (IC)

For the determination of the concentration of sulfates (SO_4^{2-}), nitrates (NO_3^-), nitrites (NO_2^-) and other anions present in the extraction media, 20 mL of medium were collected after 7, 14 and 28 days of incubation. The samples were then centrifuged 10 min at 9000 rpm and the supernatants were filtered at 0.22 µm (Millipore, United States) to remove residual particulate matter. Filtered samples were diluted (5 times to 10 times) and analysed with an ion chromatograph Dionex ICS 1600 (Thermo Fisher Scientific, United States) equipped as described in section 3.1. Data was analysed with the Chromeleon™ software (Thermo Fisher Scientific, United States).

pH measurements

During experiments with *T. denitrificans*, pH was measured at the surface of the wood using a PHM210 standard pHmeter (Radiometer analytical). pH measurements were performed with a surface electrode (Sentix Sur, WTW) calibrated using pH 4.00 and pH 7.00 buffer solutions (VWR, United States).

Raman spectroscopy

To identify the iron and sulfur compounds present in the wood samples Raman microspectroscopy was performed on the surface and inner part of wood cubes as well as on transversal and longitudinal wood slides. Micro-Raman experiments were carried out with a Jobin Yvon High Resolution Raman spectrometer (Horiba Ltd., Japan) with a microscope and a Peltier-based cooled charge-coupled device detector. The spot diameter under the 50x objective was set at 3 µm. The laser power was filtered down to 0.1 mW to avoid any

transformation of the matter by heating, and spectra were recorded at 0.2 cm^{-1} resolution with an excitation wavelength of 632.82 nm. The spectrograms were analysed using LabSpec5 software (Horiba Ltd., Japan). The obtained spectra were compared to reference spectra of mineral sulfur, mackinawite and vivianite.

Synchrotron-X-ray fluorescence (Sy-XRF)

A synchrotron source was used to distinguish different sulfur oxidation states. The In-situ X-ray fluorescence measurements were conducted at the micro-focus spectroscopy beamline I18 at the Diamond Light Source (Harwell, United Kingdom). Sy-XRF maps were collected on cross-sections obtained with a scalpel from wood cubes. Sy-XRF mapping was performed by scanning the external wood surface at the energies of 2475, 2482, 3000 eV in order to detect respectively reduced, oxidized and total sulfur. The following parameters were used: 60 x 800 µm area with 5 rows, 2 µm step size and 60 s per point (dwell time of 0.149 s). An attenuator "2m Sn" was used. During analyses, samples were placed under inert atmosphere (helium bag) on a plate oriented at 10 degrees to the incoming beam. The results were analysed by free PyMca software.

X-ray diffraction (XRD)

XRD was employed to analyse the crystalline phases in the mineral concretions adding information to the Raman studies. Freshly cut slices from wood cubes were placed directly on the diffractometer with an incidence angle of 5° to the X-ray beam. The experiments were conducted by an INEL Equinox 6000 diffractometer, using CoKα wavelength (λ = 1.7903 Angström) provided with a 90° curve detector. A voltage of 40 kV and an intensity of 40 mA were applied. The acquisition time was 30 minutes. The diffraction patterns obtained were elaborated with Eva software.

Results and discussion

Oxidation experiments

ESEM-EDS analyses of the reference-impregnated wood showed that the outer surface was covered by aggregates composed by sulfur and iron (Figure S 3.3). However, ESEM-EDS analyses of the wood inner part revealed the presence of iron and sulfur, but no precipitates were observed (Figure S 3.3). This suggested that the impregnation solution reached the inner part of the cubes and, probably that the elements in the solution formed organosulfur or iron-binding compounds with the wood components. Indeed, Sy-XRF maps showed iron along the wood, while sulfur was mostly present on the surface. Wood samples were first impregnated

with the iron-containing solution. This may have prevented the efficient penetration of the sulfur-containing solution afterwards, avoiding the formation of iron sulfides in the inner part of wood samples. Raman and XRD analyses confirmed the formation of sulfur compounds in the outer layer of the wood samples. In particular, mineral sulfur (α-S_8) was detected as spheres (Figure 3.10) and the respective Raman spectra were characterized by vibrational bands at 151, 220 and 473 cm^{-1} (Figure 3.10) characteristic of mineral sulfur [44].

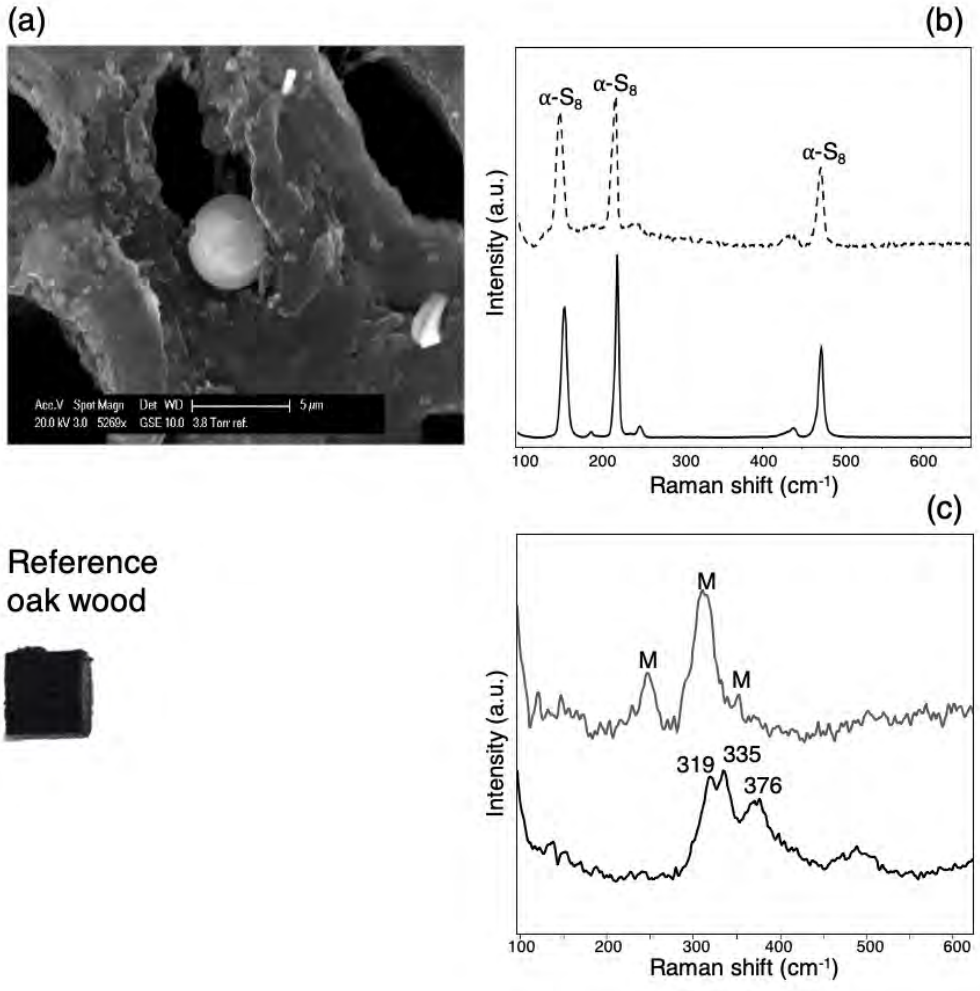

Figure 3.10. *(a) ESEM image obtained from reference wood showing spherical aggregates and (b) corresponding Raman spectrum (continuous line) and reference spectrum of elemental sulfur (α-S_8) (dashed line). (c) Raman spectra obtained from reference wood showing the presence of partially oxidized mackinawite (M) and a mix of mackinawite and greigite. Adapted from* [45]. *© 2018 Elsevier Ltd.*

Partially oxidized mackinawite (FeS: $Fe(II)_{1-3x}Fe(III)_{2x}S$) was also identified with corresponding characteristic Raman shifts at 247, 310, 314 and 349 cm^{-1} (Figure 3.10) [46]. It is worth mentioning that mackinawite can be detected by Raman spectroscopy in three different

states: nanocrystalline mackinawite, well-crystallized mackinawite and partially oxidized mackinawite. The latter state is characterized by the presence of Fe^{3+} ions inside the crystal structure [46]. As well, it seemed an oxidation process from partially oxidized mackinawite to greigite (Fe_3S_4: $Fe(II)Fe(III)_2S_4$) had occurred. Indeed, we observed a shift with respect to the mackinawite vibrational bands toward those corresponding to greigite (350 and 365 cm^{-1}) at 319, 335 and 376 cm^{-1} (Figure 3.10). No further oxidation products, such as iron oxides were identified [20]. Regarding XRD analyses, mackinawite was also observed. However, on the contrary to Raman spectroscopy, the different states of mackinawite mentioned above cannot be differentiated by XRD measurements [20]. Hence, it was assumed that mackinawite detected during XRD analyses was also in a partially oxidized state. In terms of wood degradation, the impregnation protocol appeared to be efficient as the wood composition was modified after samples were immerged in iron(II)- and sulfide-containing solutions (Figure S 3.4).

However, pyrite was not identified in our model samples. This compound has been detected in archaeological waterlogged wood [20], [47]. For example, some samples from the *Mary Rose* presented one third of the total reduced sulfur in form of pyrite [48]. According to Rémazeilles et al. (2013), pyrite is formed from mackinawite, via greigite, under certain conditions (i.e., constant supply of sulfur). In this process of oxidation from mackinawite to pyrite, partially oxidized mackinawite may be formed. This was the main iron sulfide compound detected by Raman spectroscopy in our samples. However, the detection of a mix between partially oxidized mackinawite and greigite (Figure 3.10) may be a side effect due to the slight oxidation of the samples during Raman analyses that were conducted under oxic conditions. In fact, mackinawite is solely predominant in anoxic conditions as is an oxygen-sensitive phase [49]. Moreover, Rémazeilles et al. (2013) also described that partially oxidized mackinawite in contact with the atmosphere can be transformed to mineral sulfur, which was actually quite recurrent in the samples analysed here (Figures 3.10 and 3.14).

The formation of mineral sulfur and partially oxidized mackinawite in the model samples allowed the study of the biological oxidation process by *T. denitrificans*. *T. denitrificans* was selected in this study for its ability to oxidize pyrite in a nitrate-dependent reaction [14]. Moreover, *T. denitrificans* can be motile due to a polar flagellum [50], allowing its development along the wood fibres and pores. The growth of bacteria inside the wood is one of the challenges of this biotechnological conservation method. Bacteria should be able to reach iron sulfides that are formed in the inner part of wood. Delivery systems, such as gels, have been previously considered in bioconservation [51]–[53]. These systems could allow the movement of the

bacteria. However, tests are needed to ascertain if they would allow the bacteria to go deep into the wood structure. Moreover, WAW is stored wet to prevent the wood structure from drying and collapsing. Thus, tests would also be required to establish if the humidity in the delivery system is enough to maintain the wooden objects wet. In this first experiment, the application of the bacteria was done finally in liquid media.

Thin cuts of the wood cubes incubated with *T. denitrificans* were used to observe the bacterial growth along the wood. ESEM images showed the colonization of bacteria in the wood pores and along the wood fibres suggesting that this bacterium was able to grow using the sulfur and iron compounds formed during the previous impregnation of wood (Figure 3.11). However, only superficial cuts were produced. A deeper investigation is needed to assure that the bacteria can reach, at least, a depth of few cm within the wood. Sulfur and iron accumulation has been detected specially in the first few centimetres of larger wooden objects [47].

In this case, no post-treatment was conducted to remove the bacteria from the wood. Remaining bacteria could be an issue due to the potential of the introduced biomass to be used by other microorganisms, such as fungi, which could further damage the wooden objects. Intensive rinsing coupled to filtration systems could allow the mechanical removal of the biomass without the need of applying biocides. In further experiments, investigations to analyse the efficient removal of the bacteria after treatment are planned.

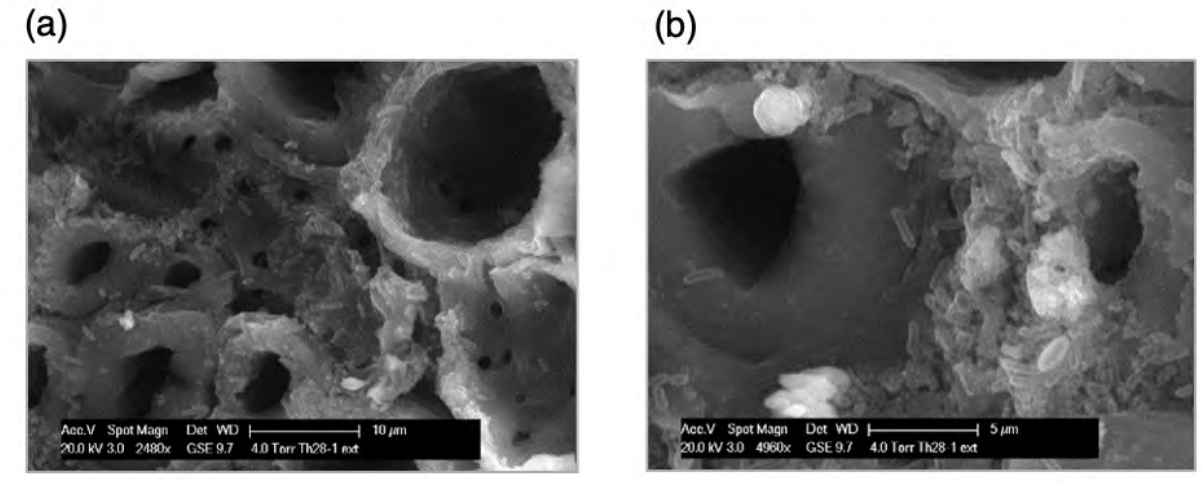

Figure 3.11. *Envirnmental scanning electron micrographs at (a) 2480x and (b) 4960x original magnification obtained from the wood treated with T. denitrificans. The bacterial rod-shaped cells are visible on the surface of the wood samples. Adapted from* [45]. *© 2018 Elsevier Ldt.*

The oxidation state of the sulfur compounds formed was ascertained by Sy-XRF measurements. The sulfur distribution in the recorded Sy-XRF maps was heterogeneous (Figure 3.12). In particular, all Sy-XRF maps collected on the reference and control wood samples indicated the presence of non-oxidized sulfur in relative high amounts (Figure 3.12). On the contrary, treated wood samples presented a large amount of oxidized sulfur respect to control and reference samples (Figure 3.12). The Sy-XRF maps obtained from wood samples treated with *T. denitrificans* suggested an effective transformation of the sulfur species formed during impregnation by the bacteria.

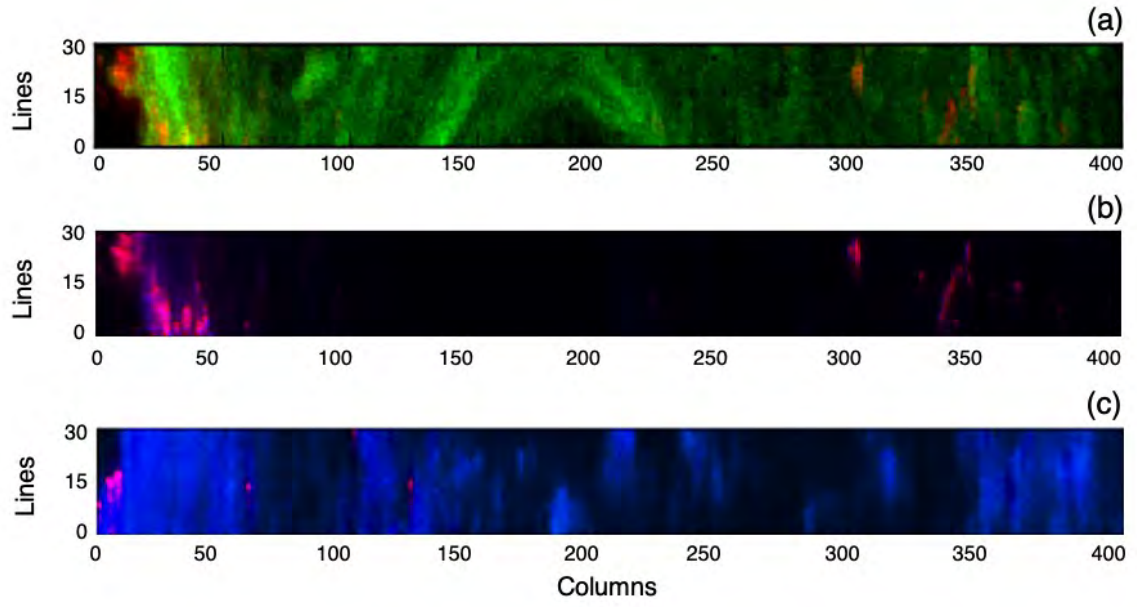

Figure 3.12. *(a) and (b) Sy-XRF maps obtained from the surface of reference wood. (c) Wood treated with T. denitrificans. Colour legend: (a)-Red: total sulfur. Green: total iron. (b and c)- Red: reduced sulfur. Blue: sulfates. Adapted from* [45]. *© 2018 Elsevier Ltd.*

Additionally, ion chromatography analyses confirmed the production of sulfates by *T. denitrificans*. Figure 3.13 shows an increasing concentration of sulfates during the treatment of impregnated wood with *T. denitrificans* suggesting that the oxidation of sulfur is part of the metabolism of the bacterium. Negative controls did not show any oxidation process. At the end of the 28-days incubation time with the wood, only small quantities of sulfates were detected in the control media (~0.03 mM), compared to the quantities measured in the media containing *T. denitrificans* (4.71 mM) (Figure 3.13 and Table 3.3). On the contrary, a depletion of nitrates was observed during the incubation time. Final concentration of nitrates was 8.65 mM (Figure 3.13), showing that 56.3% of total nitrates were reduced by the bacteria. Moreover, control

samples showed an unchanged content of nitrates during the whole time of the experience. Nitrites were produced during the incubation to a final concentration of 5.02 mM (Figure 3.13 and Table 3.3). Nitrites were not detected in the control.

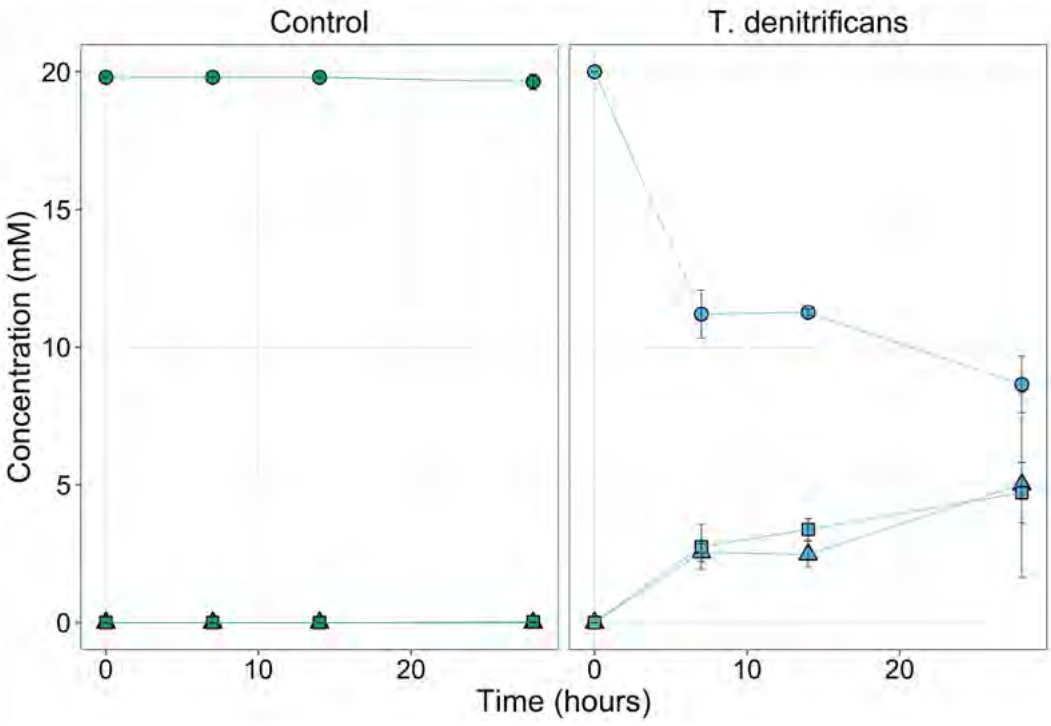

Figure 3.13. *Concentration over time of nitrates (●), nitrites (▲), and sulfates (■) in presence of T. denitrificans or in control samples without bacteria. Error bars show standard deviation of three replicates. Adapted from* [45]. *© 2018 Elsevier Ltd.*

Table 3.3. *Mass balance of educts and products for the oxidation of iron sulfides by T. denitrificans after 28 days of incubation. Adapted from* [45].

	NO_3^- depleted (mM)	**SO_4^{2-} produced (mM)**	**NO_2^- produced (mM)**	**$\Delta NO_3^-/\Delta SO_4^{2-}$ ratio**	**$\Delta NO_3^-/\Delta NO_2^-$ ratio**
Calculated	11.14 ±1.03	4.71 ±1.09	5.02 ±3.34	2.49 ±0.82	2.99 ±2.10
Theoretical	3	1.5	1	2	3

[a] Values are compared to the theoretical stoichiometry according to equation 1.

Elemental sulfur has been described as energy source for *T. denitrificans* [15], [27]. Moreover, other studies showed that mackinawite and greigite were also used by *T. denitrificans* [24]. Indeed, these phases are more easily attacked by bacteria than more stable compounds such as pyrite [54]. In the present study, partially oxidized mackinawite was not detected in treated wood, but mineral sulfur was found in both control and treated wood samples (Figure 3.14). This suggested that the bacteria used here partially oxidized mackinawite as more accessible energy source [10], [55]. The differences observed with the previous section could be due to the stability of the phases formed here. The synthesised mackinawite must have been more reactive than the purchased mackinawite of previous section. Nitrites accumulation points towards partially reduction to nitrites. The main reaction expected for this process is the equation already discussed in previous section (Equation 1):

$$1.5FeS + 3NO_3^- + 2H^+ \rightarrow N_2 + NO_2^- + 1.5Fe^{2+} + 1.5SO_4^{2-} + H_2O \quad (1)$$

Sulfate and nitrate concentrations obtained from ion chromatography allowed to calculate a $\Delta NO_3^-/\Delta SO_4^{2-}$ ratio of 2.49 ±0.82 (Table 3.3). The $\Delta NO_3^-/\Delta NO_2^-$ ratio was 2.99 ±2.01. Overall, the calculated ratios were close to the expected ones in reference to equation 1 (Table 3.3). The hypothesis would be that the bacteria used the available nitrates to oxidize iron sulfides (FeS) formed during the impregnation protocol. Therefore, this equation is suggested as the main reaction happening. However, Bosch et al. 2012 observed that when FeS_2 was used as electron donor *T. denitrificans* performed partial denitrification with the accumulation of nitrites. While, with mackinawite as electron donor, these authors observed a reduction of nitrates to nitrogen gas, with negligible production of nitrites. Still, as seen in the previous section with mineral phases, we have also observed partial denitrification when using mackinawite and other sulfur phases as energy source.

Moreover, partially oxidized mackinawite was not detected in the wood treated with *T. denitrificans* whereas this compound is present in control wood samples (Figures 3.14). Nevertheless, mineral sulfur was detected in both, treated and control wood samples (Figures 3.14). In addition, compounds that were not present in the reference-impregnated wood were observed on treated and control wood samples. In particular, ESEM-EDS micrographs of the wood showed granules along the wood fibres that contained phosphorus (Figure 3.14). Micro-Raman and XRD confirmed that these structures corresponded to an iron phosphate vivianite ($Fe_3(PO_4)_2 \cdot 8\ H_2O$) (Figure 3.14). In particular, Raman spectra showed an intense and sharp peak at 954 cm^{-1} and weak bands around 460, 580, 1020, 1055 cm^{-1} corresponding to vivianite [56]. This compound was only detected in treated and control wood samples. This result

suggested that the formation of vivianite was an abiotic reaction due to the presence of phosphates in the growth media as KH_2PO_4.

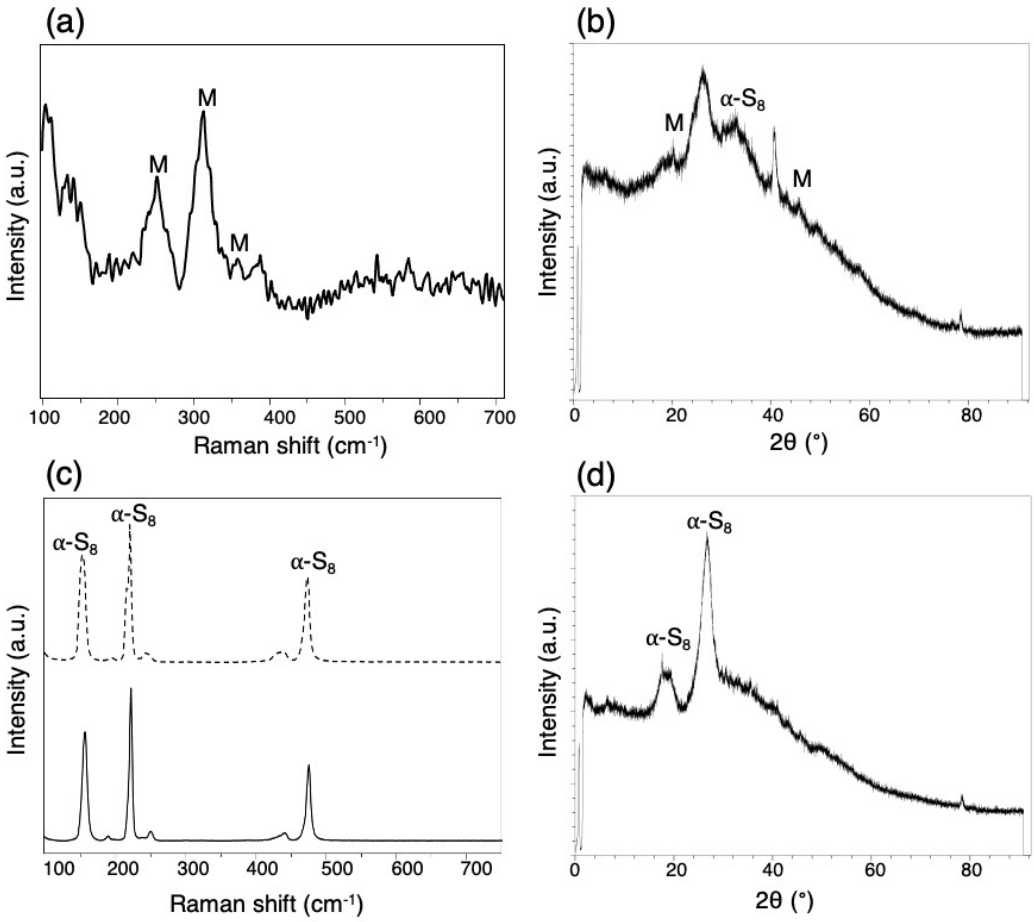

Figure 3.14. *(a) Raman spectra of the control wood where mackinawite (M) was detected. (b) XRD of the control wood with rays for mackinawite (M) and mineral sulfur (α-S_8). (c) Raman spectra showing the presence of mineral sulfur in control sample (dashed line) and reference spectrum of elemental sulfur (α-S_8) (continuous line). (d) XRD diffractogram showing rays of sulfur (α-S_8) for the wood treated with T. denitrificans. Adapted from* [45]. *© 2018 Elsevier Ltd.*

Microorganisms have certain requirements for their growth. For future research, it is important to take into account the chemical composition of the growth medium, as undesired secondary compounds may be formed. Indeed, vivianite was only found in the control and treated wood samples (Figure 3.15). This suggested that the formation of this compound is an abiotic reaction between Fe^{2+} and PO_4^{2-} from the culture medium. Vivianite is not commonly reported in wood remains. However, it is identified in waterlogged soils and iron artefacts [57]. This compound could also cause issues in the preservation of archaeological wood as it is a source of iron, even

though it has been described as an interesting mineral for the stabilization of archaeological iron [58], [59]. In fact, iron itself can cause severe wood degradation as it initiates and catalyses oxidation processes of cellulose with Fenton-type reactions occurring [60]. Thus, the polymeric chains of PEG used for the wood consolidation can be degraded in the same way by iron ions. Therefore the presence of iron compounds in PEG-consolidated wood can compromise the long-term stability of wood artefacts [61].

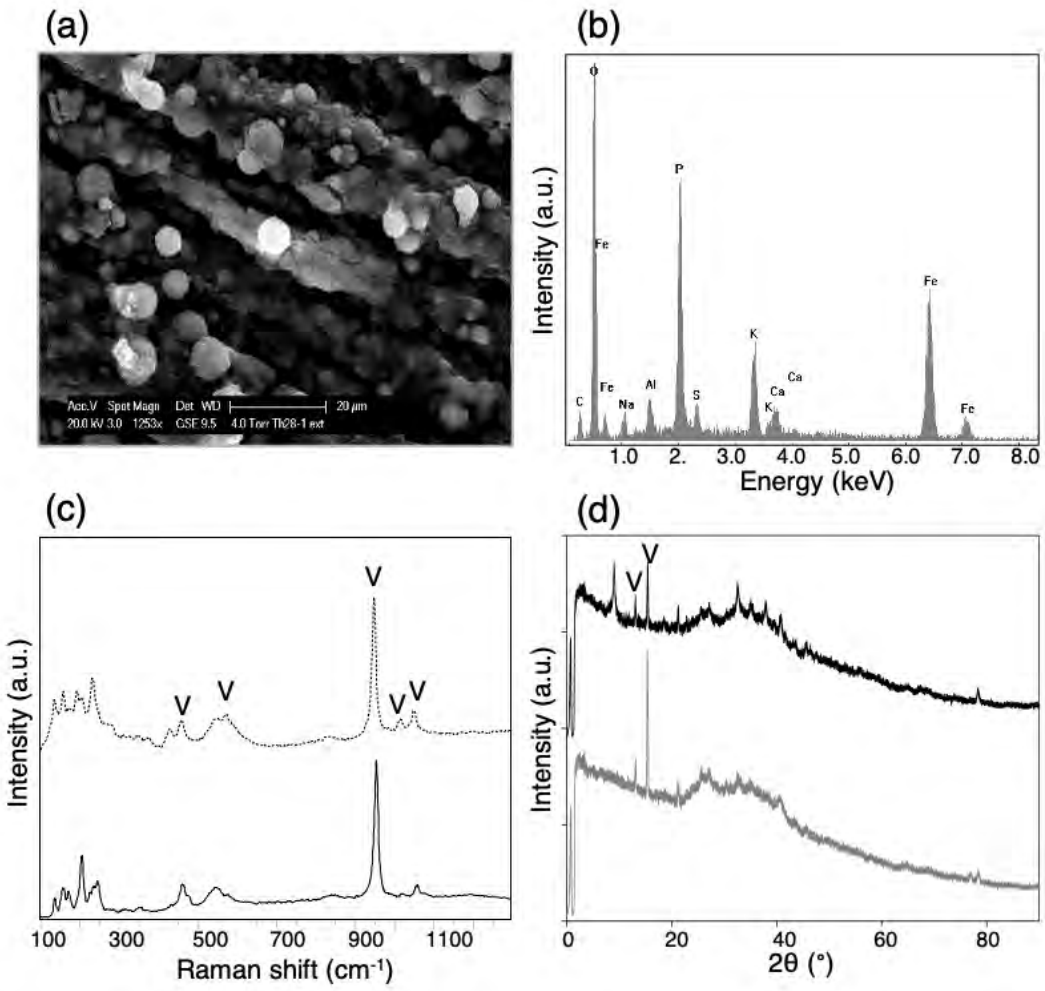

Figure 3.15. *(a) ESEM image of treated wood. (b) Corresponding EDS spectrum. (c) Raman spectra obtained from control wood (dashed line) and wood samples treated with T. denitrificans (continuous line) with peaks related to vivianite (V). (d) XRD spectra from control wood (grey) and treated wood (black) with rays related to vivianite (V). Adapted from* [45]. *© 2018 Elsevier Ltd.*

Risk evaluation

In parallel to the characterization of sulfur and iron species present before and after treatment with *T. denitrificans*, FTIR and pH measurements were performed to evaluate the impact on the wood substrate of the microbiological treatment. Indeed, the biological oxidation of iron sulfides presents several challenges that need to be addressed in order to be adequate for archaeological wood conservation. In a previous study *T. denitrificans* has been suggested as a potential candidate for biological remediation of waterlogged wood [16]. However, this study reported preliminary experiments and thus was not further validated on model wood samples. Biological transformation of sulfur minerals have been widely explored in acidic and aerobic conditions [62]–[64] but such conditions cannot be applied for wood preservation. Indeed, it is essential that the pH remains neutral during treatment to avoid any acidification and chemical damage on wood. To this purpose, *T. denitrificans* is well known as neutrophilic bacterium [41] and pH values measured during experiments were indeed neutral. During the 28 days of treatment, pH measurements on the surface of the wood treated with *T. denitrificans* did not significantly change. pH values measured on the surfaces of reference wood and treated wood samples were similar and close to 7.0.

Moreover, to the best of our knowledge, no study has yet reported its capability to degrade wood compounds. In any case as obligate chemolithoautotrophic bacterium*, T. denitrificans* generates biomass from the fixation of CO_2 and this is not expected to have an incidence on the degradation of archaeological wood. No structural changes or chemical modifications in the wood composition were observed during FTIR analyses further than those made by the impregnation. FTIR spectra recorded from fresh oak wood appeared to be slightly different from the FTIR spectra obtained from impregnated, control and treated wood samples (Figure 3.16). The peak around 1733 cm^{-1}, that corresponds to C=O vibration in hemicellulose [43], [65], [66], is indeed better defined on fresh wood samples than after impregnation and treatment. In particular, this vibrational band was weakly detected in the FTIR spectra recorded on treated wood samples and completely disappeared in impregnated and control wood samples, as shown in figure 3.16. On the contrary, the peak around 1634 cm^{-1} had a strong absorbance in all wet samples (impregnated, control and treated wood) with respect to the fresh wood. This peak is assigned to the O-H bend of absorbed H_2O [65]–[67]. The peak around 1234 cm^{-1}, assigned to C–O stretch in lignin and xylan [65], appeared as a broad peak in the fresh wood. However, for the impregnated, control and treated wood samples, the relative intensity of these vibrational bands was modified. In particular, the peak at 1234 cm^{-1} was less intense

and another peak at 1265 cm^{-1} was better defined. Finally, peaks at 1505, 1368, 1157 and 897 cm^{-1} were detected in all FTIR spectra. These bands are respectively assigned to aromatic skeletal vibration in lignin, C–H deformation in cellulose and hemicellulose, C–O–C vibration in cellulose and hemicellulose and; C–H deformation in cellulose [43].

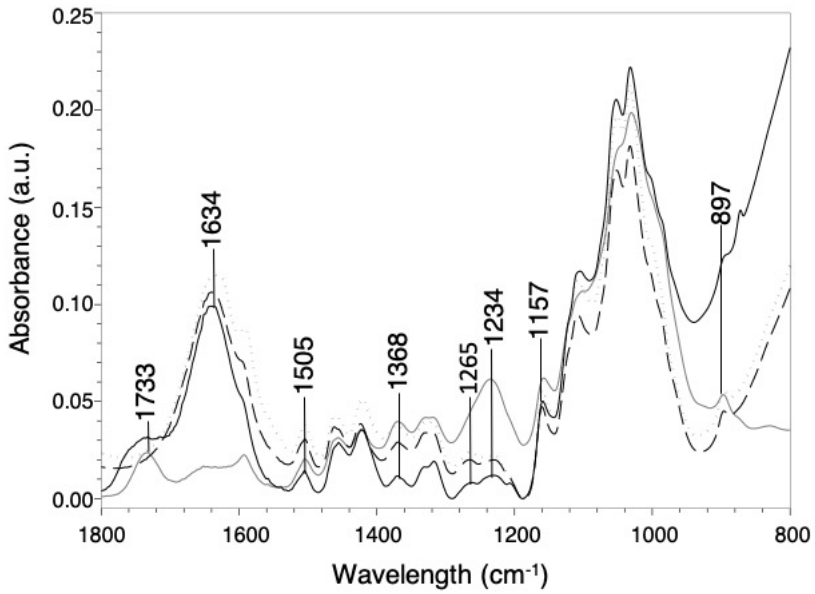

Figure 3.16. *Representative FTIR spectra of fresh wood (grey), impregnated wood (⋯), control wood (---) and wood treated with T. denitrificans (black), for the region between 1800 and 800 cm^{-1}. Adapted from* [45]*. © 2018 Elsevier Ltd.*

In order to evaluate the wood degradation related to impregnation and/or treatment, the intensity ratios between lignin absorbance (1505 cm^{-1}) against carbohydrates absorbance (either 1368, 1157 or 897 cm^{-1}) were calculated (Figure S 3.4). It appeared that the impregnation had a major impact on C–H deformation (A_{1505}/A_{1368} and A_{1505}/A_{897}) and not on C–O–C vibration (A_{1505}/A_{1157}) with higher values observed for A_{1505}/A_{1368} and A_{1505}/A_{897} than A_{1505}/A_{1157}. This suggested the efficiency of the impregnation to artificially age fresh wood samples that can be then exploited as model samples simulating degraded archaeological wood. However, only significant difference was observed for the A_{1505}/A_{1368} between fresh wood and wet wood samples (reference, control and treated). Regarding treatment, no significant differences were observed before and after bacterial treatment, suggesting the innocuousness of the proposed treatment when applied on wood substrate. These results offer promising perspectives for the application of *T. denitrificans* in the extraction of sulfur species from waterlogged wood.

3.2.2 Optimisation

Materials and Methods

Model wood samples

Balsa (*Ochroma pyramidale*) wood cubes with the following dimensions: 1×1×1 cm^3, were prepared to reproduce the characteristics of waterlogged wood. The samples were impregnated with iron and sulfur solutions as described in section 3.2.1 for oak wood. After artificial contamination, samples were kept immersed in N_2-flushed water. Before any experimental procedure, cubes samples were washed by ultrasonic bath until no more impregnation solution was released.

Bacteria and culture conditions

Thiobacillus denitrificans (DSM 12475) was obtained from the German Collection of Microorganisms and Cell Cultures (DMSZ GmbH, Germany). The strain was cultivated using standard anaerobic techniques at 30 °C in the dark using medium 113 (2017 DSMZ).

Oxidation experiments

Experiments were conducted in glass bottles without sealing at 30 °C in without agitation in the darkness. The oxidation medium consisted in the modified 113-medium (2017 DSMZ) where all the sulfur and iron compounds were removed. Moreover, as phosphates from the culture medium precipitated in the previous experience, some experiments did not include KH_2PO_4 (Table 3.4). In this case, the buffer agent was 15 mM HEPES. Also, not all conditions included KNO_3 (Table 3.4). Oxygen was the only electron acceptor in some of the experimental set-ups (Table 3.4). Therefore, final media compositions were: 1) 15 mM KH_2PO_4, 20 mM KNO_3, 19 mM NH_4Cl, 3.2 mM $MgCl_2 \cdot 6H_2O$, 30 mM $NaHCO_3$, and 2 mL of modified SL-4 oligo-elements solution for 113 medium with phosphates and nitrates (113-PN), 2) 15 mM KH_2PO_4, 19 mM NH_4Cl, 3.2 mM $MgCl_2 \cdot 6H_2O$, 30 mM $NaHCO_3$, and 2 mL of modified SL-4 oligo-elements solution for 113 medium with phosphates and without nitrates (113-PO), 3) 15 mM HEPES, 20 mM KNO_3, 19 mM NH_4Cl, 3.2 mM $MgCl_2 \cdot 6H_2O$, 30 mM $NaHCO_3$, and 2 mL of modified SL-4 oligo-elements solution for 113 medium without phosphates and with nitrates (113-HN), and 4) 15 mM HEPES, 19 mM NH_4Cl, 3.2 mM $MgCl_2 \cdot 6H_2O$, 30 mM $NaHCO_3$, and 2 mL of modified SL-4 oligo-elements solution for 113 medium without phosphates and without nitrates (113-HO).

The bottles were filled to the top and one impregnated wood cube was added in sterile conditions to each bottle. *T. denitrificans* was grown for 5-7 days to obtain high cell

concentration. Then, the cells were recovered by centrifugation and washed three time in medium 113 without nitrates, phosphates, or any sulfur or iron source. *T. denitrificans* was then inoculated to every experiment to the final cell concentration as mention in Table 4.

Negative controls without bacteria were carried out to evaluate the possible interaction of the medium with the wood substrate. Controls for internal accumulation of sulfur containing only electron acceptor and *T. denitrificans,* but no sulfur source, were also included. Experiments and controls were performed in two independent replicates. Samples were withdrawn over time for further analyses. The growth of the bacteria in solution was followed the first days of incubation by the increase in Optical Density (OD) at 600 nm, using a UV-Vis spectrophotometer (Lambda 25 Perkin Elmer, Unites States).

Table 3.4*. Overview of the different experimental conditions for the study of the oxidation of reduced sulfur species in model wood samples.*

	Exp. A	**Exp. B**	**Exp. C**	**Exp. D**	**Exp. E**	**Exp. F**	**Exp. G**	**Exp. H**
Buffer agent	KH_2PO_4	KH_2PO_4	KH_2PO_4	KH_2PO_4	HEPES	HEPES	HEPES	HEPES
Cell concentration (cells·mL^{-1})	~1x10^6	~1x10^8	~1x10^6	~1x10^8	~1x10^6	~1x10^8	~1x10^6	~1x10^8
Initial nitrates concentration (mM)	20	20	-	-	20	20	-	-
Oxygen	yes	yes	yes	yes	yes	yes	yes	yes
Wood	1 cube	1 cube	1 cube	1 cube	1 cube	1 cube	1 cube	1 cube

Analytical methods

Colorimetric measurements

Colour measurements were registered with a Minolta CM-508D spectrophotometer with the following parameters: Specular Component Included (SCI), Illuminant D65 (daylight containing UV component, colour T 6504K), d/8° geometry, 10° observer, measurement area diameter 10 mm, illumination with Xe flashlight source 100% UV containing all UV components or 0% UV containing no UV components, CIELab 1976 colour space. On each wood sample, a measurement was carried out on the centre of three faces (i.e., three

measurements per cubes). Measurements were carried out on fresh, artificially contaminated, treated and control wood samples.

Inductively Coupled Plasma-Optical Emission Spectrometry (ICP-OES)

Total iron and sulfur concentrations were determined in solution by Inductively Coupled Plasma-Optical Emission Spectrometry (ICP-OES). Samples were first filtered through a 0.22 µm PVDF membrane (BGB Analytik, Switzerland) and then diluted into the detection range (0-2 ppm). Diluted samples were loaded using a peristaltic pump, and a cyclonic spray chamber connected to a nebulizer (Perkin-Elmer, United States) to provide high sample transfer into the ICP. Total iron concentrations were determined using an Optima 2100 DV (Perkin-Elmer, United States) optical emission spectrometer.

Ion chromatography (IC)

For the determination of the concentration of sulfates (SO_4^{2-}), nitrates (NO_3^-), nitrites (NO_2^-), phosphates (PO_4^{3-}) and other anions, samples were filtered at 0.22 µm using PVDF filters (BGB Analytik, Switzerland) and then diluted before analysis. Dilutions were analysed with an ion chromatograph Dionex ICS 1600 (Thermo Fisher Scientific, Unites States) equipped as described in section 3.1. Data was inspected with the Chromeleon™ software (Thermo Fisher Scientific, Unites States).

pH measurements

A 691 pH Meter Metrohm (Metrohm AG, Switzerland) was used to control the pH of the solution over time with an ionic electrode (unitrode 6.0259.100) calibrated between pH 4 and pH 7 or pH 7 and pH 9 buffer solutions. The pH of the cubes was measured with a surface electrode (flat membrane electrode 6.0256.100), also correctly calibrated, at the beginning and end of the experiment.

Raman spectroscopy

A Jobin Yvon Horiba™ spectrophotometer coupled with Olympus BX41 microscope (Horiba Ltd., Japan) was used for measurements. Spectra were recorded at a wavelength of 632 nm, hole of 800 µm, slit of 200 µm, 100-2000 cm^{-1} range, filter 25%, 50xLWD objective and 5 sec of acquisition with 10 accumulations. The spectra were processed with LabSpec® 5 software (automatic baseline correction). Reference spectra from spectra libraries and literature were used to identify the compounds formed. Measurements were carried out on the surface of impregnated, treated and control wood samples.

Scanning Electron Microscopy coupled with Energy Dispersive X-Ray Spectroscopy (SEM-EDS)

Wood samples treated with *T. denitrificans* and controls were rinsed after the incubation time, and small slices were obtained using a razor blade. Wood segments were fixed at RT with 3% (v/v) glutaraldehyde solution in 0.1 M sodium cacodylate (pH 7.2) for 3h, washed twice and then dehydration steps were performed using different concentrations of ethanol (25%, 50%, 75%, 90%, 100% (v/v)) and then pure acetone. Finally, samples were dried in a CO_2 atmosphere.

Samples were mounted on stubs using carbon conductive tape. Samples were examined under low vacuum without coating using a Thermo Scientific™ Scios™ 2 DualBeam™ (Thermo Fisher Scientific, Unites States) equipped with an energy-dispersive X-ray analyser (EDAX, Unites States). Afterwards, the same samples were coated with a layer of gold using a Leica EM SCD050 (60 mA current, 5 cm, 5 s duration, argon gas), and examined again at high vacuum using the same instrument.

Results and Discussion

After 30 days of incubation, balsa wood cubes treated in 113-medium with KH_2PO_4 had a final appearance that was similar to oak samples discussed in the section above. The same type of yellowish precipitate was observed on the surface of the balsa cubes (Figure S 3.5), indicating that most likely iron phosphates precipitation occurred also here. Moreover, no remarkable visual differences were observed between the abiotic control cubes and treated cubes in any condition (113-PN or 113-PO) (Figures 3.17 and 3.18). On the other hand, cubes incubated in 113-medium with HEPES (113-HN and 113-HO) presented a reddish colouration (Figure 16). HEPES buffer was considered as replacement of KH_2PO_4, in the growth medium, to prevent vivianite (iron phosphate) formation. In this case, differences were observed between the wood incubated in presence of nitrates (113-HN) or just with oxygen in the solution (113-HO) (Figure 3.17). A darker hue was noticed in cubes incubated in 113-HN, for both abiotic controls and samples. Indeed, while colorimetric plots clustered together 113-PN and 113-PO samples, 113-HN and 113-HO samples were plotted separately in the colour scale (L*a*b*) (Figure 3.18).

***Figure 3.17**. Visual appearance of the balsa wood cubes after incubation with T. denitrificans in the different experimental set-ups. Medium 113 with KH_2PO_4 and with nitrates or without (113-PN and 113-PO). Medium 113 with HEPES and with nitrates or without (113-HN and 113-HO). For complete description of the experimental conditions refer to the materials and methods section.*

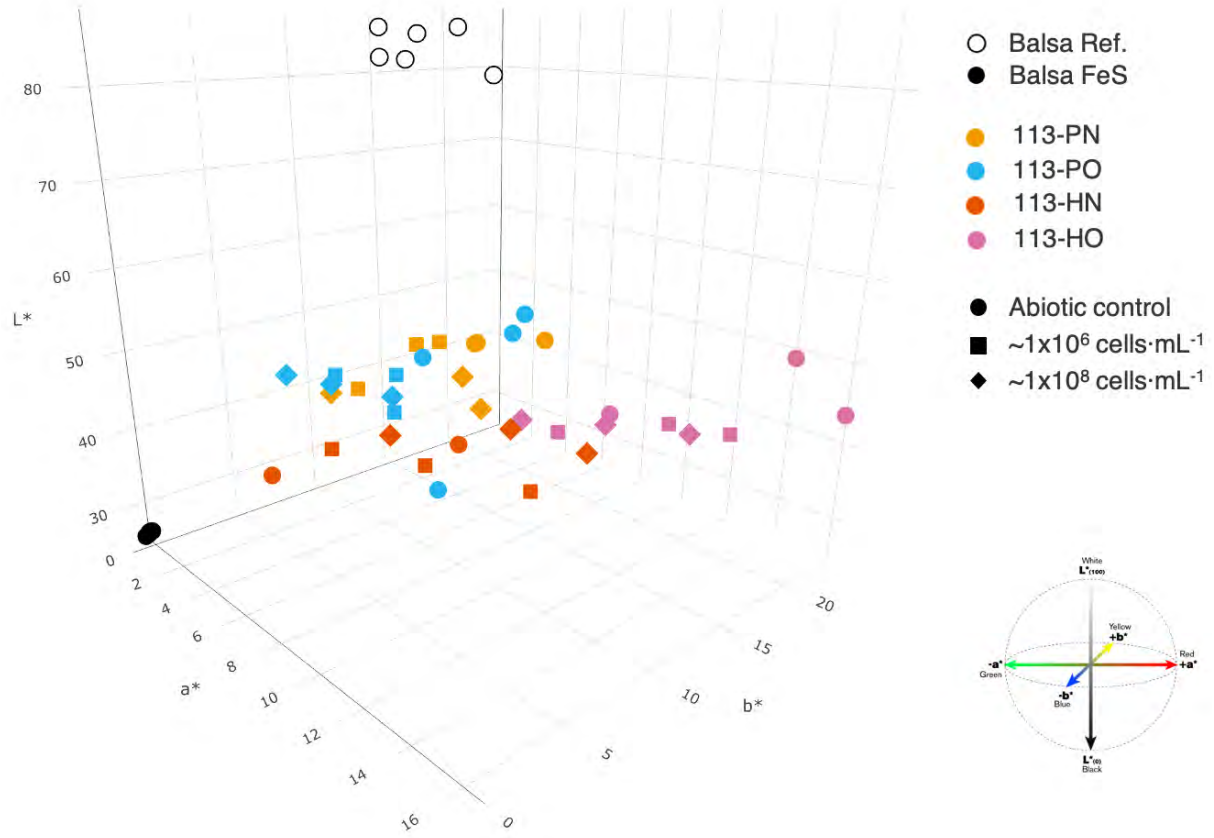

***Figure 3.18**. Colorimetry plots representing colour coordinates: L* (lightness/bright-dark), a* (red/green opponent colours) and b* (yellow/blue opponent colours). Colour measurements were taken on the wood surface of all samples after incubation with T. denitrificans or abiotic controls. The different four media are represented by different colours. Abiotic controls and the two initial cell concentration are represented by different symbols. Fresh balsa (Balsa Ref.) and balsa impregnated with iron sulfides (Balsa FeS) are included as references.*

Although similar precipitates were observed in balsa cubes, vivianite that was detected in oak cubes in the previous section was not registered here. Only one spectrum recorded on a 113-PN abiotic control cube presented a peak at ~1098 cm^{-1} that could be assigned to iron phosphates (Figure S 3.6). Iron phosphates present strong Raman frequency ranges between 1010 and 1100 cm^{-1} related to PO_3 symmetric stretch [68]. Therefore, this band could indicate formation of iron phosphates in 113-PN medium. However, as cellulose presents a strong band at 1096 cm^{-1} [69], and no other iron phosphates assigned bands were detected, identification was not obvious. Complementary SEM-EDS analyses, however, showed phosphorous on the surface of all analysed thin wood sections treated in 113-PN and 113-PO (Figures 3.19 and S 3.8).

In core sections of samples treated in 113-PN and 113-PO, sulfur was also detected (Figures 3.19 and S 3.8). In this case, Raman analysis confirmed the presence of mineral sulfur on the wood samples (Figures 3.19 and S 3.8). Other reduced sulfur species (i.e., iron sulfides) were not detected after treatment by Raman spectroscopy. However, some bands at 1343 and 1491 cm^{-1} were detected in the wood treated in Exp. A (Figure 3.19). These bands can be related to the wood substrate [69].

In samples treated in 113-HN and 113-HO, the visual appearance suggested formation of iron oxides. SEM-EDS analyses on 113-HN samples (Exp. F) revealed the formation of precipitates mostly composed of iron (Figure 3.20). However, these phases could not be identified by Raman spectroscopy. The co-existent elemental sulfur, with strong excitation, could have made difficult the identification (Figure 3.20). Oxygen samples (Exp. G and H) also showed iron in their EDS spectra, although the precipitates were not observed (Figure S 3.8). This could explain the differences observed in the appearance of these wood samples (Figure 3.17).

In exp. E and F, *T. denitrificans* produced nitrites via reduction of nitrates and oxidation of the sulfur species formed in the model samples (Figure 3.21). The nitrites formed can abiotically react with Fe^{2+}. Abiotic oxidation of Fe^{2+} to goethite has been previously studied in presence of nitrates and nitrites [70]. In fact, researchers highlight that abiotic oxidation will compete with biotic oxidation, especially if nitrites are formed in the biotic reaction [70]. Iron(II) oxidation by nitrites is faster than with nitrates. This reaction is dependant of pH, at lower pH the reaction rate is increased. Still, at neutral pH this abiotic oxidation is possible [70]. In experimental set-ups only containing oxygen (Exp. G and H), the oxidation of ferrous iron was only possible with O_2. The different oxidation processes could translate to the different appearance between 113-HN and 113-HO samples, and also the different type of precipitates detected between 113-HN and 113-HO samples.

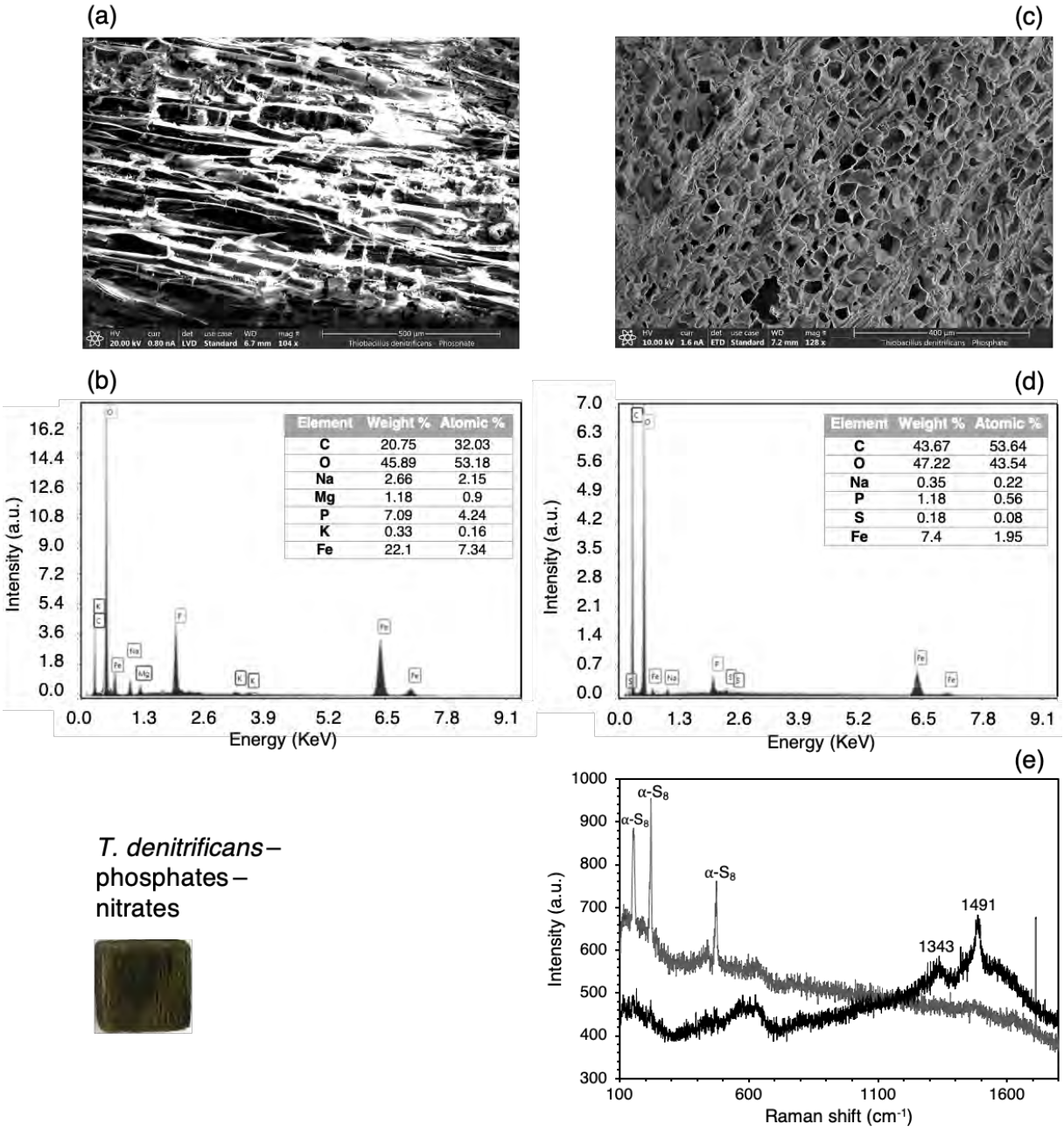

Figure 3.19. *(a) Secondary electron micrograph and (b) corresponding EDS spectrum of a tangential cut of a wood sample treated with T. denitrificans in 113-PN (Exp. A). (c) Secondary electron micrograph and (d) corresponding EDS spectrum of a cross-section cut of a wood sample treated with T. denitrificans in 113-PN (Exp. A). (e) Raman spectra obtained from two independent points on the wood sample. Characteristic peaks of elemental sulfur (α-S_8) are tagged along with some unidentified peaks.*

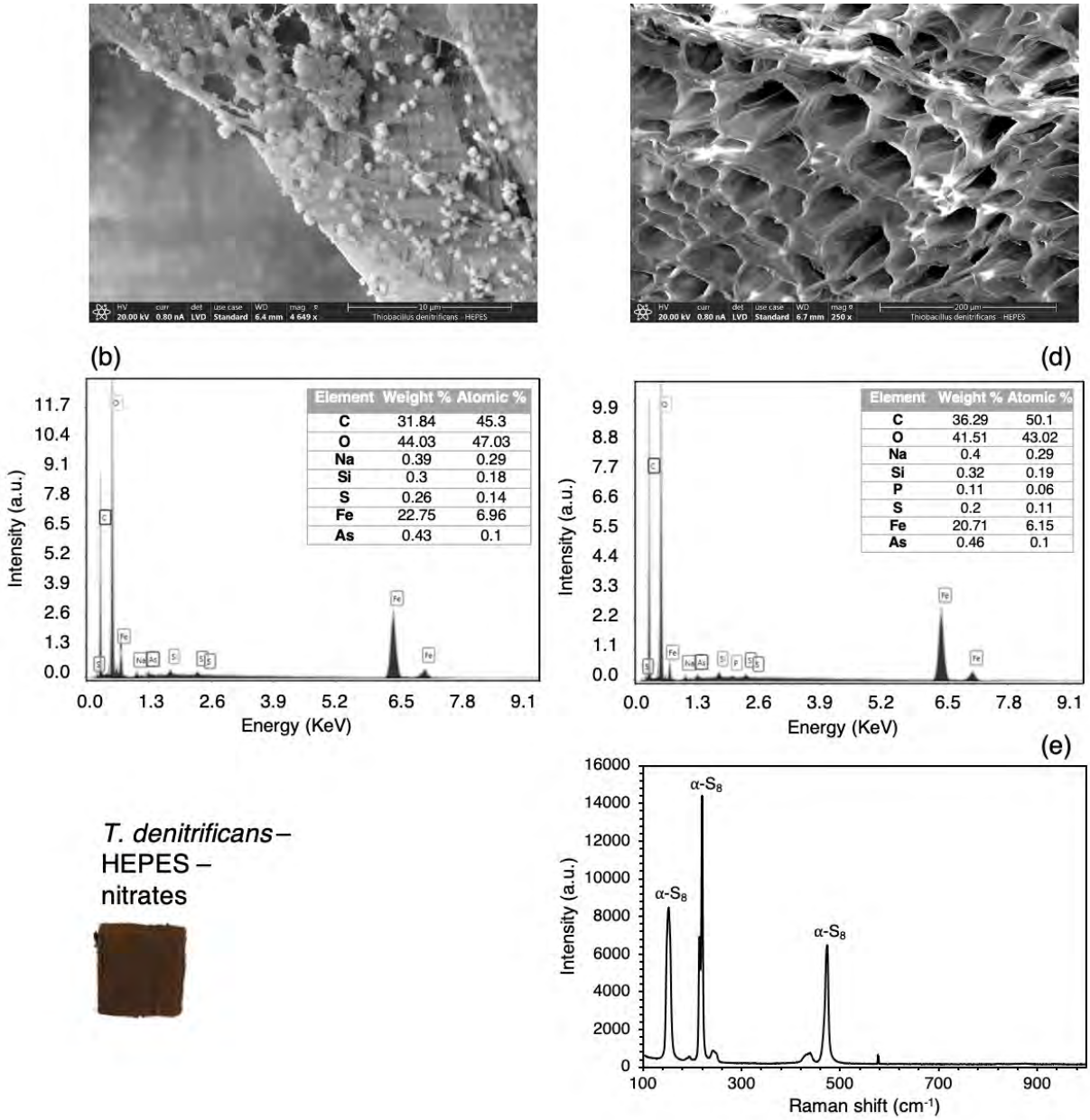

Figure 3.20. *(a) Secondary electron micrograph and (b) corresponding EDS spectrum of the precipitates observed on a cross-section of wood treated with T. denitrificans in 113-HN (Exp. F). (c) SEM image and (d) corresponding EDS spectrum of cross-sectioned wood treated with T. denitrificans (Exp. F), where the precipitates were observed. (e) Raman spectrum obtained from the surface of the wood sample. Characteristic peaks of elemental sulfur (α-S_8) are tagged.*

Complementary IC analyses revealed oxidation of the sulfur species formed during impregnation of the model samples to sulfates (Figure 3.21). In general, experimental set-ups with nitrates (Exp. A, B, E and F) were more successful in oxidising sulfur compounds to sulfates (Figure 3.21). In the first section of this chapter, we observed that in presence of oxygen and nitrates, some sulfur species were preferentially oxidised by nitrates. Only elemental sulfur was clearly oxidised using O_2. This could indicate that other phases are being oxidised prior to

elemental sulfur in presence of nitrates here. Indeed, in the proof of concept, partially oxidised mackinawite was oxidised while elemental sulfur remained. Here, elemental sulfur was detected in Raman analyses in all samples after treatment, but not mackinawite. Moreover, most $\Delta NO_3^-/\Delta SO_4^{2-}$ ratios were close to the theoretical ratios for oxidation of mackinawite (Table 3.5). Still, some sulfates were registered in experimental set-ups with only oxygen (Exp. C, D, G and H), indicating that there might have been oxidation using also this electron acceptor.

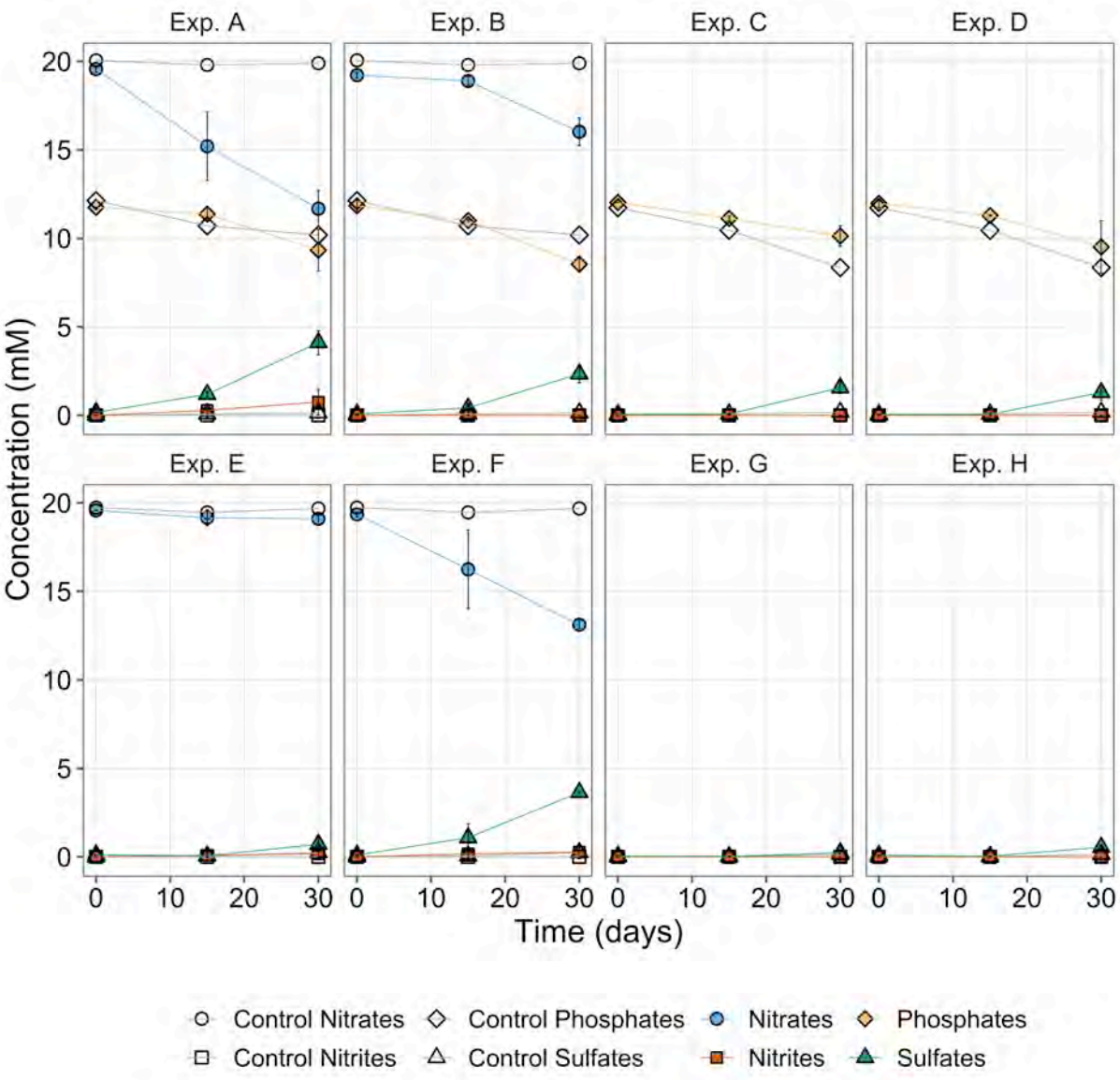

Figure 3.21. *Concentration over time of nitrates, nitrites, phosphates and sulfates in presence of T. denitrificans (closed symbols) or abiotic controls (open symbols), in all experimental set-ups. Error bars show standard deviation of two independent replicates.*

***Table 3.5**. Mass balance of educts and products for the different experimental set-ups after the 30 days of incubation of the model wood with T. denitrificans.*

	NO_3^- depleted (mM)	**SO_4^{2-} produced (mM)[a]**	**NO_2^- produced (mM)**	**$\Delta NO_3^-/\Delta SO_4^{2-}$ ratio**	**$\Delta NO_3^-/\Delta NO_2^-$ ratio**
Exp. A	7.89 ±0.84	3.97 ±0.68	0.75 ±0.73	2.00 ±0.13	19.06 ±17.49
Exp. B	3.20 ±0.96	2.20 ±0.49	-	1.54 ±0.78	-
Exp. C	-	1.38 ±0.31	-	-	-
Exp. D	-	1.11 ±0.44	-	-	-
Exp. E	0.47 ±0.35	0.46 ±0.40	0.17 ±0.24	1.10 ±0.19	1.06 ±1.49
Exp. F	6.23 ±0.10	3.39 ±0.08	0.27 ±0.38	1.84 ±0.07	5.83 ±8.25
Exp. G	-	0.09 ±0.07	-	-	-
Exp. H	-	0.40 ±0.08	-	-	-
Theoretical					
Eq. 1	3	1.5	1	2	3
Eq. 2	8	5	-	1.6	-

[a]Sulfates concentration, and therefore the calculated ratios, have been adjusted by removing the amounts of sulfates detected in the abiotic controls.

$$1.5FeS + 3NO_3^- + 2H^+ \rightarrow N_2 + NO_2^- + 1.5Fe^{2+} + 1.5SO_4^{2-} + H_2O \quad (1)$$

$$5FeS + 8NO_3^- + 8H^+ \rightarrow 4N_2 + 5Fe^{2+} + 5SO_4^{2-} + 4H_2O \quad (2)$$

Over the time of the experiment some abiotic oxidation was registered as well. In the proof of concept, where anoxic environment was kept, sulfates detected in the control were ~0.03 mM. Here, we detected values between 0.14-0.24 mM, depending on the experimental condition. In the proof of concept, the production of sulfates was over 150 times higher than in controls, while here, the biological production of sulfates was maximum 30 times higher. The sulfur extraction under oxic environment is expected to be a synergic combination between abiotic and microbial oxidation [71]. The bio-oxidation would enhance dissolution of reduced sulfur compounds under control conditions avoiding future spontaneous oxidation and production of acids.

IC analyses also showed that in 113-PN samples with ~1x10^6 cells·mL^{-1} (Exp. A), more sulfates were produced than with higher cell concentration (Exp. B) (Figure 3.21). The opposite was

observed in 113-HN samples, more sulfates were detected with the higher cell concentration (Exp. F) (Figure 3.21). The initial concentration of cells did not influence the oxidation rate, but the growth rate was the key factor. The growth followed by the OD at 600 nm showed that these two experimental set-ups had active growing bacteria for longer time (Figure S 3.9). *T. denitrificans* uses reduced sulfur species as energy source [17]. Higher oxidation rates would be achieved by actively growing rather than energy conservation.

In general, *T. denitrificans* seemed to thrive better with phosphates in the growth medium (Figure S 3.9), and with exception of the above-mentioned Exp. F, more production of sulfates was detected in these conditions (Exp. A, B, C and D). *T. denitrificans* encodes for multiple oxidation pathways for multiple sulfur compounds. Some of the enzymes participating in the overall pathway require phosphorous [17]. The presence of phosphates would benefit this metabolic route. Bacteria were detected in SEM analyses along the wood in samples from 113-PO (Figure S 3.7).

IC confirmed that in 113-PN and 113-PO samples phosphates decreased in solution over time (Figure 3.21). This influenced the pH of the abiotic control, with a slight increase in the pH from 7.23 ±0.15 to of 7.81 ±0.13. In samples, due to the biological metabolisms occurring the pH remained stable or decreased. HEPES samples maintained a more stable pH along the incubation time (~7.34 ±0.19).

Finally, we measured total iron concentration in solution by ICP-OES. Analyses of the solution detected very low levels of iron at the end of the extraction time for all conditions. In all samples using KH_2PO_4 as buffer agent, iron in solution was around 10 µM. In samples with HEPES buffer, iron concentrations did not arrive to 1 µM. These results show that even though oxidation of sulfur species was occurring the co-existent iron was not extracted. Indeed, we observed precipitation in form of iron phosphates or iron oxides (specific compounds not confirmed).

Conclusion

The extraction of sulfur compounds from waterlogged wood is necessary for the efficient long-term preservation of these specific items. This preliminary study on a preventive biological extraction method for waterlogged wood showed that *T. denitrificans* was able to directly metabolize sulfur compounds in wood substrate under anoxic conditions. This demonstrated the feasibility of a biotechnological procedure as an alternative to current extraction methods of sulfur species from WAW.

Moreover, optimization of the processes targeted the encountered problems regarding nitrites accumulation and iron phosphates precipitation. However, *T. denitrificans* conducted preferentially denitrification coupled to the oxidation of the reduced sulfur species formed in the model wood. Oxidation rates in presence of oxygen as sole electron acceptor were lower. In future research, other bacteria could be investigated to conduct circumneutral oxidation of reduced sulfur species with oxygen as electron acceptor [71].

The precipitation of iron phosphates helped preventing the formation of iron oxides, but the problematic iron was not extracted. This feature can be interesting depending on the specific requirements of the artefacts under study. The precipitation of iron phosphates did not interfere with the oxidation of the sulfur moiety. This protocol would result in extracted sulfur, and iron stabilized as iron phosphates. However, if the extraction of iron is essential, the presence of phosphates in the growth medium will be inconvenient. Still, using another buffering agent, like HEPES, we did not extract any iron either. In this case iron was precipitating, most likely as iron oxide. Moreover, *T. denitrificans* presented a better development when phosphates were included in the growth medium. Thus, when using *T. denitrificans* for the oxidation of sulfur compounds within the wood, the presence of phosphates may be essential. Another delivery system could prevent the precipitation and formation of minerals such as vivianite. For example, the use of a gel instead of complete immersion could avoid the precipitation of iron phosphates and is foreseen to be tested.

Regardless, if total sulfur an iron extraction is required, combining sulfur oxidation and iron complexation will improve the overall efficiency of the treatment.

Supplementary material 3.2

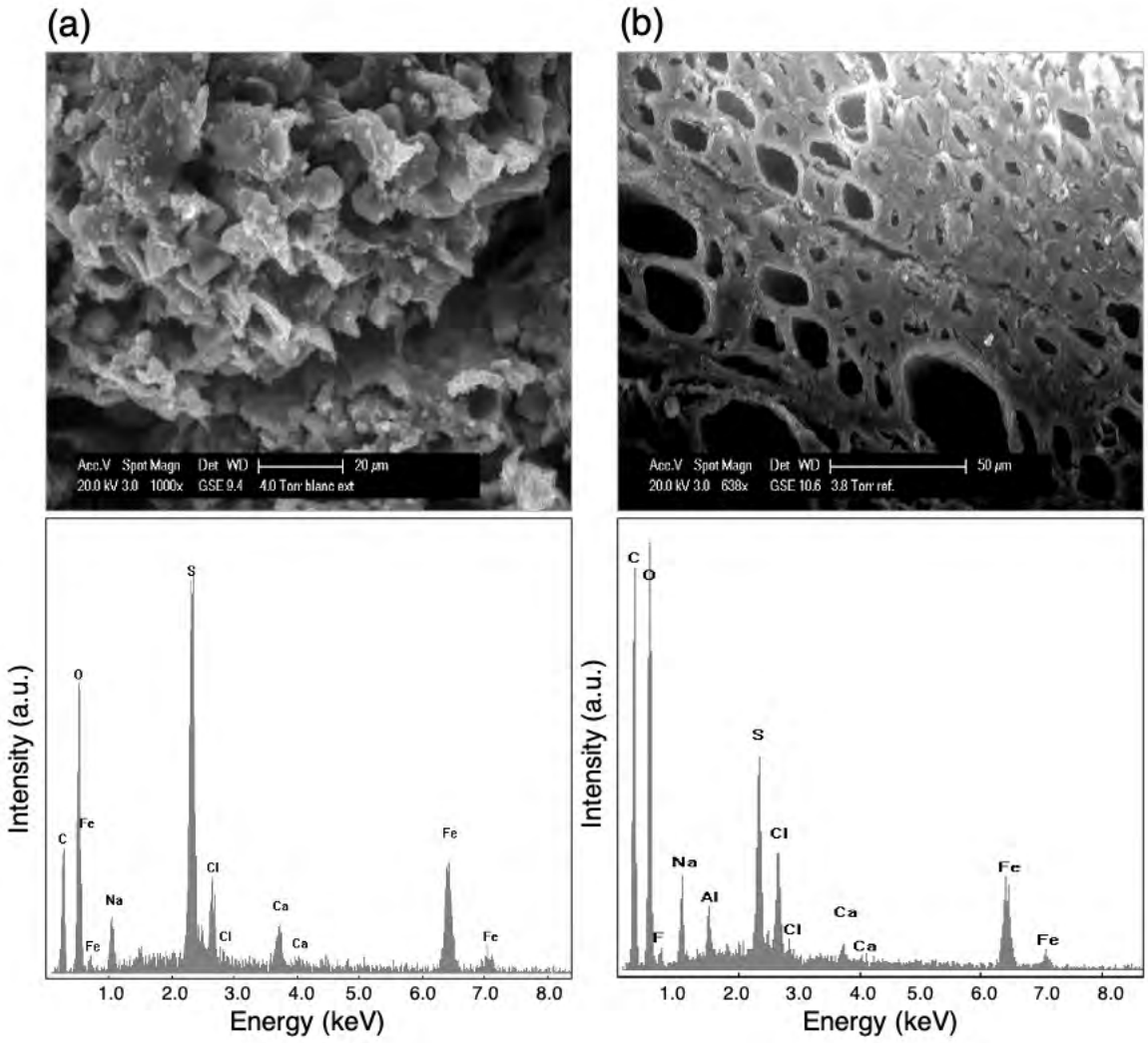

Figure S 3.3. *Envirnmental scanning electron micrographs and respective EDS spectra obtained from reference wood on (a) external surface and (b) inner transversal section. Adapted from* [45]. *© 2018 Elsevier Ldt.*

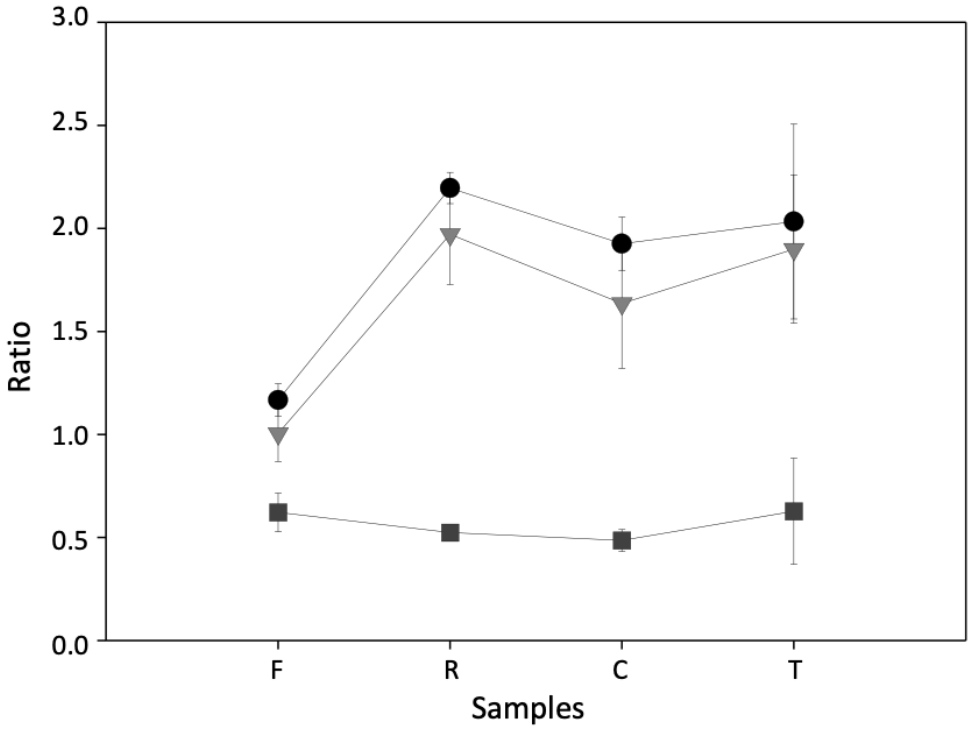

Figure S 3.4. *Intensity ratio of the absorbance band characteristic for lignin (1505 cm^{-1}) against the absorbance bands corresponding to carbohydrates at 1368 (●), 1157 (■) and 897 (▼) cm^{-1} respectively, calculated for fresh wood (F), reference wood (R), control wood (C) and wood treated with T. denitrificans (T). Error bars show standard deviation of three replicates. Adapted from* [45]. *© 2018 Elsevier Ldt.*

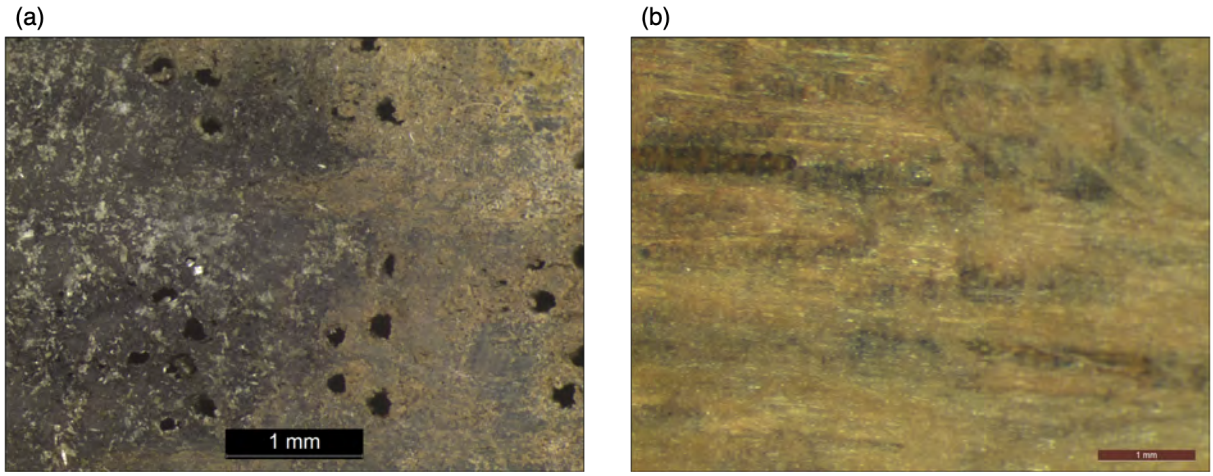

Figure S 3.5. *(a) Stereomicroscope image of an oak wood sample after treatment with T. denitrificans. (b) Stereomicroscope image of a balsa wood sample after treatment with T. denitrificans. Yellow precipitates are visible in both types of wood.*

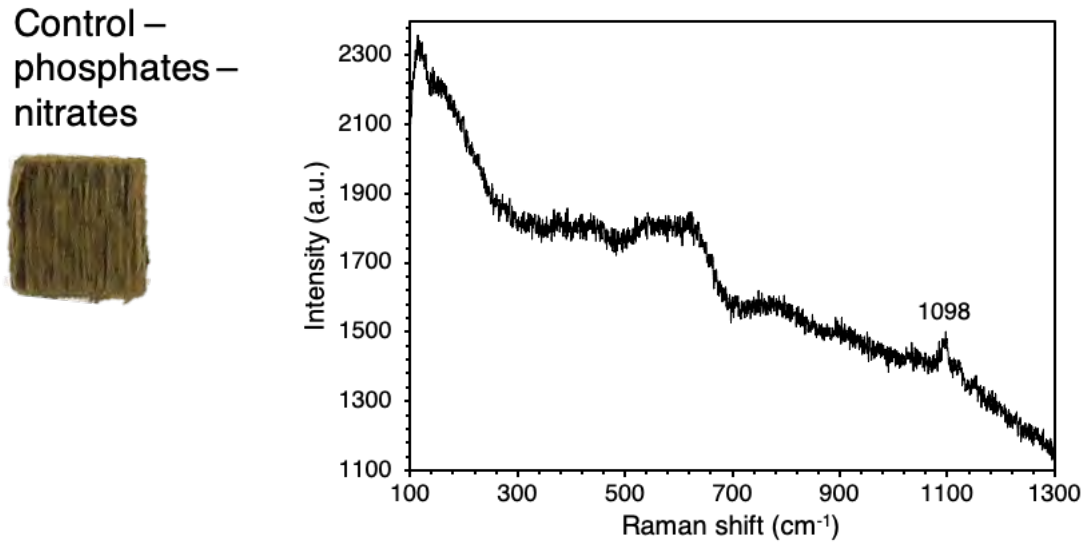

Figure S 3.6. *Raman spectrum obtained from the surface of the113-PN abiotic control wood sample.*

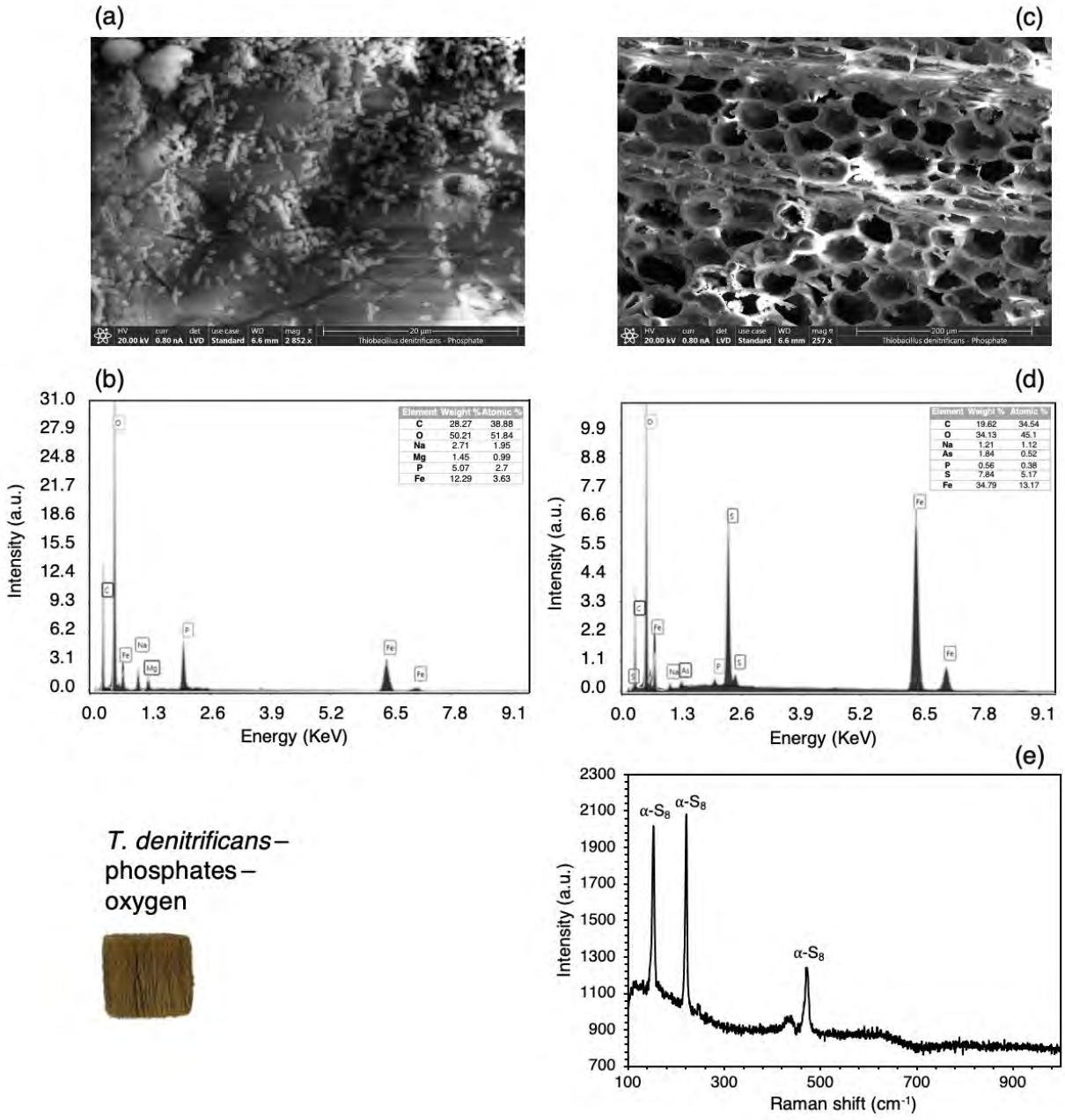

Figure S 3.7*. (a) Secondary electron micrograph of the wood sample treated with T. denitrificans in 113-PO (Exp. C) where bacterial colonies are seen. (b) EDS spectrum of the aggregates observed around the bacteria. (c) SEM image of an inner cut of the wood and (d) corresponding EDS spectrum. (e) Raman spectrum obtained from the surface of the wood sample. Characteristic peaks of elemental sulfur (α-S_8) are tagged.*

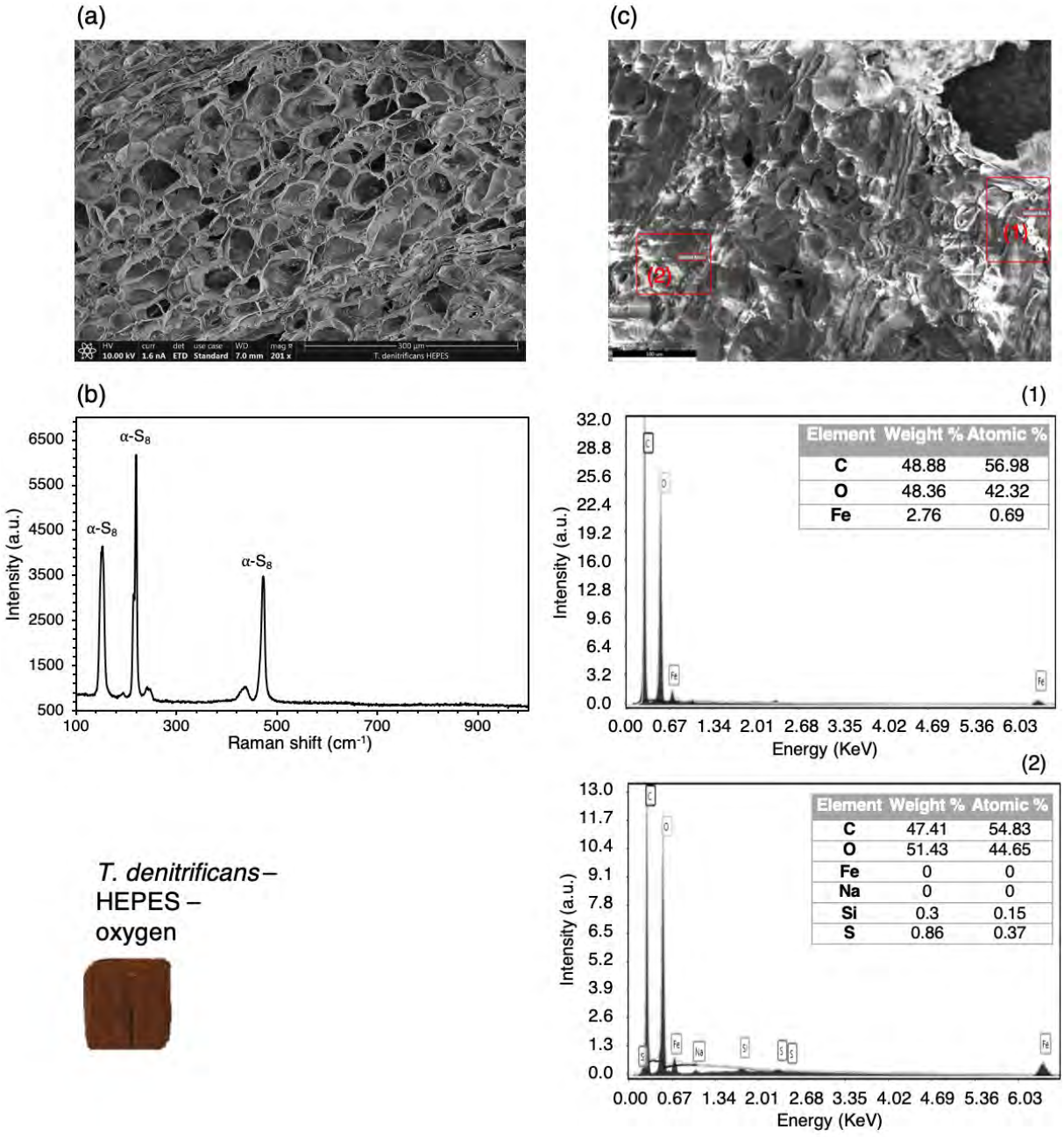

Figure S 3.8. *(a) Secondary electron micrograph of a cross section cut of the wood sample treated with T. denitrificans in 113-HO (Exp. H). (b) Raman spectrum obtained from the surface of the wood sample. Characteristic peaks of elemental sulfur (α-S_8) are tagged. (c) SEM image of the same cross section with corresponding EDS spectra (1 and 2).*

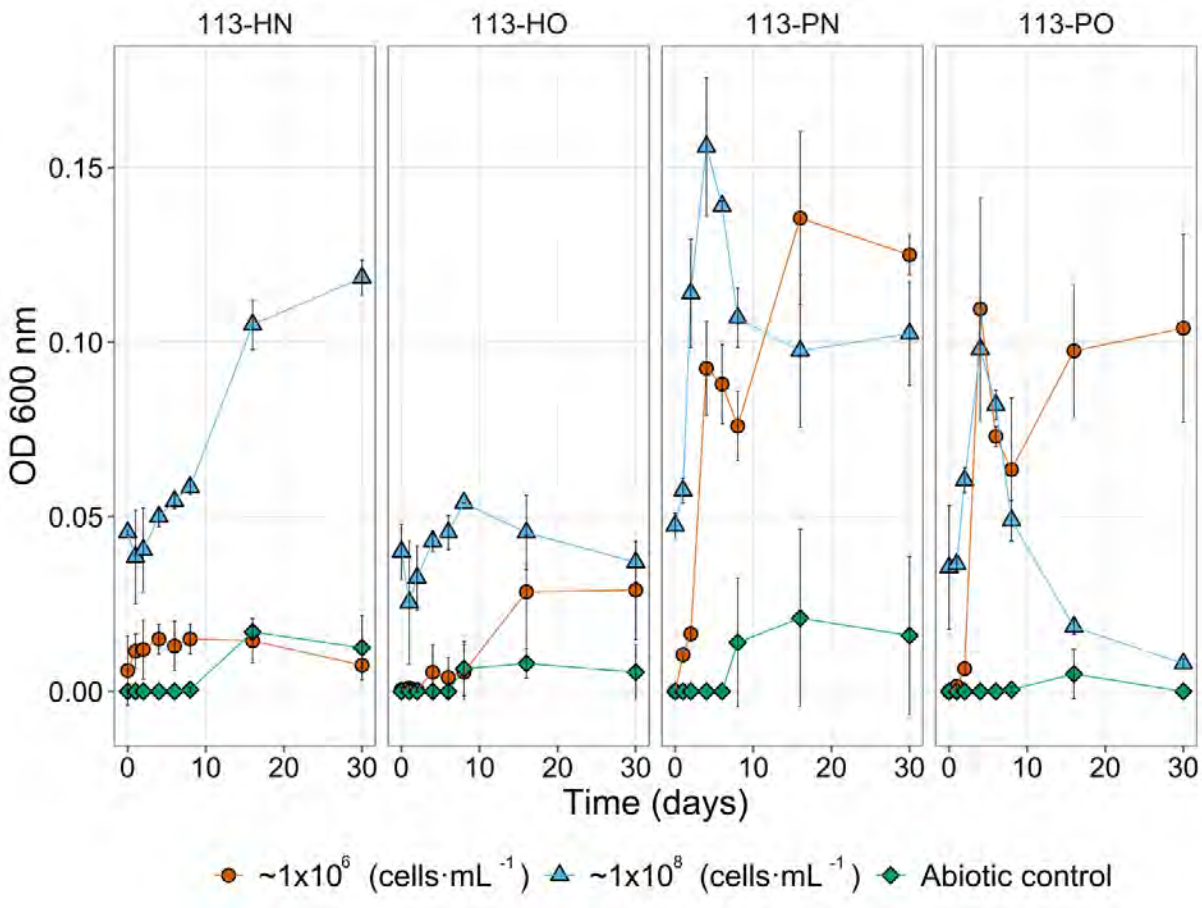

Figure S 3.9. *Growth of the bacterium T. denitrificans in presence of artificially contaminated wood in the different experimental media (113-HN, 113-HO, 113-PN, and113-PO) followed by the increase of OD at 600 nm over time.*

Author contribution

Published data (Section 3.2.1): MA-B analysed the data and wrote the manuscript. MM assisted in data analysis. CJ conducted the experiments. PJ supervised the experimental desing and data collection. CR assisted the Raman analysis. EJS assisted the Sy-XRF analysis. EJ supervised the experimental design, analysed the data, and wrote the manuscript. All co-authors corrected the manuscript.

Unpublished data (Sections 3.1 and 3.2.2): MA-B designed and performed all experiments analysed the data and wrote this chapter. MM assisted with Raman and SEM-EDS analyses. EJ supervised the experimental design, analysed the data, wrote and corrected this chapter.

References

[1] D. Rickard and G. W. Luther, "Chemistry of iron sulfides," *Chem. Rev.*, vol. 107, no. 2, pp. 514–562, 2007, doi: 10.1021/cr0503658.

[2] D. Pokorna and J. Zabranska, "Sulfur-oxidizing bacteria in environmental technology," *Biotechnol. Adv.*, vol. 33, no. 6, pp. 1246–1259, 2015, doi: 10.1016/j.biotechadv.2015.02.007.

[3] S. Vaclavkova *et al.*, "The Importance of Microbial Iron Sulfide Oxidation for Nitrate Depletion in Anoxic Danish Sediments," *Aquat. Geochemistry*, vol. 20, no. 4, pp. 419–435, Jul. 2014, doi: 10.1007/s10498-014-9227-x.

[4] Y. C. Zhang, C. P. Slomp, H. P. Broers, H. F. Passier, and P. Van Cappellen, "Denitrification coupled to pyrite oxidation and changes in groundwater quality in a shallow sandy aquifer," *Geochim. Cosmochim. Acta*, vol. 73, no. 22, pp. 6716–6726, 2009, doi: 10.1016/j.gca.2009.08.026.

[5] Y. T. Chen *et al.*, "Biogeochemical processes governing natural pyrite oxidation and release of acid metalliferous drainage," *Environ. Sci. Technol.*, vol. 48, no. 10, pp. 5537–5545, 2014, doi: 10.1021/es500154z.

[6] A. Mazumdar, T. Goldberg, and H. Strauss, "Abiotic oxidation of pyrite by Fe(III) in acidic media and its implications for sulfur isotope measurements of lattice-bound sulfate in sediments," *Chem. Geol.*, vol. 253, no. 1–2, pp. 30–37, 2008, doi: 10.1016/j.chemgeo.2008.03.014.

[7] M. Sandström, F. Jalilehvand, I. Persson, U. Gelius, P. Frank, and I. Hall-Roth, "Deterioration of the seventeenth-century warship Vasa by internal formation of sulphuric acid," *Nature*, vol. 415, no. 6874, pp. 893–897, Feb. 2002, doi: 10.1038/415893a.

[8] S. C. M. Haaijer, G. Crienen, M. S. M. Jetten, and H. J. M. Op den Camp, "Anoxic iron cycling bacteria from an iron sulfide-and nitrate-rich freshwater environment," *Front. Microbiol.*, vol. 3, no. FEB, pp. 1–8, 2012, doi: 10.3389/fmicb.2012.00026.

[9] S. Jessen, D. Postma, L. Thorling, S. Müller, J. Leskelä, and P. Engesgaard, "Decadal variations in groundwater quality: A legacy from nitrate leaching and denitrification by pyrite in a sandy aquifer," *Water Resour. Res.*, vol. 53, no. 1, pp. 184–198, Jan. 2017, doi: 10.1002/2016WR018995.

[10] J. Bosch, K.-Y. Lee, G. Jordan, K.-W. Kim, and R. U. Meckenstock, "Anaerobic, Nitrate-Dependent Oxidation of Pyrite Nanoparticles by Thiobacillus denitrificans," *Environ. Sci. Technol.*, vol. 46, no. 4, pp. 2095–2101, Feb. 2012, doi: 10.1021/es2022329.

[11] R. Yan *et al.*, "Effect of Reduced Sulfur Species on Chemolithoautotrophic Pyrite Oxidation with Nitrate," *Geomicrobiol. J.*, vol. 36, no. 1, pp. 19–29, Jan. 2019, doi: 10.1080/01490451.2018.1489915.

[12] T. Rohwerder, T. Gehrke, K. Kinzler, and W. Sand, "Bioleaching review part A:," *Appl. Microbiol. Biotechnol.*, vol. 63, no. 3, pp. 239–248, Dec. 2003, doi: 10.1007/s00253-003-1448-7.

[13] J. Bosch and R. U. Meckenstock, "Rates and potential mechanism of anaerobic nitrate-dependent microbial pyrite oxidation," *Biochem. Soc. Trans.*, vol. 40, no. 6, pp. 1280–1283, Dec. 2012, doi: 10.1042/BST20120102.

[14] C. Torrentó, J. Cama, J. Urmeneta, N. Otero, and A. Soler, "Denitrification of groundwater with pyrite and Thiobacillus denitrificans," *Chem. Geol.*, vol. 278, no. 1–2, pp. 80–91, 2010, doi: 10.1016/j.chemgeo.2010.09.003.

[15] R. Sierra-Alvarez, R. Beristain-Cardoso, M. Salazar, J. Gómez, E. Razo-Flores, and J. A. Field, "Chemolithotrophic denitrification with elemental sulfur for groundwater treatment," *Water Res.*, vol. 41, no. 6, pp. 1253–1262, 2007, doi: 10.1016/j.watres.2006.12.039.

[16] K. Tran, N. Bertout, F. Dalard, and J.-P. Magnin, "Trials on chemical and microbiological processes for the oxidation of sulphur compounds in archaeological wood," in *Proceedings of the 9th ICOM Group on Wet Organic Archaeological Materials Conference: Copenhagen, 2004*, 2004, pp. 227–242.

[17] H. R. Beller *et al.*, "The genome sequence of the obligately chemolithoautotrophic, facultatively anaerobic bacterium Thiobacillus denitrificans," *J. Bacteriol.*, vol. 188, no. 4, pp. 1473–1488, 2006, doi: 10.1128/JB.188.4.1473-1488.2006.

[18] D. P. Kelly and A. P. Wood, "Reclassification of some species of Thiobacillus Acidithiobacillus gen . nov ., Halothiobacillus," *Int. J. Syst. Evol. Microbiol.*, vol. 50, no. May, pp. 511–516, 2000.

[19] L. L. Stookey, "Ferrozine-A New Spectrophotometric Reagent for Iron," vol. 42, no. 7, pp. 779–781, 1970, doi: 10.1021/ac60289a016.

[20] C. Rémazeilles, K. Tran, E. Guilminot, E. Conforto, and P. Refait, "Study of Fe(II) sulphides in waterlogged archaeological wood," *Stud. Conserv.*, vol. 58, no. 4, pp. 297–307, 2013, doi: 10.1179/2047058412Y.0000000071.

[21] C. Rémazeilles *et al.*, "Post-treatment Study of Iron/Sulfur-containing Compounds in the Wreck of Lyon Saint-Georges 4 (Second Century ACE)," *Stud. Conserv.*, vol. 65, no. 1, pp. 28–36, Jan. 2020, doi: 10.1080/00393630.2019.1610608.

[22] Z. R. Harrold *et al.*, "Aerobic and Anaerobic Thiosulfate Oxidation by a Cold-Adapted, Subglacial

Chemoautotroph," *Appl. Environ. Microbiol.*, vol. 82, no. 5, pp. 1486–1495, Mar. 2016, doi: 10.1128/AEM.03398-15.

[23] D. Y. Sorokin, A. N. Antipov, and J. G. Kuenen, "Complete denitrification in coculture of obligately chemolithoautotrophic haloalkaliphilic sulfur-oxidizing bacteria from a hypersaline soda lake," *Arch. Microbiol.*, vol. 180, no. 2, pp. 127–133, Aug. 2003, doi: 10.1007/s00203-003-0567-y.

[24] S. Vaclavkova, N. Schultz-Jensen, O. S. Jacobsen, B. Elberling, and J. Aamand, "Nitrate-Controlled Anaerobic Oxidation of Pyrite by Thiobacillus Cultures," *Geomicrobiol. J.*, vol. 32, no. 5, pp. 412–419, 2015, doi: 10.1080/01490451.2014.940633.

[25] T. Liu, Y. Hu, N. Chen, Q. He, and C. Feng, "Microbial redox activity mediated anaerobic pyrite oxidation under circumneutral conditions," 2020. doi: https://doi.org/10.1101/2020.02.17.952168.

[26] C. Torrentó, J. Urmeneta, K. J. Edwards, and J. Cama, "Characterization of Attachment and Growth of Thiobacillus denitrificans on Pyrite Surfaces," *Geomicrobiol. J.*, vol. 29, no. 4, pp. 379–388, 2012, doi: 10.1080/01490451.2011.575912.

[27] M. I. M. Soares, "Denitrification of groundwater with elemental sulfur," *Water Res.*, vol. 36, no. 5, pp. 1392–1395, 2002, doi: 10.1016/S0043-1354(01)00326-8.

[28] Y. Yang *et al.*, "Utilization of iron sulfides for wastewater treatment: a critical review," *Rev. Environ. Sci. Biotechnol.*, vol. 16, no. 2, pp. 289–308, 2017, doi: 10.1007/s11157-017-9432-3.

[29] A. Cockburn *et al.*, "Nitrite in feed: From animal health to human health," *Toxicol. Appl. Pharmacol.*, vol. 270, no. 3, pp. 209–217, 2013, doi: 10.1016/j.taap.2010.11.008.

[30] S. Hedrich, M. Schlömann, and D. Barrie Johnson, "The iron-oxidizing proteobacteria," *Microbiology*, vol. 157, no. 6, pp. 1551–1564, 2011, doi: 10.1099/mic.0.045344-0.

[31] M. Miethke and M. A. Marahiel, "Siderophore-Based Iron Acquisition and Pathogen Control," *Microbiol. Mol. Biol. Rev.*, vol. 71, no. 3, pp. 413–451, 2007, doi: 10.1128/MMBR.00012-07.

[32] K. L. Straub, M. Benz, and B. Schink, "Iron metabolism in anoxic environments at near neutral pH," *FEMS Microbiol. Ecol.*, vol. 34, no. 3, pp. 181–186, 2000, doi: 10.1016/S0168-6496(00)00088-X.

[33] C. . G. Björdal, G. Daniel, and T. Nilsson, "Depth of burial, an important factor in controlling bacterial decay of waterlogged archaeological poles," *Int. Biodeterior. Biodegradation*, vol. 45, no. 1–2, pp. 15–26, Jan. 2000, doi: 10.1016/S0964-8305(00)00035-4.

[34] C. Rémazeilles *et al.*, "Microbiologically influenced corrosion of archaeological artefacts:Characterisation of iron(II) sulfides by Raman spectroscopy," *J. Raman Spectrosc.*, vol. 41, no. 11, pp. 1425–1433, 2010, doi: 10.1002/jrs.2717.

[35] Y. Fors *et al.*, "Sulfur and iron accumulation in three marine-archaeological shipwrecks in the Baltic Sea: The Ghost, the Crown and the Sword," *Sci. Rep.*, vol. 4, no. 1, pp. 1–6, 2014, doi: 10.1038/srep04222.

[36] J. Preston, A. D. Smith, E. J. Schofield, A. V. Chadwick, M. A. Jones, and J. E. M. Watts, "The effects of Mary Rose conservation treatment on iron oxidation processes and microbial communities contributing to acid production in marine archaeological timbers," *PLoS One*, vol. 9, no. 2, 2014, doi:

10.1371/journal.pone.0084169.

[37] K. M. Wetherall *et al.*, "Sulfur and iron speciation in recently recovered timbers of the Mary Rose revealed via X-ray absorption spectroscopy," *J. Archaeol. Sci.*, vol. 35, no. 5, pp. 1317–1328, 2008, doi: 10.1016/j.jas.2007.09.007.

[38] G. Almkvist and I. Persson, "Extraction of iron compounds from wood from the Vasa," *Holzforschung*, vol. 60, no. 6, pp. 678–684, 2006, doi: 10.1515/HF.2006.114.

[39] T. Rohwerder and W. Sand, "Oxidation of inorganic sulfur compounds in acidophilic prokaryotes," *Eng. Life Sci.*, vol. 7, no. 4, pp. 301–309, 2007, doi: 10.1002/elsc.200720204.

[40] D. H. P. Ng, A. Kumar, and B. Cao, "Microorganisms meet solid minerals: interactions and biotechnological applications," *Appl. Microbiol. Biotechnol.*, vol. 100, no. 16, pp. 6935–6946, 2016, doi: 10.1007/s00253-016-7678-2.

[41] H. R. Beller *et al.*, "Genome-enabled studies of anaerobic, nitrate-dependent oxidation in the chemolithoautotrophic bacterium Thiobacillus denitrificans," *Front. Microbiol.*, vol. 4, no. AUG, pp. 1–16, 2013, doi: 10.3389/fmicb.2013.00249.

[42] S. Montalvo, C. Huiliñir, D. Gálvez, N. Roca, and L. Guerrero, "Autotrophic denitrification with sulfide as electron donor: Effect of zeolite, organic matter and temperature in batch and continuous UASB reactors," *Int. Biodeterior. Biodegradation*, vol. 108, pp. 158–165, Mar. 2016, doi: 10.1016/j.ibiod.2015.12.022.

[43] C. Ganne-Chédeville, A. S. Jääskeläinen, J. Froidevaux, M. Hughes, and P. Navi, "Natural and artificial ageing of spruce wood as observed by FTIR-ATR and UVRR spectroscopy," *Holzforschung*, vol. 66, no. 2, pp. 163–170, 2012, doi: 10.1515/HF.2011.148.

[44] B. Meyer, "Elemental sulfur," *Chem. Rev.*, vol. 76, no. 3, pp. 367–388, 1976, doi: 10.1021/cr60301a003.

[45] M. Albelda Berenguer *et al.*, "Biological oxidation of sulfur compounds in artificially degraded wood," *Int. Biodeterior. Biodegradation*, vol. 141, no. December 2017, pp. 62–70, Jul. 2019, doi: 10.1016/j.ibiod.2018.06.009.

[46] J. A. Bourdoiseau, M. Jeannin, R. Sabot, C. Rémazeilles, and P. Refait, "Characterisation of mackinawite by Raman spectroscopy: Effects of crystallisation, drying and oxidation," *Corros. Sci.*, vol. 50, no. 11, pp. 3247–3255, 2008, doi: 10.1016/j.corsci.2008.08.041.

[47] Y. Fors and M. Sandström, "Sulfur and iron in shipwrecks cause conservation concerns," *Chem. Soc. Rev.*, vol. 35, no. 5, pp. 399–415, 2006, doi: 10.1039/b507010b.

[48] J. Preston, J. E. M. Watts, and M. Jones, "Novel bacterial community associated with 500-year-old unpreserved archaeological wood from King Henry VIII's tudor warship the Mary Rose," *Appl. Environ. Microbiol.*, vol. 78, no. 24, pp. 8822–8828, 2012, doi: 10.1128/AEM.02387-12.

[49] J. A. Bourdoiseau, M. Jeannin, C. Rémazeilles, R. Sabot, and P. Refait, "The transformation of mackinawite into greigite studied by Raman spectroscopy," *J. Raman Spectrosc.*, vol. 42, no. 3, pp. 496–504, 2011, doi: 10.1002/jrs.2729.

[50] D. P. Kelly and A. P. Wood, "Confirmation of Thiobacillus denitrificans as a species of the genus Thiobacillus, in the beta-subclass of the Proteobacteria, with strain NCIMB 9548 as the type strain.," *Int. J. Syst. Evol. Microbiol.*, vol. 50, no. 2, pp. 547–550, Mar. 2000, doi: 10.1099/00207713-50-2-547.

[51] P. Bosch-Roig, J. Regidor-Ros, P. Soriano, and R. Montes-Estelles, "Biocleaning of animal glue on wall paintings by Pseudomonas stutzeri," *Chim. Oggi/Chemistry Today*, vol. 31, pp. 50–53, Jan. 2013.

[52] P. B. Roig, J. L. Regidor Ros, and R. M. Estellés, "Biocleaning of nitrate alterations on wall paintings by Pseudomonas stutzeri," *Int. Biodeterior. Biodegrad.*, vol. 84, pp. 266–274, Oct. 2013, doi: 10.1016/j.ibiod.2012.09.009.

[53] S. S. Cameotra and T. C. Dakal, "Carbonatogenesis: microbial contribution to the conservation of monuments and artwork of stone," *Conserv. Sci. Cult. Herit.*, vol. 12, no. 1, pp. 79–108, 2012, doi: 10.6092/ISSN.1973-9494/3383.

[54] D. Rickard, "The solubility of FeS," *Geochim. Cosmochim. Acta*, vol. 70, no. 23 SPEC. ISS., pp. 5779–5789, 2006, doi: 10.1016/j.gca.2006.02.029.

[55] S. C. M. Haaijer, L. P. M. Lamers, A. J. P. Smolders, M. S. M. Jetten, and H. J. M. Op de Camp, "Iron sulfide and pyrite as potential electron donors for microbial nitrate reduction in freshwater wetlands," *Geomicrobiol. J.*, vol. 24, no. 5, pp. 391–401, 2007, doi: 10.1080/01490450701436489.

[56] K. G. Taylor, K. A. Hudson-Edwards, A. J. Bennett, and V. Vishnyakov, "Early diagenetic vivianite [Fe3(PO4)2 · 8H2O] in a contaminated freshwater sediment and insights into zinc uptake: A μ-EXAFS, μ-XANES and Raman study," *Appl. Geochemistry*, vol. 23, no. 6, pp. 1623–1633, 2008, doi: 10.1016/j.apgeochem.2008.01.009.

[57] M. Rothe, A. Kleeberg, and M. Hupfer, "The occurrence, identification and environmental relevance of vivianite in waterlogged soils and aquatic sediments," *Earth-Science Rev.*, vol. 158, pp. 51–64, Jul. 2016, doi: 10.1016/j.earscirev.2016.04.008.

[58] L. Comensoli, J. Maillard, M. Albini, F. Sandoz, P. Junier, and E. Joseph, "Use of Bacteria To Stabilize Archaeological Iron," *Appl. Environ. Microbiol.*, vol. 83, no. 9, pp. e03478-16, May 2017, doi: 10.1128/AEM.03478-16.

[59] W. M. Kooli *et al.*, "Bacterial iron reduction and biogenic mineral formation for the stabilisation of corroded iron objects," *Sci. Rep.*, vol. 8, no. 1, p. 764, Dec. 2018, doi: 10.1038/s41598-017-19020-3.

[60] J. A. Emery and H. A. Schroeder, "Iron-catalyzed oxidation of wood carbohydrates," *Wood Sci. Technol.*, vol. 8, no. 2, pp. 123–137, 1974, doi: 10.1007/BF00351367.

[61] G. Almkvist and I. Persson, "Degradation of polyethylene glycol and hemicellulose in the Vasa," *Holzforschung*, vol. 62, no. 1, pp. 64–70, 2008, doi: 10.1515/HF.2008.009.

[62] T. A. Fowler, P. R. Holmes, and F. K. Crundwell, "On the kinetics and mechanism of the dissolution of pyrite in the presence of Thiobacillus ferrooxidans," *Hydrometallurgy*, vol. 59, no. 2–3, pp. 257–270, 2001, doi: 10.1016/S0304-386X(00)00172-9.

[63] T. Huang and D. Li, "Presentation on mechanisms and applications of chalcopyrite and pyrite bioleaching

in biohydrometallurgy - A presentation," *Biotechnol. Reports*, vol. 4, no. 1, pp. 107–119, 2014, doi: 10.1016/j.btre.2014.09.003.

[64] A. Mahmoud, P. Cézac, A. F. A. Hoadley, F. Contamine, and P. D'Hugues, "A review of sulfide minerals microbially assisted leaching in stirred tank reactors," *Int. Biodeterior. Biodegrad.*, vol. 119, pp. 118–146, Apr. 2017, doi: 10.1016/j.ibiod.2016.09.015.

[65] K. K. Pandey and A. J. Pitman, "FTIR studies of the changes in wood chemistry following decay by brown-rot and white-rot fungi," *Int. Biodeterior. Biodegrad.*, vol. 52, no. 3, pp. 151–160, 2003, doi: 10.1016/S0964-8305(03)00052-0.

[66] M. Traoré, J. Kaal, and A. Martínez Cortizas, "Application of FTIR spectroscopy to the characterization of archeological wood," *Spectrochim. Acta - Part A Mol. Biomol. Spectrosc.*, vol. 153, pp. 63–70, 2016, doi: 10.1016/j.saa.2015.07.108.

[67] G. Müller, C. Schöpper, H. Vos, A. Kharazipour, and A. Polle, "FTIR-ATR spectroscopic analyses of changes in wood properties during particleand fibreboard production of hardand softwood trees," *BioResources*, vol. 4, no. 1, pp. 49–71, 2009, doi: 10.15376/BIORES.4.1.49-71.

[68] L. Zhang and R. K. Brow, "A Raman study of iron-phosphate crystalline compounds and glasses," *J. Am. Ceram. Soc.*, vol. 94, no. 9, pp. 3123–3130, 2011, doi: 10.1111/j.1551-2916.2011.04486.x.

[69] U. P. Agarwal and S. A. Ralph, "FT-Raman Spectroscopy of Wood: Identifying Contributions of Lignin and Carbohydrate Polymers in the Spectrum of Black Spruce (Picea Mariana)," *Appl. Spectrosc.*, vol. 51, no. 11, pp. 1648–1655, Nov. 1997, doi: 10.1366/0003702971939316.

[70] F. Picardal, "Abiotic and microbial interactions during anaerobic transformations of Fe(II) and NOx-," *Front. Microbiol.*, vol. 3, no. MAR, pp. 1–7, 2012, doi: 10.3389/fmicb.2012.00112.

[71] E. Percak-Dennett *et al.*, "Microbial acceleration of aerobic pyrite oxidation at circumneutral pH," *Geobiology*, vol. 15, no. 5, pp. 690–703, 2017, doi: 10.1111/gbi.12241.

Chapter 4

EVALUATION OF A BIOLOGICAL EXTRACTION METHOD

Pole in Lake Biel. © Archaeological Service Caton Bern

Section 4.2 of this chapter is partially based on the following articles:

- M. Monachon, M. Albelda-Berenguer, T. Lombardo, E. Cornet, F. Moll-Dau, J. Schramm, K. Schmidt-Ott and E. Joseph, "Evaluation of bio-based extraction methods by spectroscopic methods," *Minerals*, vol. 10, no. 2, pp. 1–17, 2020, doi: 10.3390/min10020203.
- M. Monachon, M. Albelda-Berenguer, T. Lombardo, E. Cornet, F. Moll-Dau, J. Schramm, K. Schmidt-Ott and E. Joseph, "Evaluation of an alternative bio-treatment for the preservation of waterlogged wood," *Eur. Phys. J. - Plus*, 2020. Submitted.

Results from sections 4.1 and 4.3 are not published.

Summary

In this chapter an application protocol for the developed extraction method was defined. The first step was to stablish an application protocol that included both iron extraction and sulfur oxidation. Two sequential steps (labelled 1B-2S and 1S-2B) and one-step (labelled 1SB) protocols were studied in our model wood matrix (i.e., artificially contaminated balsa wood). The sequential application protocol that involved first the use of the siderophore DFOM, i.e., iron complexation, followed by the oxidation of sulfur by *Thiobacillus denitrificans* was selected as the best performance. We selected this application protocol as the most successful since: 1) it respected the dark appearance of archaeological wood, 2) it avoided precipitation of iron phosphates, and 3) the bacteria were more efficient in the oxidation of sulfur to sulfates translating to the highest sulfur extraction rates.

The second section of this chapter focused on the evaluation of the selected extraction method with the application protocol defined previously. Fresh balsa, fresh and archaeological oak, and fresh and archaeological pinewood were selected here to study the performance of the proposed extraction method in different types and species of wood. Our bio-based treatment was compared to a two-step chemical treatment currently applied for the extraction of harmful salts from waterlogged wood. FTIR and Raman spectroscopies were used along with ICP-OES and IC to evaluate the overall performance of the different treatments under study. No wood degradation was observed after any of the treatments. However, the tested chemical treatment tended to bleach the samples. The total sulfur extraction rates were higher for the biological treatment, while the chemical treatment presented higher extraction rates of iron. Overall, the biological treatment had iron and sulfur extraction rates over 50%. Moreover, reduced sulfur species were still identified by Raman analyses in the cubes chemically treated but no in the biologically treated wood.

In parallel, we studied the autochthonous microbial community of waterlogged wood samples to have an insight of possible secondary reactions and drawbacks when applying the bio-based extraction method. The existing microbial community of the wood could decrease the overall efficiency of our treatment if interactions occur. Solutions may need to be defined in case of opposite interactions.

4.1 Definition of an application protocol

Abstract

The definition of an application protocol is essential for the development of a treatment. In this section, three different application protocols (labelled 1B-2S, 1S-2B, and 1SB) were developed combining iron complexation and sulfur oxidation. 1B-2S and 1S-2B included sequential steps, applying first the bacteria or the siderophore and vice versa. 1SB was a one-step protocol where DFOM and *T. denitrificans* were applied together. The different protocols were tested in artificially contaminated balsa wood. Before and after treatment, the visual aspect of the cubes was assessed, and the efficiency of extraction calculated by measuring total iron and sulfur concentrations in the cubes. IC allowed to follow the oxidation of sulfur. All protocols presented rates of extraction of iron higher than 80%. Overall, sulfur extraction was less efficient. Highest sulfur extraction rate was just under 50% when using 1S-2B. The bacteria acted best when cubes were pre-treated with DFOM (1S-2B protocol). This application protocol gave the most promising results and was selected for further experiments.

Introduction

Conservation practices must follow some basic principles: materials should be safe and stable, and the treatment should be durable and if possible reversible, or at least retreatable [1]. Therefore, new conservation methods should be designed to follow these ethical criteria. Moreover, simple protocols involving not many application steps, mild conditions, and easily available reagents, are preferred against more complicated procedures.

As example, current extraction methods for waterlogged archaeological wood (WAW) that involve strong iron chelators are easy to apply. A concentrated solution in water is prepared from an available commercial product [2]. Moreover, the temperature is usually not adjusted [2], [3]. Thus, the objects are placed in the solution at RT for an established amount of time. However, these methods may involve drawbacks as toxicity of the chemicals or highly alkaline pH [2], and therefore the protocols have to consider safety regulations. Some methods also involve other solvents such as iso-propanol [4], which require extra safety considerations for the user and the environment.

On the contrary, green chelators such as deferoxamine are safe to use and there is no associated toxicity [5]. Moreover, DFOM is commercially available in pharmacies under the name of Desferal®. It has been previously suggested for conservation of wood and textiles, and it was

successfully applied in gel to remove iron stains [6], [7]. In this study, we combine the use of DFOM with the action of sulfur-oxidising bacteria.

Biological treatments usually require maintaining conditions such as temperature and pH over the time of the treatment, allowing microbial activity [8]. *Thiobacillus denitrificans* has an optimal growth at 30 ºC and pH between 6.8 - 7.4. These are mild conditions that could be maintained with current installations used by conservators [2]. Moreover, *T. denitrificans* is a facultative anaerobe. During this thesis, anoxic and oxic conditions were tested to assess the best conditions for bacterial growth and effective treatment. We have ascertained that reducing the exchange of oxygen is suitable to the bacterial growth and the stability of the iron sulfides. Maintaining strict anoxic conditions could be complicated for end-users.

In the previous chapters, iron complexation and sulfur oxidation has been tested separately. The goal of this study was to test different application protocols combining the biological processes previously studied in this thesis. Three different application protocols were developed:

1) Oxidation of sulfur by *T. denitrificans* followed by chelation of iron by DFOM
2) Extraction of iron ions by DFOM followed by the oxidation of the remaining sulfur
3) One-step application were iron complexation and sulfur oxidation act at the same time

Materials and Methods

Model wood samples

Balsa wood was employed as a simplified model simulating waterlogged wood. Balsa (*Ochroma pyramidale*) wood cubes with the following dimensions: 1×1×1 cm^3were prepared. The samples were impregnated with iron and sulfur solutions by immersing them in 1 L iron(II) chloride tetrahydrate (0.5 M $FeCl_2 \cdot 4\ H_2O$) solution under vacuum (-600 mbars) for 4 h. The samples were dried overnight at 45 °C. Afterwards, the samples were immersed in a solution of hydrated sodium sulfide (0.5 M $Na_2S \cdot nH_2O$) under vacuum (-600 mbars) for also 4 h. Samples were kept immersed in N_2-flushed water. Before any experimental procedure, cubes samples were washed by ultrasonic bath until no more impregnation solution was released.

Bacteria and iron chelators

Thiobacillus denitrificans (DSMZ 12475) was obtained from the German Collection of Microorganisms and Cell Cultures (DMSZ, Germany). The strain was cultivated using standard anaerobic techniques at 30 °C in the dark. Deferoxamine mesylate salt (DFOM) was purchased as Desferal® (Novartis Pharma Schweiz AG, Switzerland).

Application protocol

The combination of iron complexation and sulfur oxidation can be done in sequential steps or at once. Three different possibilities exist: 1) Application of the sulfur-oxidising bacteria followed by chelators; 2) The extraction of iron ions by siderophores and then the oxidation of the remaining sulfur species; and 3) In one application step, add both siderophores and sulfur-oxidising bacteria together.

In table 4.1, the conditions of the three extraction protocols are defined. DFOM was applied in water to a final concentration of 20 mM. *T. denitrificans* was always inoculated to modified 113 medium from a 5 days culture to a final concentration of $1x10^6$ cells/mL. Cells were recovered by centrifugation and washed twice in physiological solution before inoculation.

Table 4.1*. Definition of the three different extraction methods tested to extract sulfur and iron from contaminated waterlogged wood.*

Extraction methods	Step 1	Between steps	Step 2
1) Bacteria → Siderophore (1B-2S)	Incubate for 23 days with *T. denitrificans* in 113 medium at 30 ªC in agitation	Rinse with H_2O_d twice in sonication bath	Incubate for 3 days in a solution of 20 mM DFOM (in water) in agitation
2) Siderophore → Bacteria (1S-2B)	Incubate for 3 days in a solution of 20 mM DFOM (in water) in agitation	Rinse with H_2O_d twice in sonication bath	Incubate for 23 days with *T. denitrificans* in 113 medium at 30 ªC
3) Siderophore + Bacteria (1SB)	Incubate for 23 days with *T. denitrificans* and 20 mM DFOM, in 113 medium at 30 ªC in agitation	---	---

Several controls were included. Wood cubes were incubated in 113 media without bacteria as control for the medium solution (Control M). Some cubes were only treated with DFOM and some only with *T. denitrificans*, as control for each treatment (control S and control B, respectively). Finally, two wood cubes were kept in water without any treatment.

All solutions used were N_2-flushed for 10 min previous addition to the wood cubes. Bottles were filled to the top, close tightly and wrapped with Parafilm® to prevent oxygen exchange.

Two bottles with two wood cubes each were carried out for each extraction method and one bottle with two wood samples for each control.

Analytical methods

Visual appearance and pH

Wood samples were monitored during the whole duration of the experiment. Changes in the appearance of the cubes were noted down and documented. Moreover, a 691 pH Meter Metrohm (Metrohm AG, Switzerland) was used to control the pH of the solution over time with an ionic electrode (unitrode 6.0259.100) calibrated with buffer solutions (pH 4, 7 and 9). The pH of the cubes was measured with a surface electrode (flat membrane electrode 6.0256.100), also correctly calibrated, at the beginning and end of the experiment.

Ion chromatography (IC)

For the determination of the concentration of sulfates (SO_4^{2-}), nitrates (NO_3^-), nitrites (NO_2^-), and phosphates (PO_4^{3-}), 2 mL of sample were filtered at 0.22 µm (BGB Analytik, Switzerland) to remove residual particulate matter. Filtered samples were correctly diluted and analysed by ion chromatography (Dionex ICS-1600). The instrument was equipped with a conductivity detector, a Dionex Ion Pac™ AS14A (4 x 250 mm) anion exchange column, and a Dionex Ion PacTM RFIC™ (4 x 50 mm) guard column. A solution of 8 mM Na_2CO_3 and 1 mM $NaHCO_3$ was used at a flow rate of 1.3 $mL \cdot min^{-1}$ as mobile phase. The detection limit was 0.05 $mg \cdot L^{-1}$. Data was analysed with the Chromeleon™ software (Thermo Fisher Scientific, United States).

Inductively Coupled Plasma - Optical Emission Spectrometry (ICP-OES)

Total iron and sulfur concentrations were determined in the extraction solutions and in the wood cubes by Inductively Coupled Plasma-Optical Emission Spectrometry (ICP-OES). Samples from the solutions were filtered through a 0.22 µm PVDF membrane (BGB Analytik, Switzerland) before analysis. Wood cubes were dissolved in a concentrated solution of ultrapure nitric acid 65% (v/v) (Suprapur, Merck KGaA) by reflux for 24 hours. All types of samples were first diluted into the detection range (0-2 ppm), and then loaded into the ICP using a peristaltic pump, and a cyclonic spray chamber connected to a nebulizer (Perkin-Elmer, United States). Then, concentrations of iron and sulfur were determined using an Optima 2100 DV (Perkin-Elmer, United States) optical emission spectrometer. The extraction rates were calculated based on the concentration of species remaining in the samples before and after extraction.

Results and Discussion

Visual characterisation and pH

The selection of an extraction method will define the conditions for future treatments and praxis. Dealing with WAW usually implies several conservation concerns that are induced by iron and sulfur species, respectively. Different biological metabolisms (i.e., iron complexation using siderophores and sulfur oxidation) have been selected here to tackle the different issues of long-term conservation of waterlogged wooden objects. Distinct performances were observed with the different extraction protocols tested.

***Figure 4.1**. Visual appearance of the wood cubes. Balsa wood was artificially impregnated with iron sulfides, and then treated with three different application protocols (1B-2S, 1S-2B, and 1SB).*

The first visual observations showed that the untreated samples (i.e., wood cubes immersed in water) were getting oxidised over time (Figure 4.1). After 23 days, the characteristic black colour attributed to iron sulfides changed in some areas to a bright orange colour that can be assigned to the presence of iron oxides [3]. However, no further characterisation of the wood samples was made at this stage, and the specific species of iron and sulfur formed remained unknown. Controls for the 113 medium solution were not oxidised, instead a brownish precipitate started to accumulate in the surface after 3-4 days (Figure 4.1). The same happened

to the samples treated by the 1B-2S protocol after the first few days of incubation with *T. denitrificans*. Due to previous experiences, we know that these precipitates are likely iron phosphates (Chapter 3). Moreover, when we observe the IC results, we can see a clear decline of phosphates in the control M and 1B-2S solutions that is not observed in the 1S-2B and 1SB treatments (Figure 4.3). The problematic of having phosphates in 113 medium has already been discussed in Chapter 3. The consequences of this precipitation are a clearer hue in this case than for the other extraction methods (Figure 4.1). Cubes treated by 1S-2B and 1SB protocols showed a closer appearance at the end of the treatment. The final appearance was a darker hue closer to the artificially impregnated sample before treatment (Figure 4.1). The wood samples treated only with DFOM, i.e., control S, presented a reddish appearance (Figure 4.1), that was distant to untreated samples. When DFOM is bound to iron, it forms a strong red-colour complex (i.e., ferrioxamine) that could change the colour of the wood if not properly rinsed out [6]. Further analyses are needed to stablish the compounds formed.

pH is also an important parameter as a very alkaline pH and a very acidic pH are both harmful for the wood components [9], [10]. pH values measured on the surface of the wood cubes are presented in Table S 4.1. After artificial contamination with iron and sulfur species, the pH of the cubes increased. We measured pH of ~9 – 11 in surface, while before artificial contamination pH was around 5. The impregnation solution is very alkaline with the presence of Na_2S. Therefore, the wood samples present a very high pH on surface right after artificial contamination that persisted over time, even if the cubes are rinsed with deionized water. However, the pH on surface of the wood cubes changed after all treatments (Table S 4.1). In general, for all the extraction protocols the pH on the samples surface changed back to values closer to the original pH of balsa (pH ~5). This change also indicates a removal/transformation of the iron and sulfur species formed during artificial contamination of the wood cubes. The pH for all three extraction methods, and control M and control B was in the range between 4 and 5.5. Only control S presented a pH on surface that was alkaline. Indeed, the surfaces of the wood samples only treated with DFOM presented a final pH ~8.3 ±0.2. This fact links to the idea that the ferrioxamine complex was not well rinsed out of the wood giving the red appearance and maintaining the pH close to the calculated value of $pKa_1 \approx 8.4$ [11], [12].

The final pH on most of the samples surface was not related to the pH in solution over the treatment time. During the bacteria step (or bacteria and siderophore step for 1SB), the pH of the solution was initially buffered to pH ~7. However, the addition of the cubes to the medium increased slightly the pH to values around ~7.5. Over time, the pH in controls M and B, and

1B-2S extraction method increased, while the pH for 1SB remained stable and decreased slightly for 1S-2B (Table S 4.2). The cause for the increase in pH in the case of the controls and 1B-2S could be related to the precipitation of iron phosphates. 113 medium is buffered with a phosphate buffer. When the phosphates precipitate the buffer loses capacity. This effect is not observed for 1S-2B and 1SB protocols, because the iron ions have already been extracted or chelated and, consequently, there is no precipitation of phosphates (Figure 4.3). On the contrary, during the siderophore step the pH in solution was not buffered. However, all solutions finished with pH values around the $pKa_1 \approx 8.4$ of deferoxamine.

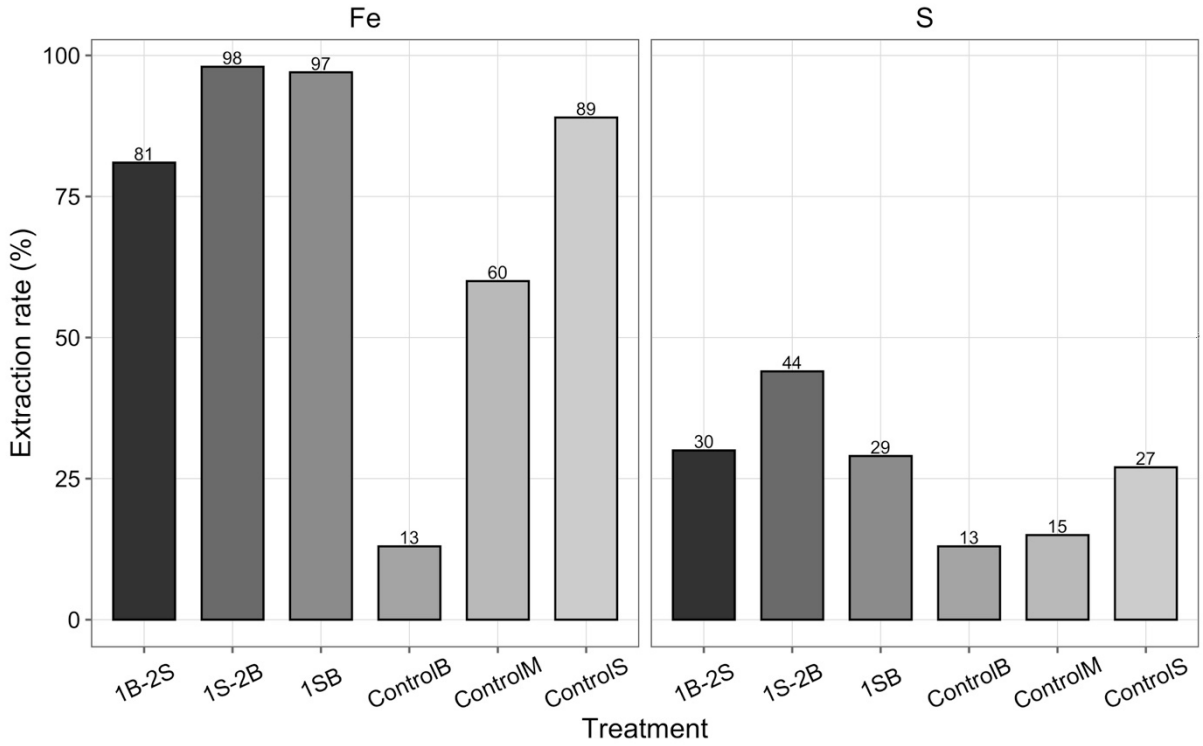

Figure 4.2. *Percentage of total iron (Fe) and sulfur (S) extraction for the different extraction methods (1B-2S, 1S-2B and 1SB) and controls (control for the bacterial step (control B), control for the 113 medium (control M), and control for the siderophore step (control S).*

Efficiency of the different extraction protocols

The total extraction of iron and sulfur from the cubes was measured by ICP-OES. We measured the initial quantities of iron and sulfur in the cubes after the impregnation protocol and compared them to the values after extraction methods. The remaining amounts of iron and sulfur in wood and the calculated extraction rates for total iron and sulfur are presented in Table

S 4.3 and S 4.4, respectively. Three artificially contaminated wood cubes were used to measure the initial concentration of total iron and sulfur. This analytical method is destructive, therefore the cubes analysed for the initial concentrations were not used after in the experiment. We assume that the impregnation with iron and sulfur species is similar in all cubes, but some variance was observed (Table S 4.3 and S 4.4). Moreover, after treatment only one cube was analysed to measure the remaining concentration of iron and sulfur. It is important to consider this when analysing the data as no statistical approach was possible. However, this preliminary test gave us some insight to the best possible application protocol.

Overall, 1S-2B method obtained the best rates of extraction of total iron and sulfur (Figure 4.2). An iron extraction rate close to 100% was achieved in balsa when applying 1S-2B. On the contrary, the sulfur extraction rate was not over 50% (Figure 4.2). The same pattern was observed for all extraction methods. Iron extraction rates were higher than for sulfur. 1SB presented extraction rates of iron of 97%, while the sulfur extraction rates was 29% (Figure 4.2). 1B-2S showed similar results to 1SB for sulfur extraction rates −30%−. However, the extraction rate of iron was the lowest −81%− (Figure 4.2).

A correlation exists between extraction of iron and sulfur. In general, when the extraction of iron is higher the extraction of sulfur is also increased [2]. We observed in our model wood that the iron extraction was much higher (from 80% to almost 100%) than sulfur (from 30% to 45%). Iron sulfides such as mackinawite (FeS), with a relation 1:1, could translate to similar extraction rates for iron and sulfur. The ratio of remaining iron/remaining sulfur in the wood was much lower than 1, for all extraction protocols. If mineral sulfur or other sulfur compounds (e.g. organosulfur) are formed, the extraction of iron does not correlate with the extraction of sulfur [2]. Current methods applied in conservation of wood that use strong iron chelators show iron extraction rates that vary from ~60 to 100% [2], [3]. Our iron extraction rates are within the range of current extraction methods. However, these studies were mostly focused on objects that may present already oxidised forms of iron sulfides, or they work with other wood species, which could influence in the extraction procedure [2], [3].

Additionally, ICP-OES measurements performed on the extraction solutions revealed some additional information regarding each individual step of the extraction methods. In one hand, insignificant amounts of iron were detected in the solutions after incubation with only *T. denitrificans* (Table S 4.5). Therefore, all iron extraction seems to be achieved by the siderophores. In the case of control M, where no siderophore was present, differences observed between iron concentrations in solutions and calculated iron extraction rates can be due to initial

differences in iron content between wood cubes. On the other hand, sulfur was detected in solution at the end of each step for 1B-2S and 1S-2B protocols (Table S 4.5). Sulfur extraction can be consequence of bacterial metabolism, iron complexation with DFOM and/or iron precipitation with phosphates. However, the highest amounts of sulfur were always detected when siderophores were in solution (Table S 4.5). Indeed, the wood cubes treated at some point with DFOM presented the highest calculated sulfur extraction rates (Figure 4.2).

DFOM was thus responsible for most of the extraction of iron and sulfur in all protocols tested. However, previous studies have shown that when only an iron chelator is applied, the sulfur bound in lignin-rich parts remains in the wood [2]. The bacteria step is then needed to oxidise and extract this reduced sulfur and other sulfur species remaining (e.g. mineral sulfur). Without the bacteria the sulfur extracted is most likely in sulfide forms, such as hydrogen sulfide (H_2S) (egg-like smell noticed). IC analysis was able to detect sulfate anions but no other species of sulfur. However, the chromatograms showed an intense peak at ~4.75 min retention time, that could match with hydrosulfide (Figure S 4.1) [13]. IC results show that when bacteria were active, sulfur species were successfully transformed to sulfates (Figure 4.3). In 1S-2B protocol, we observed the typical decrease of nitrates and increase of sulfates related to *T. denitrificans* metabolism (Figure 4.3). In 1B-2S protocol, the bacteria activity was much lower or even inexistent than in 1S-2B, probably due to an increase in pH. In these samples, phosphates precipitation was higher than in experiments in chapter 3. Maybe more free iron was in solution, increasing the precipitation rate. *T. denitrificans* has an optimal pH of growth close to neutrality. The increase in pH (Table S 4.2), could negatively affect its development and consequently slower sulfur metabolism observed.

After incubation, only 0.24 ±0.03 mM of sulfates were detected in 1SB. This value is in the range with the value detected in the control M (abiotic oxidation). However, in the control, the nitrates value did not change while in 1SB a small consumption of nitrates was detected over time. The hypothesis is that the extraction of iron produces high quantities of hydrogen sulfide (Figure S 4.1), which is toxic for bacteria [14]. This would explain the very low or inexistent growth of bacteria in the 1SB extraction method.

The relation between nitrates consumed and sulfates produced in the solution of 1S-2B protocol was in the range with the following reactions [15], [16]:

$$5S_{(0)} + 6NO_3^- + 2H_2O \rightarrow 5SO_4^{2-} + 3N_2 + 4H^+ \quad (1)$$

$$17S_{(0)} + 24NO_3^- + 8H_2O \rightarrow 6NO_2^- + 9N_2 + 17SO_4^{2-} + 16H^+ \quad (2)$$

The calculated $\Delta NO_3^-/\Delta SO_4^{2-}$ ratio was 1.37 ±0.45, while the theoretical ratios are 1.2 and 1.4 for equations 1 and 2, respectively. As we observed a small production of nitrites, we can assume that both reactions are could be occurring. These results point that in the first step of 1S-2B protocol, DFOM is able to solubilize iron sulfides, extracting iron and sulfur, while the second step is needed for the bacteria to solubilize other possibly remaining sulfur compounds. However, without other complementary analyses, such as Raman spectroscopy, we cannot assume which sulfur species were left at the end of the treatment.

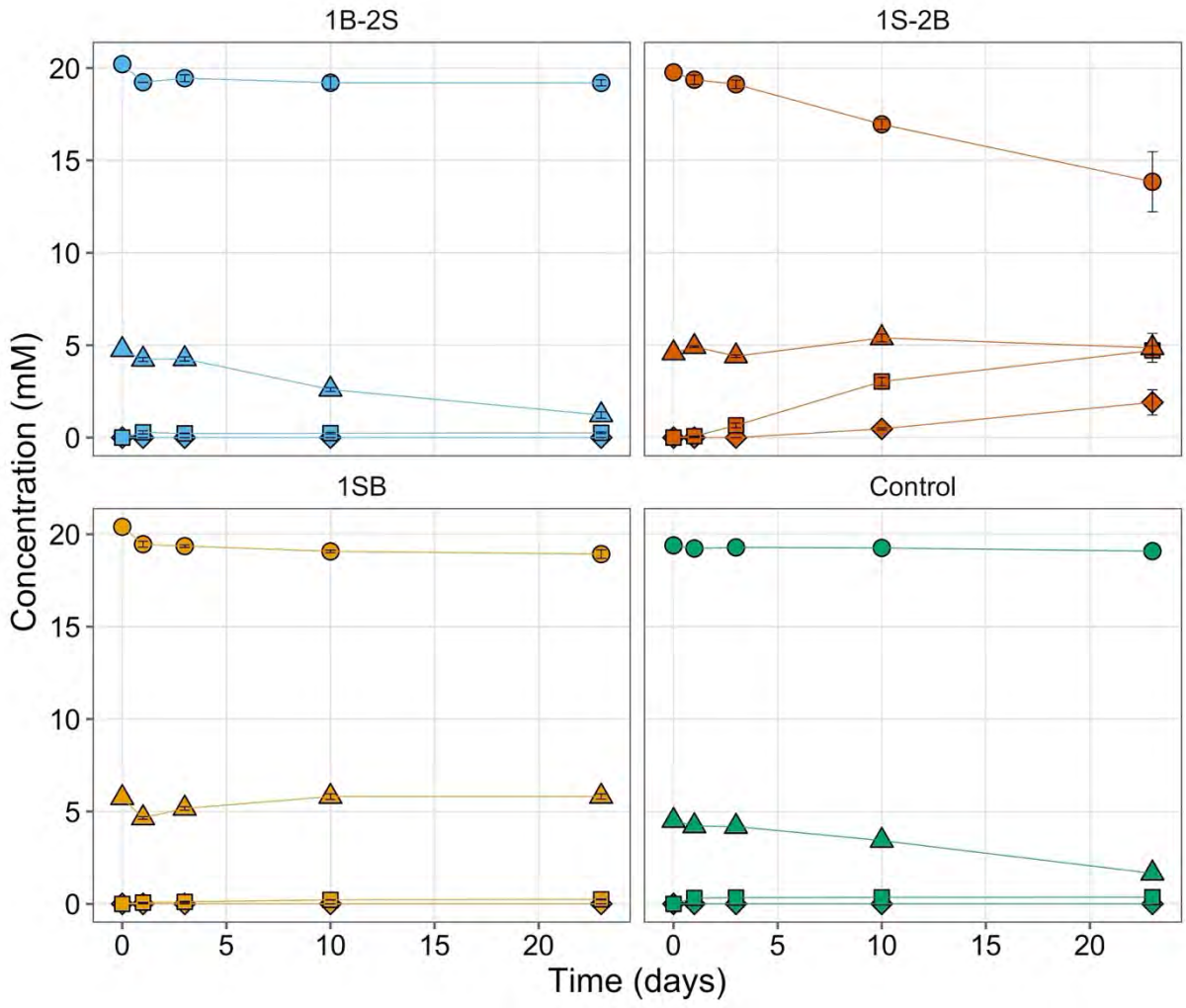

Figure 4.3. *Nitrates (●), nitrites (♦), sulfates (■), and phosphates (▲) concentrations (mM) over time. Anions concentrations were measured in solutions containing balsa wood cubes, for the three different extraction protocols: 1B-2S, 1S-2B and 1SB, as well as a control solution (medium 113). Error bars indicate standard deviation of two replicates.*

Conclusion

This preliminary study allowed us to select an adequate extraction protocol for future assays of the biological treatment. Of all three extraction protocols tested, 1S-2B presented some of the highest extraction rates for both iron and sulfur. Moreover, this application protocol was the only one that successfully converted sulfur into sulfates. 1SB also extracted sulfur but only a small amount of sulfates were detected in IC. We assume that the sulfur species were mostly in hydrogen sulfide form, which can still react with the wood to form organosulfur species leading to possible future conservation issues.

In this experiment we encounter some issues with bacterial growth. Bacteria grew better in 1S-2B method. We hypothesized that the bacteria were not able to properly grow in some conditions with high levels of hydrogen sulfide and relative higher pH (1SB and 1B-S treatment, respectively). 1S-2B is a “safer” extraction protocol. The DFOM pre-treatment allows to eliminate high quantities of iron and sulfur. In the second step, the bacteria can metabolise remaining sulfur species (organosulfur, mineral sulfur, some iron sulfides still present) to sulfates.

Further tests are needed to better develop an application protocol. Higher number of cubes have to be treated to add statistical value to the results. This initial experiment sets the basis for future studies. Up to this point, we chose the 1S-2B extraction protocol as the best to be used in further experiments.

Supplementary material 4.1

***Table S 4.1**. pH values on the surface of the wood cubes during the application of the different extraction methods under study.*

Extraction method	pH of fresh balsa wood	pH T0[a]	pH TF[b]
1B-2S	5.1 ±0.1	9.8 ±0.6	4.5 ±0.1
1S-2B		9.7 ±0.5	4.9 ±0.1
1SB		9.8 ±0.5	5.5 ±0.2
Control M		10.1 ±0.5	4.4 ±0.1
Control B		10.0 ±0.3	4.1 ±0.1
Control S		9.8 ±0.1	8.3 ±0.2

[a] T0 refers to artificially contaminated wood cubes right before experiment.
[b] TF refers to the end of the treatment. In protocols with two steps is at the end of both steps.
Values are presented as the mean of three independent replicates ±standard deviation.

***Table S 4.2**. pH values measured in the extraction solutions during the application of the different extraction methods under study.*

Extraction method	pH values in solution			
	Step 1		Step 2	
	T0[a]	TF[b]	T0[a]	TF[b]
1B-2S	7.5 ±0.03	8.5 ±0.01	5.8 ±0.03	8.4 ±0.03
1S-2B	5.4 ±0.1	8.3 ±0.1	7.6 ±0.03	7.2 ±0.1
	Single step			
	T0[a]		TF[b]	
1SB	7.5 ±0.01		7.6 ±0.1	
Control M	7.6		8.4	
Control B	7.5		8.8	
Control S	5.3		8.3	

[a] T0 refers to the values at the beginning of the extraction step.
[b] TF refers to the end the extraction.
Values are presented as the mean of two independent replicates ±standard deviation for extraction methods and as a single value (no replicates) for the controls.

***Table S 4.3**. Extraction rates of total iron for the three different extraction protocols under study and controls.*

Extraction method	Total iron in wood before treatment (mg Fe / g wood)	Total iron remaining in wood after treatment (mg Fe / g wood)	% of iron extracted
1B-2S	17.50 ±1.55[a]	3.27	81.34
1S-2B		0.40	97.74
1SB		0.61	96.53
Control medium		6.97	60.12
Control S		2.67	88.62
Control B		17.39	12.77

[a] Standard deviation for three cubes.

***Table S 4.4**. Extraction rates of total sulfur for the three different extraction protocols under study and controls.*

Extraction method	Total sulfur in wood before treatment (mg S / g wood)	Total sulfur remaining in wood after treatment (mg S / g wood)	% of sulfur extracted
1B-2S	32.55 ±3.29[a]	22.82	29.90
1S-2B		18.29	43.81
1SB		23.21	28.69
Control medium		27.71	14,87
Control S		23.73	27.08
Control B		28.21	13.33

[a] Standard deviation for three cubes.

***Table S 4.5**. Concentration of total iron and sulfur in the extraction solutions at the end of each step of every extraction protocol and controls.*

Extraction method	Total iron in solution at TF (mM)		Total sulfur in solution at TF (mM)	
	Step 1	Step 2	Step 1	Step 2
1B-2S	0.003 ±0.001	4.76 ±0.41	6.90 ±0.28	9.24 ±0.57
1S-2B	4.97 ±0.13	1.15 ±0.03	14.99 ±1.82	6.75 ±0.57
	Single step			
1SB	5.51 ±0.11		15.31 ±0.19	
Control M	0		7.17	
Control B	0.006		6.61	
Control S	4.84		14.74	

Values are presented as the mean of two independent replicates ±standard deviation for extraction methods and as a single value (no replicates) for the controls.

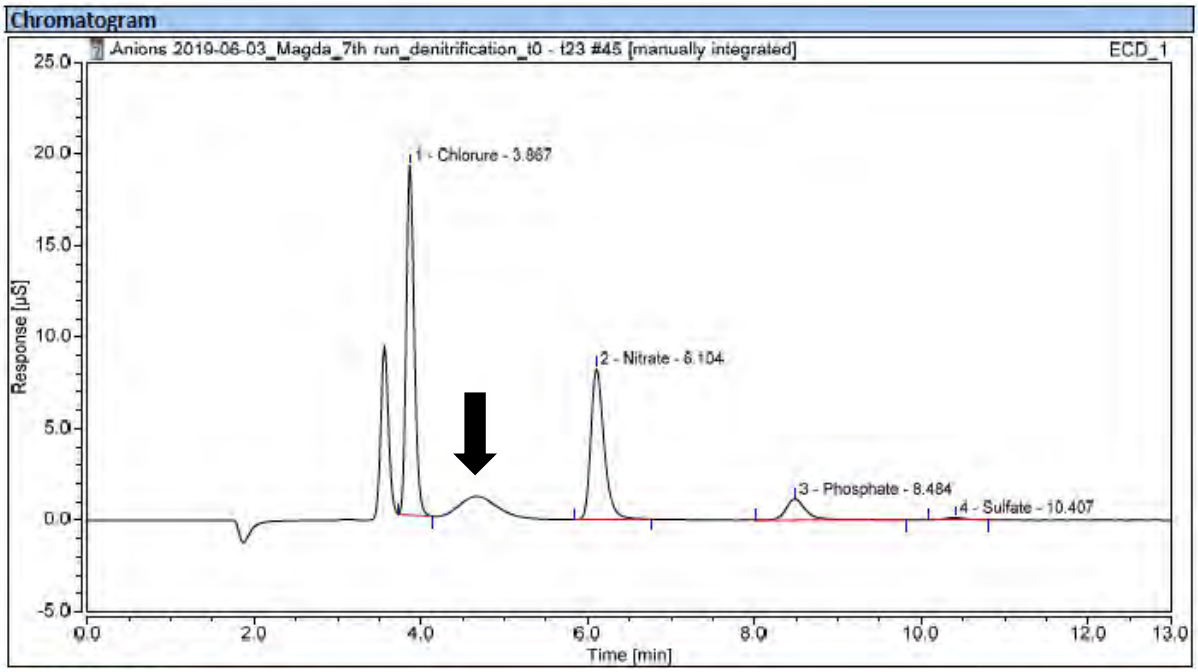

Figure S 4.1. *Chromatogram of IC analysis of the solution of 1SB protocol after 10. The arrow points out the peak that could be assigned to hydro sulfide [13].*

4.2 Evaluation of the application protocol

Abstract

New technologies are in development regarding the preservation of waterlogged archaeological wood items contaminated with Fe/S species. A bio-based treatment to extract these harmful species before further damages occur was developed. *Thiobacillus denitrificans* and DFOM were employed based on their specific properties to solubilize iron sulfides and uptake iron. The biological treatment was compared with chemical oxidizing and complexing agents traditionally used in conservation-restoration. Mock-ups of fresh balsa as well as fresh and archaeological oak and pinewood were prepared to simulate degraded waterlogged wood. Biological and chemical extraction methods were evaluated through FTIR and Raman spectroscopies. Total iron and sulfur extraction were measured with ICP. The biological oxidation of sulfur was investigated with IC. Results showed that extraction methods did not affect the wood composition, meaning that no wood degradation was induced. However, the chemical method tended to bleach the samples. The extraction rates of sulfur were higher for the biological extraction, while the chemical treatment presented higher extraction rates of iron. Overall, the biological treatment had iron and sulfur extraction rates over 50%. Moreover, reduced sulfur species were still identified by Raman analyses in the cubes chemically treated but no in the biologically treated wood.

Introduction

Accumulation of iron sulfides within waterlogged archaeological wood is a long-known issue [17]–[19]. This problematic often linked to marine environments is also common in lakes and riverbeds when oxygen levels are low. Recent studies shown the high levels of pyrite (FeS_2) inside wood remains coming from fresh water locations [20]. However, no defined protocol/procedure exists to deal with the consequences of this accumulation in the wood pores. So far, only precautions can be taken to avoid uncontrolled oxidation of iron and sulfur species [20]. The development of extraction methods that can prevent the formation of salts and strong acids is essential in the long-term preservation.

Biotechnology has proven to offer sustainable solutions for the preservation of heritage artefacts [8], [21]. Microbial processes can be used for consolidation, cleaning or inhibition of reactive corrosion products while reducing the toxicity related to traditionally used treatments [22]. Profiting some specific microbial metabolisms, iron sulfides can be extracted from within the wood. For example, siderophores are produced by many bacteria under iron-deficient

conditions and they present the highest iron affinity, allowing their use in pharmacology, agriculture, medicine and other applications [23]. The application of siderophores has already been investigated on paper and wooden artefacts to remove iron staining [7]. The results showed that siderophores were the most effective regarding the extraction of iron in comparison to commonly used complexing agents. They represent a promising green alternative to current chemical iron extraction methods. Moreover, sulfur oxidizing bacteria, such as *Thiobacillus denitrificans*, can be used to oxidise sulfur species to soluble sulfates under controlled conditions.

A two-step protocol has been developed using DFOM and *T. denitrificans* (see section 4.1). In the first step, DFOM chelates iron avoiding the formation of iron hydroxides and other species that are insoluble [24]. Once this solution is rinsed out, a *T. denitrificans* culture is used to oxidise remaining sulfur species still present in the wood. Current extraction methods show that the application of only iron chelating compounds is not enough to co-extract all sulfur species [2]. The development of a new treatment needs to assure efficacy on both iron and sulfur. Moreover, recent research revealed that the accumulation of iron sulfides inside the wood varies with the species of wood [25]. The extraction of these compounds could also be influenced by the type and species of wood. An extensive campaign is essential to evaluate the treatment in different woods.

Our goal in this study is to evaluate, on different wooden mock-ups, the effectiveness of the proposed bio-based treatment in comparison with chemical methods usually employed.

Materials and Methods

Wood samples

Three woods were selected: balsa (*Ochroma pyramidale*), oak (*Quercus* sp.) and pine/fir (*Pinaceae* family). These woods have already been reported as mock-ups to model waterlogged wood [3], [26]–[28]. Oak and pine are the main wood species found on waterlogged wood artefacts and the most described cases in literature [29].

Fresh and archaeological wood samples were tested. Fresh balsa was purchased from Coop Brico + Loisirs (Neuchâtel, Switzerland). Fresh oak and pine were obtained from a carpenter, J.F. Liabeuf (Cernier, Switzerland). Concerning archaeologic samples, poles and boards of oak and silver fir were provided by the Archaeological Service of Bern Canton (ADB), and two other Neolithic oak poles were provided by the Swiss National Museum (SNM).

From all samples, cubes of 2×2×2 cm^3 and 1×1×1 cm^3 were prepared. Concerning archaeological wood, the samples were cut on the external layer of the poles (sapwood) and following the wood ring to have homogeneous samples sets. All the samples present the transversal (Tr), tangential (Ta) and Radial (R) cutting sections.

10 sets of 19 samples each were prepared. The set distribution is described in Table 4.2. All samples were stored in N_2-flushed deionized water until further experiments. For each set, one sample was kept as reference, on which no artificial contamination or extraction was performed.

***Table 4.2**. Description of the prepared sets. Sample distribution was based on wood specie and wood type.*

Set	Wood specie	Wood type	Dating	Degradation state	Artificial contamination
A1	Balsa (*Ochroma pyramidale*)	Fresh	Recent	low	Yes
A2	Balsa (*Ochroma pyramidale*)	Fresh	Recent	low	Yes
B	Oak (*Quercus* sp.)	Fresh	Recent	low	Yes
C	Oak (*Quercus* sp.)	Archaeologic	2753 BC	high	Yes
D1	Oak (*Quercus* sp.)	Archaeologic	3840 BC	high	No
D2	Oak (*Quercus* sp.)	Archaeologic	Bronze age	high	No
E	Pine (*Pinus* sp.)	Fresh	Recent	low	Yes
F	Silver fir (*Abies alba*)	Archaeologic	1878 AC	low	Yes
G1	Pine (*Pinus* sp.)	Archaeologic	3840 BC	high	No
G2	Oak (*Quercus* sp.)	Archaeologic	Neolithic	high	No

Sets A1, A2, B, C, E and F were artificially contaminated with iron and sulfur species according to the protocol previously described (Section 4.1). A water pre-immersion treatment under vacuum (600 mbars) was also applied for sets A1, A2, B and E before impregnation to enhance the desired wood degradation and to simulate the state of degradation observed on real waterlogged wood artefacts. Regarding D1, D2, G1 and G2 sets, spot tests to detect iron(II), iron(III), sulfides and sulfates were performed. Potassium thiocyanate 33% and barium chloride test were used to detect iron and sulfates, respectively. Machery-Nagel® test paper n°90761 (Fisher Scientific AG, Switzerland) was employed for sulfides detection [30].

Labelling

All the cubes of each set were named depending on the treatment applied on them. In each set, 3 groups of 6 cubes: untreated (NT), biologically treated (BT) and chemically treated (CT), plus, the reference cube, were included. The samples were named NT-1 to NT-6, BT-1 to BT-6, and CT-1 to CT-6.

Extraction methods

The proposed biological treatment was compared to current chemical extraction treatment. Before extraction, the samples were washed in 400 mL of deionized water and sonicated for 2 and then 4 min. The water was changed between the two-sonication baths. The final volume of extraction solution was set to 200 mL. At the end of treatment, BT and CT samples were immersed in N_2-flushed deionized water, and several cycles of 2 × 20 min vacuum (1 mbars) followed by 1 h sonication were applied on the samples until constant pH was reached and storage solution conductivity was in the range 10–30 μS/cm (as the rinsing water).

Biological treatment

T. denitrificans (DSMZ 12475) was obtained from the German Collection of Microorganisms and Cell Cultures (DMSZ, Germany). The strain was cultivated using standard anaerobic techniques at 30 °C in the dark. Deferoxamine mesylate salt (DFOM) was purchased as Desferal® (Novartis Pharma Schweiz AG, Switzerland). Wood cube samples were used for the extraction without any previous sterilization protocol. BT samples were directly immersed in a N_2-flushed water solution with a final concentration of DFOM 84 mM, after the above-described rinsing. The six wood cubes were treated in the same extraction solution. The concentration of DFOM was the maximum possible for its solubility. Samples were kept at room temperature and with orbital agitation for 10 days. After rinsing with deionized water in a sonication bath, the samples were incubated for 23 days with *T. denitrificans* in N_2-flushed modified 113 medium. Inoculation of the bacteria was done as described in the previous section. Samples inoculated with the bacteria were incubated at 30 °C in darkness without agitation.

Chemical treatment

The applied chemical protocol was based on a previous study [3]. Briefly, the samples were immersed in sodium persulfate 0.1 M for 1 day to oxidize sulfur species. After rinsing with deionized water, the samples were then immersed in EDTA 0.125 M for 7 days to complex free iron ions. During the whole process, the samples were kept at room temperature without agitation.

Analytical methods

Documentation and colorimetry

Each set was photographically documented. The samples were always placed on the same position. The sets were photographed with a Canon Power Shot G5X camera on auto mode. Each face of the cubes was documented. The pictures were taken in a white chamber (48x48 cm) dedicated for photography. The sets were illuminated with 2 halogen lights (23W/lamp). The camera was placed on a tripod (135 cm from the floor) and tilted at 90° to be above the tent and the samples. Colour and lengths scales were used.

Colorimetry measurements were investigated to determine the changes in samples appearance. A Minolta CM-508D spectrophotometer was used for the colour measurements, with the following parameters: Specular Component Included (SCI), Illuminant D65 (daylight containing UV component, colour T 6504 K), d/8° geometry, 10° observer, measurement area diameter 10 mm, illumination with Xe flashlight source 100% UV containing all UV components or 0% UV containing no UV components, CIELab 1976 colour space (EN ISO 11664-5:2016). On each sample, one measurement was recorded through a plastic film.

The parameters L^* (lightness), a^* (green–red chromatic coordinate) and b^* (blue-yellow chromatic coordinate) were determined, and the ΔE* (i.e., difference between two colours) was calculated following equation 1 [31]:

$$\Delta E^* = \sqrt{(\Delta L^*)^2 + (\Delta a^*)^2 + (\Delta b^*)^2} \quad (1)$$

pH measurements and conductivity

Over time, pH was measured at the surface of the wood samples and within the extraction solutions. A 691 pH Meter Metrohm (Metrohm AG, Switzerland) with surface electrode (flat membrane electrode 6.0256.100) and ionic electrode (unitrode 6.0259.100) calibrated with buffer solutions (pH 4, 7 and 9) was used.

The conductivity of the wash out solutions was measured with a WTW Multi 3410 conductometer. Deionised water was used as reference.

Fourier Transformed Infrared spectroscopy (FTIR)

Fourier transformed infrared spectroscopy (FTIR) was used to evaluate the wood degradation. A Nicolet iS5 Thermo Fisher™ (Thermo Fisher Scientific, United States) was used for measurements, with the following parameters: range 650-4000 cm^{-1}, spectral resolution of 4 cm^{-1} and 16 scans. The measurements were done in an ATR (Attenuated Total Reflectance)

mode using a diamond ATR crystal without any sample preparation. Spectra were recorded at the surface of all faces with 3 points per face with a mask. The spectra were analysed with the Thermo® OMNIC software (Thermo Fisher Scientific, United States). 2 cubes per treatment per set were analysed: NT-2, NT-4, BT-2, BT-4, CT-2 and CT-4.

The height of vibrational bands at: 1) 1034 cm^{-1} assigned to C–O stretching in holocellulose and lignin, 2) 1158 cm^{-1} related to C–O–C vibration in cellulose and hemicellulose, 3) 1374 cm^{-1} assigned to C–H deformation in holocellulose and cellulose, and 4) 1506 cm^{-1} assigned to aromatic skeletal vibration in lignin, were used to calculate three ratios: R1=I(1158)/I(1506), R2=I(1374)/I(1506) and R3=I(1034)/I(1506) according to literature [32]–[34].

Raman spectroscopy

The minerals formed during the impregnation protocols were determined by Raman spectroscopy. A Jobin Yvon Horiba™ spectrophotometer was used for the measurements coupled with Olympus BX41 microscope (Horiba Ltd., Japan). Spectra were recorded at a wavelength of 632.8 nm, pinhole of 1000 µm, spectrometer entrance slit of 100 µm, 1800 lines/cm grating, 100-1500 cm^{-1} range, with 0.99 mW (D1 filter, 10%) of laser power to avoid over heating of the compounds, 100x objective (0.9 numerical aperture) and acquisition with 10 accumulations of 5 seconds. Then, one long-acquisition spectrum was recorded, with the same parameters, and an acquisition of 25x10s. The spectra were acquired with the LabSpec® 5 software (Horiba Ltd., Japan). Reference spectra were used to identify the compounds formed. The analyses were performed on the samples immersed in their stock solution. A thin layer of solution over the cubes surface allowed the laser power to be increased. One measurement at the centre of each face was carried out. 2 cubes per treatment per set were analysed: NT-1, NT-3, BT-1, BT-3, CT-1 and CT-3.

Ion chromatography (IC)

For the determination of the concentration of sulfates (SO_4^{2-}), nitrates (NO_3^-), nitrites (NO_2^-), and phosphates (PO_4^{3-}), in the solution of the biological extraction method samples, an ion chromatograph Dionex ICS 1600 (Thermo Fisher Scientific, United States) was used. Samples were prepared as in the previous section. Data was analysed with the Chromeleon™ software (Thermo Fisher Scientific, United States).

Inductively Coupled Plasma - Optical Emission Spectrometry (ICP-OES)

Inductively Coupled Plasma-Optical Emission Spectrometry (ICP-OES) was applied to determine total iron and sulfur concentrations in the wood cubes and in the extraction solutions.

Same protocol and detection system as in the previous section were applied. The cubes used for measuring the remaining amount of iron and sulfur after the extraction protocols were extra cubes of 1×1×1 cm^3, treated together with the 2×2×2 cm^3 samples. The extraction rates were calculated based on the concentration of species remaining in the samples before and after extraction.

Results and Discussion

Visual appearance after treatment

The effects of two extraction treatments (BT and CT) were compared on six artificially contaminated woods (A1, A2, B, C, E, and F), and four different waterlogged archaeological woods naturally contaminated with iron and sulfur species (D1, D2, G1, and G2). The impregnation with Fe/S species gave a darker colour to artificially contaminated sets that resemble then to archaeological wood (Figure 4.4). This change was especially remarkable in fresh wood sets A1, A2, B, and E (Figure 4.4). Colorimetric measurements confirmed the visual observations clustering together all samples after artificial contamination (Figure S 4.2). Only set G1 was cluster away. Pine usually presents a clearer hue than oak, and it could be that this set is not highly contaminated with iron and sulfur species preserving its original colour. Set G2 also presented some cubes clustered away. This set presented an heterogenous colour what would explain the wide distribution.

After extraction the chemical treatment presented the higher variation in colour in comparison to the samples before extraction (Figure 4.5). The larger the value for the calculated ΔE*, the greater the colour difference between the treated samples and the reference groups [31]. CT presented high ΔE* values for all artificial contaminated samples. (Figure 4.5). D1, D2, G1, and G2 sets also suffered colour changes but in lesser degree. Overall, all samples treated by CT presented a colour changer superior to 5. ΔE* higher than 5 is considered to be a clearly perceptible colour difference [35]. On the contrary, the biological treatment presented smaller ΔE* values for all sets. The ΔE* for BT cubes was below 5 for C, D2, and G2 sets (Figure 4.5). Appearance was especially similar in sets C and D2 with values below 3. The higher colour change was observed for set G1 (ΔE*=16.5) (Figure 4.5). In general, the biological treatment affected the appearance of oak samples less than the other species of wood, while the chemical treatment affected all woods (Figure 4.5).

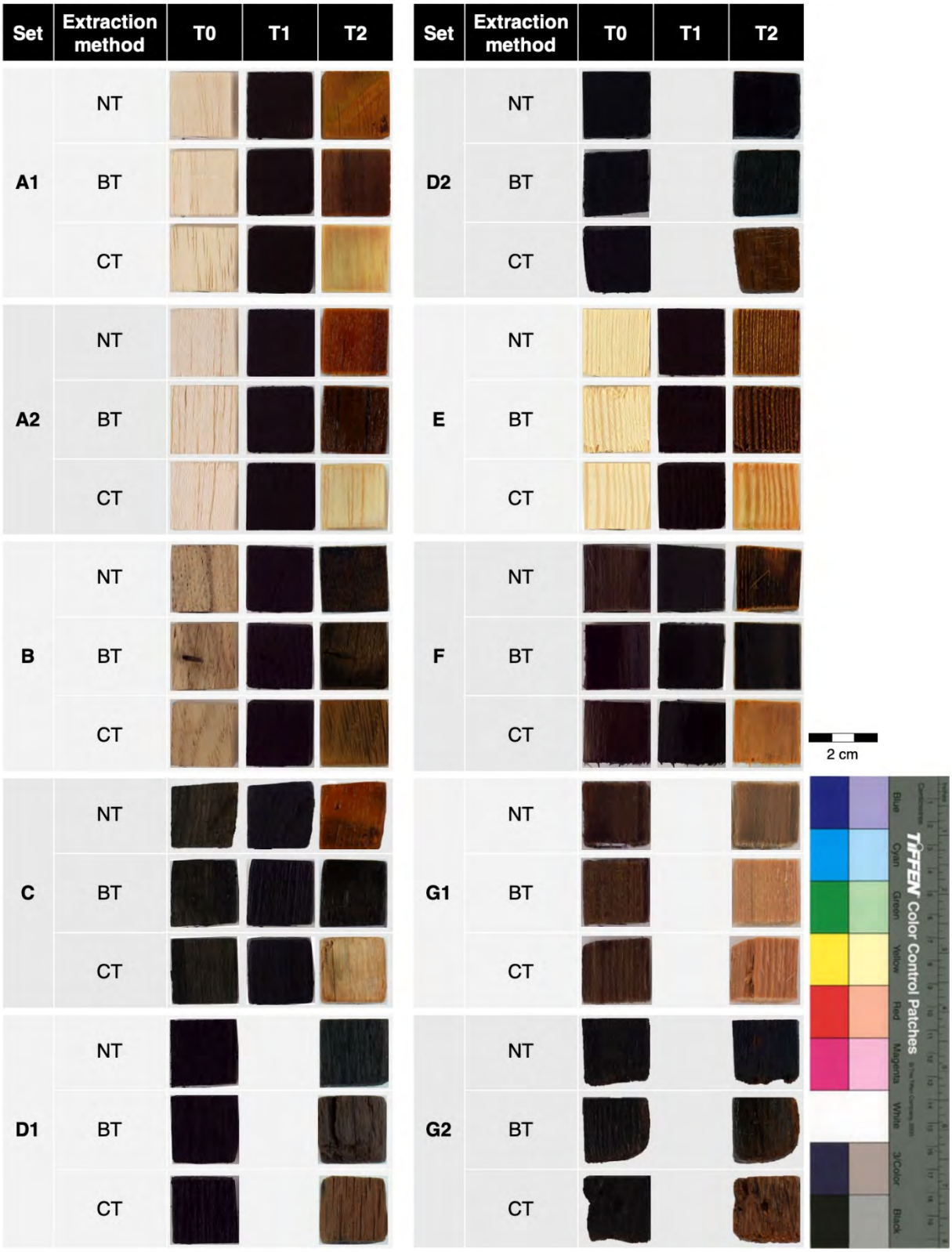

***Figure 4.4**. Visual aspect of the wood samples at different steps of the experiment (T0: before impregnation, T1: after impregnation and T2: after extraction). NT: untreated samples, BT: biological treatment, CT: chemical treatment. A1 and A2 sets are fresh balsa, B set is fresh oak, C set is Neolithic oak, D1 and D2 sets are archaeological oak, E set is fresh pine, F set is waterlogged silver fir, G1 set is archaeological pine, and G2 set is archaeological oak.*

However, when comparing to the reference sample the picture changes. In this case, BT presented colour changes for fresh balsa, oak and pine (Figure 4.5). The artificial contamination achieves wooden mock-ups that resemble waterlogged archaeological wood items. Therefore, it is important that the treatments respect the appearance after artificial contamination. However, in the case of fresh wood, past studies have used recovering the original colour as an indicator of for successful iron extraction [3]. The biological treatment allowed maintaining the aesthetical appearance from artificial contamination, while extracting considerable amounts of iron (see below). For fresh wood, CT recovered a clearer colour closer to the "original" appearance (Figure 4.4), but the colour variation was still superior than 5 (Figure 4.5). Moreover, in the case of waterlogged wood artificially impregnated (C and F sets), the chemical treatment seemed quite aggressive, and the final colour after treatment was not similar to the original colour (Figure 4.4). Sodium persulfate used here as oxidant agent is known as an oxidizing bleach. It can remove colour by adding oxygen to a dye structure.

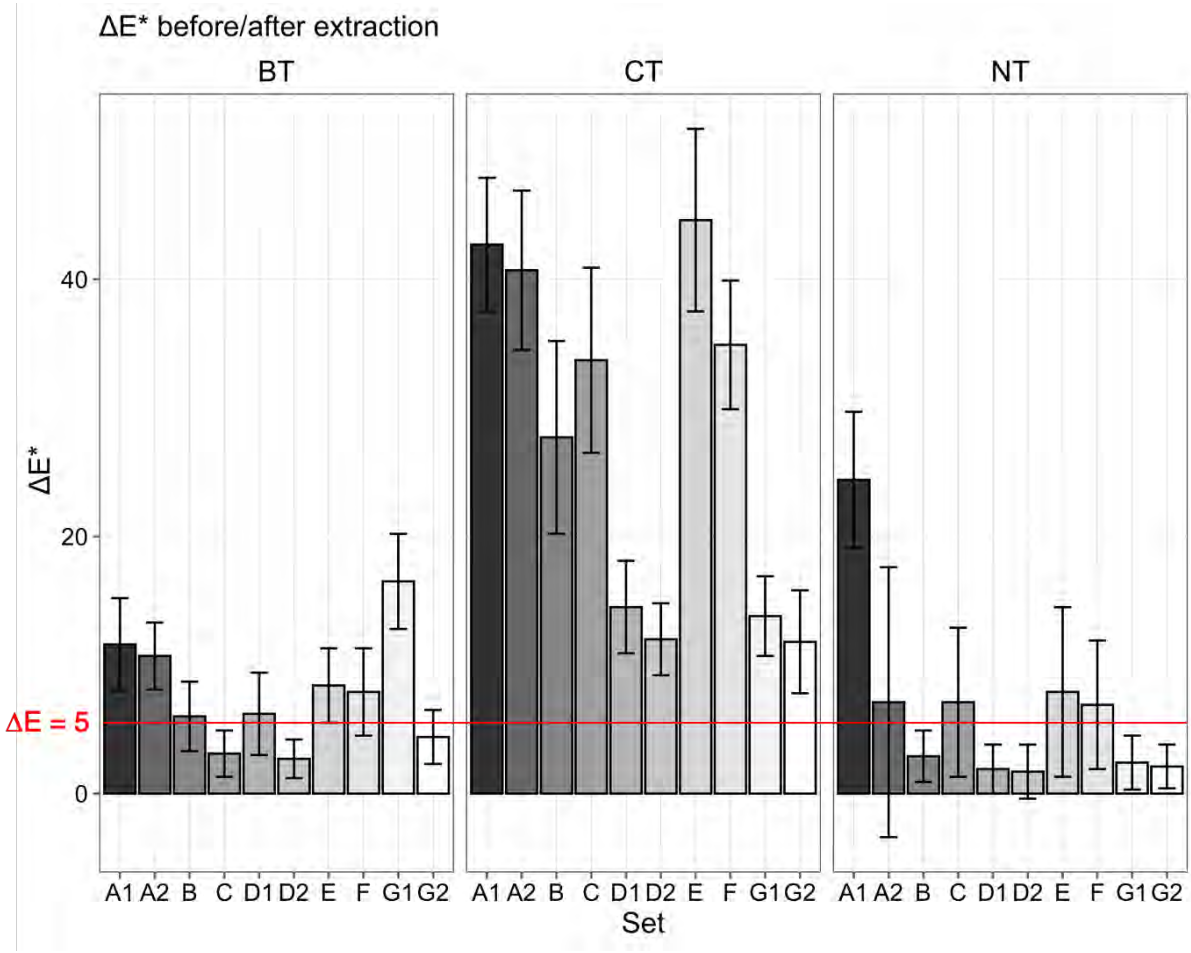

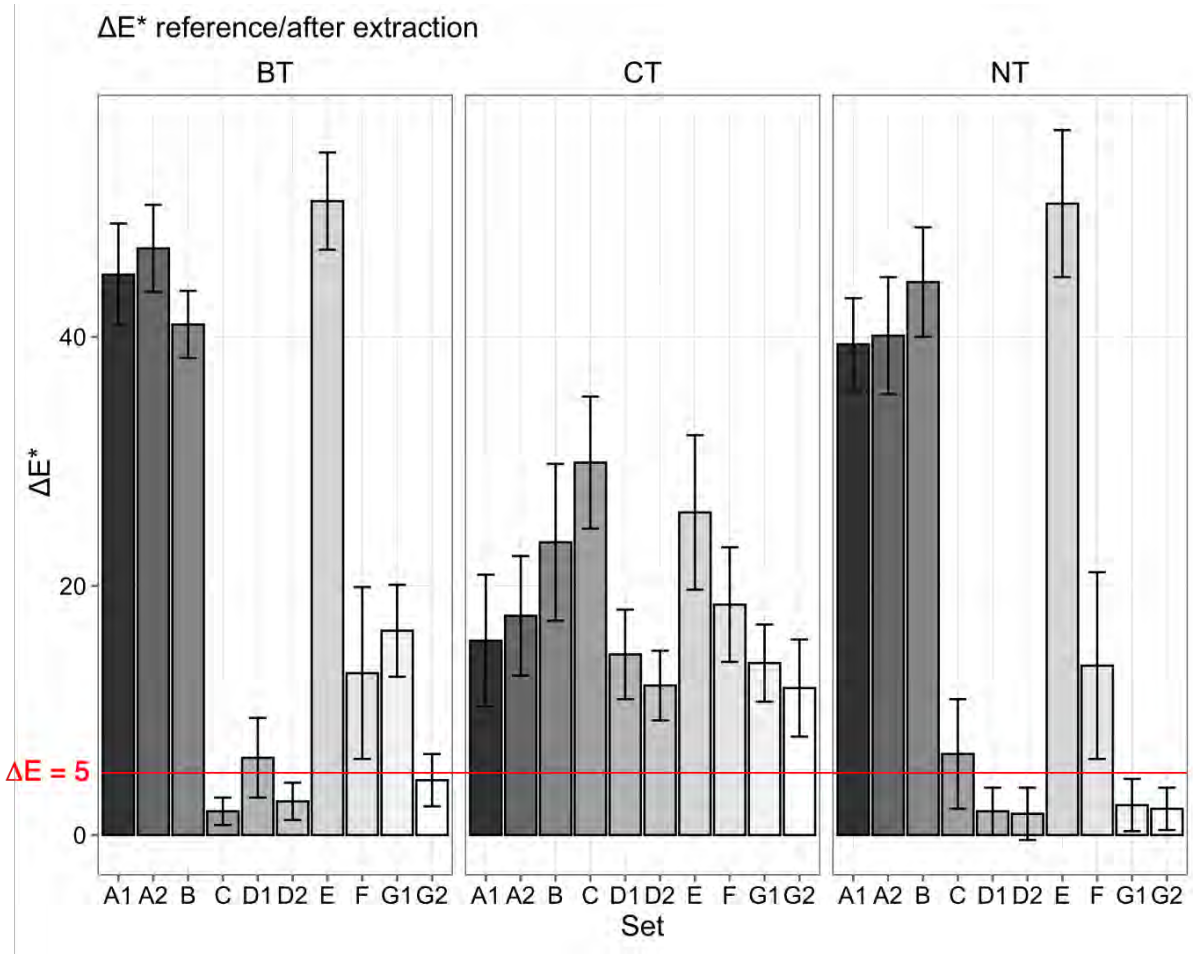

***Figure 4.5**. Difference between colour (ΔE*) depending on the extraction method applied (BT or CT) and in untreated samples (NT); before and after extraction (above), and in reference to before any artificial contamination (below).*

Untreated samples were employed to evaluate present iron sulfides in wood without any treatment. The colour variation shows that specially balsa wood suffers changes over time (Figure 4.5). We observed a slight oxidation especially on the samples manipulated for analysis (Figure 4.4). These are the expected changes when iron sulfides within the wood oxidise. The transformation of iron sulfides to iron oxides and other salts is translated to a big change in visual appearance [10].

Efficiency of the treatment

Raman analysis

Raman analyses allowed to characterize iron sulfides and other sulfur forms within the wood [19], [36], [37]. Raman analyses of the NT wood samples showed that reduced sulfur compounds were present on the artificially contaminated samples. Sets A1, A2, C, E and F displayed the same spectrum as reference $Fe_{1-x}S$ (Table 4.3 and Figure S 4.3). Thus, the

artificial contamination applied on some of the sets led to the formation of partially oxidized mackinawite ($Fe_{1-x}S$). Elemental sulfur was identified only on set B samples (fresh oak) with characteristics bands at 152, 220 and 473 cm^{-1} (Table 4.3 and Figure S 4.3). Raman spectra on the surface of sets D1, D2, G1 and G2 did not reveal the presence of any inorganic compounds. Therefore, iron and sulfur detected in these samples with the previous spot test skipped the detection with Raman spectroscopy. Their concentration within the wood may be low or heterogeneous. EDS analyses described in section 4.3, confirmed this hypothesis.

After extraction, Raman analyses did not detect reduced sulfur compounds on the surface of BT samples (Table 4.3 and Figure S 4.3). These results together with the extraction rates suggest that the proposed microbial treatment was efficient in extracting iron and sulfur at least from the surface of wood cubes. On the contrary, CT samples still presented some reduced sulfur compounds, what agrees with the lower sulfur extraction rates calculated. Mainly, elemental sulfur was identified on sets A2, C, E and F (Table 4.3 and Figure S 4.3).

***Table 4.3**. Compounds identified by Raman spectroscopy depending on the treatment: untreated (NT), biological treatment (BT), and chemical treatment (CT). Adapted from* [38].

Set	**Compounds identified:**		
	Mineral sulfur (α-S_8) 152, 220, 470 cm^{-1}	Partially oxidized mackinawite ($Fe_{1-x}S$) 119, 282, 360 cm^{-1}	Wood substrate 400, 580, 650, 930, 1270, 1330, 1480 cm^{-1}
A1		NT	NT, BT, CT
A2	CT	NT	NT, BT, CT
B	NT		NT, BT, CT
C	CT	NT	NT, BT, CT
D1			NT, BT, CT
D2			NT, BT, CT
E	NT, CT	NT	NT, BT, CT
F	CT	NT	NT, BT, CT
G1			NT, BT, CT
G2			NT, BT, CT

For all sets, some bands at 400, 580, 650, 930, 1270, 1330 and 1480 cm^{-1} (Figure S 4.4) were observed and attributed to wood substrate [39]. Raman analyses on the wood could also be used in parallel to FTIR as risk evaluation in the future. In this case, is also possible to measure the difference between peaks corresponding to wood components that may change if degradation occur over the extraction. Also, further analyses should be performed on the samples core, before and after extraction, to evaluate how deep extraction of iron and sulfur species occurred. Moreover, this technique allows statistical analyses to be performed to assess the efficiency of the treatments under study.

Total extraction rates

The preservation strategy for waterlogged archaeological wood may vary depending on the species of wood, the level of degradation of the wood, and the sulfur and iron species within the wood. Three different species of wood with different degradation states, and different iron and sulfur species allowed us to evaluate the efficiency of the biological treatment under study. The artificial contaminated samples (Sets A1, A2, B, C, E, and F), in comparison with the no contaminated samples (Sets D1, D2, G1, and G2), showed a much higher concentration of iron and sulfur within the wood (Table S 4.5 and S 4.6). The archaeological samples without artificial contamination come from freshwater locations. Moreover, the samples are pre-Iron age and no iron artefacts co-exist in the burial environment. These conditions are not expected to favour high iron sulfides accumulation within these woods [20]. All the iron measured within the wood must come from the surrounding burial environment.

The efficient extraction of iron and sulfur species from all the tested sets was followed over time. The release of iron and sulfur was measured in the extraction solutions. Moreover, at the end of the different treatments, the remaining amounts of iron and sulfur in the wood were controlled. The iron extraction rates for the bio-treatment were in general around 50-75% (Figure 4.6). These rates are lower than the observed previously in section 4.1. Differences may be consequence of treating six cubes of bigger dimensions with a concentration in DFOM only ~4 times higher. However, sulfur rates were closer pointing out that the differences in iron extraction may be due to the diffusion of the iron-siderophore complex out of the wood being slower in bigger wood samples.

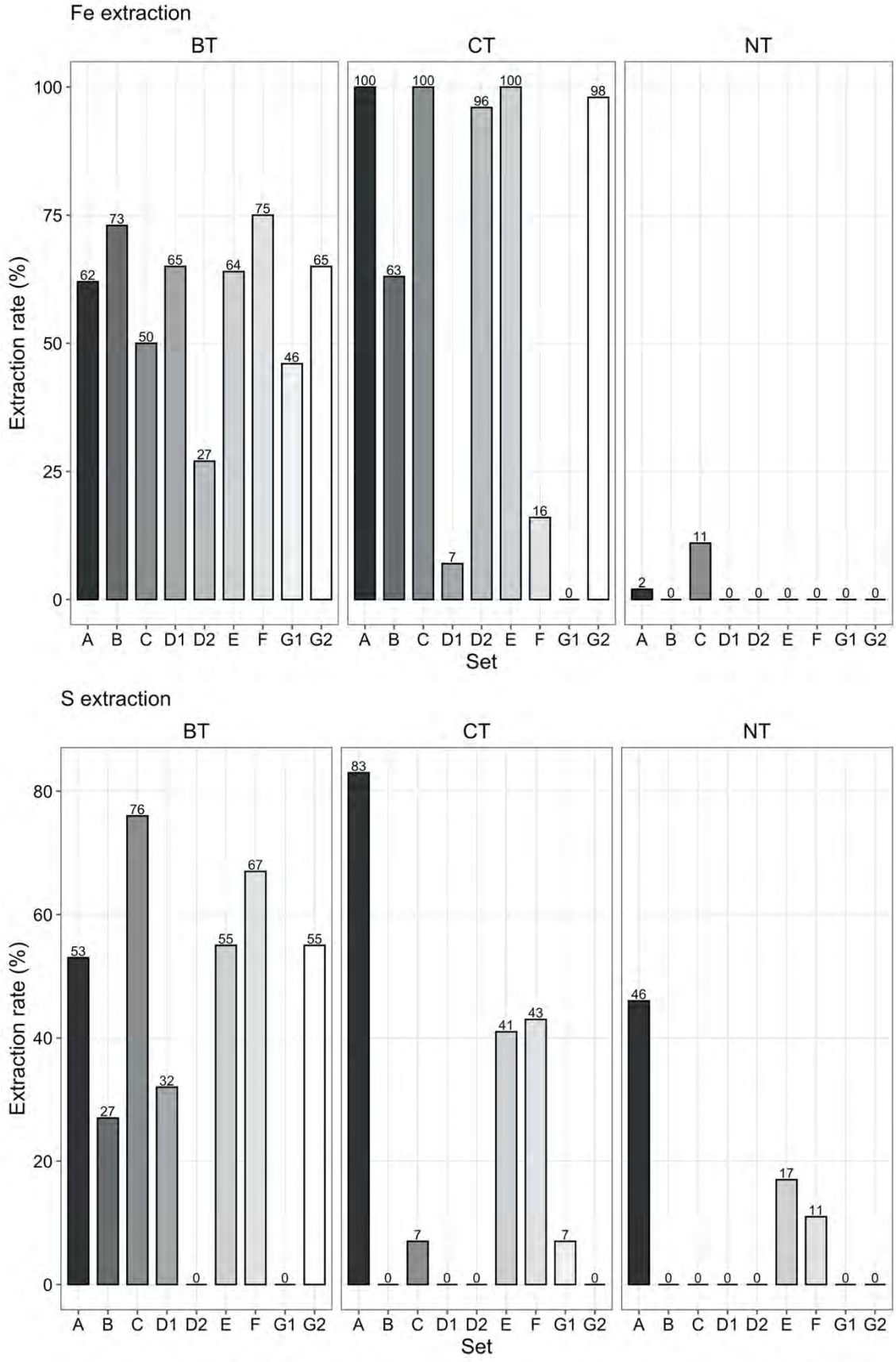

***Figure 4.6**. Percentage of total iron (above) and sulfur (below) extraction for treated (BT and CT) and untreated (NT) sets of wood (A, B, C, D1, D2, E, F, G1, and G2).*

Extraction rates lower of 50% were calculated for set D2 (Figure 4.6). This set is ancient oak highly decayed without artificial contamination. The reason why this group of wood showed a lower efficiency of the bio-treatment is uncertain. Different factors influence the extraction rate: 1) Diffusion of the ligand into the matrix, 2) formation of the iron-ligand complex 3) diffusion of the complex out of the wood, and 4) amount of iron-chelator complex already existing in solution [40]. All listed factors could influence the lower extraction rates. No further experiments were carried out at this point to define formation constants or diffusion rates. However, we observed that even after intensive rinsing of the cubes with deionised water, iron-DFOM complex was still being released from the cubes. We assume that the diffusion of the complex out of the wood cubes is slow.

Nonetheless, similar iron extraction rates in the majority of the sets treated with BT give encouraging results in terms of application of DFOM to different wooden objects with different characteristics (e.g. degradation state, wood specie, iron and sulfur compounds, etc.). The extraction rates can be increased by longer time of application, or by renew of the chelating solution [40].

In parallel, the chemical treatment used as reference in this study showed very good iron extraction rates for almost all treated woods (Figure 4.6). Iron extraction rates of almost 100% were achieved for A, C, D2, E, and G2 sets. This method was previously used in archaeological oak samples giving the best results [3]. 30% iron was extracted there after 24 h. In our case, a longer time may have allowed higher extraction rates. However, sodium persulfate is a harmful compound that requires safety precautions [3]. Also, it appeared to be highly corrosive. The samples were tagged with iron steel needles that corroded completely during this treatment. That would explain why in some cases the extraction rate was negative, having more iron after than before extraction (set G1). This was not observed with the biological treatment. The strong specificity of DFOM for iron as Fe^{3+} ($\log K_f \approx 30$) prevents the siderophore from corroding iron steel [11] Moreover, DFOM is safe to use and does not require special safety equipment [5].

Sulfur extraction was not as efficient when applying CT. Only balsa wood presented an extraction rate of 83% (Figure 4.6). For the other sets, the rates were always 40% or below and, in some cases, the treatment even seemed to add sulfur to the wooden mock-ups. Sodium persulfate ($Na_2S_2O_8$) could have left residual sulfur that bond to the wood and was not removed with the intensive rinsing. These first results showed that the biological treatment, was more efficient regarding sulfur extraction.

In BT treated samples, the average sulfur extraction for all sets is around 40%. However, differences are observed between the sets. The higher sulfur extraction was 76% for set C (Figure 4.6). On the contrary, no sulfur extraction or very low amount was measured for D2 and G1 sets. In this case, the variation between sulfur extraction rates did not correlate with wood species or state of degradation (Figure 4.6). In general, higher sulfur extraction rates were observed for the wood sets artificially contaminated. Both D2 and G1 sets are archaeological samples used as reference for natural iron and sulfur contamination. The contamination of iron and sulfur here could be heterogenous. ICP-OES analyses are destructive and the samples used as before were not the ones being treated. Therefore, it could be that by chance the cubes used for the analysis after treatment had higher amounts of sulfur in the starting point. ICP-OES and IC analyses detected sulfur in solutions when treating these two sets (Table S 4.5 and S 4.6).

Oxidation of sulfur species

Most sulfur and iron was extracted from the wood in the first step of the bio-treatment. Studies have shown that the extraction of iron correlates with the extraction of sulfur species [2]. In the first step of the biological treatment, we measured high amounts of sulfur in solution (Table S 4.6). However, not all sulfur can be co-extracted with iron [2]. The goal of the *T. denitrificans* step is the oxidation of the remaining sulfur.

Raman analyses detected different sulfur species on the wood surfaces of the cubes (Figure S 4.4). Partially oxidised mackinawite ($Fe_{1-x}S$) and elemental sulfur (α-S_8) were detected on some artificially contaminated cubes. The oxidation of these species by *T. denitrificans* has been previously described [15], [41]:

$$5FeS + 8NO_3^- + 8H^+ \rightarrow 4N_2 + 5Fe^{2+} + 5SO_4^{2-} + 4H_2O \quad (2)$$

$$5S_{(0)} + 6NO_3^- + 2H_2O \rightarrow 5SO_4^{2-} + 3N_2 + 4H^+ \quad (3)$$

Assuming that some of these species were still in the different woods after the DFOM step, ratios of depleted nitrates/produced sulfates were calculated for all wood sets (Table 4.4).

Some of the artificial contaminated sets (A1, A2, C, E, and F) showed a slight decrease of nitrates related to a slight increase of sulfates over time (Figure 4.7). Partially oxidised mackinawite was detected in both sets of balsa wood (A1 and A2), in untreated samples (Table 4.4). However, the calculated $\Delta NO_3^-/\Delta SO_4^{2-}$ ratios were higher than the theoretical one for equation 2 (Table 4.4). Previous studies have shown that the presence of high concentrations of hydrogen sulfide could change denitrification ($NO_3^- \rightarrow N_2$) towards dissimilatory nitrate

reduction to ammonia ($NO_3^- \rightarrow NH_4^+$) [42]. The levels of sulfide and ammonia were not controlled, but this could be an explanation for the higher consumption of nitrates.

Partially oxidised mackinawite was also detected in sets C, E, and F (Table 4.3). The calculated $\Delta NO_3^-/\Delta SO_4^{2-}$ ratios here were 1.68, 2.02 and 1.71, respectively (Table 4.4), and partially oxidised mackinawite was not detected after biological extraction (Table 4.3). Untreated samples of set E also presented elemental sulfur, that was not detected after BT (Table 4.3). In this case, it is possible the oxidation of both sulfur species at the same time.

Among the artificially contaminated sets, set B presented a high decrease in nitrates arriving to complete depletion (Figure 4.7). Mineral sulfur was detected in untreated samples of this set by Raman spectroscopy (Table 4.3). However, the total consumption of nitrates is higher than expected for the total amount of sulfates detected, if we consider a complete oxidation of mineral sulfur to nitrogen (Eq. 3). Some studies have seen that a partially reduction of nitrogen to nitrites can also occur here [16], [43]:

$$17S_{(0)} + 24NO_3^- + 8H_2O \rightarrow 6NO_2^- + 9N_2 + 17SO_4^{2-} + 16H^+ \quad (4)$$

$$S_{(0)} + 3NO_3^- + H_2O \rightarrow 3NO_2^- + SO_4^{2-} + 2H^+ \quad (5)$$

A considerable number of nitrites (615.99 mg/L) was detected in the solution of set B after 23 days. Moreover, the calculated consumed nitrates/produced nitrites ratio ($\Delta NO_3^-/\Delta NO_2^-$ =1.48) is closer to the theoretical $\Delta NO_3^-/\Delta NO_2^-$ ratio of the last reaction. Still, equation 5 does not relate the production of sulfates to the consumption of nitrates detected. Theoretical ratio $\Delta NO_3^-/\Delta SO_4^{2-}$ is 3, while the calculated one is 13.24. The high consumption of nitrates could be due again to reduction to ammonia [42]. Another possibility for the high consumption of nitrates is the heterotrophic denitrification using organic compounds from cell lysis or from the wood material [41], [44], [45]. However, this would imply that other microorganisms are thriving in the solution as *T. denitrificans* is an obligately chemolithoautotrophic bacterium [46]. The samples used in this experiment were not sterilised before treatment. There is the possibility that other microorganisms could have developed. Controls with sterile wood could help to understand the influence of other microorganisms in future experiments.

The four archaeological wood sets (D1, D2, G1, and G2) also showed a remarkable consumption of nitrates over time, arriving also to complete depletion in set D1 (Figure 4.7). However, sulfur species were not detected in these sets by Raman spectroscopy before treatment (Table 4.3). Spot tests conducted to select the samples, ICP-OES and EDS analyses

(section 4.3), only revealed sulfur but not which species. Therefore, the calculated ratios shown in Table 4.4 are an assumption that some sulfur species were present in these sets.

Nevertheless, the amounts of sulfates detected in solution did not correlate with the high number of nitrates consumed. High $\Delta NO_3^-/\Delta SO_4^{2-}$ ratios were calculated for naturally contaminated sets (Table 4.4). Nitrates could have been used for other metabolisms by autochthonous bacteria [47]. For example, wood chips have been suggested as a method for denitrification of wastewaters [45]. Bacteria use the wood as carbon source and carry out a heterotrophic denitrification. This hypothesis could explain why we observe only a slight increase of sulfates over time, against a high decrease in nitrates (Figure 4.7). No pre-treatment, such as biocides or autoclave sterilization, was performed in in any of the wood sets. We assume a natural community could be inhabiting these woods (see section 4.3). As before, controls where the wood was previously sterilised could help to establish the effects of autochthonous microbiota in the overall efficiency of the bio-treatment.

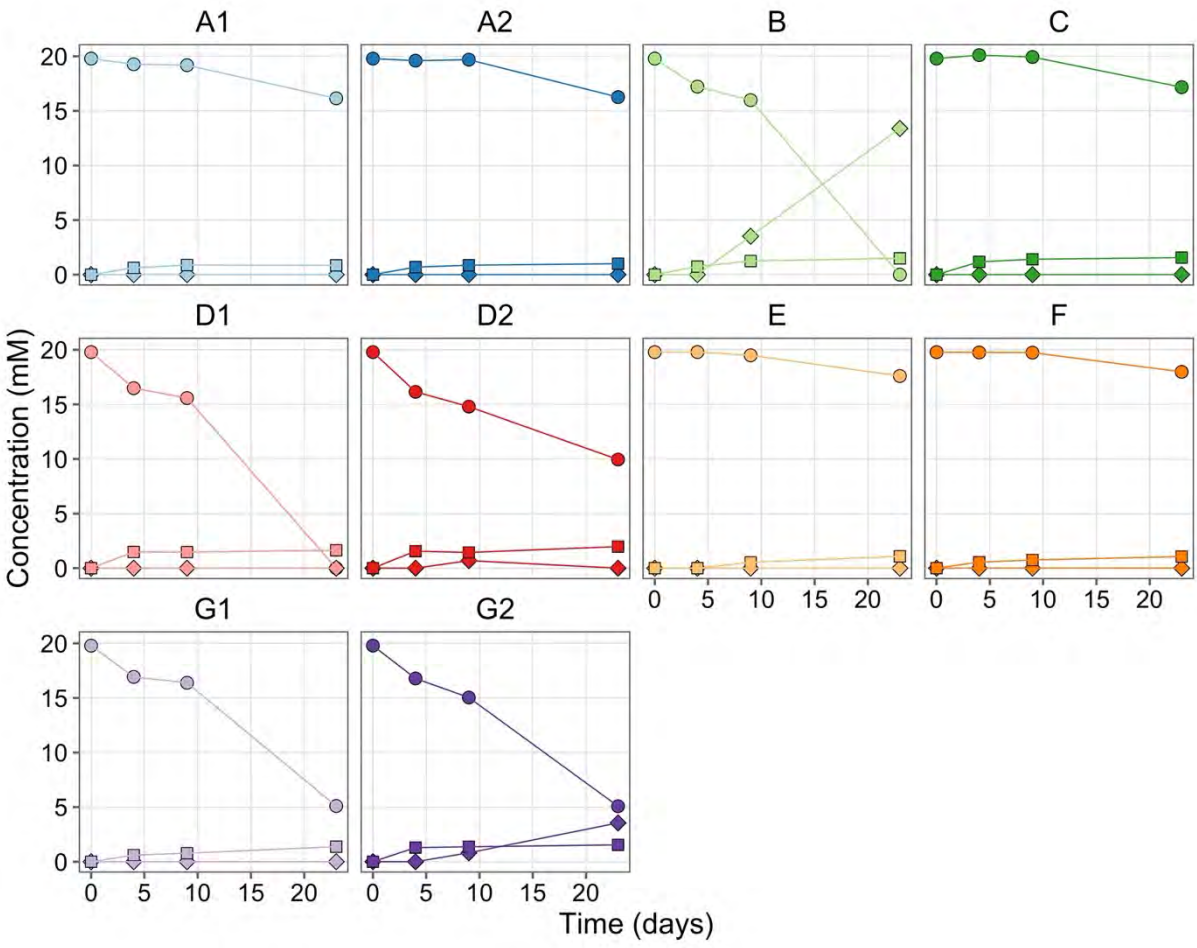

***Figure 4.7**. Nitrates (●), nitrites (♦), and sulfates (■) concentrations (mM) over time. Anions concentrations were measured in the different solutions containing the six wood cubes of each set (A1, A2, B, C, D1, D2, E, F, G1, and G2).*

***Table 4.4**. Mass balance of educts and products for the oxidation of reduced sulfur compounds by T. denitrificans after 23 days of incubation.*

	Set	NO_3^- depleted [mM]	SO_4^{2-} produced [mM]	NO_2^- produced [mM]	$\Delta NO_3^-/\Delta SO_4^{2-}$ ratio	$\Delta NO_3^-/\Delta NO_2^-$ ratio
Calculated	A1	3.64	0.85	-	4.28	-
	A2	3.53	1.01	-	3.51	-
	B	19.79	1.49	13.38	13.24	1.48
	C	2.62	1.56	-	1.68	-
	D1	19.79	1.64	-	12.08	-
	D2	9.84	1.97	-	4.98	-
	E	2.19	1.08	-	2.02	-
	F	1.81	1.06	-	1.70	-
	G1	14.69	1.38	-	10.68	-
	G2	14.71	1.54	3.55	9.54	4.14
Theoretical	Eq. 2	8	5		1.6	
	Eq. 3	6	5		1.2	
	Eq. 4	24	17	6	1.4	4
	Eq. 5	3	1	3	3	1

Nitrites were observed in solution in set G2. Again, Raman analysis did not show any sulfur specie in the surface of this wood. However, if we assume that sulfur species may be found within the wood, the calculated $\Delta NO_3^-/\Delta NO_2^-$ ratio was close to the theoretical ratio for equation 4 (Table 4.4). Still, the theoretical $\Delta NO_3^-/\Delta SO_4^{2-}$ ratio for this reaction is also much lower than the calculated one (Table 4.4), what implies one more time, that nitrates had to be consumed by other parallel pathways. IC results compared to ICP-OES results showed that only a small fraction of the total sulfur detected in solution after step 2 of the BT was as sulfates (Table 4.4). In fact, ICP-OES detected much more sulfur in solution than IC. Previous studies have shown that the detection of sulfur by these techniques can be compared and no differences are observed [48]. Therefore, we still have sulfur extraction here that could be due to residual DFOM from the first step. The wood cubes were rinsed between steps until no more DFOM solution was observed to leave the cube. However, after some time in incubation with *T. denitrificans*, the solution turned orange-red, characteristic colour of Fe-DFOM complex [6]. The diffusion of

the iron-siderophore complex from the wood is a slow process. Intensive rinsing after BT was needed to clean out all the extraction solution.

In general, sets where more depletion of nitrates was observed presented a higher percentage of sulfates (Table 4.5). One exception is set E, where a 50.53% of sulfates was calculated. If we check the amount of total sulfur in solution for set E (Table 4.5), is much lower than for the other sets. In this case, most of the sulfur must have already been extracted in step 1 of the BT.

***Table 4.5**. Comparison of amounts of sulfur in solution after the second step of the biotreatment.*

Set	Amount of sulfur in solution as sulfate (mM)[a]	Amount of total sulfur in solution (mM)[b]	% of sulfur as sulfate
A1	0.85	32.75	2.60
A2	1.01	64.60	1.56
B	1.49	6.25	19.95
C	1.56	32.71	4.77
D1	1.64	12.62	12.98
D2	1.97	15.10	13.08
E	1.08	2.15	50.53
F	1.06	97.59	1.09
G1	1.38	17.18	8.01
G2	1.54	18.70	8.24

[a] Calculated with IC.

[b] Calculated with ICP-OES.

Risk evaluation

pH measurements

After artificial contamination, the pH of the cubes increased to values between 10 and 13 due to the impregnation solution. This elevated pH reduced after the application of the different extraction treatments (Figure 4.8).

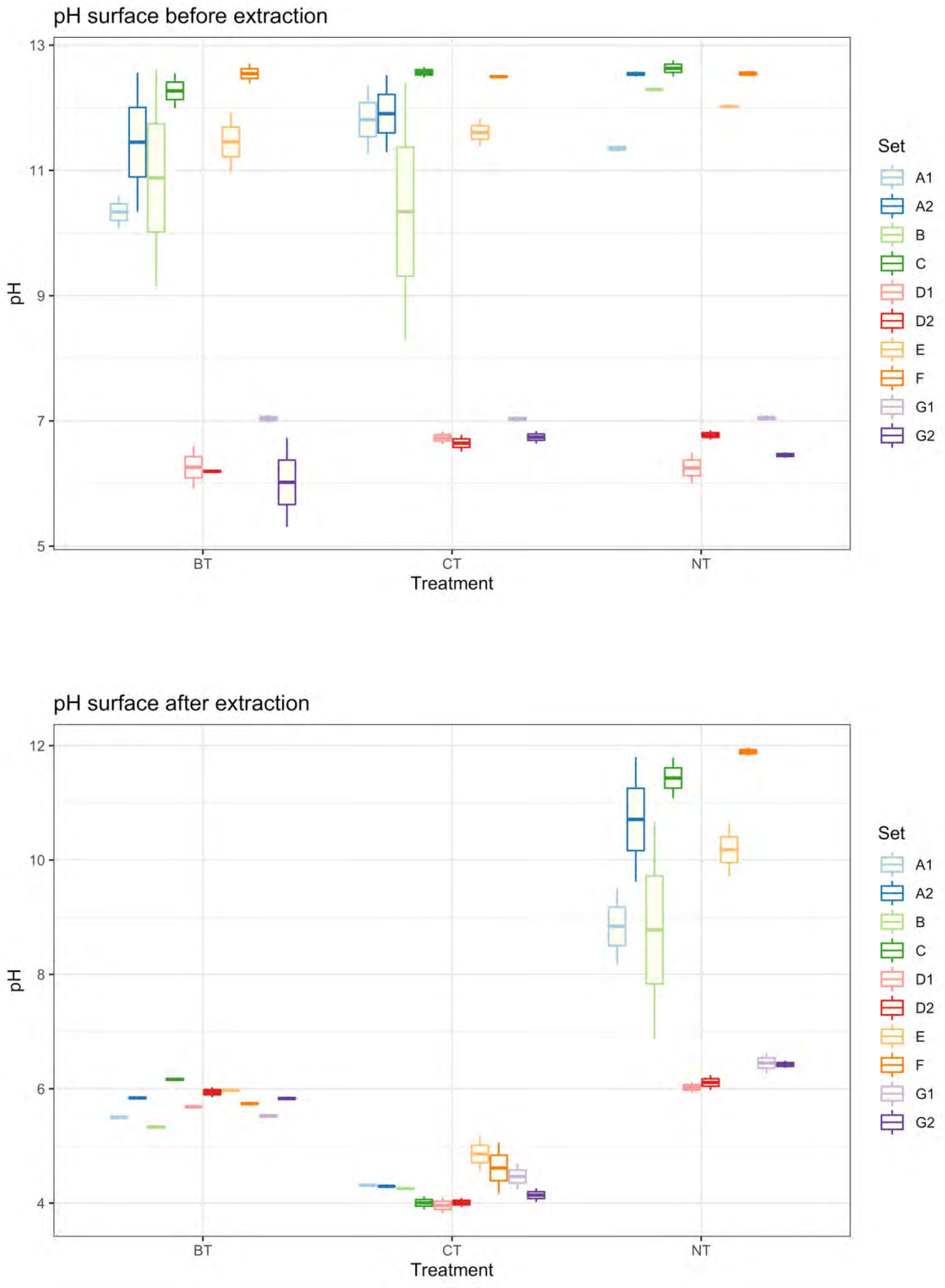

***Figure 4.8**. pH variation measured on the surface of the cubes for all sets before and after extraction treatment. BT: biological treatment, CT: chemical treatment, and NT: untreated.*

The pH was measured on the cubes surfaces after extraction and rinsing with deionised water. The biological treatment is not buffered during the DFOM step and buffered to neutrality (pH 7) during the bacteria step (Figure S 4.5). During the DFOM step, the pH varies depending the amount of iron in solution. With high amounts of iron, the pH is quite constant around 8.4 (pKa_1 DFO≈8.4) [11], [12]. Sets D1, D2, G1 and G2 that presented lower concentrations of iron, maintained a lower pH in solution (5-6) during this step. During the application of *T. denitrificans*, all solutions remained close to pH 7, some increasing a little (Figure S 4.5). However, the pH on the surface of the cubes after BT and rinsing was close to the pH of deionised water, between 5.3 and 6.1 (Figure 4.8). The extraction solutions were efficiently removed, and the pH was in range to the values observed in the reference woods. Fresh woods presented a pH ~5 before contamination.

The CT used as reference here presents acidic conditions (pH 1.5–4). The first step of the CT is the most acidic, the cubes were exposed to pH of 1.5 for 24 h (Figure S 4.5). However, at the end of CT and after rinsing, the cubes recovered to a pH on surface ~4 (Figure 4.8). Most species of wood are naturally acidic, having a pH between 4.0 and 5.5 [49]. Still, cellulose and hemicellulose dissolve in strong acids [50]. In case longer application times are needed, this protocol would be very harmful for the wood components.

Untreated cubes suffered a decrease in the surface pH over time. This could be due to the wash out of the impregnation solution or because of the oxidation of the iron and sulfur species formed. The oxidation of these species is usually related to the production of acids and decrease in pH [10].

FTIR analyses

The secondary effects of the treatment in the wood were controlled by FTIR. Before extraction, differences could be observed between the spectra from fresh and archaeological wood sets (Figure S 4.4). Vibrational bands at 1034 and 1059 cm^{-1} were very intense for fresh wood and decreased in intensity for archaeological wood sets. Only set F (Figure S 4.54 which is lake pinewood presented a mean spectrum similar to fresh samples. These bands were assigned to C–O stretching of holocellulose and lignin [51]. Moreover, the intensity of vibrational band at 1738 cm^{-1} assigned to C=O stretching in xylan, a component of hemicellulose [52], decreased for archaeological wood sets. All these observations suggested a higher decay of holocellulose within the archaeological wood sets. Archaeological samples displayed intense band at 1650 cm^{-1} attributed to H_2O deformation due to the water absorbed by the wood during burial time

(Figure S 4.4). The vibrational bands at 1237 and 1267 cm^{-1} were assigned to C–O stretching (lignin and xylan) and to C–H and O–H wagging (cellulose and xylan) [27], [53]. Generally, a higher intensity of these bands was observed for fresh wood presenting differences between the wood species.

After extraction, FTIR spectra recorded on untreated (NT) samples were considered as reference for the characterization campaign. The bands at 1034 and 1059 cm^{-1} were still observed for fresh samples (Figure S 4.4). All sets presented adsorbed water with a characteristic band at 1650 cm^{-1} after artificial contamination. Archaeological samples still had bands less intense in the range 1400–1200 cm^{-1}, suggesting that the protocol of degradation of fresh wood was not comparable to natural degradation. However, none of the sets displayed the band at 1738 cm^{-1}, meaning that xylan content was probably successfully degraded for all wood samples (Figure S 4.4).

Table 4.6 shows the calculated ratios from FTIR bands (R1=I(1158)/I(1506), R2=I(1374)/I(1506), and R3=I(1034)/I(1506)). Ratios estimate the amount of carbohydrates over lignin. When comparing to fresh wood, a general decrease of the ratios was observed. This suggests a degradation of holocellulose content after artificial degradation and contamination. However, pinewood artificially contaminated sets showed special behaviour. The artificial contamination did not degrade wood content as the values for R3 ratio in NT samples in sets E and F are in the same range as fresh pine. R3 ratio is based on the height of the vibrational band at 1034 cm^{-1} attributed to C–O stretching of holocellulose and lignin [52]. Comparing with literature, waterlogged pine wood generally present higher ratio values than oak species [54]. It seems that the impregnation protocol has a different effect depending on wood specie leading to different states of carbohydrates degradation. Intern structure of these pinewood species (porosity, presence of resin canals) may lead to different degradation processes. For example, Neolithic pine was reported to be a yellow and hard wood while Neolithic oak was described as yellow-red wood with the heartwood well preserved, but the sapwood often decayed [55]. To reach similar state of degradation, a longer water pre-immersion time or increase of vacuum, forcing the structure to collapse should be applied on fresh wood samples (A1, A2, B and E) in further experiments.

After extraction, whatever the treatment (BT or CT) applied, the ratios calculated were in range with the reference ones (NT) (Table 4.6). This observation suggests that the extraction methods did not have any impact on the wood matrix. The treatment applied on the samples did not affect the carbohydrates content, whether it was a chemical or a biological treatment. Previous

experiments have already demonstrated that *T. denitrificans* was harmless for wood substrate (Chapter 3). Iron extraction with siderophores as first extraction step did not interfere with the substrate neither. However, CT application led to an important aesthetic change (Figure 4.4). If the ratios are not impacted, the hypothesis is that minor wood components such as extractives may react during extraction, or the action of the persulfate could lead to discoloration of the wood surface.

***Table 4.6**. FTIR ratios (R1=I(1158)/I(1506), R2=I(1374)/I(1506) and R3=I(1034)/I(1506)) calculated. Adapted from* [38].

	Set	Extraction method	R1 (H/L)	R2 (C/L)	R3 (H/L)
Ref.:	Fresh balsa	-	1.16 (±0.05)	1.07 (±0.03)	1.65 (±0.24)
	Fresh oak	-	1.08 (±0.04)	1.01 (±0.03)	1.55 (±0.20)
	Fresh pine	-	1.05 (±0.01)	1.00 (±0.00)	1.21 (±0.04)
	A1	BT	0.91 (±0.03)	0.94 (±0.01)	1.05 (±0.07)
		CT	0.93 (±0.02)	0.94 (±0.00)	1.10 (±0.07)
		NT	0.88 (±0.02)	0.93 (±0.01)	0.97 (±0.05)
	A2	BT	0.93 (±0.02)	0.94 (±0.01)	1.07 (±0.07)
		CT	0.92 (±0.03)	0.95 (±0.01)	1.07 (±0.07)
		NT	0.89 (±0.02)	0.94 (±0.01)	0.99 (±0.05)
	B	BT	0.95 (±0.04)	0.94 (±0.01)	1.21 (±0.13)
		CT	0.98 (±0.03)	0.94 (±0.01)	1.30 (±0.11)
		NT	0.92 (±0.04)	0.98 (±0.03)	1.17 (±0.11)
	C	BT	0.87 (±0.01)	0.91 (±0.01)	0.95 (±0.03)
		CT	0.85 (±0.01)	0.91(±0.01)	0.90 (±0.03)
		NT	0.90 (±0.01)	0.91 (±0.01)	0.99 (±0.03)
	D1	BT	0.89 (±0.02)	0.91 (±0.01)	0.98 (±0.03)
		CT	0.88 (±0.03)	0.91 (±0.01)	0.98 (±0.03)
		NT	0.90 (±0.01)	0.92 (±0.01)	1.01 (±0.03)
	D2	BT	0.86 (±0.01)	0.91 (±0.01)	0.94 (±0.03)
		CT	0.87 (±0.06)	0.92 (±0.03)	0.96 (±0.12)
		NT	0.85 (±0.02)	0.92 (±0.00)	0.91 (±0.04)

Table 4.6. Continuation

E	BT	1.01 (±0.06)	0.97 (±0.02)	1.47 (±0.02)
	CT	1.00 (±0.05)	0.96 (±0.02)	1.42 (±0.18)
	NT	0.97 (±0.03)	0.95 (±0.01)	1.24 (±0.11)
F	BT	0.95 (±0.09)	0.95 (0.03)	1.31 (±0.37)
	CT	0.98 (±0.09)	0.96 (±0.03)	1.37 (±0.34)
	NT	0.98 (±0.06)	0.95 (±0.02)	1.27 (±0.26)
G1	BT	0.85 (±0.02)	0.92 (±0.01)	0.93 (±0.07)
	CT	0.87 (±0.04)	0.93 (±0.02)	0.98 (±0.10)
	NT	0.84 (±0.01)	0.92 (±0.01)	0.90 (±0.06)
G2	BT	0.85 (±0.01)	0.91 (±0.01)	0.89 (±0.02)
	CT	0.88 (±0.03)	0.91 (±0.01)	0.95 (±0.09)
	NT	0.83 (±0.00)	0.92 (±0.01)	0.84 (±0.03)

Conclusion

Eco-friendly solutions for the conservation of cultural heritage are promising if their outcomes are comparable with traditional methodologies. After application of the defined biological treatment (BT), reduced sulfur compounds identified by Raman spectroscopy were not detected anymore, while elemental sulfur was still present in softwood samples (sets E and F) after chemical treatment (CT). The wood type may have higher impact on the efficiency of the chemical extraction than in the one of the bio-based treatment. BT was compatible with all the different type of wood used in this study. Performance was not influenced by the species of wood nor the state of degradation. However, iron extraction was lower for BT than CT. EDTA was applied in higher concentrations than DFOM, and the latest has a higher molecular weight, what may influence diffusion. Even so, we obtained extraction rates of ~75% for five wood sets (B, D1, E, F and G2). Improving the efficiency of the BT for iron extraction could involve longer extraction times, or ideally several consecutive extractions with DFOM.

On the contrary, sulfur extraction rates were higher for BT than CT, as expected taking into account the Raman results. Sulfates were detected in solutions with all wood sets treated with *T. denitrificans*. In some cases, higher concentrations of sulfates were expected in relation to the number of nitrates consumed. Especially in archaeological samples not artificially contaminated, we observed high $\Delta NO_3^-/\Delta SO_4^{2-}$ ratios. Other metabolisms, such as

heterotrophic denitrification, may have participated and/or autochthonous bacteria may have used the sulfates produced to form again hydrogen sulfide. In the next section (section 4.3), the study of the microbial community of samples from wood sets C and F, before any treatment or artificial contamination, revealed bacteria from genera that are known as denitrifying bacteria and others that are sulfate-reducing bacteria. Therefore, for future applications, is important to keep in mind the effect that the inhabiting bacteria may have in our extraction protocol. Further experiments including sterilized wood cubes could help to understand the effects of the autochthonous microbial community. Moreover, in this first experiment abiotic controls were not included. Therefore, the sulfates produced could also come from abiotic oxidation. Future research should determine up to what point the oxidation step with *T. denitrificans* is needed, especially if this step allows the development of autochthonous bacteria, and to evaluate the impact of extracting sulfur as dissolved sulfides instead of sulfates during the DFOM step.

Both treatments showed no further wood degradation as observed with FTIR measurements. Although, CT had a higher impact on the visual aspect of the wood samples. pH during treatment was highly acidic at some points of the CT, while the bio-based protocol kept more circumneutral conditions. Moreover, the bio-treatment can be considered more respectful for the environment and human health. EDTA is consider problematic as it tends to bioaccumulate in natural environments [56], and sodium persulfate is consider hazardous for the user requiring a specific training to be handled. Deferoxamine is not toxic and expected to degrade in the environment. *T. denitrificans* is a non-pathogenic bacterium (risk group 1) and the growth medium used does not represent either big environmental issues.

Mock-ups were useful in this study as the access to WAW samples is not always possible. However, the use of WAW samples with higher accumulation of iron sulfides is essential to further evaluate the defined extraction protocol.

Supplementary Material 4.2

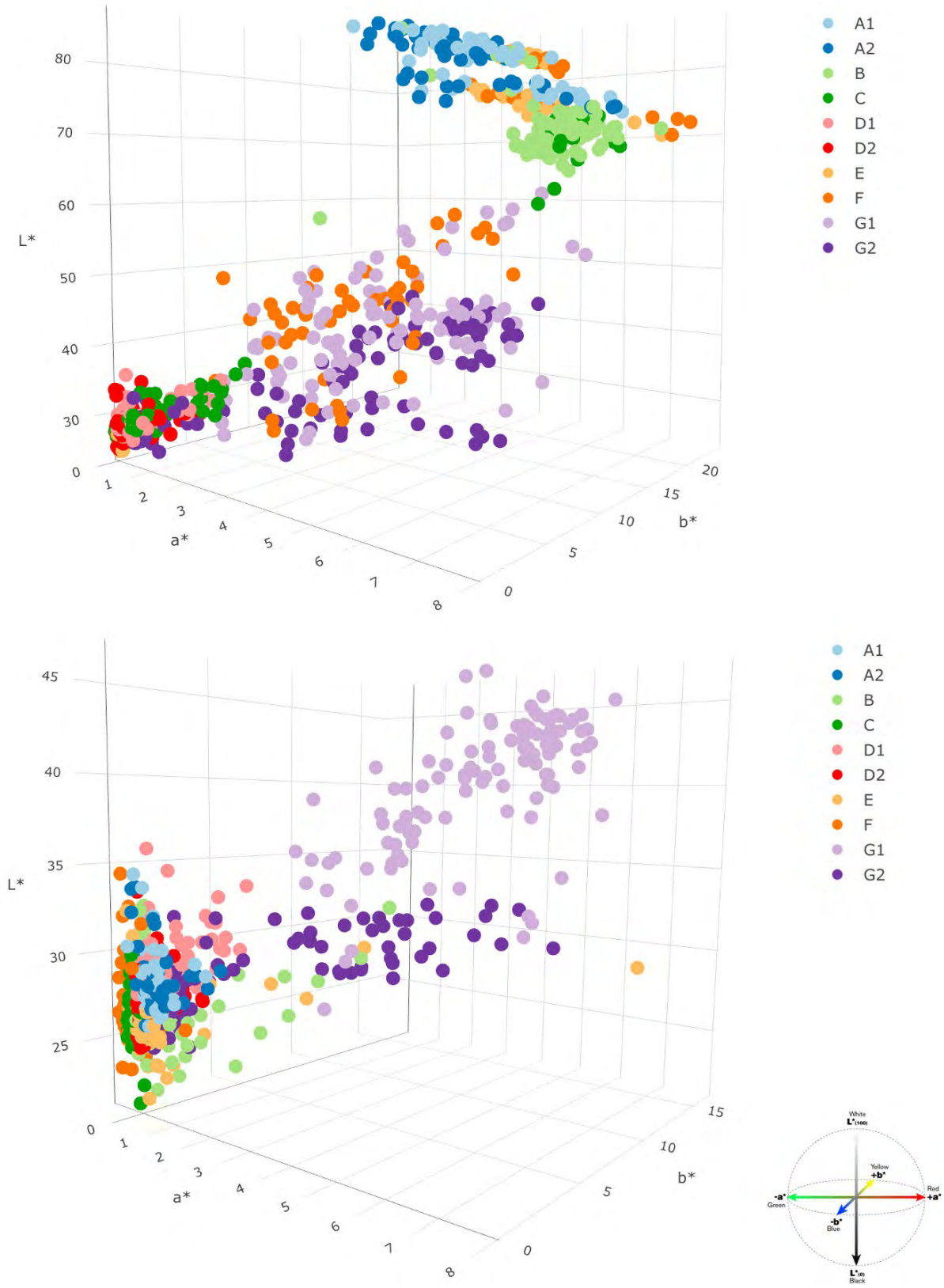

***Figure S 4.2**. Distribution of the wood cubes of all the different sets (A1, A2, B, C, D1, D2, E, F, G1 and G2) in L*-a*-b* colour space at T0 (above), and after impregnation-before extraction (T1) (below).*

***Table S 4.6**. Extraction rates of total iron for the two extraction methods (biological treatment (BT), and chemical treatment (CT)) under study.*

Treatment	Set	Total iron in solution after 1st step (mg Fe / g wood)[a]	Total iron in solution after 2nd step (mg Fe / g wood)[b]	Total iron in wood before treatment (mg Fe / g wood)	Total iron remaining in wood after treatment (mg Fe / g wood)	% of iron extracted
BT	A	2.68	1.43	17.41	6.62	61.97
	B	1.17	0.53	8.22	2.23	72.91
	C	2.48	1.67	14.64	7.40	49.46
	D1	0.32	0.15	1.36	0.47	65.15
	D2	0.41	0.15	3.10	2.26	27.14
	E	2.86	1.56	10.11	3.63	64.07
	F	1.95	1.34	7.58	1.93	74.59
	G1	0.07	0.05	0.30	0.16	46.16
	G2	0.48	0.20	2.04	0.69	65.75
CT	A	6.03	2.82	17.41	0.02	99.88
	B	2.75	2.38	8.22	3.05	62.89
	C	5.44	6.31	14.64	0.05	99.63
	D1	0.59	1.33	1.36	1.27	6.56
	D2	0.72	2.96	3.10	0.12	99.59
	E	2.98	5.07	10.11	0.02	99.78
	F	1.87	3.86	7.58	6.38	15.75
	G1	0.64	0.58	0.30	5.37	0.00
	G2	0.51	139.19	2.04	0.05	97.50

[a] 1st step of the extraction method refers to the siderophores (DFOM) solution for BT, and sodium persulfate solution for CT.

[b] 2nd step of the extraction method refers to the bacteria (*T. denitrificans*) solution for BT, and EDTA solution for CT.

Table S 4.7*. Extraction rates of total sulfur for the two extraction methods (biological treatment (BT), and chemical treatment (CT)) under study.*

Treatment	Set	Total sulfur in solution after 1st step (mg S / g wood)[a,*]	Total sulfur in solution after 2nd step (mg S / g wood)[b]	Total sulfur in wood before treatment (mg S / g wood)	Total sulfur remaining in wood after treatment (mg S / g wood)	% of sulfur extracted
BT	A	-	10.79	32.33	15.07	53.37
	B	-	3.26	7.21	5.24	27.24
	C	-	4.78	16.69	4.08	75.58
	D1	-	1.82	2.09	1.42	32.15
	D2	-	1.93	2.09	4.02	0.00
	E	-	1.86	28.41	12.85	54.77
	F	-	15.96	12.01	4.01	66.66
	G1	-	2.47	3.81	4.01	0.00
	G2	-	2.95	3.07	1.39	54.90
CT	A	0	7.83	32.33	5.47	83.07
	B	0	5.21	7.21	23.36	0.00
	C	0	6.86	16.69	15.54	6.92
	D1	4.05	8.59	2.09	4.51	0.00
	D2	9.12	6.32	2.09	5.11	0.00
	E	0	3.99	28.41	16.86	40.64
	F	11.73	7.01	12.01	6.38	43.30
	G1	11.85	5.04	3.81	3.53	7.25
	G2	7.46	6.45	3.07	3.47	0.00

[a] 1st step of the extraction method refers to the siderophores (DFOM) solution for BT, and sodium persulfate solution for CT.
[b] 2nd step of the extraction method refers to the bacteria (*T. denitrificans*) solution for BT, and EDTA solution for CT.
[*] Accurate calculations of sulfur concentrations in the solution of the BT-DFOM step were not possible due to interferences in the method used (ICP-OES).

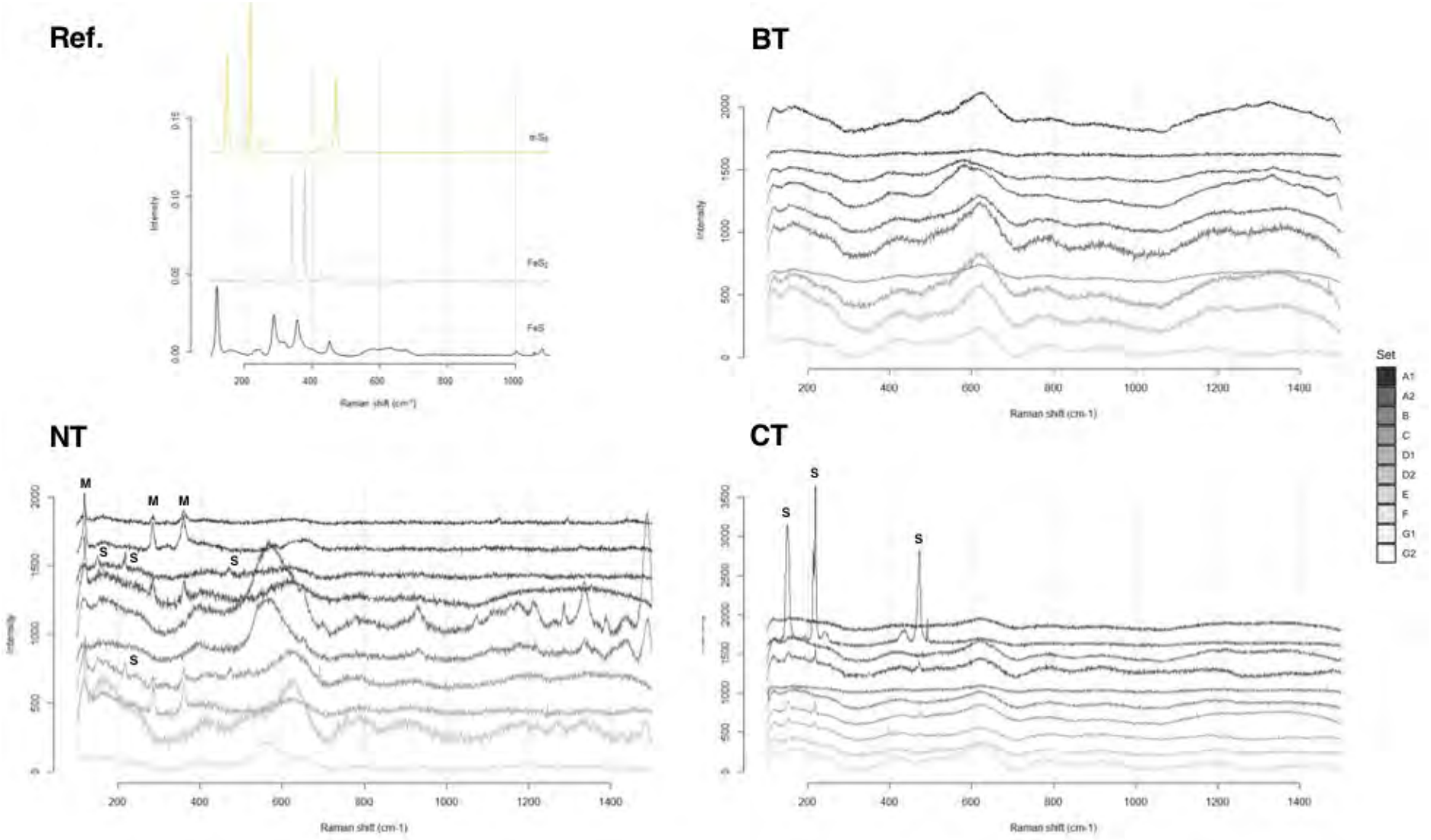

Figure S 4.3. *Raman spectra of reference (Ref.) compounds sulfur (α-S_8), pyrite (FeS_2), and partially oxidized mackinawite ($Fe_{1-x}S$). Raman spectra obtained on untreated (NT), biologically treated (BT), and chemically treated (CT) samples. Elemental sulfur (S) and partially oxidized mackinawite (M) characteristics shifts are indicated.*

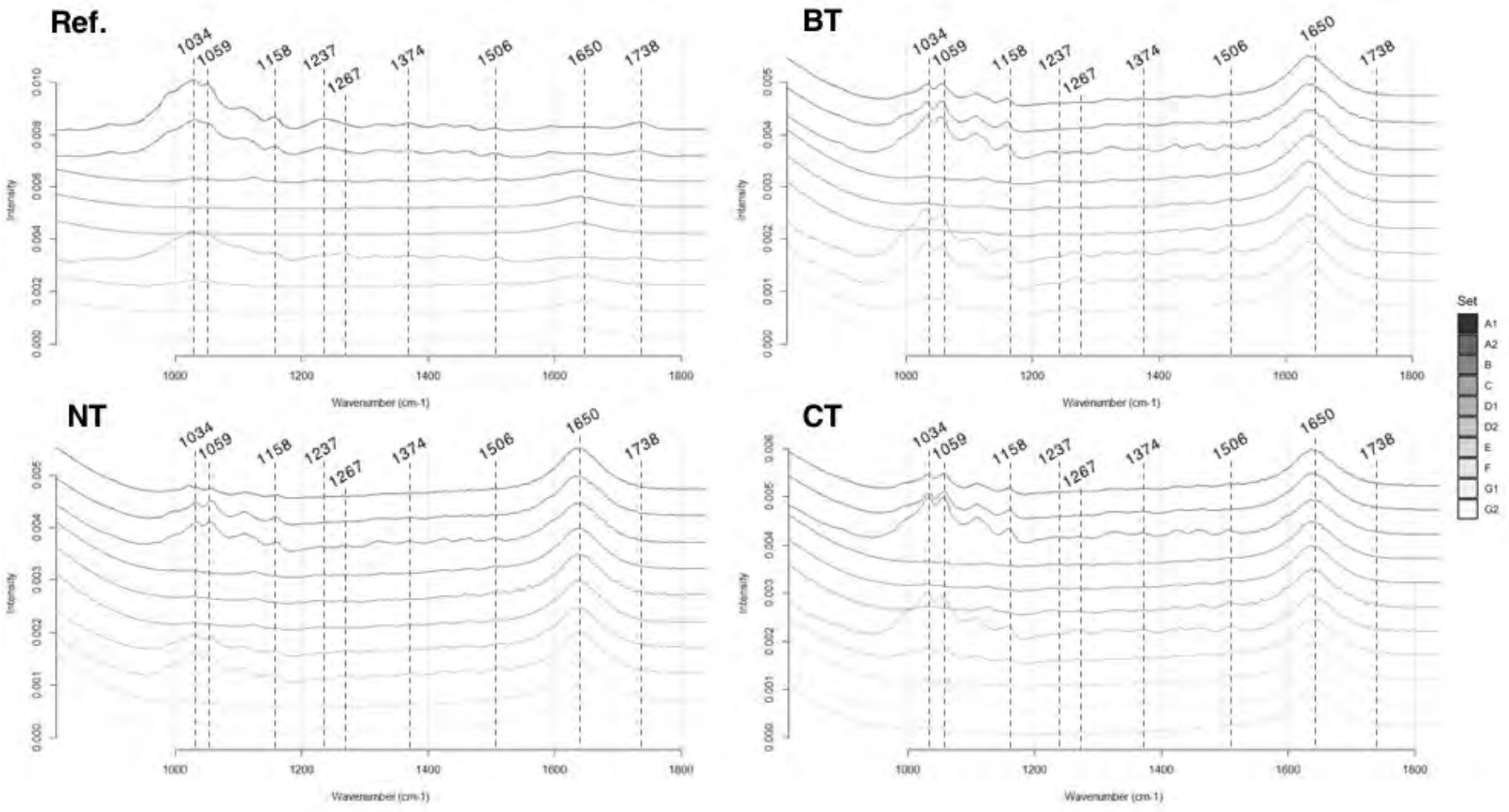

Figure S 4.4. *FTIR spectra recorded on the surface of the cubes before any treatment or artificial contamination (Ref.), untreated (NT), biologically treated (BT) and chemically treated (CT). In the reference spectra, first spectrum corresponds to sets A1 and A2 combined. The peak values indicated are related to wood components and defined in the text.*

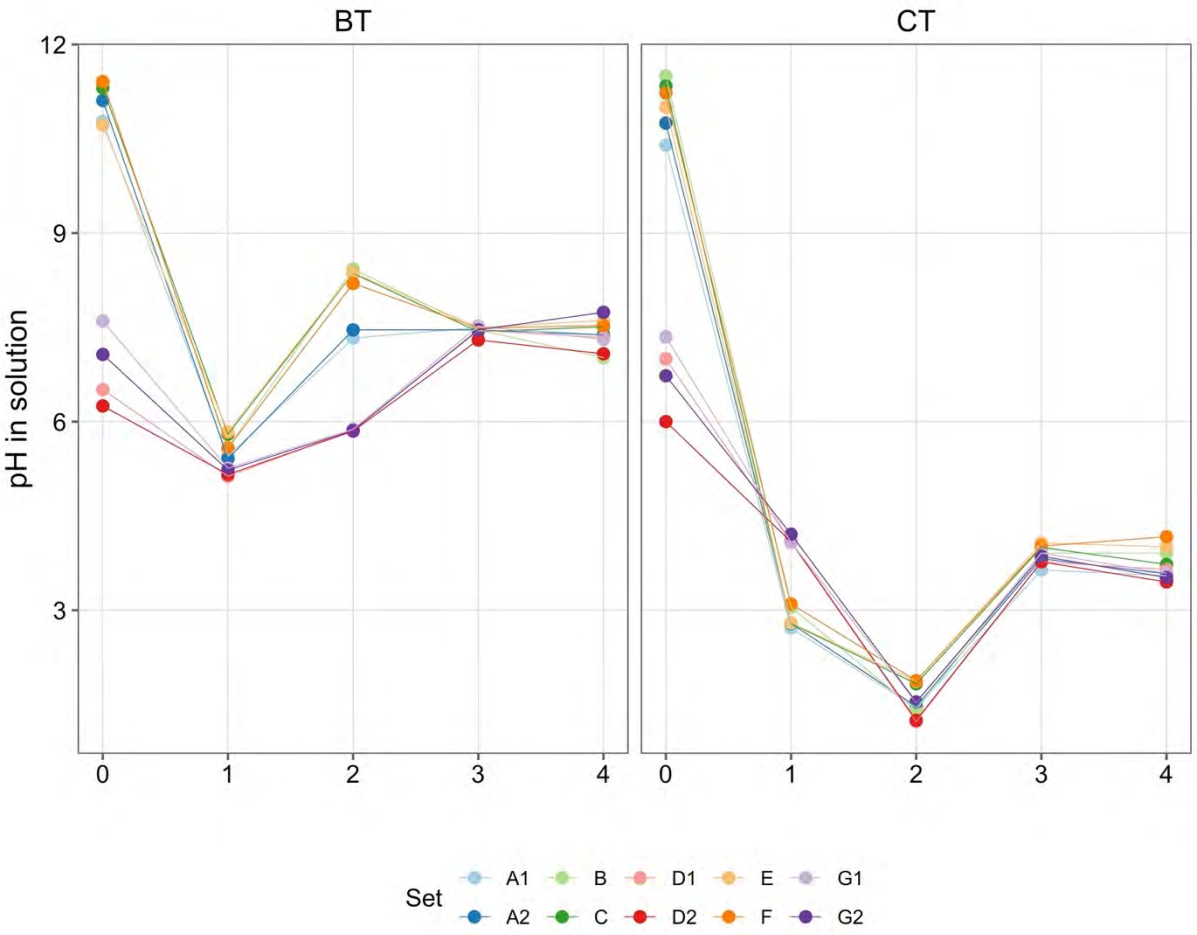

Figure S 4.5. *pH variation measured on the extraction solutions of the biological treatment (BT) and the chemical treatment (CT) at the different steps of the extraction protocol. 0: pH in solution after adding the cubes, 1: pH in solution at T0 of the first step (BT-DFOM, CT-Sodium persulfate), 2: pH in solution at the end of the first step, 3: pH in solution at T0 of the second step (BT-T. denitrificans, CT-EDTA), and 4: pH in solution at the end of the second step.*

4.3 Study of the microbial community

Abstract

Waterlogged wood represents an ideal habitat for the development of a specialised microbial community. Culture, microscopic and DNA analyses have shown a hydrolytic population that is responsible for the biodegradation of the wood material. Moreover, the decay microorganisms are often accompanied by others with specific metabolisms, such as sulfate-reducing bacteria (SRB). The autochthonous microbial community could interfere with the above-defined extraction treatment, for instance, SRB metabolism is opposite to the desired oxidation of sulfur. In this preliminary study, we investigated the microbial community of different waterlogged wood samples. First, freshwater wood samples from Biel Lake and other Swiss locations were incubated with fresh wood to detect if the microbial community was still active. Growth was positive, but microscopic analysis revealed that the colonization of the fresh wood samples was very low or inexistent. Longer time periods are needed for the proper establishment of the community in fresh wood. The biodegradation process by bacteria is usually defined as slow. Fungi development was not observed with our samples. Also, microscopic analysis did not show sign of fungal attack. Finally, DNA was extracted from some of the wood samples and the bacterial community was analysed. Differences were observed between oak and silver fir samples in terms of alpha and beta diversity. Overall, silver fir samples presented higher bacterial diversity. The taxonomy composition indicated that oak samples were dominated by the phylum Proteobacteria; while silver fir samples had taxa belonging to the phyla Proteobacteria, Firmicutes, Actinobacteria and Chloroflexi in higher abundance. Genera *Janthinobacterium*, *Pseudomonas* and *Flavobacterium* were detected in all samples, showing some members of the wood degraders community. Moreover, genera like *Desulfomonile*, *Desulfosporosinus* and *Desulfovibrio* were also detected. These results confirmed a bacterial community composed by wood degraders and scavenging bacteria, including SRB.

Introduction

Bio-based methods constitute a promising approach for the preservation of cultural heritage. Many examples have shown the effectiveness of biological processes to clean, repair, and protect heritage artefacts [57]–[60]. However, to define an efficient strategy for the preservation of cultural heritage, it is important to characterize the present autochthonous microbial community. Undesired metabolisms or uncontrolled microbial colonization could occur as

consequence of the treatment [61]. For example, in the past, some biocide treatments triggered the development of more resistant and harmful microorganisms [62]. Today, molecular methods to identify the inhabiting microbial community are widely adopted in the field of cultural heritage to have a clearer picture of possible interactions with preservation treatments [62], [63].

Waterlogged wood is decayed mostly by bacteria as fungal activity is reduced in waterlogged environments [64]. Many studies have investigated the degrative activity of microorganisms in WAW through microscopic and isolation/culture analysis [28], [51], [65]–[67]. The visual observations detected specific morphologies of wood decay, and the bacteria were divided into three groups, i.e. erosion, tunnelling, and cavitation bacteria [28]. These bacteria form the group of primary degraders of waterlogged wood (or simply referred as erosion bacteria, EB). Moreover, EB are usually associated with scavenging bacteria. Scavenging bacteria profit from the residual material left by the proper wood degraders. Sulfate-reducing bacteria (SRB), are commonly detected as scavenging bacteria, and a possible consortia between primary wood degraders and SRB cannot be ruled out [28]. Yet, little is known about the taxonomy of the bacteria colonising WAW. Some studies in pure cultures of erosion bacteria revealed species belonging to the CFB (*Cytophaga–Flavobacterium Bacteroides*) complex [67], [68]. Other research, also in pure cultures, showed the presence of Spirochaetes, Alpha-, Beta- and Gamma-Proteobacteria [69]. However, culture-based analysis can skip part of the population. More recently, next-generation sequencing (NGS) was applied to study WAW samples and gain insight of the autochthonous microbial community of such objects. These studies certified the presence of CFB bacteria, and also revealed the presence of other microorganisms with ability to degrade complex organic materials, such as *Pseudomonas*, *Janthinobacterium* or *Halomonas* [70], [71]. Moreover, in all cases bacteria involved in the iron and/or sulfur cycle were found representing a small fraction of the community [70]–[72].

In this preliminary study, the aim was to analyse different waterlogged wood pieces to better understand possible interaction between the defined biological extraction treatment and the autochthonous microbial community. In this experiment, we focused only on the archaeological samples from the previous section (wood sets C, D1, D2, F, G1 and G2). Moreover, DNA analyses were conducted in wood samples only before the biological extraction treatment. Therefore, the original microbial community of WAW samples was studied here and not the community present during treatment. Still, complementary culturing and DNA analyses gave

us a better understanding of the wood microbial community and the possible interaction with the bio-treatment.

Materials and Methods

Isolation of EB-SRB

Parallelly to the extraction experiments of section 4.2, two pieces of wood of every waterlogged wood set (C, D1, D2, F, G1 and G2) were incubated each with one cube of fresh pine of and one cube of fresh oak wood of 2x2x2 cm^3 in independent jars. The wood cubes did not suffer any artificial contamination or sterilization protocol before incubation with the new fresh wood.

Prior to addition of the wood, jars were filled with sterile BAK-7 medium [67], and autoclaved. Fresh pine and oak wood were autoclaved in dry mode. The fresh and waterlogged wood were then added to the jars in sterile conditions. Jars were incubated up-side down at RT. The growth of EB-SRB was monitored over time taking small samples of fresh wood in sterile conditions and analysing them under light microscopy. The production of hydrogen sulfide in the jars detected as strong egg-like smell was also an indicator of growth.

Microscopy analysis

Light microscopy

Samples from the waterlogged wood sets (C, D1, D2, F, G1 and G2) were analysed before incubation. Samples of fresh wood were investigated over time using light microscopy to detect attack of EB. Thin cross, radial and tangential sections were cut by hand using a razor blade. Sections were observed directly without staining and also after staining with 1% (w/v) red safranin in ethanol to highlight the wood morphology.

Scanning Electron Microscopy coupled with Energy Dispersive X-Ray Spectroscopy (SEM-EDS) analyses

Samples from the waterlogged wood sets (C, D1, D2, F, G1 and G2) were analysed before incubation. After incubation, samples of fresh wood were selected to be analysed. Wood samples were cut into small slices using a razor blade. Wood segments were fixed at RT with 3% (v/v) glutaraldehyde solution in 0.1 M sodium cacodylate (pH 7.2) for 3h, washed twice and then dehydration steps were performed using different concentrations of ethanol (25%, 50%, 75%, 90%, 100% (v/v)) and then pure acetone.

Samples were mounted on stubs using carbon conductive tape. Samples were examined under low vacuum without coating using a Thermo Scientific™ Scios™ 2 DualBeam™ (Thermo

Fisher Scientific, United States) equipped with an energy-dispersive X-ray analyser (EDAX, United States). Afterwards, the same samples were coated with a layer of gold using a Leica EM SCD050 (60 mA current, 5 cm, 5 s duration, argon gas), and examined again at high vacuum using the same instrument.

DNA Sequencing

DNA extraction

In parallel to the isolation of EB-SRB and the extraction methods of previous section, DNA analyses of some of the wood cubes were also conducted. At this point, the microbial community of WAW coming from freshwater was studied. Eight wood samples were collected from sets C (oak) and F (silver fir) right after excavation from Biel Lake (Switzerland). From each wood, two samples were recovered right under the surface of the wood pole, and two from the core of the wood pole. The samples were collected with the help of a sterile scalpel. All samples were frozen right after collection and kept at -20 °C until analysis. Description of the samples is included in table S 4.8. Later, 500 mg of each sample were used to extract total DNA. Prior to extraction, wood samples were homogenized using an agate mortar previously sterilized with ethanol. FastDNA® SPIN kit for soil was used according to the manufacturer's instructions (MP Biomedicals, Unites States). After extraction, DNA concentrations were measured with Qubit Fluorometer using the dsDNA BR (broad range) and HS (high sensitivity) Assay Kit (Invitrogen, United States).

Ethanol Precipitation of DNA

Ethanol precipitation of DNA was performed following the next protocol: 0.1 volumes of 3 M sodium acetate were added with 2.5-3 volumes of pure ethanol (ice cold) to the extracted DNA. The whole suspension was mixed thoroughly. Precipitation was done overnight at -20 °C. Precipitated DNA was centrifuged at full speed (13000 rpm) at 4 °C for 30 min. The pellet was washed twice with 0.5 mL ice cold 75% ethanol and centrifuged again for 10 min each time. The ethanol was removed, and the pellet was spined quickly to remove trace amounts of ethanol. The pellet was air dried and resuspended in an appropriate volume of nuclease free water. DNA concentrations were measured again with a Qubit Fluorometer using the dsDNA HS Assay Kit (Invitrogen, United States).

Polymerase Chain Reaction (PCR)

First assessment of the presence of bacteria and fungi in the samples was conducted by polymerase chain reaction (PCR). PCR amplifications of the *16S rRNA* gene (for bacterial) and

the internal transcribed spacer (ITS) region (for fungi) were done using Taq DNA polymerase (NEB) with ThermoPol buffer (New England Biolabs, United States). The reaction was performed in a final volume of 25 µL containing 1X ThermoPol Buffer, 0.2 µM of forward (16S: gm3f, ITS: ITS1F) and reverse primers (16S: gm4r, ITS: ITS 4), 0.2 µM of deoxynucleotide triphosphate mix (Promega, United States), 1X bovine serum albumin (BSA), 1 U of Taq DNA polymerase and 2 µL (for 16S) and 1 µL (for ITS) of diluted sample (4 ng DNA·µL^{-1}). The volume was completed with double sterilized Milli-Q® water. DNA of *Bacillus subtilis* was used as positive control for the bacterial PCR and *Aspergillus sp.* for the fungal PCR. In both cases, sterile distilled water was used as negative control.

PCR was performed with Thermo Scientific Arktik Thermal Cycler (Thermo Fisher Scientific, United states). The program for the bacterial PCR was the following: initial denaturation at 94 °C for 10 min, followed by 35 cycles of 1) denaturation at 94 °C for 30 s, 2) annealing at 51 °C for 45 s, and 3) elongation at 68 °C for 1 min. The final elongation was performed at 68 °C for 5 min. The program for the fungal PCR was the following: initial denaturation at 95 °C for 2 min, followed by 35 cycles of 1) denaturation at 95 °C for 30 s, 2) annealing at 61 °C for 30 s, and 3) elongation at 68°C for 1min. The final elongation was performed at 68 °C for 5 min.

PCR products were checked by gel electrophoresis. The gel consisted of 1% (w/v) agarose in 0.5X TAE (Tris base, acetic acid and EDTA) buffer. 3 µL of StainIN™ GREEN Nucleic Acid Stain (HighQu GmbH, Germany) were added to the gel. 5 µL of PCR product plus 1 µL of loading buffer (Biotium, United States) were loaded to the gel along with a 1Kb Bench Top ladder (Promega, United States) and run for 30 min at 100 V. The gels containing DNA were visualized in GenoPlex chamber (VWR, United States). PCR showed no ITS amplification. Further sequencing was conducted only for bacterial community.

Sequencing

Amplicon sequencing was performed on an Illumina MiSeq platform, using the services of Fasteris SA (Switzerland). For the bacterial community analysis, the regions V3-V4 of the *16S rRNA* gene were targeted using universal primers 341F (5'-CCTACGGGNGGCWGCAG-3') and 805R (5'-GACTACHVGGGTATCTAATCC-3') [73]

The Illumina reads were processed with QIIME 2 (version 2020.6) [74], according to the standard pipelines. Raw sequence data was received demultiplexed. Directly after importing was denoised using DADA2 (via q2-dada2) [75]. All amplicon sequence variants (ASVs) were aligned with mafft [76] and used to construct a phylogeny with FastTree 2 [77] (via q2-

phylogeny align-to-tree-mafft-fasttree). Alpha diversity metrics (Shannon's diversity index [78], Chao1 index [79], Pielou's evenness [80] and Faith's phylogenetic diversity [81]) and beta diversity metrics (Bray-Curtis dissimilarity [82], and weighted UniFrac distance [83]) were estimated using q2-diversity after samples were rarefied to 44698 sequences per sample (Figure S 4.9). Taxonomy was assigned to ASVs using the q2-feature-classifier [84] classify-sklearn Naïve Bayes taxonomy classifier, trained against the most updated version of the SILVA database (release 132) [85]. Assessment of significant variation of alpha diversity between categories was determined using the Kruskal–Wallis test. Beta diversity significance was calculated with PERMANOVA test. Graphics about taxonomic composition, multivariate analyses and diversity analyses were done using Calypso [86].

Results and Discussion

Isolation and microscopy analyses

All analysed wood samples presented a high state of degradation, except for the samples of set F (Figure 4.9). SEM analyses revealed highly decayed cells where the secondary cell wall was detached from the middle lamella (Figure 4.9). The degradation was particularly evident when comparing, set F samples to the other wood. Set F presented cells without cell wall detachment or any kind of visual decay (Figure 4.9). The other samples showed the accumulation of debris from the degradation in the lumen, a part of detached cell walls (Figure 4.9). The accumulated granular material has been described as a mixture of bacteria, slime and residual lignin [64]. The observed decay is representative from the attack of EB [51], [64].

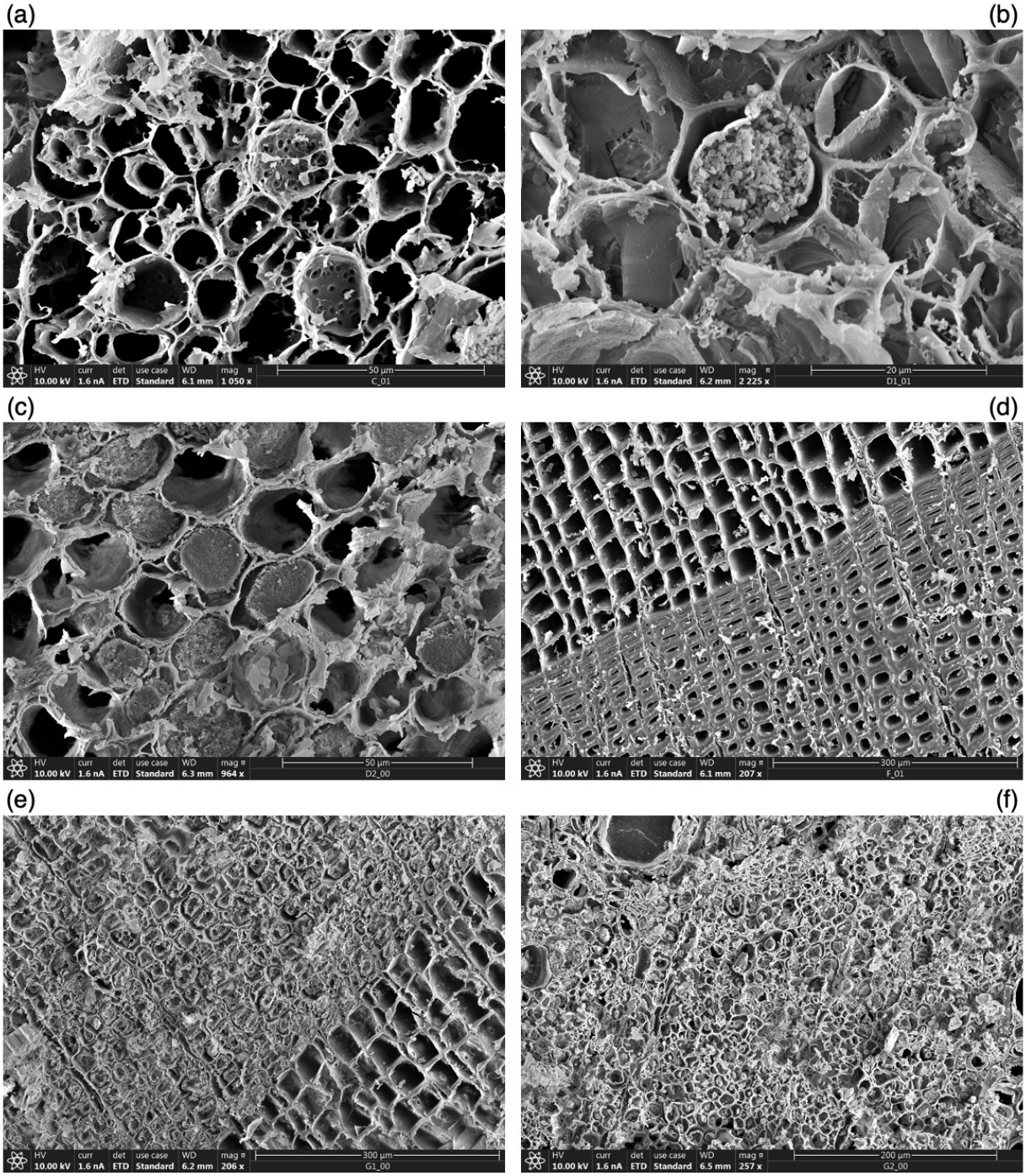

Figure 4.9. *Secondary electron micrographs of cross-sections from archaeological wood sets: (a) C, (b) D1, (c) D2, (d) F, (e) G1, and (f) G2.*

Sulfur and iron were detected in some samples with EDS (Figure 4.10 and Figure S 4.6). The detection was heterogenous with only some of the spots analysed showing these elements (44% and 16% of iron and sulfur detection, respectively, in relation to all analysed samples). As discussed in the previous section, these wood samples come from freshwater locations (Switzerland) and are originated from pre-Iron age. These conditions are not expected to favour high iron sulfides accumulation within the woods [20]. Even so, after a month of incubating the WAW sets with fresh wood some of the bottles already presented a strong egg-like smell. This indicates that sulfur bacteria were present in WAW and that although iron sulfides were not detected (see Raman analysis in previous section), reduced sulfur is likely to be present.

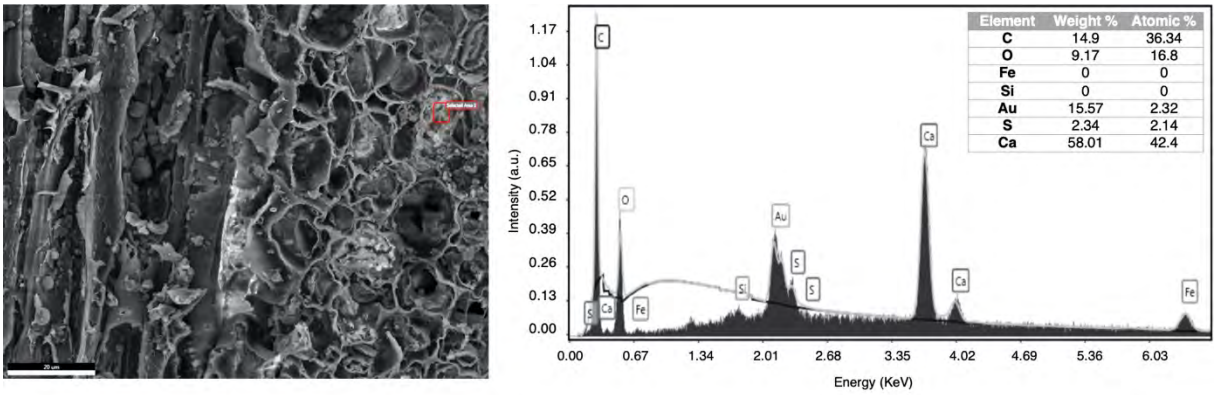

***Figure 4.10**. SEM image and correspondent EDS spectrum (red area) of a thin wood cut from set G2.*

At the end of the incubation experiment (4 months), most of the bottles had egg-like smell. Especially, bottles incubated with sets C and D1 wood presented the strongest smell, and the fresh wood acquired a black coloration (Figure 4.11). Thin sections from the fresh wood incubated with sets C and D1 were selected to be analysed with SEM-EDS. Analyses revealed some precipitates on the surface (Figure 4.11). In the case of wood incubated with set D1, some sulfur and iron was detected with EDS (Figure 4.11). For the fresh wood incubated with set C, mineral concretions were observed with SEM, but in this case, the elemental composition was mostly phosphorous and iron (Figure 4.11). Sulfur was also detected in the analysed fresh wood samples incubated with set C, but in lower proportion (Figure S 4.7). Previous studies that incubated an EB-SRB consortium with fresh pine wood detected high accumulation of sulfur in all samples [28]. However, this study incubated the samples for over 2 years and the inoculum

was an isolated EB-SRB consortium instead of wood pieces [28]. Long incubation periods may turn out to similar accumulation of sulfur in the fresh woods.

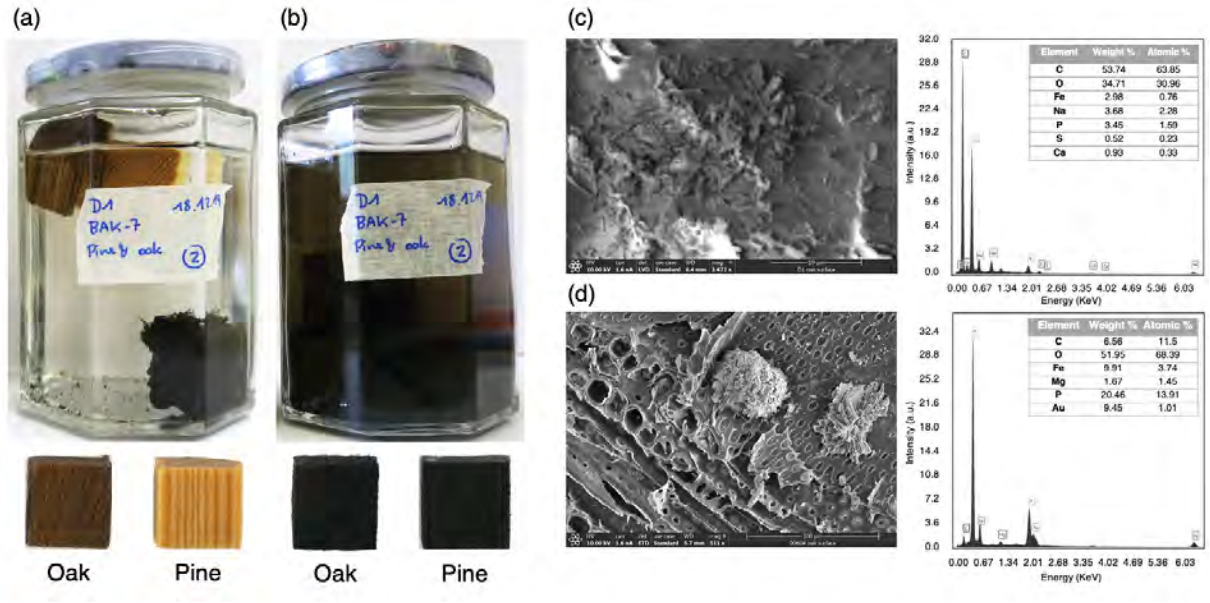

Figure 4.11. *Visual aspect of the culture bottles and fresh wood (oak and pine) at (a) T0 of the experiment and (b) at the end of the incubation time. (c) Secondary electron micrograph and corresponding EDS spectrum from a selected sample of fresh oak wood incubated with D1 wood. (d) Secondary electron micrograph from a selected sample of fresh oak wood incubated with C wood. EDS spectrum corresponding to a point from the mineral concretions observed.*

Light microscopy also showed highly decayed cells for some archaeological wood (Figure 4.12). The detachment of the cell wall was clearly detected in some cells, with accumulation of decay products in the lumen (Figure 4.12). However, the incubated fresh wood did not present as highly damaged cells (Figure 4.12). Samples taken over time presented early stages of EB attack (Figure 4.12). In figure 4.12-c, the invasion of EB through the rays of the fresh pine wood is seen as dark areas. Also, the dark mass observed in the lumen of some cells, in both oak and pine fresh wood (Figure 4.12), could be representative of the accumulation of cell wall degradation products [28]. Moreover, complementary SEM analyses of selected samples showed bacteria attached to the wood surface (Figure 4.12).

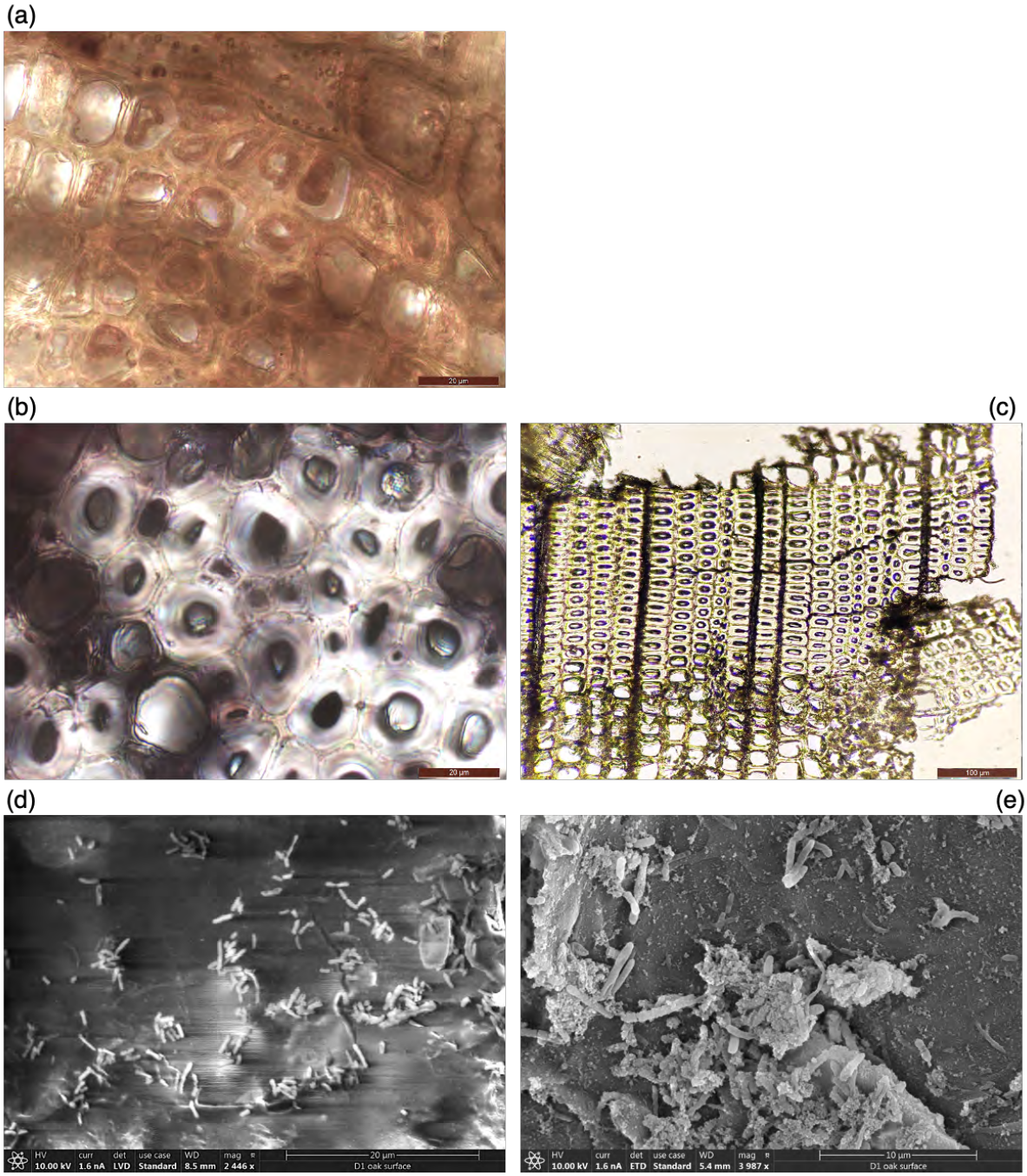

Figure 4.12. *Light microscopy images from cross-sections from (a) D1 wood, (b) fresh oak wood incubated with D1 wood and (c) fresh pine wood incubated with G2 wood. d and e) Secondary electron micrographs from fresh oak incubated with D1 wood.*

Microbial community

DNA extraction was successful for all samples, and precipitation with ethanol allowed concentration and purification of the extracted DNA (Table S 4.8). However, no ITS PCR amplification was obtained while all samples were positive for *16S* amplification (Figure S 4.8). The analysed samples came directly from the collection point in Biel Lake (Switzerland) to the laboratory. Samples were taken from the sediments where fungal activity is considered to be reduced [64]. Indeed, most studies in waterlogged wood microbial community focused in bacteria and archaea populations [87]–[90]. Moreover, microscopy analyses discussed above did not detect either the presence of fungal attack. For example, soft rot fungi produce holes in the cell walls [51], that were not observed here. Still, recent studies in WAW microbial community showed the presence of fungal communities [70], [71]. These investigations focused on samples taken in previous years and stored in the laboratory or museum facilities over time. They were interested on the negative consequences that the microbial community may have in the WAW after recovery from the burial locations. [70], [71]. Storage is usually in water at RT or refrigerated. In these conditions, it is possible that the development of a fungal community happened after sample collection.

The negative result in the ITS PCR amplification led to only sequencing for the bacterial community. A total number of 2553 of amplicon sequence variants (AVSs) were identified after denoising with DADA2. Overall, silver fir (set F) samples presented a higher number of AVSs. Three samples were in the range between 607-751, while one of the samples from the core presented only 479 AVSs. Except for this one samples, oak samples (set C) had lower number of observed features, between 325 to 564.

Diversity analyses revealed that the alpha diversity was not significantly different between oak and silver fir samples for AVSs diversity, richness and evenness (Shannon index, Chao1 estimator and Pielou's evenness, respectively) (Figure 4.13). Sample 8 decreased the diversity, richness and evenness for the group of silver fir samples (Figure S 4.9). This sample was the one with less observed features (479 AVSs) and the presence of relative more abundant genera decreased diversity and evenness also. However, significant differences were detected in the phylogenetic diversity between oak and silver fir ($p=0.02$) (Figure 4.13). Silver fir samples had a more diverse phylogeny than oak samples. Oak samples presented a much higher state of degradation than silver fir samples, as seen in the microscopy analyses presented above. More specialised metabolisms may have defined the community in oak samples

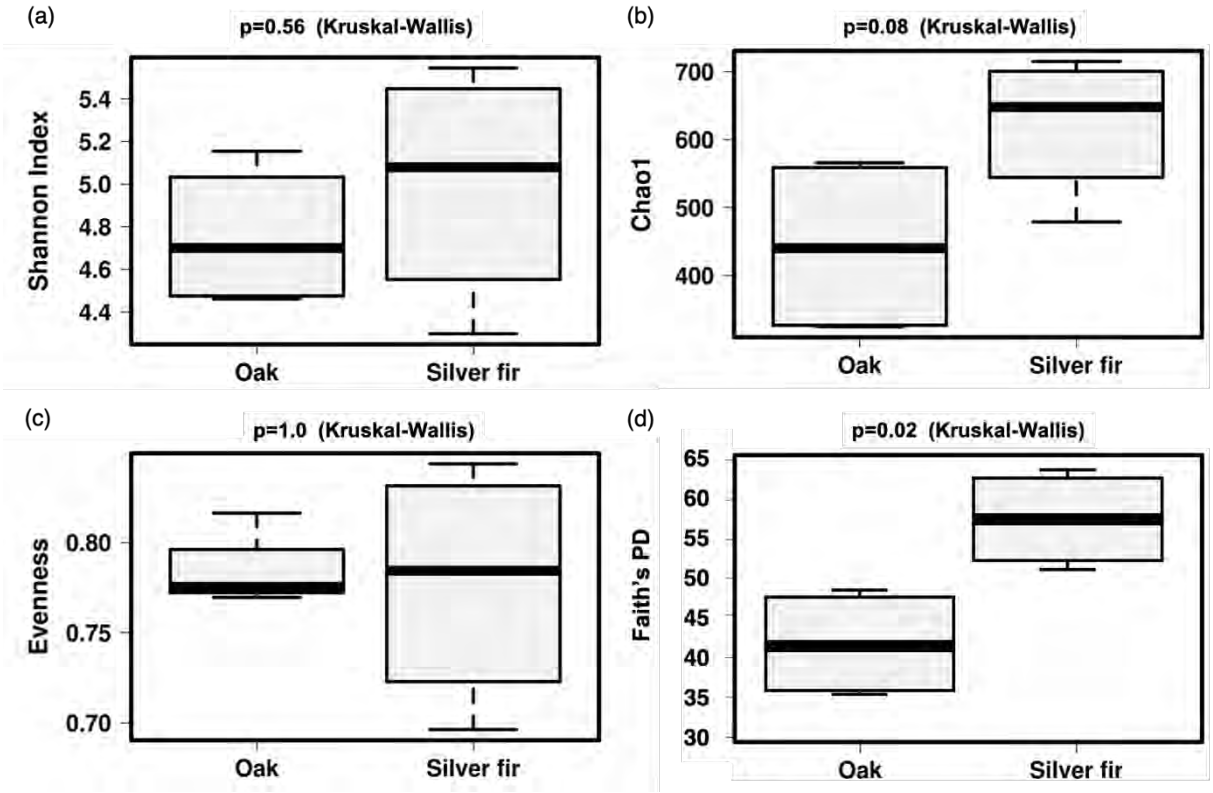

Figure 4.13. *Bacterial community richness and diversity for the two types of wood under study, oak and silver fir. (a) bacterial AVSs diversity (Shannon index). (b) bacterial AVSs richness (Chao1 index). (c) bacterial AVSs evenness (Pielou's evenness). (d) phylogenetic diversity (Faith's PD). The indexes were calculated using a sampling depth of 44698. Significant differences between the two wood types were calculated with Kruskal-Wallis test.*

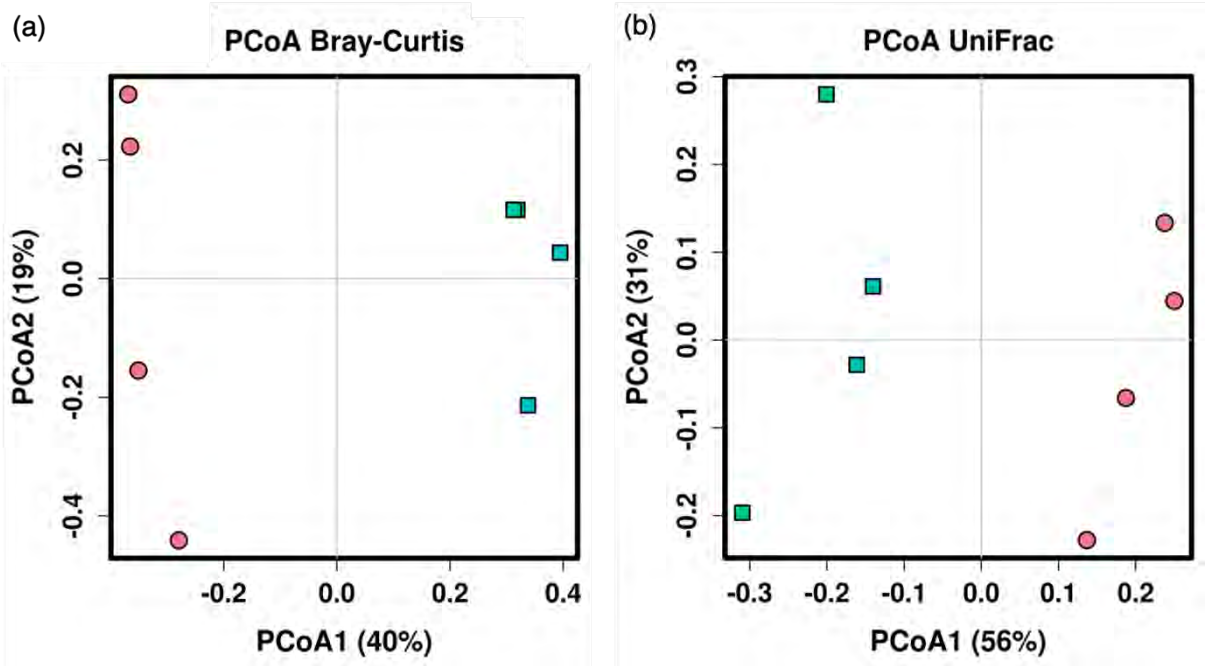

Figure 4.14. *Bacterial beta diversity between oak (●) and silver fir (■) samples by principal coordinate analysis (PCoA). PCoA was calculated based on (a) Bray-Curtis dissimilarity, and (b) weighted UniFrac distance matrix.*

Principal Coordinates Analyses (PCoA) were made based on Bray-Curtis dissimilarity and weighted UniFrac distance matrix (Figure 4.14). Both methods used are abundance-based indices. However, Bray-Curtis dissimilarity quantifies the compositional differences between samples, based on different features [82], while UniFrac distances are based on phylogenetic diversity [83]. PCoA analyses revealed, in both cases, a separation between oak and silver fir samples. PERMANOVA test showed significant differences in both Bray-Curtis dissimilarity and weighted UniFrac distance matrix ($p=0.02$ and $p=0.03$, respectively). Moreover, differences were observed between core and surface samples. PCoA based on weighted UniFrac distance matrix showed a separation between core and surface samples, in both oak and silver fir wood (Figure 4.14). In Bray-Curtis based PCoA, differences were more evident between core and surface oak samples. The alpha diversity already showed that within the oak wood samples the diversity and richness were different between core and surface samples. The beta diversity results corroborate that not only there is a difference between the bacterial communities of the different woods, but also between sections of the same wood.

The taxonomy composition of the wood samples indicated that oak samples were dominated by taxa belonging to the phylum Proteobacteria; while silver fir samples had taxa belonging to the phyla Proteobacteria, Firmicutes, Actinobacteria and Chloroflexi in similar abundance (Figure 4.15). Unclassified bacteria were present in both woods (40-45% relative abundance).

Proteobacteria made up to 39-47% of the total AVSs in oak samples. The next most abundant phylum was Firmicutes with relative frequency between 4 to 7%, followed by Bacteroidetes and Chloroflexi that made between 1 to 5%, and 1 to 3%, respectively, of the total community. The rest of phyla were under 1%. In silver fir samples, Proteobacteria made up to 16-24% of the total community, what is a reduction of half compared to their abundance in oak samples. Firmicutes made between 9 to 19%, Actinobacteria between 4 to 11%, and Chloroflexi between 2 to 4%. In silver fir samples, other phyla such as Bacteroidetes, Acidobacteria and Planctomycetes, still had a relative frequency of ~1-4% each, what explains the higher alpha diversity of silver fir samples.

Proteobacteria is a commonly found phylum in waterlogged wood samples, along with Bacteroidetes and Firmicutes [70]–[72], [88]. Within the Proteobacteria, Gammaproteobacteria was the most abundant in oak samples, due to the high abundance of one specific genus, *Janthinobacterium* (3-18% of the total community) (Figure 4.16). The incidence of Gammaproteobacteria was reduced in silver fir samples were. Here, other genera outside of this class were more abundant, as *Exiguobacterium* belonging to Bacilli (Firmicutes) (Figure 4.16).

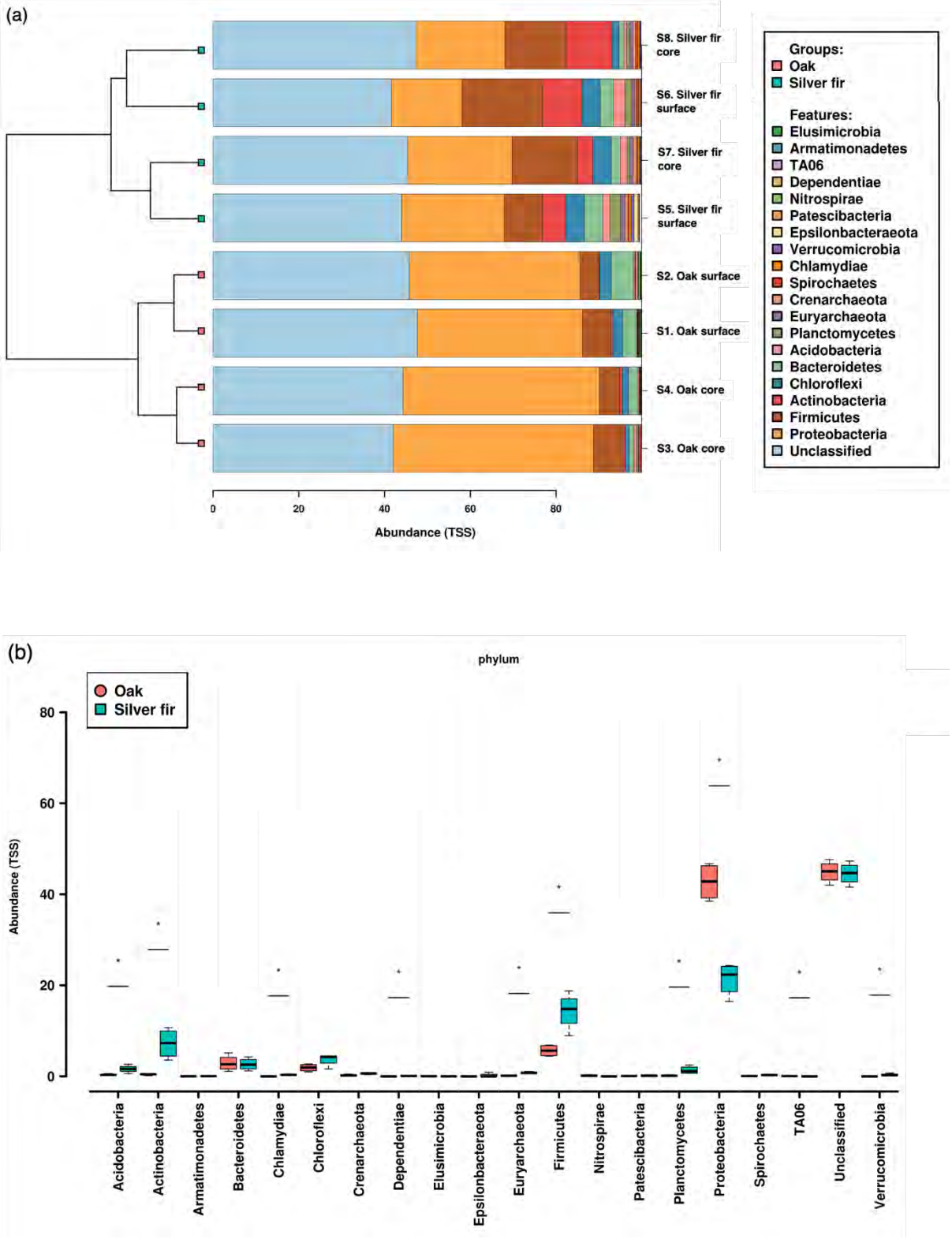

Figure 4.15. *(a) Stacked bar chart of the taxonomic profile at phylum level showing the 20 most abundant phyla. (b) Comparison between the type of wood of the 20 most abundant phyla. Significant differences are marked with a star.*

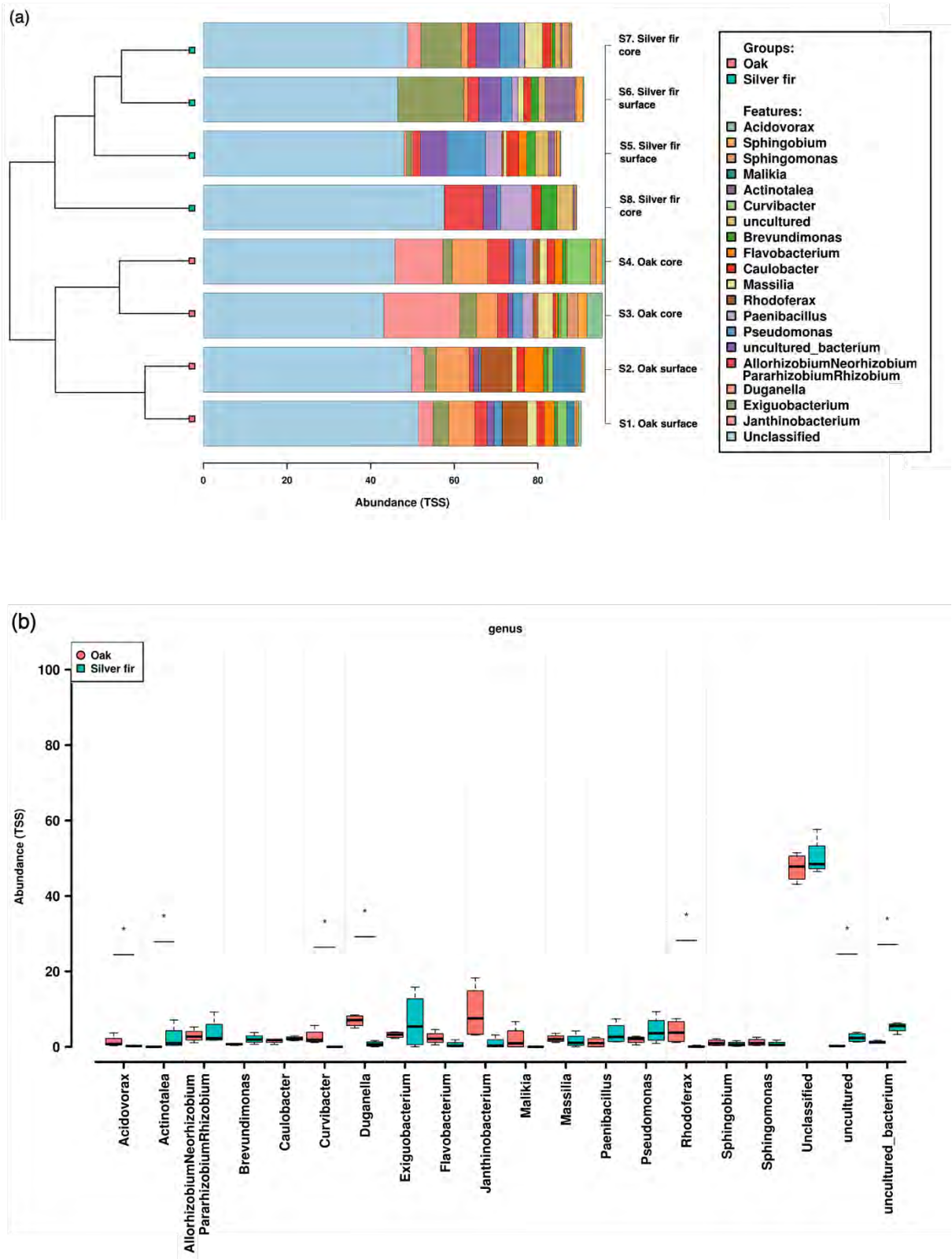

Figure 4.16. *(a) Stacked bar chart of the taxonomic profile at genus level showing the 20 most abundant genera. (b) Comparison between the type of wood of the 20 most abundant genera. Significant differences are marked with a star.*

Still, *Janthinobacterium* was also detected in some silver fir samples (Figure 4.16). The genus *Janthinobacterium* has been already detected in WAW samples, and forms part of the microbial community usually associated to waterlogged wood [70], [87]. This genus belongs to the group of wood degraders as it has been demonstrated that has cellulolytic activity [91], [92].

Previous studies in WAW samples showed Gammaproteobacteria and Alphaproteobacteria to be among the most detected classes also [70], [72]. In one of the studies, the abundancy of Gammaproteobacteria was related to the high presence of the genus *Pseudomonas* [70]. Here, *Pseudomonas* made up to 3% in some oak samples and 9% in silver fir samples (Figure 4.16). *Pseudomonas* spp. have been detected in waterlogged wood samples from different origins [87], [93], [94]. Moreover, microorganisms belonging to the genus *Pseudomonas* are involved in very different metabolisms. Some species participate in sulfur and iron metabolism [87]. Others may present cellulolytic activity, and even ligninolytic activity [95], [96]. Also, some species are denitrifying bacteria [44].

Other frequent genus for both type of woods was the already mentioned *Exiguobacterium*. This genus was detected in all oak samples (2-4%), and in silver fir samples, it made up to 16% of the total community in sample 6. This genus has been found in diverse environments, from permafrost to freshwater lakes [97], [98]. Moreover, species from this genus have been studied for their cellulolytic activity [99], [100].

The *Allorhizobium-Neorhizobium-Pararhizobium-Rhizobium* (ANPR) clade was also quite abundant in all samples (1-9%). Rhizobiales are common soil bacteria that have also been described for their cellulolytic activity [101]. In both wood, *Paenibacillus* (1-7%), *Massilia* (0.7-4%), *Brevundimonas* (0.3-4%), *Flavobacterium* (0.1-5%), *Caulobacter* (0.6-3%), *Sphingomonas* (0.4-3%) and *Sphingobium* (0.1-2%) were found. After, each wood presented some specific genera. For example, in oak wood samples *Duganella* (5-8%), *Rhodoferax* (1-7%), *Curvibacter* (1-6%), *Malikia* (2-7%) and *Acidovorax* (0.3-4%) were significantly more abundant than in silver fir samples. *Actinotalea* (0.4-7%), on the contrary, was more abundant in silver fir samples. Moreover, sample 8 (silver fir core), where the diversity and evenness were smaller, presented a dominant feature that is much less represented in the other silver fir samples. Namely an uncultured Actinobacteria of the order Coriobacteriales made up to 9% of the total community in this sample.

All the above-mentioned bacteria constituted the 20 most abundant genera of the community. They made up to 85-95% and 70-80% of the total bacterial community (along with unclassified bacteria) for oak and silver fir, respectively. Between these bacteria, wood degraders were

detected. Apart from the already discussed *Janthinobacterium, Pseudomonas*, *Exiguobacterium* and ANPR, other bacteria such as *Flavobacterium* present cellulolytic activity [102]. In fact, pure cultures of erosion bacteria (EB) suggested that they have species belonging to the CFB (*Cytophaga-Flavobacterium-Bacteroides*) complex [68], [87]. Here, the genera *Cytophaga* and *Bacteroides* were not detected. Other analyses in WAW samples already reported *Flavobacterium* but not the other two genera [70]. Some of the other bacteria detected also present hydrolytic abilities. Members from Actinobacteria, *Caulobacteraceae* (including *Caulobacter* and *Brevundimonas*), *Sphingomonadaceae* (including *Sphingomonas* and *Sphingobium*), Burkholderiales (including *Massilia*, *Duganella*, and *Acidovorax*) and *Paenibacillus* have been described for their cyllulolytic/ligninolytic capacities [91], [95], [100], [101], [103]–[107], and have also been previously detected in WAW samples [70], [71], [87].

Genera such as *Marinomonas*, *Marinobacter* and *Halomonas* were not detected in this study. These bacteria are highly described in marine WAW samples [71], [72], and they also produce cellulases and xylanases [108]. These results highlight that the degraders community is more complicated and diverse than just the suggested CFB complex [68], and that bacteria from other groups also participate as primary wood degraders.

The other bacteria found could be part of the secondary wood degraders or scavenging bacteria group, profiting from the metabolic products of the primary wood degraders [66]. Some of the bacteria found are related to the iron and sulfur cycles. For instance, members of the Dehalococcoidia class (Chloroflexi) were currently found, although they were not between the 20 most abundant genera. Species from this class are involved in the sulfur cycle [109]. Moreover, genera like *Desulfomonile*, *Desulfosporosinus* and *Desulfovibrio* were detected in all samples, even though in less proportion (~0.2%). These genera have bacteria that reduce sulfates to hydrogen sulfide [110]–[112], and they have all been previously detected in WAW samples [70], [72], [87]. Iron and sulfur related metabolisms leads to accumulation of reduced iron and sulfur compounds in WAW [25], [28]. The incubation of wood samples from the analysed oak (set C) and silver fir (set F) with fresh woods produced egg-like smell, and accumulation of iron and sulfur in the fresh woods (Figures 4.11 and S 4.7). The presence of these bacteria ratify that longer incubation times could turn out in a higher occurrence of reduced sulfur compounds in the incubated fresh woods.

Overall, WAW samples although having a diverse inhabiting bacterial community are often dominated by wood degraders and scavenging bacteria, including SRB [28], [67], [70]–[72]. The bacterial community seems to remain after excavation and storage in terms of wood

degraders. However, sulfur- and iron-oxidising bacteria that were detected in stored WAW [70], were not found here. Moreover, in samples from the *Mary Rose* where acidification was high, another microbial community was enriched, detecting also iron and sulfur oxidisers [113]. Therefore, after recovery, depending on the conditions, a shift in the community of secondary wood degraders could occur changing from sulfate reducers towards iron and sulfur oxidisers.

Conclusion

The use of biocides is common in conservation of WAW. However, developing more eco-friendly solutions needs a better understanding of the community living within waterlogged wood artefacts. Our defined bio-based extraction protocol does not involve the use of biocides, and at this point we studied the extraction protocol without any previous sterilization. Therefore, interactions between the treatment and the inhabiting microbial community may arise. In this study, we have analysed WAW samples from freshwaters sites including different types of wood and state of degradation. All samples but one showed the effects of EB attack in microscopic analyses. Moreover, sulfur was detected in some of the analysed wood. This indicated that EB-SRB could still be active in the wood. Incubation with fresh wood samples showed that the bacteria could develop. Egg-like smell, related to the production of hydrogen sulfur, was detected in all culture bottles. Moreover, early stages of degradation were observed in the fresh wood samples. DNA analyses confirmed the presence of microbial taxa with cellulolytic abilities, and sulfur metabolism. The bacterial community varied between the two types of wood analysed (silver fir and oak), but in both cases the presence of wood degraders and scavenging bacteria, like SRB, was detected.

The presence of wood degraders in WAW samples could be of concern if the defined extraction protocol enhances their development. For instance, in the previous section we registered a high consumption of nitrates in some samples that did not correlate with the amounts of sulfates produced. Genera with denitrifying species where detected in this study and others [70]. Therefore, it is important to control that the bio-treatment does not enhance wood decay. For instance, woodchips have been suggested as solution for denitrification of wastewater. Denitrifying microorganisms used the wood as carbon source removing nitrates from the contaminated water [45]. In our case, heterotrophic denitrifying bacteria, such as some *Pseudomonas*, could further decay the wood using the nitrates from the medium. Moreover, if the nitrates from the medium are being used by other microorganisms, the development of *T. denitrificans* could be affected. Here, FTIR analysis (section 4.2) did not reveal further wood

degradation after treatment. Therefore, even though these bacteria could develop, their effect was negligible in terms of wood decay. However, we observed that the production of sulfates was lower than expected. Thus, even if the wood was not further damaged the action of *T. denitrificans* could have been challenged.

SRB bacteria could also interfere with the protocol re-cycling the oxidised sulfates again to reduced sulfur. Levels of hydrogen sulfide were not registered during treatment. Future research is needed to also evaluate if the effects of this group are also negligible. Further DNA and RNA analyses at different stages of the protocol could help understand the changes in the community during treatment. Especially, reveal which microorganisms are active.

Supplementary material 4.3

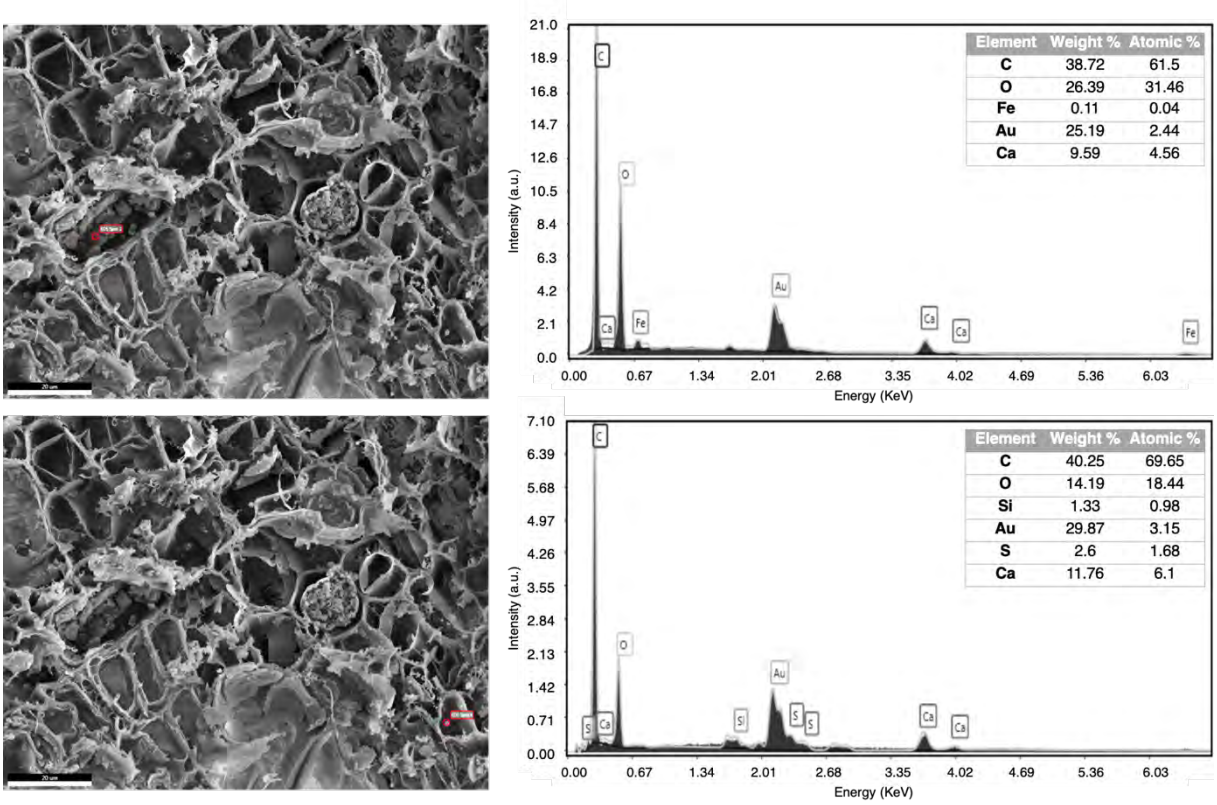

***Figure S 4.6**. SEM images and correspondent EDS spectra (red points) of a thin wood cut from set D1.*

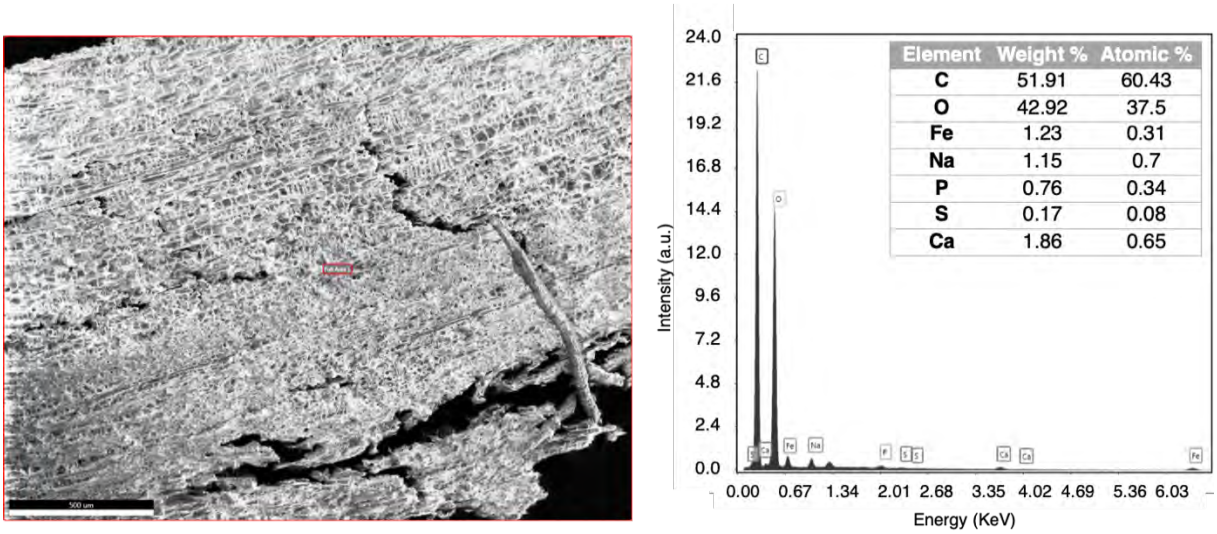

***Figure S 4.7**. SEM image and correspondent EDS spectrum (full area) of a thin wood cut from oak samples incubated with set C samples.*

***Table S 4.8**. Concentrations of DNA after extraction and after purification.*

Sample no.	Set	Description	DNA ng/µl before precipitation	DNA ng/µl after precipitation
1	C	Neolithic oak surface	5.98	29.00
2	C	Neolithic oak surface	2.36	10.30
3	C	Neolithic oak core	3.91	25.40
4	C	Neolithic oak core	4.30	19.50
5	F	Silver fir surface	0.60	4.78
6	F	Silver fir surface	2.05	19.30
7	F	Silver fir core	0.31	4.64
8	F	Silver fir core	0.17	1.32

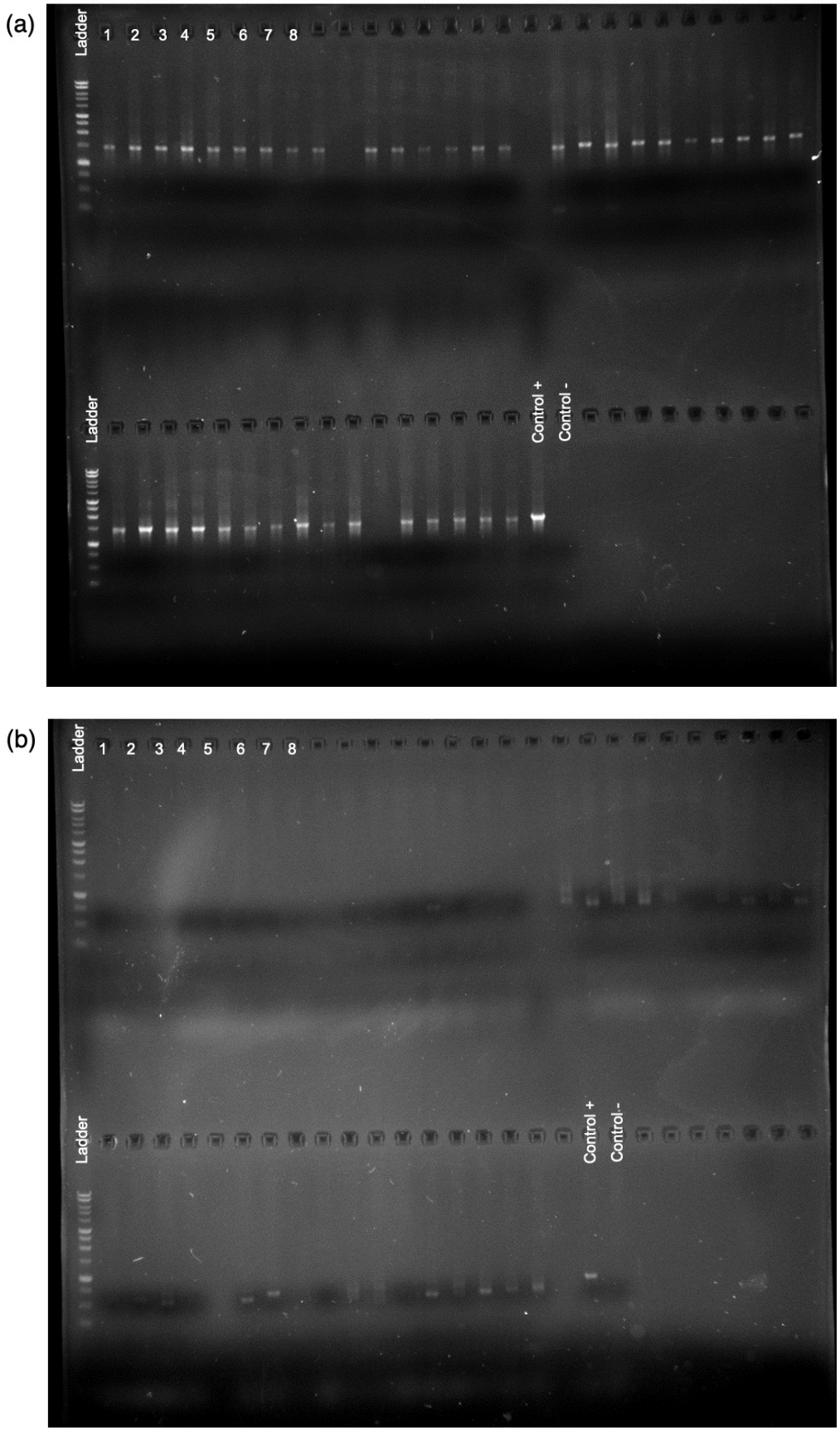

***Figure S 4.8**. Electrophoresis gels showing the DNA amplificons for (a) 16S rRNA and (b) ITS. Samples follow the classification by numbers of table S 4.8. Bands without number correspond to a different study.*

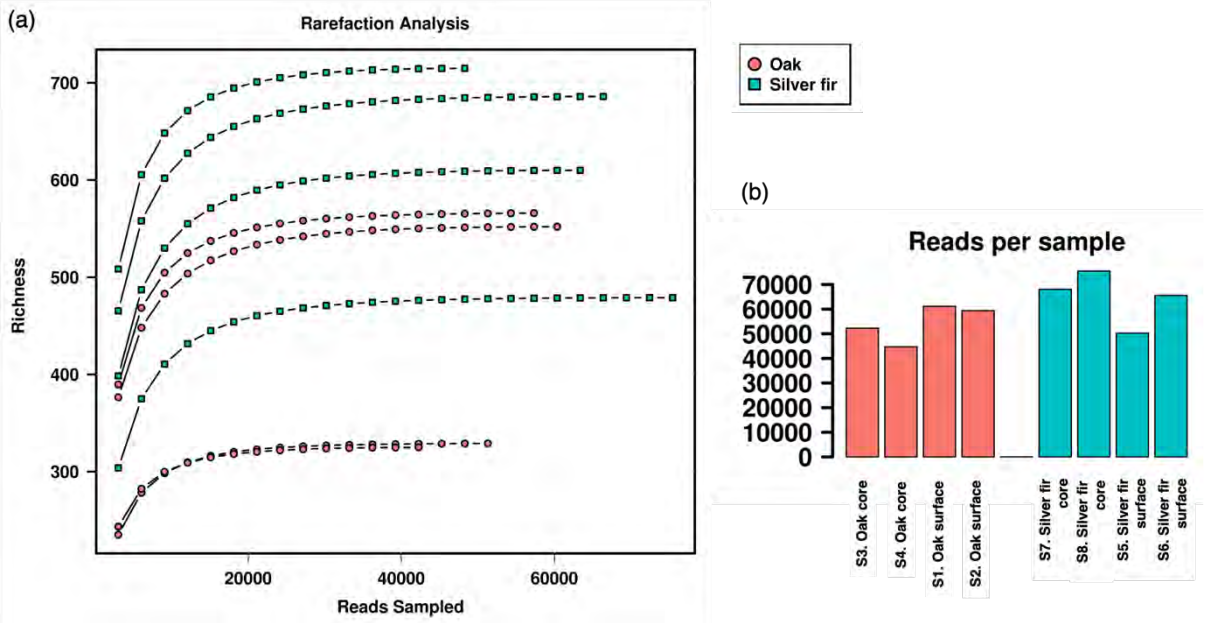

***Figure S 4.9**. (a) Number of reads per sample as function of the richness. Rarefaction allowed to determine the minimum sampling depth. (b) Direct representation of the reads per sample.*

***Table S 4.9**. Community richness and diversity estimates for all the samples analysed.*

Sample no.	Set	Description	Shannon index	Chao1	Evenness	Faith's PD
1	C	Neolithic oak surface	5.15	552	0.816	48.14
2	C	Neolithic oak surface	4.91	566	0.775	44.86
3	C	Neolithic oak core	4.46	329	0.769	37.37
4	C	Neolithic oak core	4.49	325	0.776	35.56
5	F	Silver fir surface	5.54	715	0.843	62.69
6	F	Silver fir surface	4.81	610	0.751	58.57
7	F	Silver fir core	5.35	686	0.829	55.04
8	F	Silver fir core	4.29	479	0.695	50.63

Author contribution

Published data (Section 4.2): MM designed the experimental protocol, performed the chemical treatment and the Raman and FTIR analyses, analysed the data and wrote the manuscripts. MA-B designed the experimental protocol, performed the biological treatment, and analysed the data. TL assisted in the experimental design and the Raman analysis. EC performed the colirimetry measurements. FM-D assisted in the experimental design. JS assisted in the experimental design. KS-O assisted in the experimental design EJ supervised the experimental design, analysed the data, and wrote the manuscripts. All co-authors corrected the manuscripts.

Unpublished data (Sections 4.1 and 4.3): MA-B designed and performed all experiments, analysed the data and wrote this chapter. MM assisted with SEM-EDS analyses. EJ supervised the experimental design, analysed the data, wrote and corrected this chapter.

References

[1] B. Appelbaum, "Criteria for treatment: Reversibility," *J. Am. Inst. Conserv.*, vol. 26, no. 2, pp. 65–73, 1987, doi: 10.1179/019713687806027852.

[2] G. Almkvist and I. Persson, "Extraction of iron compounds from wood from the Vasa," *Holzforschung*, vol. 60, no. 6, pp. 678–684, 2006, doi: 10.1515/HF.2006.114.

[3] C. Pelé, E. Guilminot, S. Labroche, G. Lemoine, and G. Baron, "Iron removal from waterlogged wood: Extraction by electrophoresis and chemical treatments," *Stud. Conserv.*, vol. 60, no. 3, pp. 155–171, May 2015, doi: 10.1179/2047058413Y.0000000110.

[4] E. J. Schofield *et al.*, "Strontium carbonate nanoparticles for the surface treatment of problematic sulfur and iron in waterlogged archaeological wood," *J. Cult. Herit.*, vol. 18, pp. 306–312, 2016, doi: 10.1016/j.culher.2015.07.013.

[5] M. G. Papich, "Deferoxamine Mesylate," *Saunders Handb. Vet. Drugs*, no. 1907, pp. 210–211, 2016, doi: 10.1016/b978-0-323-24485-5.00596-9.

[6] S. Rapti, S. Boyatzis, S. Rivers, A. Velios, and A. Pournou, "Removing iron stains from wood and textile objects: assessing gelled siderophores as novel green chelators," Aug. 2017.

[7] S. Rapti, S. Rivers, and A. Pournou, "Removing iron corrosion products from museum artefacts : Investigating the effectiveness of innovative green chelators," no. November 2015, 2016.

[8] P. Junier and E. Joseph, "Microbial biotechnology approaches to mitigating the deterioration of construction and heritage materials," *Microb. Biotechnol.*, vol. 10, no. 5, pp. 1145–1148, 2017, doi: 10.1111/1751-7915.12795.

[9] Y. Fors and V. Richards, "The Effects of the Ammonia Neutralizing Treatment on Marine Archaeological

Vasa Wood," *Stud. Conserv.*, vol. 55, no. 1, pp. 41–54, Mar. 2010, doi: 10.1179/sic.2010.55.1.41.

[10] K. M. Wetherall *et al.*, "Sulfur and iron speciation in recently recovered timbers of the Mary Rose revealed via X-ray absorption spectroscopy," *J. Archaeol. Sci.*, vol. 35, no. 5, pp. 1317–1328, 2008, doi: 10.1016/j.jas.2007.09.007.

[11] P. M. Ihnat, J. L. Vennerstrom, and D. H. Robinson, "Solution equilibria of deferoxamine amides," *J. Pharm. Sci.*, vol. 91, no. 7, pp. 1733–1741, 2002, doi: 10.1002/jps.10168.

[12] E. A. Christenson and J. Schijf, "Stability of YREE complexes with the trihydroxamate siderophore desferrioxamine B at seawater ionic strength," *Geochim. Cosmochim. Acta*, vol. 75, no. 22, pp. 7047–7062, 2011, doi: 10.1016/j.gca.2011.09.022.

[13] S. I. Ohira and K. Toda, "Ion chromatographic measurement of sulfide, methanethiolate, sulfite and sulfate in aqueous and air samples," *J. Chromatogr. A*, vol. 1121, no. 2, pp. 280–284, 2006, doi: 10.1016/j.chroma.2006.05.074.

[14] K. L. Subletta, "Aerobic oxidation of hydrogen sulfide byThiobacillus denitrificans," *Biotechnol. Bioeng.*, vol. 29, no. 6, pp. 690–695, Apr. 1987, doi: 10.1002/bit.260290605.

[15] M. I. M. Soares, "Denitrification of groundwater with elemental sulfur," *Water Res.*, vol. 36, no. 5, pp. 1392–1395, 2002, doi: 10.1016/S0043-1354(01)00326-8.

[16] R. Yan *et al.*, "Effect of Reduced Sulfur Species on Chemolithoautotrophic Pyrite Oxidation with Nitrate," *Geomicrobiol. J.*, vol. 36, no. 1, pp. 19–29, Jan. 2019, doi: 10.1080/01490451.2018.1489915.

[17] M. Sandström *et al.*, "Sulfur accumulation in the timbers of King Henry VIII's warship Mary Rose: a pathway in the sulfur cycle of conservation concern.," *Proc. Natl. Acad. Sci. U. S. A.*, vol. 102, no. 40, pp. 14165–70, 2005, doi: 10.1073/pnas.0504490102.

[18] M. Sandström, F. Jalilehvand, I. Persson, U. Gelius, P. Frank, and I. Hall-Roth, "Deterioration of the seventeenth-century warship Vasa by internal formation of sulphuric acid," *Nature*, vol. 415, no. 6874, pp. 893–897, Feb. 2002, doi: 10.1038/415893a.

[19] C. Rémazeilles, K. Tran, E. Guilminot, E. Conforto, and P. Refait, "Study of Fe(II) sulphides in waterlogged archaeological wood," *Stud. Conserv.*, vol. 58, no. 4, pp. 297–307, 2013, doi: 10.1179/2047058412Y.0000000071.

[20] C. Rémazeilles *et al.*, "Post-treatment Study of Iron/Sulfur-containing Compounds in the Wreck of Lyon Saint-Georges 4 (Second Century ACE)," *Stud. Conserv.*, vol. 65, no. 1, pp. 28–36, Jan. 2020, doi: 10.1080/00393630.2019.1610608.

[21] P. Bosch-Roig and G. Ranalli, "The safety of biocleaning technologies for cultural heritage," *Front. Microbiol.*, vol. 5, no. APR, pp. 1–3, 2014, doi: 10.3389/fmicb.2014.00155.

[22] E. Joseph and P. Junier, "Metabolic processes applied to endangered metal and wood heritage objects: Call a microbial plumber!," *N. Biotechnol.*, vol. 56, pp. 21–26, May 2020, doi: 10.1016/J.NBT.2019.11.003.

[23] L. O. De Serrano, "Biotechnology of siderophores in high-impact scientific fields," *Biomol. Concepts*, vol. 8, no. 3–4, pp. 169–178, 2017, doi: 10.1515/bmc-2017-0016.

[24] P. U. Reichard, R. Kretzschmar, and S. M. Kraemer, “Dissolution mechanisms of goethite in the presence of siderophores and organic acids,” *Geochim. Cosmochim. Acta*, vol. 71, no. 23, pp. 5635–5650, Dec. 2007, doi: 10.1016/j.gca.2006.12.022.

[25] C. G. Björdal and Y. Fors, “Correlation between sulfur accumulation and microbial wood degradation on shipwreck timbers,” *Int. Biodeterior. Biodegradation*, vol. 140, no. January, pp. 37–42, May 2019, doi: 10.1016/j.ibiod.2019.03.010.

[26] S. Norbakhsh, I. Bjurhager, and G. Almkvist, “Impact of iron(II) and oxygen on degradation of oak – modeling of the Vasa wood,” *Holzforschung*, vol. 68, no. 6, pp. 649–655, 2014, doi: https://doi.org/10.1515/hf-2013-0197.

[27] G. Almkvist, S. Norbakhsh, I. Bjurhager, and K. Varmuza, “Prediction of tensile strength in iron-contaminated archaeological wood by FT-IR spectroscopy-a study of degradation in recent oak and Vasa oak,” *Holzforschung*, vol. 70, no. 9, pp. 855–865, 2016, doi: https://doi.org/10.1515/hf-2015-0223.

[28] Y. Fors, T. Nilsson, E. D. Risberg, M. Sandström, and P. Torssander, “Sulfur accumulation in pinewood (Pinus sylvestris) induced by bacteria in a simulated seabed environment: Implications for marine archaeological wood and fossil fuels,” *Int. Biodeterior. Biodegrad.*, vol. 62, no. 4, pp. 336–347, 2008, doi: 10.1016/j.ibiod.2007.11.008.

[29] A. Sandak, J. Sandak, L. Babiński, D. Pauliny, and M. Riggio, “Spectral analysis of changes to pine and oak wood natural polymers after short-term waterlogging,” *Polym. Degrad. Stab.*, vol. 99, pp. 68–79, Jan. 2014, doi: 10.1016/J.POLYMDEGRADSTAB.2013.11.018.

[30] N. Odegaard, S. Carroll, W. S. Zimmt, D. Spurgeon, and S. K. Lane, *Material Characterization Tests for Objects of Art and Archaeology*. Archetype Publications, 2005.

[31] J. Sheng *et al.*, “Changes in the chemical composition of young Chinese fir wood exposed to different soil temperature and water content,” *Cellulose*, vol. 3, 2020, doi: 10.1007/s10570-020-03039-3.

[32] V. Emmanuel, B. Odile, and R. Céline, “FTIR spectroscopy of woods: A new approach to study the weathering of the carving face of a sculpture,” *Spectrochim. Acta - Part A Mol. Biomol. Spectrosc.*, vol. 136, no. PC, pp. 1255–1259, 2015, doi: 10.1016/j.saa.2014.10.011.

[33] I. Dobrică, P. Bugheanu, I. Stănculescu, and C. Ponta, “FT-IR spectral data of wood used in Romanian,” *Analele Univ. din Bucuresti*, vol. I, pp. 33–37, 2008.

[34] C. Ganne-Chédeville, A. S. Jääskeläinen, J. Froidevaux, M. Hughes, and P. Navi, “Natural and artificial ageing of spruce wood as observed by FTIR-ATR and UVRR spectroscopy,” *Holzforschung*, vol. 66, no. 2, pp. 163–170, 2012, doi: 10.1515/HF.2011.148.

[35] B. Buchelt and A. Wagenführ, “Evaluation of colour differences on wood surfaces,” *Eur. J. Wood Wood Prod.*, vol. 70, no. 1–3, pp. 389–391, Jan. 2012, doi: 10.1007/s00107-011-0545-z.

[36] J. A. Bourdoiseau, M. Jeannin, R. Sabot, C. Rémazeilles, and P. Refait, “Characterisation of mackinawite by Raman spectroscopy: Effects of crystallisation, drying and oxidation,” *Corros. Sci.*, vol. 50, no. 11, pp. 3247–3255, 2008, doi: 10.1016/j.corsci.2008.08.041.

[37] C. Rémazeilles *et al.*, "Microbiologically influenced corrosion of archaeological artefacts:Characterisation of iron(II) sulfides by Raman spectroscopy," *J. Raman Spectrosc.*, vol. 41, no. 11, pp. 1425–1433, 2010, doi: 10.1002/jrs.2717.

[38] M. Monachon *et al.*, "Evaluation of bio-based extraction methods by spectroscopic methods," *Minerals*, vol. 10, no. 2, pp. 1–17, 2020, doi: 10.3390/min10020203.

[39] U. P. Agarwal and S. A. Ralph, "FT-Raman Spectroscopy of Wood: Identifying Contributions of Lignin and Carbohydrate Polymers in the Spectrum of Black Spruce (Picea Mariana)," *Appl. Spectrosc.*, vol. 51, no. 11, pp. 1648–1655, Nov. 1997, doi: 10.1366/0003702971939316.

[40] G. Almkvist, "The chemistry of the Vasa," Doctoral Thesis, Uppsala, 2008.

[41] S. Vaclavkova *et al.*, "The Importance of Microbial Iron Sulfide Oxidation for Nitrate Depletion in Anoxic Danish Sediments," *Aquat. Geochemistry*, vol. 20, no. 4, pp. 419–435, Jul. 2014, doi: 10.1007/s10498-014-9227-x.

[42] R. C. Brunet and L. J. Garcia-Gil, "Sulfide-induced dissimilatory nitrate reduction to ammonia in anaerobic freshwater sediments," *FEMS Micorbiol. Ecol.*, vol. 21, pp. 131–138, 1996.

[43] D. Pokorna and J. Zabranska, "Sulfur-oxidizing bacteria in environmental technology," *Biotechnol. Adv.*, vol. 33, no. 6, pp. 1246–1259, 2015, doi: 10.1016/j.biotechadv.2015.02.007.

[44] C. Torrentó, J. Cama, J. Urmeneta, N. Otero, and A. Soler, "Denitrification of groundwater with pyrite and Thiobacillus denitrificans," *Chem. Geol.*, vol. 278, no. 1–2, pp. 80–91, 2010, doi: 10.1016/j.chemgeo.2010.09.003.

[45] V. Grießmeier, A. Bremges, A. C. McHardy, and J. Gescher, "Investigation of different nitrogen reduction routes and their key microbial players in wood chip-driven denitrification beds," *Sci. Rep.*, vol. 7, no. 1, pp. 1–12, 2017, doi: 10.1038/s41598-017-17312-2.

[46] H. R. Beller *et al.*, "The genome sequence of the obligately chemolithoautotrophic, facultatively anaerobic bacterium Thiobacillus denitrificans," *J. Bacteriol.*, vol. 188, no. 4, pp. 1473–1488, 2006, doi: 10.1128/JB.188.4.1473-1488.2006.

[47] J. T. Lin and V. Stewart, "Nitrate assimilation by bacteria.," *Adv. Microb. Physiol.*, vol. 39, pp. 1-30,379, 1998, doi: 10.1016/s0065-2911(08)60014-4.

[48] M. F. Mesko, M. G. Crizel, D. L. R. Novo, C. A. Hartwig, F. S. Rondan, and C. A. Bizzi, "New and feasible method for total phosphorus and sulfur determination in dietary supplements by ion chromatography," *Arab. J. Chem.*, vol. 13, no. 1, pp. 2076–2083, 2020, doi: 10.1016/j.arabjc.2018.03.006.

[49] A. Geffert, J. Geffertova, and M. Dudiak, "Direct method of measuring the pH value of wood," *Forests*, vol. 10, no. 10, pp. 6–10, 2019, doi: 10.3390/f10100852.

[50] A. C. Wiedenhoeft and R. B. Miller, "Structure and function of wood," in *Handbook of Wood Chemistry and Wood Composites*, R. M. Rowell, Ed. CRC Press LLC, 2012, pp. 9–32.

[51] N. Macchioni, C. Capretti, L. Sozzi, and B. Pizzo, "Grading the decay of waterlogged archaeological wood according to anatomical characterisation. The case of the Fiavé site (N-E Italy)," *Int. Biodeterior.*

Biodegradation, vol. 84, pp. 54–64, Oct. 2013, doi: 10.1016/j.ibiod.2013.05.028.

[52] K. K. Pandey and A. J. Pitman, "FTIR studies of the changes in wood chemistry following decay by brown-rot and white-rot fungi," *Int. Biodeterior. Biodegrad.*, vol. 52, no. 3, pp. 151–160, 2003, doi: 10.1016/S0964-8305(03)00052-0.

[53] K. K. Pandey and H. C. Nagveni, "Rapid characterisation of brown and white rot degraded chir pine and rubberwood by FTIR spectroscopy," *Holz als Roh- und Werkst.*, vol. 65, no. 6, pp. 477–481, Nov. 2007, doi: 10.1007/s00107-007-0181-9.

[54] G. Giachi, C. Capretti, N. Macchioni, B. Pizzo, and I. D. Donato, "A methodological approach in the evaluation of the efficacy of treatments for the dimensional stabilisation of waterlogged archaeological wood," *J. Cult. Herit.*, vol. 11, no. 1, pp. 91–101, 2010, doi: 10.1016/j.culher.2009.04.003.

[55] F. H. Schweingruber and E. anstalt für das forstliche versuchswesen, *Microscopic Wood Anatomy*. Swiss Federal Institute of Forestry Research, 1978.

[56] K. Asemave, "Greener Chelators for Recovery of Metals and Other Applications," *Org. Med. Chem. Int. J.*, vol. 6, no. 4, May 2018, doi: 10.19080/OMCIJ.2018.06.555694.

[57] G. Ranalli *et al.*, "Onsite advanced biocleaning system for historical wall paintings using new agar-gauze bacteria gel," *J. Appl. Microbiol.*, vol. 126, no. 6, pp. 1785–1796, Jun. 2019, doi: 10.1111/jam.14275.

[58] F. Jroundi *et al.*, "Protection and consolidation of stone heritage by self-inoculation with indigenous carbonatogenic bacterial communities," *Nat. Commun.*, vol. 8, no. 1, pp. 1–12, Dec. 2017, doi: 10.1038/s41467-017-00372-3.

[59] E. Caselli *et al.*, "Characterization of biodegradation in a 17 th century easel painting and potential for a biological approach," *PLoS One*, vol. 13, no. 12, pp. 1–18, 2018, doi: 10.1371/journal.pone.0207630.

[60] P. Bosch-Roig, J. Regidor-Ros, P. Soriano, and R. Montes-Estelles, "Biocleaning of animal glue on wall paintings by Pseudomonas stutzeri," *Chim. Oggi/Chemistry Today*, vol. 31, pp. 50–53, Jan. 2013.

[61] J. Preston, A. D. Smith, E. J. Schofield, A. V. Chadwick, M. A. Jones, and J. E. M. Watts, "The effects of Mary Rose conservation treatment on iron oxidation processes and microbial communities contributing to acid production in marine archaeological timbers," *PLoS One*, vol. 9, no. 2, 2014, doi: 10.1371/journal.pone.0084169.

[62] K. Sterflinger and G. Piñar, "Microbial deterioration of cultural heritage and works of art - Tilting at windmills?," *Appl. Microbiol. Biotechnol.*, vol. 97, no. 22, pp. 9637–9646, 2013, doi: 10.1007/s00253-013-5283-1.

[63] I. Soffritti *et al.*, "The potential use of microorganisms as restorative agents: An update," *Sustainability (Switzerland)*, vol. 11, no. 14. pp. 1–17, 2019, doi: 10.3390/su11143853.

[64] C. G. Björdal, T. Nilsson, and G. Daniel, "Microbial decay of waterlogged archaeological wood found in Sweden. Applicable to archaeology and conservation," *Int. Biodeterior. Biodegrad.*, vol. 43, no. 1–2, pp. 63–73, 1999, doi: 10.1016/S0964-8305(98)00070-5.

[65] C. G. Björdal and T. Nilsson, "Reburial of shipwrecks in marine sediments: a long-term study on wood

degradation," *J. Archaeol. Sci.*, vol. 35, no. 4, pp. 862–872, 2008, doi: 10.1016/j.jas.2007.06.005.

[66] C. . G. Björdal, G. Daniel, and T. Nilsson, "Depth of burial, an important factor in controlling bacterial decay of waterlogged archaeological poles," *Int. Biodeterior. Biodegradation*, vol. 45, no. 1–2, pp. 15–26, Jan. 2000, doi: 10.1016/S0964-8305(00)00035-4.

[67] T. Nilsson and C. Björdal, "Culturing wood-degrading erosion bacteria," *Int. Biodeterior. Biodegrad.*, vol. 61, no. 1, pp. 3–10, 2008, doi: 10.1016/j.ibiod.2007.06.006.

[68] T. Nilsson, C. Björdal, and E. Fällman, "Culturing erosion bacteria: Procedures for obtaining purer cultures and pure strains," *Int. Biodeterior. Biodegrad.*, vol. 61, no. 1, pp. 17–23, 2008, doi: 10.1016/j.ibiod.2007.06.010.

[69] A. C. Helms, A. C. Martiny, J. Hofman-Bang, B. K. Ahring, and M. Kilstrup, "Identification of bacterial cultures from archaeological wood using molecular biological techniques," *Int. Biodeterior. Biodegrad.*, vol. 53, no. 2, pp. 79–88, 2004, doi: 10.1016/j.ibiod.2003.10.003.

[70] F. Antonelli *et al.*, "Microbiota in waterlogged archaeological wood: Use of next-generation sequencing to evaluate the risk of biodegradation," *Appl. Sci.*, vol. 10, no. 13, pp. 1–21, 2020, doi: 10.3390/app10134636.

[71] Z. Liu *et al.*, "Microbial community analysis and biodeterioration of waterlogged archaeological wood from the Nanhai No. 1 shipwreck during storage," *Sci. Rep.*, vol. 8, no. 1, pp. 1–11, 2018, doi: 10.1038/s41598-018-25484-8.

[72] Q. Li *et al.*, "Analysis of the bacterial communities in the waterlogged wooden cultural relics of the Xiaobaijiao No. 1 shipwreck via high-throughput sequencing technology," *Holzforschung*, vol. 72, no. 7, pp. 609–619, 2018, doi: 10.1515/hf-2017-0132.

[73] D. P. R. Herlemann, M. Labrenz, K. Jürgens, S. Bertilsson, J. J. Waniek, and A. F. Andersson, "Transitions in bacterial communities along the 2000 km salinity gradient of the Baltic Sea," *ISME J.*, vol. 5, no. 10, pp. 1571–1579, 2011, doi: 10.1038/ismej.2011.41.

[74] E. Bolyen *et al.*, "Reproducible, interactive, scalable and extensible microbiome data science using QIIME 2," *Nat. Biotechnol.*, vol. 37, no. 8, pp. 852–857, 2019, doi: 10.1038/s41587-019-0209-9.

[75] B. J. Callahan, P. J. McMurdie, M. J. Rosen, A. W. Han, A. J. A. Johnson, and S. P. Holmes, "DADA2: High-resolution sample inference from Illumina amplicon data," *Nat. Methods*, vol. 13, no. 7, pp. 581–583, 2016, doi: 10.1038/nmeth.3869.

[76] K. Katoh, K. Misawa, K. I. Kuma, and T. Miyata, "MAFFT: A novel method for rapid multiple sequence alignment based on fast Fourier transform," *Nucleic Acids Res.*, vol. 30, no. 14, pp. 3059–3066, 2002, doi: 10.1093/nar/gkf436.

[77] M. N. Price, P. S. Dehal, and A. P. Arkin, "FastTree 2 - Approximately maximum-likelihood trees for large alignments," *PLoS One*, vol. 5, no. 3, 2010, doi: 10.1371/journal.pone.0009490.

[78] C. E. Shannon and W. Weaver, "The mathematical theory of communication," Jan. 1949, doi: 10.1145/584091.584093.

[79] A. Chao, "Nonparametric Estimation of the Number of Classes in a Population," *Scand. J. Stat.*, vol. 11, no. 4, pp. 265–270, Sep. 1984, [Online]. Available: http://www.jstor.org/stable/4615964.

[80] E. C. Pielou, "The measurement of diversity in different types of biological collections," *J. Theor. Biol.*, vol. 13, pp. 131–144, 1966, doi: https://doi.org/10.1016/0022-5193(66)90013-0.

[81] D. P. Faith, "Conservation evaluation and phylogenetic diversity," *Biol. Conserv.*, vol. 61, no. 1, pp. 1–10, 1992, doi: https://doi.org/10.1016/0006-3207(92)91201-3.

[82] J. R. Bray and J. T. Curtis, "An Ordination of the Upland Forest Communities of Southern Wisconsin," *Ecol. Monogr.*, vol. 27, no. 4, pp. 325–349, 1957, doi: 10.2307/1942268.

[83] C. A. Lozupone, M. Hamady, S. T. Kelley, and R. Knight, "Quantitative and qualitative β diversity measures lead to different insights into factors that structure microbial communities," *Appl. Environ. Microbiol.*, vol. 73, no. 5, pp. 1576–1585, 2007, doi: 10.1128/AEM.01996-06.

[84] N. A. Bokulich *et al.*, "Optimizing taxonomic classification of marker-gene amplicon sequences with QIIME 2's q2-feature-classifier plugin," *Microbiome*, vol. 6, no. 1, pp. 1–17, 2018, doi: 10.1186/s40168-018-0470-z.

[85] C. Quast *et al.*, "The SILVA ribosomal RNA gene database project: Improved data processing and web-based tools," *Nucleic Acids Res.*, vol. 41, no. D1, pp. 590–596, 2013, doi: 10.1093/nar/gks1219.

[86] M. Zakrzewski *et al.*, "Calypso: A user-friendly web-server for mining and visualizing microbiome-environment interactions," *Bioinformatics*, vol. 33, no. 5, pp. 782–783, 2017, doi: 10.1093/bioinformatics/btw725.

[87] E. T. Landy, J. I. Mitchell, S. Hotchkiss, and R. A. Eaton, "Bacterial diversity associated with archaeological waterlogged wood: Ribosomal RNA clone libraries and denaturing gradient gel electrophoresis (DGGE)," *Int. Biodeterior. Biodegrad.*, vol. 61, no. 1, pp. 106–116, 2008, doi: 10.1016/j.ibiod.2007.07.007.

[88] S. K. Fagervold, P. E. Galand, M. Zbinden, F. Gaill, P. Lebaron, and C. Palacios, "Sunken woods on the ocean floor provide diverse specialized habitats for microorganisms," *FEMS Microbiol. Ecol.*, vol. 82, no. 3, pp. 616–628, 2012, doi: 10.1111/j.1574-6941.2012.01432.x.

[89] C. Palacios *et al.*, "Microbial ecology of deep-sea sunken wood: Quantitative measurements of bacterial biomass and cellulolytic activities," *Cah. Biol. Mar.*, vol. 47, no. 4, pp. 415–420, 2006.

[90] C. Palacios, M. Zbinden, M. Pailleret, F. Gaill, and P. Lebaron, "Highly similar Prokaryotic communities of sunken wood at shallow and deep-sea sites across the oceans," *Microb. Ecol.*, vol. 58, no. 4, pp. 737–752, 2009, doi: 10.1007/s00248-009-9538-4.

[91] R. C. Wilhelm, R. Singh, L. D. Eltis, and W. W. Mohn, "Bacterial contributions to delignification and lignocellulose degradation in forest soils with metagenomic and quantitative stable isotope probing," *ISME J.*, vol. 13, no. 2, pp. 413–429, 2019, doi: 10.1038/s41396-018-0279-6.

[92] L. M. Avellaneda-Torres, C. P. G. Pulido, and E. T. Rojas, "Assessment of cellulolytic microorganisms in soils of Nevados park, Colombia," *Brazilian J. Microbiol.*, vol. 45, no. 4, pp. 1211–1220, 2014, doi:

10.1590/S1517-83822014000400011.

[93] S. Wagner *et al.*, "Europe PMC Funders Group High-Throughput DNA sequencing of ancient wood," vol. 27, no. 5, pp. 1138–1154, 2018, doi: 10.1111/mec.14514.High-Throughput.

[94] F. Palla, G. Barresi, and E. Di Carlo, "Identification of bacterial taxa in archaeological waterlogged wood," *Conserv. Sci. Cult. Herit.*, pp. 247–254.

[95] T. D. H. Bugg, M. Ahmad, E. M. Hardiman, and R. Singh, "The emerging role for bacteria in lignin degradation and bio-product formation," *Curr. Opin. Biotechnol.*, vol. 22, no. 3, pp. 394–400, 2011, doi: https://doi.org/10.1016/j.copbio.2010.10.009.

[96] J. Shui Yang, J. Ren Ni, H. Li Yuan, and E. Wang, "Biodegradation of three different wood chips by Pseudomonas sp. PKE117," *Int. Biodeterior. Biodegradation*, vol. 60, no. 2, pp. 90–95, 2007, doi: https://doi.org/10.1016/j.ibiod.2006.12.006.

[97] R. Raichand, S. Pareek, N. K. Singh, and S. Mayilraj, "Exiguobacterium aquaticum sp. nov., a member of the genus exiguobacterium," *Int. J. Syst. Evol. Microbiol.*, vol. 62, no. 9, pp. 2150–2155, 2012, doi: 10.1099/ijs.0.035790-0.

[98] T. A. Vishnivetskaya, S. Kathariou, and J. M. Tiedje, "The Exiguobacterium genus: Biodiversity and biogeography," *Extremophiles*, vol. 13, no. 3, pp. 541–555, 2009, doi: 10.1007/s00792-009-0243-5.

[99] R. C. Kasana and C. B. Pandey, "Exiguobacterium: an overview of a versatile genus with potential in industry and agriculture," *Crit. Rev. Biotechnol.*, vol. 38, no. 1, pp. 141–156, 2018, doi: 10.1080/07388551.2017.1312273.

[100] V. Thakur, V. Kumar, S. Kumar, and D. Singh, "Diverse culturable bacterial communities with cellulolytic potential revealed from pristine habitat in indian trans-Himalaya," *Can. J. Microbiol.*, vol. 64, no. 11, pp. 798–808, 2018, doi: 10.1139/cjm-2017-0754.

[101] P. Talia *et al.*, "Biodiversity characterization of cellulolytic bacteria present on native Chaco soil by comparison of ribosomal RNA genes," *Res. Microbiol.*, vol. 163, no. 3, pp. 221–232, 2012, doi: https://doi.org/10.1016/j.resmic.2011.12.001.

[102] L. M. Herrera, V. Braña, L. Franco Fraguas, and S. Castro-Sowinski, "Characterization of the cellulase-secretome produced by the Antarctic bacterium Flavobacterium sp. AUG42," *Microbiol. Res.*, vol. 223–225, pp. 13–21, 2019, doi: https://doi.org/10.1016/j.micres.2019.03.009.

[103] R. Berlemont *et al.*, "Cellulolytic potential under environmental changes in microbial communities from grassland litter," *Front. Microbiol.*, vol. 5, no. NOV, pp. 1–10, 2014, doi: 10.3389/fmicb.2014.00639.

[104] A. Bettache, Z. Azzouz, N. Boucherba, C. Bouiche, and S. Hamma, "Lignocellulosic Biomass and Cellulolytic Enzymes of Actinobacteria," *SAJ Biotechnol*, vol. 5, no. 2, p. 106, 2018, [Online]. Available: www.scholarena.com.

[105] V. A. Dumova and Y. V. Kruglov, "A cellulose-decomposing bacterial association," *Microbiology*, vol. 78, no. 2, pp. 234–239, 2009, doi: 10.1134/S0026261709020155.

[106] E. Masai, Y. Katayama, S. Nishikawa, and M. Fukuda, "Characterization of Sphingomonas paucimobilis

SYK-6 genes involved in degradation of lignin-related compounds," *J. Ind. Microbiol. Biotechnol.*, vol. 23, no. 4–5, pp. 364–373, 1999, doi: 10.1038/sj.jim.2900747.

[107] V. Tláskal, J. Voříšková, and P. Baldrian, "Bacterial succession on decomposing leaf litter exhibits a specific occurrence pattern of cellulolytic taxa and potential decomposers of fungal mycelia," *FEMS Microbiol. Ecol.*, vol. 92, no. 11, p. fiw177, 2016, doi: 10.1093/femsec/fiw177.

[108] C. Yang *et al.*, "Metabolic versatility of halotolerant and alkaliphilic strains of Halomonas isolated from alkaline black liquor," *Bioresour. Technol.*, vol. 101, no. 17, pp. 6778–6784, 2010, doi: https://doi.org/10.1016/j.biortech.2010.03.108.

[109] K. Wasmund *et al.*, "Single-Cell Genome and Group-Specific dsrAB Sequencing Implicate Marine Members of the Class Dehalococcoidia (Phylum Chloroflexi) in Sulfur Cycling," *MBio*, vol. 7, no. 3, pp. 1–15, Jul. 2016, doi: 10.1128/mBio.00266-16.

[110] Y. Sato *et al.*, "Desulfosporosinus spp. were the most predominant sulfate-reducing bacteria in pilot- and laboratory-scale passive bioreactors for acid mine drainage treatment," *Appl. Microbiol. Biotechnol.*, vol. 103, no. 18, pp. 7783–7793, 2019, doi: 10.1007/s00253-019-10063-2.

[111] A. Loy, K. Küsel, A. Lehner, H. L. Drake, and M. Wagner, "Microarray and functional gene analyses of sulfate-reducing prokaryotes in low-sulfate, acidic fens reveal cooccurrence of recognized genera and novel lineages," *Appl. Environ. Microbiol.*, vol. 70, no. 12, pp. 6998–7009, 2004, doi: 10.1128/AEM.70.12.6998-7009.2004.

[112] M. N. Price *et al.*, "The genetic basis of energy conservation in the sulfate-reducing bacterium Desulfovibrio alaskensis G20," *Front. Microbiol.*, vol. 5, no. OCT, pp. 6–12, 2014, doi: 10.3389/fmicb.2014.00577.

[113] J. Preston, J. E. M. Watts, and M. Jones, "Novel bacterial community associated with 500-year-old unpreserved archaeological wood from King Henry VIII's tudor warship the Mary Rose," *Appl. Environ. Microbiol.*, vol. 78, no. 24, pp. 8822–8828, 2012, doi: 10.1128/AEM.02387-12.

Chapter 5

FINAL DISCUSSION AND PERSPERCTIVES

Animal head posts from Oseberg. © Museum of Cultural History, University of Oslo/ Kirsten Helgeland

Waterlogged archaeological wood (WAW) encounters serious conservation issues after excavation [1]. In presence of oxygen and high humidity, iron and sulfur species accumulated during the burial time can oxidise leading to the formation of acids and salts efflorescence [2]. In the long-term perspective, the extraction of these compounds is essential for the stabilization of the recovered wooden objects [3].

The goal of the MICMAC (Microbes for the Archaeological wood Conservation) project is to develop sustainable bio-based strategies for the extraction of problematic iron and sulfur compounds from WAW. These strategies need to be compatible with the wood matrix and other conservation treatments applied to WAW (i.e., consolidation of the wood structure), present a comparable effectiveness to current extraction methods, and be cost-effective. Moreover, any treatment should respect as much as possible the original appearance [4], be safe for the user and environment, durable and, if possible, reversible or at least retreatable [5].

The MICMAC project is an interdisciplinary research that involves scientists with different backgrounds. The presented work within the MICMAC project focused on studying microbial metabolisms that could meet the requirements listed above. The objective was to identify and characterize microorganisms or bioproducts that could be used to extract iron and sulfur species from WAW.

The first approach (Chapter 2) was the extraction of iron using bacterial siderophores. Iron compounds detected in WAW are mostly iron sulfides accumulated during burial [6], and oxidation products, such as iron oxides and oxyhydroxides, formed during recovery and storage [7]. Therefore, both ferric and ferrous iron compounds are found within WAW. Siderophores have a higher affinity for iron(III) than iron(II) [8], and many studies have focused on the dissolution of iron(III) phases by siderophores [9]–[11]. However, some researchers highlight the capacity of siderophores to oxidize ferrous iron and then form the iron(III)-siderophore complex [12], [13]. Moreover, the dissolution of pyrite (FeS_2) has been enhanced by siderophores [14]. Hence, siderophores seem good candidates to extract problematic iron from WAW.

Siderophore-producing bacteria are currently used to extract minerals from different ores via production of siderophores [9], [15]. *Escherichia coli* (strain K12), *Pseudomonas putida* (strain 90), *Serratia ureilytica* (strain Lr5/4), and *Streptomyces pilosus* (strain ETH 11686) were selected between several bacterial strains for the capability to produce siderophores. However, the first trial to extract iron from artificially contaminated wood mock-ups (i.e., balsa wood impregnated with iron- and sulfur-containing solutions) was not efficient. After treatment with

the bacteria, low levels of iron were registered in solution, and SEM-EDS analyses still detected iron in all wood samples. Previous studies showed that *E. coli* and *P. putida* developed and produced siderophores in presence of goethite (α-FeOOH) and hematite (Fe_2O_3). While with iron sulfides like mackinawite (FeS) and pyrite, *P. putida* and *S. ureilytica* developed but did not produce siderophores. In presence of all solid phases studied, *S. pilosus* was able to grow but without production of siderophores. This shows that, although, the chelation of iron by bacteria is mainly via siderophores production, other mechanisms may also participate in iron acquisition [16]. Still, interesting results were obtained with siderophore-producing bacteria that can be considered for future applications. For instance, some bacteria, like *P. putida* and specially *S. ureilytica*, although did not extract iron from wood prevented the oxidation of iron sulfides. The mechanisms behind this stabilization are not identified. Previous studies using these species for the prevention of iron corrosion suggest several metabolisms involved, such as the scavenging of oxygen and/or production of protective metabolites (coating) [17]. Long-term evaluation would determine if the stabilization effects are durable over time.

The direct use of isolated siderophores resulted in the extraction of iron from all solid phases tested, as well as, from the artificially contaminated wood samples. The results obtained with the commercial siderophore Desferal® (deferoxamine mesylate, DFOM) were comparable to the chemical iron chelator ethylenediaminetetraacetic acid (EDTA). DFOM treatment arrived at the same extraction levels than EDTA. Moreover, siderophores were more compatible with the wood matrix. On opposite to EDTA, they did not enhance the production of reactive oxygen species (ROS). Moreover, EDTA and derivatives involve environmental and health concerns [18], [19]. Siderophores are a safer alternative for the objects, the users and the environment.

However, the costs of using siderophores are at this moment much higher than EDTA. Purification of siderophores in the laboratory was time-consuming. Around 70 mg of purified PVD per 1 L of culture were recovered after a long process. The small amounts and the instability of the products made the long-term usage challenging. Commercial siderophores are a good alternative, but they are still much more expensive than EDTA and derivatives. One solution to reduce costs is the synergic use of low molecular weight organic acids (LMWO). We have seen the positive effect of using citric acid along with the siderophores. The mechanism behind this increased dissolution suggests that the organic acid is adsorbed into the solid surface promoting dissolution. Then, the rapid ligand exchange between siderophore and acid allows rapid re-adsorption of the organic acid, promoting more dissolution [20]. Moreover, citric acid meets the requirements to be considered sustainable. It is a biodegradable molecule

that can be obtained from natural sources [21]. Another alternative to reduce costs is to improve the in-house production of siderophores. The implementation of continuous cultures, where the bacteria are in production state over extended periods of time, will allow to reduce production costs [22]. Also, the siderophore obtained from *S. ureilytica* Lr5/4, not yet identified, could be more stable than the purified pyoverdine (PVD) from *P. putida*.

Overall, the use of siderophores was in line with the conservation requirements mentioned above. Moreover, the change in the appearance of the model wood samples after siderophore treatment were within the standards when extracting high quantities of iron [3], [23]. The treatment is also retreatable and further characterization is in place to determine the durability of such treatment.

The chelation of iron from iron sulfides usually co-extracts the associated sulfur [23]. During experiments in chapter 2, the co-extraction of sulfur was indeed detected. However, after few days, sulfur in solution was precipitating on the wood samples. The extraction of reduced sulfur species using biological metabolisms was the second line of research on this work (Chapter 3).

T. denitrificans is a well-known sulfur-oxidising bacterium [24], [25]. It was selected in this study for its capability to oxidise several reduced sulfur species, including iron sulfides, at neutral pH and in anoxic conditions [26]–[29]. Under these conditions, *T. denitrificans* was able to oxidise elemental sulfur at rates of 0.11 ±0.02 mM $SO_4^{2-}\cdot day^{-1}$. Similar rates have been observed before with this bacterium [30]. Mackinawite was oxidised at rates of 0.03 ±0.00 mM $SO_4^{2-}\cdot day^{-1}$, that is also in agreement with previous works [27]. To enhance oxidation of more stable phases, such as pyrite, we added a more accessible sulfur source, as sodium thiosulfate, to increase initial growth. However, even in these conditions, pyrite oxidation only led to Fe^{3+} ions production. Release of sulfates was of the same order as in control.

Furthermore, *T. denitrificans* was also applied to extract reduced sulfur species from artificially contaminated model wood samples in neutral pH and anoxic environment. Here, we detected rates of 0.17 ±0.04 mM $SO_4^{2-}\cdot day^{-1}$. Raman spectroscopy analyses and the study of chemical equations, however, suggested that partially oxidised mackinawite was the main reduced sulfur compound oxidised. The oxidation rates were higher than for the experiments with solid phases. This could be due to the lower chemical stability of the compounds present on the wood than the purchased mackinawite tested previously. No other sulfur species, apart from mackinawite, were clearly oxidised on the wood samples. Nonetheless, the oxidation rates showed that *T. denitrificans* was able to directly metabolize sulfur compounds present in the wood substrate.

This demonstrated the feasibility of a biological extraction as an alternative to current chemical oxidation methods.

Originally, the research idea was to oxidise problematic sulfur species without the presence of oxygen. However, after deeper discussion with conservation scientists and conservators, they suggested that the application of a total anoxic immersion bath would be difficult in real praxis. Moreover the accumulation of nitrites could be problematic [31]. Therefore, we also studied the oxidation in presence of oxygen. *T. denitrificans* was still our model organism as it as a facultative anaerobe that could also oxidise sulfur species in oxic conditions [24]. Oxidation rates of elemental sulfur increased in these conditions to of 0.19 ±0.05 mM $SO_4^{2-}\cdot day^{-1}$. For the other tested solid phases, the presence of oxygen turned out in abiotic oxidation in control samples, and therefore, we ruled out biological oxidation occurring in these samples. In artificially contaminated wood samples, *T. denitrificans* was able to oxidise reduced sulfur compounds with oxygen as electron acceptor, but the oxidation rates were lower (0.04-0.05 mM $SO_4^{2-}\cdot day^{-1}$). In this case, the bacteria also used preferentially partially oxidized mackinawite over other reduced sulfur species (mainly elemental sulfur).

WAW present high amounts of pyrite [1], [7], [32], while our model samples presented mostly partially oxidised mackinawite and elemental sulfur when analysed with Raman spectroscopy. Studies with pure mineral phases showed that pyrite was only partially oxidised by *T. denitrificans*. Therefore, the use of WAW samples with pyrite accumulation (i.e., marine samples) would be essential to ascertain the efficacy of the proposed biological treatment.

Moreover, future investigation could focus on other model bacteria to conduct the oxidation of iron sulfides. *T. denitrificans* is a model bacteria for anaerobic, nitrate-dependent oxidation of pyrite at neutral pH [26], [27]. However, other bacteria like *Thiobacillus thioparus* could be used, alone or in co-culture [33]. Previous studies showed the increased oxidation of pyrite when *T. denitrificans* and *T. thioparus* were used in a co-culture [33]. Moreover, if the treatment is finally defined in oxic conditions, the microbial oxidation of reduced sulfur species has the potential to accelerate the dissolution of these species. Recent work has shown rates of pyrite oxidation an order of magnitude higher in the presence of certain bacteria compared to abiotic control [34]. Bacteria from the order *Rhizobiales* and *Ralstonia* species were detected in the cultures [34].

The application of *T. denitrificans* to wood samples was compatible with the matrix, as no degradation of the wood components was observed by FTIR analyses. Chemical oxidative

agents are, so far, more efficient in terms of oxidation rate. Yet, they are very aggressive towards the wood, resulting in bleaching [35]. Treatment with *T. denitrificans* also altered the appearance of the wood. However, in some cases it was mostly due to the precipitation of phosphates from the growth medium. When using a different buffering agent, oxidation occurred, and the wood samples acquired the typical dark appearance of WAW contaminated with iron oxides [2]. Therefore, further research is still needed to improve the biological oxidation of sulfur species in wood samples, in terms of appearance and efficiency.

As observed during this work, the extraction of iron and sulfur independently always resulted in the other moiety precipitating or interfering. Therefore, we defined an application protocol that combined the use of siderophores and *T. denitrificans* (Chapter 4). For this first treatment campaign, DFOM (Desferal®) was selected as we required high quantities of chelating agent, and the costs of producing siderophores overtook the cost of the commercial one. DFOM is a useful reference of the feasibility of applying siderophores to treat WAW.

The biological treatment was defined as a two sequential steps protocol:

1. Extraction of iron ions by DFOM
2. Oxidation of the remaining sulfur by *T. denitrificans*

This protocol was the most efficient in a first trial. The DFOM pre-treatment eliminated high quantities of iron and sulfur, and in the second step, the bacteria metabolised remaining sulfur species to sulfates.

This protocol was then evaluated on different wood species with different degrees of degradation and contamination with iron and sulfur compounds. This study was conducted in direct collaboration with the Archaeological Service of Bern Canton and the Swiss National Museum. Their experience in wood conservation gave important feedback to approach the biological treatment to real praxis. As already mentioned, complete anoxic conditions were discarded. Instead, flushing the treatment solutions with nitrogen was an approach they suggested feasible in conservation departments. Moreover, after collaborative discussion, they trusted our experience in microbiology and were not concerned that the biological treatment will produce further biodeterioration. They presented big interest in alternative extraction methods to current treatments.

After application of the defined biological treatment, reduced sulfur compounds identified by Raman spectroscopy were not detected anymore. In this case, not even elemental sulfur was observed after treatment. In the previous chapters with only siderophores or bacteria, elemental

sulfur was still present after treatment. Here, sulfur extraction rates reached 80% in some samples, and iron extraction rates were in average of 65%. These results were comparable to the reference chemical protocol based on successive immersion in oxidant and complexing solutions. However, the biological treatment had a longer duration. To reduce treatment times, an increase in siderophore concentration could be considered along with improvement of the bacterial culture. As studied in chapter 3, *T. denitrificans* presented a better growth when the growth medium presented phosphates. Other nutritional requirements could be considered to improve bacterial growth.

In this study, the performance of the bio-treatment was not influenced by the species of wood nor the state of wood degradation, and finally the biological treatment preserved the original appearance better than the chemical treatment. The final appearance of the wood cubes would be further evaluated after conservation treatments (i.e., consolidation and freeze-drying). These processes also affect the final appearance of the wood. A survey among conservators is planned with the final consolidated cubes to ascertain that the final aspect respects conservation guidelines.

Both extraction protocols were compatible with the wood substrate as no further wood degradation was observed with FTIR measurements. However, the chemical protocol presented more aggressive conditions (pH of 1.5-4). Moreover, some of the chemicals used in the chemical protocol are classified as health hazard (i.e., sodium persulfate, hazard statements: H302, H315, H317, H319, H334). Still, this chemical protocol is currently used due to its short-time application duration and low cost. Improving the efficiency of the bio-treatment is essential for end-users to switch from one protocol to the other. As discussed above, the synergic use of LMWO could enhance the overall extraction rate.

Moreover, for future applications, is important to keep in mind the interactions between the wood autochthonous microorganisms and the proposed extraction protocol. During the *T. denitrificans* treatment step, samples representing freshwater WAW (sets D1, D2, G1 and G2) presented nitrate reduction rates of 0.43-0.86 mM $NO_3^{-}\cdot day^{-1}$, but sulfur oxidation rates were in the range of 0.06-0.09 mM $SO_4^{2-}\cdot day^{-1}$. However, with almost all artificially contaminated wood model samples (exception of set B: fresh oak artificially contaminated) denitrification rates of 0.08-0.16 mM $NO_3^{-}\cdot day^{-1}$, were coupled with sulfur oxidation rates of 0.04-0.07 mM $SO_4^{2-}\cdot day^{-1}$. Moreover, in other previous experiments, like the first trial of the application protocol (Section 4.1), denitrification rates were higher (~0.26 mM $NO_3^{-}\cdot day^{-1}$) because of higher sulfates production rates (~0.21 mM $SO_4^{2-}\cdot day^{-1}$). These values indicate that with

freshwater WAW samples (sets D1, D2, G1 and G2), the consumption of nitrates was higher than expected for denitrification coupled to oxidation of the studied reduced sulfur compounds. Complementary analyses on the inhabiting bacteria of lake WAW samples revealed a diverse microbial community that could explain the extra consumption of nitrates. For example, *Pseudomonas* species were detected in DNA sequencing analysis. This genus contains bacteria that are able to conduct heterotrophic denitrification [26]. Moreover, further analyses of the autochthonous bacterial community showed a consortium of bacteria including sulfate-reducing bacteria (SRB). These bacteria developed along with erosion bacteria (EB) in incubated fresh wood samples. The presence of SRB was confirmed by the DNA analyses. These group of bacteria could affect the efficiency of treatment if the sulfates produced are reduced again [36]. Further experiments are needed to observe if this specific group of bacteria and others could alter the overall performance of the biological extraction protocol proposed or if their effect could be considered negligible. Experiments conducted in sterile wood versus experiments in wood containing the autochthonous microbiota could help to establish the overall impact of the inhabiting bacteria in the biological treatment.

Overall, both metabolisms under study, namely siderophores complexation and sulfur oxidation, can be useful to extract problematic iron and sulfur species from WAW. Depending on the specific requirements of the recovered artefacts one or the other pathway would be recommended. Still, we observed that together, the use of siderophores and biological oxidation performed similarly to current extraction treatments and are in line with conservation ethics. The bio-based treatment resulted promising and future efforts would be made to improve performance, reduce costs and develop a ready-to use protocol.

The Swiss National Science Foundation has granted the MICMAC project a two-year extension up to January 2023. The project will continue to deepen in the biological solutions proposed in this thesis, and to develop towards real praxis.

References

[1] M. Sandström, F. Jalilehvand, I. Persson, U. Gelius, P. Frank, and I. Hall-Roth, "Deterioration of the seventeenth-century warship Vasa by internal formation of sulphuric acid," *Nature*, vol. 415, no. 6874, pp. 893–897, Feb. 2002, doi: 10.1038/415893a.

[2] Y. Fors and M. Sandström, "Sulfur and iron in shipwrecks cause conservation concerns," *Chem. Soc. Rev.*, vol. 35, no. 5, pp. 399–415, 2006, doi: 10.1039/b507010b.

[3] C. Pelé, E. Guilminot, S. Labroche, G. Lemoine, and G. Baron, "Iron removal from waterlogged wood: Extraction by electrophoresis and chemical treatments," *Stud. Conserv.*, vol. 60, no. 3, pp. 155–171, May 2015, doi: 10.1179/2047058413Y.0000000110.

[4] D. W. Grattan and R. W. Clarke, "Conservation of waterlogged wood," *Conserv. Mar. Archaeol. Objects*, pp. 164–206, Jan. 1987, doi: 10.1016/B978-0-408-10668-9.50015-0.

[5] C. Caple, *Conservation skills: judgement, method and decision making*. Routledge, 2000.

[6] C. Rémazeilles *et al.*, "Microbiologically influenced corrosion of archaeological artefacts:Characterisation of iron(II) sulfides by Raman spectroscopy," *J. Raman Spectrosc.*, vol. 41, no. 11, pp. 1425–1433, 2010, doi: 10.1002/jrs.2717.

[7] C. Rémazeilles, K. Tran, E. Guilminot, E. Conforto, and P. Refait, "Study of Fe(II) sulphides in waterlogged archaeological wood," *Stud. Conserv.*, vol. 58, no. 4, pp. 297–307, 2013, doi: 10.1179/2047058412Y.0000000071.

[8] S. Dhungana and A. L. Crumbliss, "Coordination chemistry and redox processes in siderophore-mediated iron transport," *Geomicrobiol. J.*, vol. 22, no. 3–4, pp. 87–98, 2005, doi: 10.1080/01490450590945870.

[9] B. E. Kalinowski, L. J. Liermann, S. Givens, and S. L. Brantley, "Rates of bacteria-promoted solubilization of Fe from minerals: A review of problems and approaches," *Chem. Geol.*, vol. 169, no. 3–4, pp. 357–370, 2000, doi: 10.1016/S0009-2541(00)00214-X.

[10] D. Parrello, A. Zegeye, C. Mustin, and P. Billard, "Siderophore-mediated iron dissolution from nontronites is controlled by mineral cristallochemistry," *Front. Microbiol.*, vol. 7, no. MAR, pp. 1–11, 2016, doi: 10.3389/fmicb.2016.00423.

[11] S. M. Kraemer, "Siderophores and the Dissolution of Iron-Bearing Minerals in Marine Systems," *Rev. Mineral. Geochemistry*, vol. 59, no. 1, pp. 53–84, 2005, doi: 10.2138/rmg.2005.59.4.

[12] E. Farkas, É. A. Enyedy, L. Zékány, and G. Deák, "Interaction between iron(II) and hydroxamic acids: Oxidation of iron(II) to iron(III) by desferrioxamine B under anaerobic conditions," *J. Inorg. Biochem.*, vol. 83, no. 2–3, pp. 107–114, 2001, doi: 10.1016/S0162-0134(00)00197-5.

[13] R. Xiao and W. S. Kisaalita, "Fluorescent pseudomonad pyoverdines bind and oxidize ferrous ion," *Appl. Environ. Microbiol.*, vol. 64, no. 4, pp. 1472–1476, 1998.

[14] D. Lukasz, R. Liwia, M. Aleksandra, and S. Aleksandra, "Dissolution of arsenic minerals mediated by dissimilatory arsenate reducing bacteria: Estimation of the physiological potential for arsenic

mobilization," *Biomed Res. Int.*, vol. 2014, 2014, doi: 10.1155/2014/841892.

[15] F. Edberg, B. E. Kalinowski, S. J. M. Holmstroḿ, and K. Holm, "Mobilization of metals from uranium mine waste: The role of pyoverdines produced by Pseudomonas fluorescens," *Geobiology*, vol. 8, no. 4, pp. 278–292, 2010, doi: 10.1111/j.1472-4669.2010.00241.x.

[16] S. S. Sasnow, H. Wei, and L. Aristilde, "Bypasses in intracellular glucose metabolism in iron-limited Pseudomonas putida," *Microbiologyopen*, vol. 5, no. 1, pp. 3–20, 2016, doi: 10.1002/mbo3.287.

[17] A. Pedersen and M. Hermansson, "Inhibition of metal corrosion by bacteria," *Biofouling*, vol. 3, no. 1, pp. 1–11, 1991, doi: 10.1080/08927019109378157.

[18] C. Oviedo and J. Rodríguez, "EDTA: The chelating agent under environmental scrutiny," *Quim. Nova*, vol. 26, no. 6, pp. 901–905, 2003, doi: 10.1590/S0100-40422003000600020.

[19] J. Arts, S. Bade, M. Badrinas, N. Ball, and S. Hindle, "Should DTPA, an Aminocarboxylic acid (ethylenediamine-based) chelating agent, be considered a developmental toxicant?," *Regul. Toxicol. Pharmacol.*, vol. 97, no. April, pp. 197–208, 2018, doi: 10.1016/j.yrtph.2018.06.019.

[20] P. U. Reichard, R. Kretzschmar, and S. M. Kraemer, "Dissolution mechanisms of goethite in the presence of siderophores and organic acids," *Geochim. Cosmochim. Acta*, vol. 71, no. 23, pp. 5635–5650, Dec. 2007, doi: 10.1016/j.gca.2006.12.022.

[21] K. Asemave, "Greener Chelators for Recovery of Metals and Other Applications," *Org. Med. Chem. Int. J.*, vol. 6, no. 4, May 2018, doi: 10.19080/OMCIJ.2018.06.555694.

[22] A. Sijerčić and N. Price, "Hydroxamate siderophore secretion by Pseudoalteromonas haloplanktis during steady-state and transient growth under iron limitation," *Mar. Ecol. Prog. Ser.*, vol. 531, pp. 105–120, Jul. 2015, doi: 10.3354/meps11338.

[23] G. Almkvist and I. Persson, "Extraction of iron compounds from wood from the Vasa," *Holzforschung*, vol. 60, no. 6, pp. 678–684, 2006, doi: 10.1515/HF.2006.114.

[24] D. P. Kelly and A. P. Wood, "Confirmation of Thiobacillus denitrificans as a species of the genus Thiobacillus, in the beta-subclass of the Proteobacteria, with strain NCIMB 9548 as the type strain.," *Int. J. Syst. Evol. Microbiol.*, vol. 50, no. 2, pp. 547–550, Mar. 2000, doi: 10.1099/00207713-50-2-547.

[25] H. R. Beller *et al.*, "The genome sequence of the obligately chemolithoautotrophic, facultatively anaerobic bacterium Thiobacillus denitrificans," *J. Bacteriol.*, vol. 188, no. 4, pp. 1473–1488, 2006, doi: 10.1128/JB.188.4.1473-1488.2006.

[26] C. Torrentó, J. Cama, J. Urmeneta, N. Otero, and A. Soler, "Denitrification of groundwater with pyrite and Thiobacillus denitrificans," *Chem. Geol.*, vol. 278, no. 1–2, pp. 80–91, 2010, doi: 10.1016/j.chemgeo.2010.09.003.

[27] J. Bosch, K.-Y. Lee, G. Jordan, K.-W. Kim, and R. U. Meckenstock, "Anaerobic, Nitrate-Dependent Oxidation of Pyrite Nanoparticles by Thiobacillus denitrificans," *Environ. Sci. Technol.*, vol. 46, no. 4, pp. 2095–2101, Feb. 2012, doi: 10.1021/es2022329.

[28] J. Pu *et al.*, "Pyrite-based autotrophic denitrification for remediation of nitrate contaminated groundwater,"

Bioresour. Technol., vol. 173, pp. 117–123, 2015, doi: 10.1016/j.biortech.2014.09.092.

[29] Y. Yang *et al.*, "Utilization of iron sulfides for wastewater treatment: a critical review," *Rev. Environ. Sci. Biotechnol.*, vol. 16, no. 2, pp. 289–308, 2017, doi: 10.1007/s11157-017-9432-3.

[30] R. Yan, A. Kappler, and S. Peiffer, "Interference of Nitrite with Pyrite under Acidic Conditions: Implications for Studies of Chemolithotrophic Denitrification," *Environ. Sci. Technol.*, vol. 49, no. 19, pp. 11403–11410, Oct. 2015, doi: 10.1021/acs.est.5b02981.

[31] A. Cockburn *et al.*, "Nitrite in feed: From animal health to human health," *Toxicol. Appl. Pharmacol.*, vol. 270, no. 3, pp. 209–217, 2013, doi: 10.1016/j.taap.2010.11.008.

[32] C. Rémazeilles *et al.*, "Post-treatment Study of Iron/Sulfur-containing Compounds in the Wreck of Lyon Saint-Georges 4 (Second Century ACE)," *Stud. Conserv.*, vol. 65, no. 1, pp. 28–36, Jan. 2020, doi: 10.1080/00393630.2019.1610608.

[33] S. Vaclavkova, N. Schultz-Jensen, O. S. Jacobsen, B. Elberling, and J. Aamand, "Nitrate-Controlled Anaerobic Oxidation of Pyrite by Thiobacillus Cultures," *Geomicrobiol. J.*, vol. 32, no. 5, pp. 412–419, 2015, doi: 10.1080/01490451.2014.940633.

[34] E. Percak-Dennett *et al.*, "Microbial acceleration of aerobic pyrite oxidation at circumneutral pH," *Geobiology*, vol. 15, no. 5, pp. 690–703, 2017, doi: 10.1111/gbi.12241.

[35] K. Tran, N. Bertout, F. Dalard, and J.-P. Magnin, "Trials on chemical and microbiological processes for the oxidation of sulphur compounds in archaeological wood," in *Proceedings of the 9th ICOM Group on Wet Organic Archaeological Materials Conference: Copenhagen, 2004*, 2004, pp. 227–242.

[36] Y. Fors, T. Nilsson, E. D. Risberg, M. Sandström, and P. Torssander, "Sulfur accumulation in pinewood (Pinus sylvestris) induced by bacteria in a simulated seabed environment: Implications for marine archaeological wood and fossil fuels," *Int. Biodeterior. Biodegrad.*, vol. 62, no. 4, pp. 336–347, 2008, doi: 10.1016/j.ibiod.2007.11.008.

[37] G. Almkvist, "The chemistry of the Vasa," Doctoral Thesis, Uppsala, 2008.

I. Acknowledgments

First, I would like to express my gratitude to my supervisor **Edith Joseph**. I appreciate the opportunity you gave me to be part of your new forming team. Together, we have battled many obstacles to develop this beautiful project in wood conservation. I really thank you for your support and advice during all these years.

The adventure of the MICMAC project would not have been the same without **Mathilde Monachon**. I remember the day I learnt that the project would be a close collaboration between two PhDs. We did not know each other, and we had to work together all the time. I could not have imagined a better turn out. From the first day, we created a perfect work dynamic. We have learnt from each other, and we have helped each other all the time. You have been the best lab/office partner ever, and personally I have gained a friend forever.

I would also like to thank the rest of the LATHEMA team. The former PhD students that helped me so much when I started. Their shared their experiences and gave me advice. **Wafa**, **Lucrezia** and **Monica** a huge thank you. Then, the PhDs that have joined afterwards that have been a great addition to the team. It has been so much fun all the time spent together. **Sarah**, **Arianna**, **Luana** and **Silvia**, I wish you all the best in your starting theses. A special mention goes to **Lidia Mathys**. Lidia, merci pour tout le support dans ces ans. Le laboratoire ne fonctionne pas sans toi !

I really need to thank all the people from my second home during these four years, the institute of chemistry. It has been hard and awkward at times, and so much laughter and fun at other times. In particular, **Marie**, **Yassine**, **Cristina**, **Siva** and **Giau**, it was so nice to share this experience with you. Also, **Stephan Von Reuss** thank you for all your help and advice. Your tips over the years have been great.

I also want to express my appreciation to my second supervisor, **Pilar Junier**. Pilar, I want to thank you for your help any time I have asked. You gave me the first opportunity to come to Neuchâtel, already six years ago. You encouraged me then into the field of microbiology, and it has turned out into a career. Also, LAMUN has always been opened, and I profit to also thank all the members that have also helped me during the years. In particular, **Saskia** and **Isha**, you have helped me to open my eyes to bioinformatics.

A big thank you goes to all the people that helped me to carry out all my analyses. All the colleagues from the NPAC, specially **Armelle Vallat** for the many ICP-OES runs. **Vincent**

Gruber, from the CHYN, for all the IC, and all the collaborators from CSEM that nicely assisted my experiences there.

I also want to thank other people that kindly supported me. **Matthieu Bueche**, your help was crucial for me. You taught me how to grow anaerobes, and you have always been there to share your advice. Also, all the personal from the Atelier de construction mécanique. You have accommodated your facilities to cut all our wood during the years.

I also really appreciate all the things I learnt in collaboration with people from different backgrounds during the MICMAC project. Therefore, I really thank **Emilie Cornet**, **Friederike Moll-Dau**, **Tiziana Lomabrdo**, **Jannet Scharmm** and **Katharina Schmidt-Ott**.

During these four years, the support of my family has been essential for me. They have been next to me in the distance, always there to comfort me. The greatest thank you is for them. **Mama**, **Papa** y **Tete**, muchas gracias por vuestro apoyo. Siempre aceptáis todas mis decisiones, aunque eso signifique vivir alejados. Lucky, I had my starting family in Switzerland with me. **Nick**, you have shared with me all the best and worst moments of these four years. You have been my balance. Also, two years ago we decided to adopt into our family our little **Russel**, who bring us so much joy and laughter.

This doctoral research has been financially supported by the Swiss National Science Foundation (Professorship Grant PP00P2_163653/1, 2016–2020). I appreciate the big investment of Switzerland for science.

Finally, I would like to acknowledge my thesis committee: **Prof. Pilar Bosch Roig** and **Dr. Jakob Zopfi**. Thank you for your invested time in evaluating my work. Your comments and recommendations would help me improve the quality of my present and future research.

II. Figures Index

III. Tables Index

IV. List of Publications and Dissemination

Publications:

1. M. Monachon, **M. Albelda-Berenguer**, T. Lombardo, E. Cornet, F. Moll-Dau, J. Schramm, K. Schmidt-Ott and E. Joseph (2020). "Evaluation of an alternative bio-treatment for the preservation of waterlogged wood," *Eur. Phys. J. - Plus*. In preparation.

2. E.Joseph, S. James, **M. Albelda Berenguer**, M. Albini, L. Comensoli, E. Cornet, E. Domon Beuret, W. Kooli, L. Brambilla, L. Mathys, M. Monachon and J. Schröter. "Ground-breaking approaches for a green and sustainable metal conservation". In preprints of ICOM-CC 18th triennial conference, Transcending Boundaries: Integrated Approaches to Conservation. Bridgland, J., managing ed. International Council of Museums Committee for Conservation (ICOM-CC): Beijing, China, 2020 (postponed to 17-21 May 2021).

3. E. Joseph, **M. Albelda-Berenguer**, E. Cornet, L. Cuvillier, S. James, L. Mathys, M. Monachon, A. Passaretti and S. Russo. (2020). "Innovative approaches towards a green and sustainable metal conservation". *Chimia*, 74, 611.

4. M. Monachon, **M. Albelda-Berenguer**, T. Lombardo, E. Cornet, F. Moll-Dau, J. Schramm, K. Schmidt-Ott and E. Joseph. (2020). "Evaluation of Bio-Based Extraction Methods by Spectroscopic Methods". *Minerals*, vol. 10, no. 2, pp. 1–17, 2020, doi: 10.3390/min10020203.

5. M. Monachon, **M. Albelda-Berenguer**, C. Pelé, E. Cornet, E. Guilminot, C. Rémazeilles and E. Joseph. (2020). "Characterization of model samples simulating degradation processes induced by iron and sulfur species on waterlogged wood". *Microchem. J.,* vol. 155, p. 104756, 2020.

6. M. Monachon*, **M. Albelda-Berenguer*** and E. Joseph. "Bio-based treatment for the extraction of problematic iron sulfides from waterlogged archaeological wood". In 14th ICOM-CC Wet Organic Archaeological Materials (WOAM) Conference Proceedings. Portsmouth, United Kingdom, 20th-24th May 2019; accepted. *Both first authors have the same contribution.

7. M. Monachon, **M. Albelda Berenguer** and E. Joseph. (2019). "Biological oxidation of iron sulphides". In *Advances in Applied Microbiology*, vol. 107, G. M. Gadd and S. B. T.-A. in A. M. Sariaslani, Eds. Academic Press, 2019, pp. 1–27, doi: 10.1016/bs.aambs.2018.12.002. 1 citation

8. **M. Albelda-Berenguer**, M. Monachon and E. Joseph. (2019). "Roles and applications of siderophores". In *Advances in Applied Microbiology*, vol. 106, G. M. Gadd and S. B. T.-A. in A. M. Sariaslani, Eds. Academic Press, 2019, pp. 193–225, doi: 10.1016/bs.aambs.2018.12.001. 6 citations

9. **M. Albelda Berenguer**, M. Monachon, C. Jacquet, P. Junier, C. Rémazeilles, E. J. Schofield and E. Joseph (2019). "Biological oxidation of sulfur compounds in artificially degraded wood". *Int. Biodeterior. Biodegradation*, vol. 141: pp. 62-70, doi: 10.1016/j.ibiod.2018.06.009. 1 citation

Conferences and meetings attended:

1. **M. Albelda-Berenguer**, M. Monachon, E. Joseph. Biotechnology to the rescue of waterlogged archaeological wood. Green conservation of cultural heritage 2019. Porto, Portugal, October 10-12 2019. (oral presentation)

2. **M. Albelda-Berenguer**, M. Monachon, E. Joseph. Pyrite, or not pyrite, that is the question. Studying the capacity of *Thiobacillus denitrificans* to carry out nitrate-dependent pyrite oxidation. Swiss Society for Microbiology annual meeting, Zurich, Switzerland, September 3-4 2019. (poster)

3. M. Monachon, **M. Albelda-Berenguer**, E. Joseph. Bio-based treatment for the extraction of problematic iron sulfides from waterlogged archaeological wood. 14th ICOM-CC Wet Organic Archaeological Materials (WOAM) Conference Proceedings. Portmouth, United Kingdom, May 20-24 2019. (oral presentation)

4. **M. Albelda-Berenguer**, M. Monachon & E. Joseph. Bio-based remediation of iron contamination in waterlogged archaeological wood. IBBS 2018, Conference on New Trends in Cultural Heritage Biodeterioration, Coimbra, Portugal, September 5 - 7 2018. (poster)

5. **M. Albelda-Berenguer**, M. Monachon, L. Schärer, M. Ramstein, P. Junier, E. Joseph. Swiss pile dwellings as model location for natural ageing of wood. IBBS17, 17th International Biodeterioration & Biodegradation Symposium, Manchester, United Kingdom, September 6-8 2017. (poster)

6. **M. Albelda-Berenguer**, M. Monachon, C. Jacquet, P. Junier, C. Rémazeilles, E. J. Schofield, E. Joseph. Biotechnology for the preservation of archaeological waterlogged wood. Swiss Society for Microbiology annual meeting, Basel, Switzerland, August 30-September 1 2017. (poster)

7. **M. Albelda-Berenguer**, M. Monachon, C. Jacquet, P. Junier, C. Rémazeilles, E. J. Schofield, E. Joseph. Microbiological extraction of sulfur compounds from simulated waterlogged wood. TECHNART2017, Bilbao, Spain, May 2-6 2017. (poster)

8. **M. Albelda-Berenguer**. A biotechnological treatment for the preservation of archaeological waterlogged wood. *Annual PhD students meeting 2017*, *Interuniversity Doctoral Program in Organismal Biology*, Neuchâtel, Switzerland, March 29, 2017. (oral presentation: 2nd prize).

V. *Curriculum Vitae*

CONTACT INFORMATION

Name: Magdalena Albelda Berenguer

Nationality: Spanish

Date of birth: 30-12-1991

Email: magdalenaalbe@gmail.com

Phone: +34 76 638 71 40

Address: Rue des Saars 2, 2000 Neuchâtel

EXPERIENCE

Neuchâtel, Switzerland
Sep 2016 – Oct 2020

Research assistant – PhD thesis

University of Neuchâtel

- Applied microbiology to the conservation of cultural heritage
- Production, purification and characterisation of bacterial iron chelators (siderophores)
- Culture and metabolic study of anaerobic bacteria
- DNA extraction, sequencing and data analysis
- Practical experience in Raman spectroscopy, optical microscopy and scanning electron microscopy - energy dispersive X-ray spectroscopy, UV-Vis spectroscopy, Fourier-transform infrared spectroscopy
- Assistance in practical lessons of bachelor students

Supervisor: Prof. Edith Joseph

Madrid, Spain
Feb 2015 – Jul 2015

Master thesis

CIB - CSIC

- Production and recovery of fungal lipases/esterases
- Esterification of hydroxycinnamic acids
- Immobilisation of enzymatic extracts

Supervisors: Dr. Alicia Prieto and Dr. María Jesús Martínez

Valencia, Spain	**Bachelor thesis**
Nov 2013 – Aug 2014	University of Valencia

- Isolation and characterisation of hydrocarbon degrading bacteria

Supervisor: Prof. Elena G. Biosca

EDUCATION

Neuchâtel, Switzerland	**PhD in Sciences**
Sep 2016 – Oct 2020	University of Neuchâtel
Madrid, Spain	**Master of Science in Microbiology**
Sep 2014 – Jul 2015	Autonomous University of Madrid
Valencia, Spain	**Bachelor of Science in Biotechnology**
Sep 2009 – Sep 2014	University of Valencia

Feb – Jun 2014: Erasmus Plus, University of Neuchâtel, Switzerland

Aug 2011– Jun 2012: Erasmus, «La Sapienza» University of Rome, Italy

SKILLS

Languages	Spanish (native), English (C1), French (B1), Catalan (B1), Italian (A2)
Software	Microsoft Office (advance), Adobe Programs (intermediate), R (intermediate)